The role of ligand and receptor dimerisation in control of CD28 and CTLA4 function

Erin Andrea Waters

A thesis submitted to University College London for the degree of Doctor of Philosophy

2023

Supervised by:
Professor David Sansom
Institute of Immunity and Transplantation
University College London

Statement of declaration

I, Erin Waters, confirm that the work presented in this thesis is my own. Where information has been derived from other sources, I confirm that this has been indicated in the thesis.

Erin Waters

Abstract

The CD28-CTLA4 system is central to the regulation of T cell responses, with dysregulation associated with autoimmune disease and cancer progression. CD28 and CTLA4 are homodimeric T cell receptors providing co-stimulatory and inhibitory functions, respectively, through their shared ligands, CD80 and CD86. Whilst CD86 exists as a monomer, CD80 can form non-covalent dimers in the cell membrane and is therefore able to form higher-order lattice structures with CTLA4, providing an avidity advantage and a unique membrane organization compared to CD86. CD80 also interacts in *cis* with PDL1 at the CD80 dimer interface, although the function of this interaction is unknown. Functionally, CTLA4 removes CD80 and CD86 from opposing cells, targeting ligand for destruction via transendocytosis. However, why two ligands are required for this regulation, and how the properties of ligand:CTLA4 interactions contribute to this mechanism are poorly understood.

We removed the avidity influence on receptor-ligand interactions by creating mutants unable to form functional dimers. We demonstrate that following transendocytosis, CD80 remains bound to CTLA4, resulting in ubiquitination and reduced CTLA4 availability. We show this is due to CD80:CTLA4 lattice formation, as dimer disruption by mutation or presence of PDL1 averts CTLA4 ubiquitination. We show loss of avid CD80:CTLA4 paradoxically enhances sensitivity to CTLA4 mediated transendocytosis, as the ability of CD80 to dissociate from CTLA4 following transendocytosis is augmented, permitting CTLA4 recycling and further transendocytosis - a feature normally seen with CD86. Finally, we detected signs of altered CD28 engagement resulting from mutant CD80 co-stimulation indicating monomeric ligands may have improved

CD28 signalling. Our results provide further detail on CTLA4 transendocytosis, where dimerisation and avidity of ligand interactions, (including those regulated by PDL1), are significant in altering the fate of CTLA4, and influencing CD28 mediated co-stimulation.

Impact statement

The work presented in this thesis will have positive academic implications, with the potential to have an impact upon several areas of clinical research. CTLA4 itself is known as an immune checkpoint, acting to limit autoimmunity by dampening T cell responses following activation. Due to this critical role, inhibition of CTLA4 through targeted blockade has the potential to reactivate T cells when in a state of hypo-responsiveness, known as anergy. This approach, alongside blockade of another immune checkpoint PD-1, received the 2018 Nobel Prize in Physiology or Medicine for revolutionising the field of cancer immunotherapy, paving the way for development of other immune checkpoint inhibitors. However, anti-CTLA4-antibodies often cause severe immunotherapy-related adverse events (irAEs) which limit their use in clinic. Thus, a tool which targets CTLA4 but limits irAEs is an active area of research. Our work advances the knowledge of how CTLA4 functions to control CD28- mediated co-stimulation, by differentially targeting shared ligands CD80 and CD86 resulting in separate fates for CTLA4 following transendocytosis. Further, we demonstrate these alternate fates are dictated by the valency of ligands and ability of CTLA4:CD80 to form higher-order structures at a cell-cell synapse. This enhanced understanding will provide additional insight into the successful design of tools which target this axis not only in terms of CTLA4, but in therapeutics that directly target CD80 and CD86, such as CTLA4-Ig (Abatacept). Additionally, our demonstration that CTLA4 acts in this way on Tregs may impact the field of Tregs as cell-based therapies, where a full understanding of how Tregs function will impact disease focus. Furthermore, our observations that CD86 provides superior CD28 co-stimulation could impact the protocols for Treg isolation and expansion for this purpose.

Academically, our work shows advancement in the understanding of CTLA4 biology and the differences between co-stimulatory ligands, CD80 and CD86. Our data supporting a differential role for CD80 and CD86 in controlling the fate of CTLA4, post-transendocytosis has been published in *Nature Immunology*, following peer review. This data has also been communicated at major international conferences, including the Immunoreceptors and Immunotherapy FASEB Science Research Conference, New Orleans July 2022. Further manuscripts are in preparation to disseminate this work to the academic community.

Acknowledgments

I would firstly like to thank my supervisor Prof David Sansom for his unwavering support, encouragement, and confidence in me for the last 5 years. I am so grateful to have been offered the switch from technician to PhD student within his lab, alongside all the opportunities that were brought with it. The advice and guidance he's provided on my project, career and life have been invaluable. I would also like to thank my secondary supervisor, Dr Anne Pesenaker for always making time for me, and putting in the upmost effort into providing feedback at every stage of my PhD – her insight has been of huge impact.

I'd also like to thank all the members of the Sansom lab, past and present, who made my PhD experience so enjoyable. I would especially like to thank Dr Alan Kennedy, whose help goes far beyond generating cell-lines. His expertise, and occasional sarcasm, have helped me personally on so many occasions, and this work really would not have been possible without his collaboration. I'm also thankful to Dr Cayman Williams, who has been there since the beginning and is always around to brighten a tough day.

I am unbelievably grateful to my best friends (you know who you are), who are always on hand to provide the greatest distractions. To Dan, my biggest support, his constant encouragement has seen me all the way to the end and is something I can't thank enough. Finally, to my family, especially my Mum and Dad. I feel so lucky to have their love and support behind everything I do.

Publications arising from this work

Papers

- Khailaie S, Rowshanravan B, Robert PA, **Waters E**, Halliday N, Herrera JDB, Walker LSK, Sansom D, Meyer-Hermann M (2018). Characterization of CTLA4 trafficking and implications for its function, Biophysical Journal, 115(7):1330-1343

- Halliday N, Williams C, Kennedy A, **Waters E**, Pesenacker AM, Soskic B, Hinze C, Hou TZ, Rowshanravan B, Janman D, Walker LSK, Sansom DM. CD86 Is a Selective CD28 Ligand Supporting FoxP3+ Regulatory T Cell Homeostasis in the Presence of High Levels of CTLA-4. Front Immunol. 2020 Dec 8;11:600000.

- Janman D, Hinze C, Kennedy A, Halliday N, **Waters E**, Williams C, Rowshanravan B, Hou TZ, Minogue S, Qureshi OS, Sansom DM. Regulation of CTLA-4 recycling by LRBA and Rab11. Immunology. 2021 Sep;164(1):106-119.

- Kennedy A*, **Waters E***, Rowshanravan B*, Hinze C, Williams C, Janman D, Fox TA, Booth C, Pesenacker AM, Halliday N, Soskic B, Kaur S, Qureshi OS, Morris EC, Ikemizu S, Paluch C, Huo J, Davis SJ, Boucrot E, Walker LSK, Sansom DM. Differences in CD80 and CD86 transendocytosis reveal CD86 as a key target for CTLA-4 immune regulation. Nat Immunol. 2022 Sep;23(9):1365-1378. (***Joint first author**)

- Fox T, Houghton B, Peterstone L, **Waters E**, Edner N, Mckenna A, Preham O, Hinze C, Williams C, Albuquerque A, Kennedy A, Pesenaker A, Genovese P, Walker LSK, Burns S, Sansom DM, Booth C, Morris EC. Therapeutic gene editing of T cells to correct CTLA-4 insufficiency. Science Translational Medicine. 2022 Oct;668(14).

- Kennedy A, Robinson M, Hinze C, **Waters E**, Williams C, Halliday N, Dovedi S, Sansom DM. CTLA-4 regulates PD-L1-PD-1 interactions via transendocytosis of CD80. EMBO Journal. 2023. (*Accepted*)

Book Chapters

- **Waters E**, Williams C, Kennedy A, Sansom DM. In Vitro Analysis of CTLA-4-Mediated Transendocytosis by Regulatory T Cells. Methods Mol Biol. 2023;2559:171-187.

Contents

List of Figures

List of Tables

List of Abbreviations

ANOVA – Analysis of variance

AP1 – Activator protein 1

APC – Antigen presenting cell

BRET- Bioluminescence resonance energy transfer

CD – Cluster of differentiation

CHO – Chinese hamster ovary cells

cSMAC – Central supramolecular activation cluster

CTLA4 – Cytotoxic T lymphocyte antigen 4

CTV – Cell trace violet

DC – Dendritic cell

DMEM – Dulbecco's modified Eagle media

DNA – Deoxyribonucleic acid

EAE – Experimental allergic encephalomyelitis

EDTA – Ethylenediaminetetraacetic acid

Erk – Extracellualr-signal-regulated kinase

Fab – Fragment antibody binding

FACS – Fluorescence-actived cell sorting

Fc – Fragment crystalline

FcR – Fcγ Receptor II

FoxP3 – Forkhead box P3

GFP – Green fluorescent protein

H – Histidine

HLA – Human leukocyte antigen

I - Isoleucine

ICAM-1 – intracellular adhesion molecule 1

ICOS – Inducible T cell costimulator

IDO – Indoleamine 2,3-dioxygenase

IFN – Interferon

Ig – Immunoglobulin

IHL – Intrahepatic lymphocytes

IL – Interleukin

IS – Immunological synapse

ITAM – Immuno-receptor tyrosine-based activation motif

JNK – c-Jun N-terminal kinases

kDa – Kilodalton

L – Leucine

Lck – Lymphocyte-specific protein tyrosine kinase

LFA-1 – Lymphocyte function-associated antigen-1

LPS – Lipopolysaccharide

LRBA – Lipopolysaccharide-responsive and beige-like anchor protein

mDC – Monocyte derived dendritic cell

MFI – Median fluorescence intensity

MHC – Major histocompatibility complex

mTEC - Medullary thymic epithelial cell

mTOR – mammalian/ mechanistic target of rapamycin

NFAT – Nuclear factor of activated T cells

NFκB – Nuclear factor κ-light-chain-enhancer of activated B cells

NK – Natural Killer

P – Proline

P/DAMP – Pathogen/danger associated molecular pattern

PBMC – Peripheral blood mononuclear cell

PBS – Phosphate buffered saline

PD1 – Programmed cell death protein 1

PD-L1 – Programmed death-ligand 1

PI3K – Phosphatidyl-inositol 3-kinase

PKB/Akt – Protein kinase B/ Ak strain transforming

PLCγ – Phospholipase C gamma

pSMAC – Peripheral supramolecular activation cluster

pTreg – Peripherally derived Treg

PPR – Pattern recognition receptors

R- Arginine

RAG – Recombination activation gene

RPMI – Roswell Park Memorial Institute media

SH – Scr homology

SEM – Standard error of the mean

T – Threonine

Tcon – Conventional T cell

TCR – T cell receptor

Tfh – T follicular helper cell

TFI – Total fluorescence intensity

TGFβ – Transforming growth factor β

Th – T helper cell

TLR – Toll like receptor

Treg – Regulatory T cell

tTreg – Thymus derived Treg

ZAP70 - Zeta-chain-associated protein kinase 70

Chapter 1: Introduction

1.1. Introduction to Immune Regulation

The immune system is a complex network of organs, cells and proteins that work together to protect against infection from diverse pathogens such as viruses and bacteria, as well as being able to discriminate between 'self' and 'nonself' antigens. Broadly, the immune system is made up of two arms: the innate and the adaptive immune systems.

The innate immune system acts to provide immediate defence against infection, comprising physical barriers to prevent entry of foreign material, such as skin and mucous membranes, as well as chemical/cellular barriers, activated if foreign molecules enter the body. These latter defences consist of plasma proteins including complement and antimicrobial peptides, and germ-line encoded receptors which recognise molecular signatures present on microorganisms termed pathogen-associated molecular patterns (PAMPs). Recognition of highly conserved PAMPs by pattern-recognition receptors (PRRs) initiates various responses including rapid recruitment of immune effector cells and induction of phagocytosis, ultimately resulting in elimination of the pathogen (Mogensen, 2009). The cornerstone of this system recognition is the toll like receptors (TLRs). For example, the extensively studied TLR4 detects the constitutive gram-negative bacteria surface molecule lipopolysaccharide (LPS), with TLR2/1 heterodimers binding bacterial and mycobacterial cell wall components (Takeuchi et al., 1999). In addition to PAMPs, molecules released from dying cells, or following tissue damage are known as damage-associated molecule patterns (DAMPs) and can also activate the innate response (Bianchi, 2007). All innate immune cells such as macrophages, neutrophils, natural killer

(NK) cells and dendritic cells (DCs) express PRRs, transmitting through well studied adaptor molecules, kinases, and transcription factors via diverse signalling pathways to produce pro-inflammatory cytokines. Cytokine production is critical for initiating effector cellular recruitment as well as activating the adaptive immune response, where required (Janeway et al., 2001).

1.1.1. Adaptive immune system

One key delineation between the two systems is whilst the innate rapidly eliminates evolutionarily conserved 'non-self' targets, the adaptive generates a specific immune response against any microbe encountered and is critical when innate immunity is ineffective in pathogen elimination (Chaplin, 2010). Adaptive immunity is regulated by antibody producing B lymphocytes, and T lymphocytes, expressing B and T cell receptors (BCR and TCR) of highly diverse specificity, potentially able to recognise any 'non-self' antigen. After pathogen elimination, antigen-specific long-lived memory lymphocytes persist, supporting rapid secondary responses following re-exposure to antigens. This effect is known as immunological memory and is perhaps the most important consequence of an adaptive immune response, as well as forming the basis behind vaccination (Alkan et al., 2011; Cano and Lopera, 2013).

The link between innate and adaptive immunity is mainly through antigen-presenting cells (APCs), classically DCs, which internalise a bound PAMP or DAMP through phagocytosis, pinocytosis, or clathrin-mediated endocytosis (Turvey et al., 2010). Post-internalisation, the molecule is degraded and then displayed as a peptide by major histocompatibility complexes (MHC). There are two main classes of MHC complex, class I and II. Whist MHC class I presents peptides to CD8+ T cells, MHC class II presents to CD4+ cells, with each subset

conducting distinct functional roles dependant on the response required (Werner et al., 2017).

Broadly, CD8+ T cells are known to have cytotoxic functions, killing infected cells by perforin and granzyme release to trigger apoptosis. Ubiquitous MHC class I expression on all nucleated cells enables this MHC restricted effector response (Diering et al., 2018a; Zinkernagel and Doherty, 1974). Conversely, MHC class II expression is restricted to 'professional' APCs, e.g. DCs, macrophages or B cells, leading to the co-ordination and regulation of CD4+ effector cells. Primarily classified as helper cells (Th), CD4+ cells do not directly kill infected cells but instead produce cytokines for effector cell recruitment, aid activation of CD8+ T cells or enable B cell antibody class switching. Indeed, CD4+ T cells exhibit extreme heterogeneity, broadly characterised by cytokine production profiles and resultant effector phenotype. Well-characterised subsets include Th1, Th2, Th17 and Th22, as well as follicular helper T cells (Tfh) key for B cell responses, and regulatory T cells (Treg) which act a suppressor T cells (Golubovskaya and Wu, 2016).

1.1.2. T cell development and receptor repertoire generation

T cells are derived from bone marrow hematopoietic stem cells and mature in the thymus (Yang et al., 2010). Each T cell has a unique TCR sequence generated by recombination of genomic DNA sequences, and therefore unique antigen specificity. In 95% of T cells, the TCR is composed of an α chain undergoing variable (V) and joining (J) gene segment stochastic recombination, and a β chain undergoing V, diversity (D) and J recombination. There are multiple varieties of each VDJ gene segment which, in addition to the pairing of two TCR chains, results in a potential receptor sequence repertoire of up to 10^{15} (Davis

and Bjorkman, 1988). This combinational diversity is exponentially increased by junctional diversity, generated by template-independent deletion and insertion of random nucleotides at the junction of V-D and D-J segments. In this way, adaptive immunity can potentially recognise any antigen, including those never seen before and those generated by novel evolving pathogens in a mammal's lifetime (Nikolich-Žugich et al., 2004). Therefore, a T cell may never encounter the antigen it is capable of recognising, but if it does it has the capacity to rapidly proliferate and differentiate in response. This process of antigen-specific T cell clonal expansion is a hallmark of adaptive immunity.

1.1.3. Central tolerance

Whilst random generation is crucial to produce large receptor repertoires required to recognise anything non-self, it also raises the possibility of TCRs with high affinity for our own 'self' molecules. Therefore, the adaptive immune system has evolved to achieve immunity against foreign antigens, without causing harm to the host. This is known as immune tolerance and is defined as lack of reactivity to self-antigens (Janeway et al., 2001b).

Central tolerance mechanisms exist in the thymus, and act to eliminate potentially autoreactive T cells. During T cell maturation, CD4/CD8 double-negative progenitor cells enter the thymic cortex and undergo rapid and extensive proliferation following TCR recombination, generating CD4/CD8 double-positive progenitor cells. Immature thymocytes are first positively selected as those that have affinity for MHC complexes, with Class I or Class II affinity dictating CD4 or CD8 lineage (Alam et al., 1996; Diering et al., 2018b). Those which do not bind will undergo apoptosis, removing non-reactive TCRs from the TCR repertoire (Surh et al., 1994). Reactive T cells migrate to the medulla, where thymic DCs

and medullary thymic epithelial cells (mTECs) present self-antigens to thymocytes. This process is possible due to the transcription factor Aire, which is selectively expressed in mTECs and drives ectopic expression of tissue-specific antigens, permitting self-antigen challenge within the thymus (Anderson et al., 2002; Derbinski et al., 2016). Developing thymocytes with high self-antigen affinity then undergo clonal deletion, whilst those with a low or intermediate affinity retained in a process termed negative selection (Klein et al., 2014). T Cells which survive this selection will downregulate either CD4 or CD8 and emerge from the thymus as a single positive resting, "naïve" T cell which can migrate to secondary lymphoid tissues e.g. the spleen and lymph nodes, and await activation.

1.1.4. Requirement of CD28 co-stimulation in T cell activation

Since negative selection in the thymus is regarded as incomplete, additional mechanisms are required to regulate peripheral T cell responses. Naïve T cells continuously circulate through the blood to secondary lymphoid tissues until they encounter an APC presenting an antigen specific for their TCR, and the process of activation begins. Antigen-MHC recognition by TCR and CD4/CD8 initiates membrane reorganisation, generating microclusters of TCRs alongside recruitment of other key adhesion and signalling molecules which together form a highly organised, molecular network known as the supramolecular activation complex (SMAC), present within an immunological synapse (Monks et al., 1998; Grakoui et al., 1999; Krummel et al., 2000). TCR microclusters are at the central point of this network (cSMAC), associated with a complex of proteins collectively known as CD3 that upon TCR ligation are phosphorylated by downstream Src family kinases Lck and Fyn, which in turn

recruits ζ-chain-associated protein kinase 70 (ZAP70) to form signalosomes required for activation (Chan et al., 1995; Holdorf et al., 1999; Palacios and Weiss, 2004).   Whilst the function of the immune synapse is still debated, it is clear that molecules within the immune synapse organise according to size with small molecules such as the TCR in the cSMAC and larger molecules, e.g. ICAM-1 and CD45 excluded (Van der Merwe et al., 2000). Embracing these features, it has been proposed that TCR tiggering involves the exclusion of phosphatases such as CD45 away from the T cell – APC contact zone, allowing the previously constitutive cycle of tyrosine phosphorylation and dephosphorylation of the TCR complex to be stably in a state of phosphorylation and allowing the multi-step signalling process of activation to occur. This is known as the kinetic-segregation model, and is an active process of TCR triggering (Davis and Van der Merwe, 2006).

It is known that for activation T cells require not just a TCR signal, but also a secondary co-stimulatory signal. Indeed, in the absence of co-stimulation, T cells are in a hyporesponsive state, generally known as anergy. Therefore, the cSMAC also contains receptors which provide a second, co-stimulatory signal. Whilst there are many co-stimulatory molecules identified, the archetypal receptor is CD28 (Linsley et al., 1993) (**Figure 1.1A).** CD28 is a member of the immunoglobulin superfamily (IgSF), existing as a 44kDA homodimeric surface glycoprotein with a short (41aa) cytoplasmic tail, expressed on the surface of the majority of CD4+ T cells, and ~50% of CD8+ T cells (Aruffo and Seed, 1987; Esensten et al., 2016). CD28 has two ligands, CD80 and CD86, which are differentially expressed on subsets of APCs. Consequently, antigen presentation is context dependent, with different ligands expressed in diverse immunological niches. Upon ligation, CD28 initiates signal transduction events dependent on

association of proteins to highly conserved tail signalling motifs (Boomer and Green, 2010). This includes the membrane proximal YMNM motif, and distal PYAP motif, shown to act as docking sites for Src Homology 2 (SH2) and/or SH3 domain-containing kinases and adaptor proteins following TCR and CD28 dependent phosphorylation. For example, tyrosine phosphorylation of the YMNM motif permits binding of the p85 subunit of phosphatidyl-inositol 3-kinase (PI3K) via an SH2 interaction, as well as Grb2 and Gads, whilst the PYAP motif binds SH3 containing Lck (Holdorf et al., 1999; Pagès et al., 1994; Prasad et al., 1994; Toma et al., 2006). Recruitment of these downstream interactors results in activation of transcription factors belonging to families such as NF-kB, NFAT and AP-1, functionally important for enhanced transcription of genes essential for T cell expansion, survival and critically, in IL-2 production (Appleman et al., 2000; Riha and Rudd, 2010).

At the most basic level, CD28 ligation lowers the T cell activation threshold, increasing sensitivity to TCR signals and therefore permitting a response to low-affinity or low abundance antigens. CD28 co-stimulation is thought to be critically required for naïve T cell proliferation, differentiation into T cell subsets and memory cells, as well as protection from anergy. Accordingly, CD28 deficient mice display an array of immune defects including impaired T cell activation and poor memory responses (Green et al., 1994; Shahinian et al., 1993). Ligation of CD28 has diverse and profound consequences, related to both the immunological setting of activation and the co-ordination of TCR and CD28 signals. Consequently, a clear understanding of how CD28 optimises T cell responses following antigen-recognition has proven difficult to delineate, despite much effort. It is currently thought that CD28 functions primarily to augment TCR-dependent signalling through general amplification of gene expression patterns

initiated by TCR ligation, but it can also deliver unique signals to T cells (Kunkl et al., 2019, 2020; Miller et al., 2009). For example, CD28 autonomous signalling has been shown to play a critical role in T cell metabolism and in cytoskeletal remodelling, aiding full downstream TCR signals (Kunkl et al., 2019; Salazar-Fontana et al., 2003). However, some studies have tried to investigate the relative requirements of TCR and CD28 signals in naïve and memory T cell subsets and have suggested a stronger requirement for CD28 in human memory T cells, whilst naïve T cells are more sensitive to TCR control, reflecting the importance of the immunological setting wherein activation occurs (Glinos et al., 2020; Pennock et al., 2013).

In addition to its critical role on pro-inflammatory effector T cells (Teffs), the role of CD28 ligation on anti-inflammatory Tregs is a very active area of research. It is known that CD28 co-stimulation is required for generation of Tregs in the thymus and their survival in the periphery, with CD28-deficient mice having an 80% reduced Treg repertoire (Deppong et al., 2010; Shahinian et al., 1993). This is in part due to the requirement of co-stimulation during generation, as well as due to loss of proliferating Tregs following self-antigen TCR recognition, key to maintenance of self-tolerance (Gogishvili et al., 2013; Salomon et al., 2000; Tang et al., 2003). Together, the outcomes of CD28 mediated co-stimulation are highly pleiotropic indicating a prominent and multifaceted role for T cell regulation.
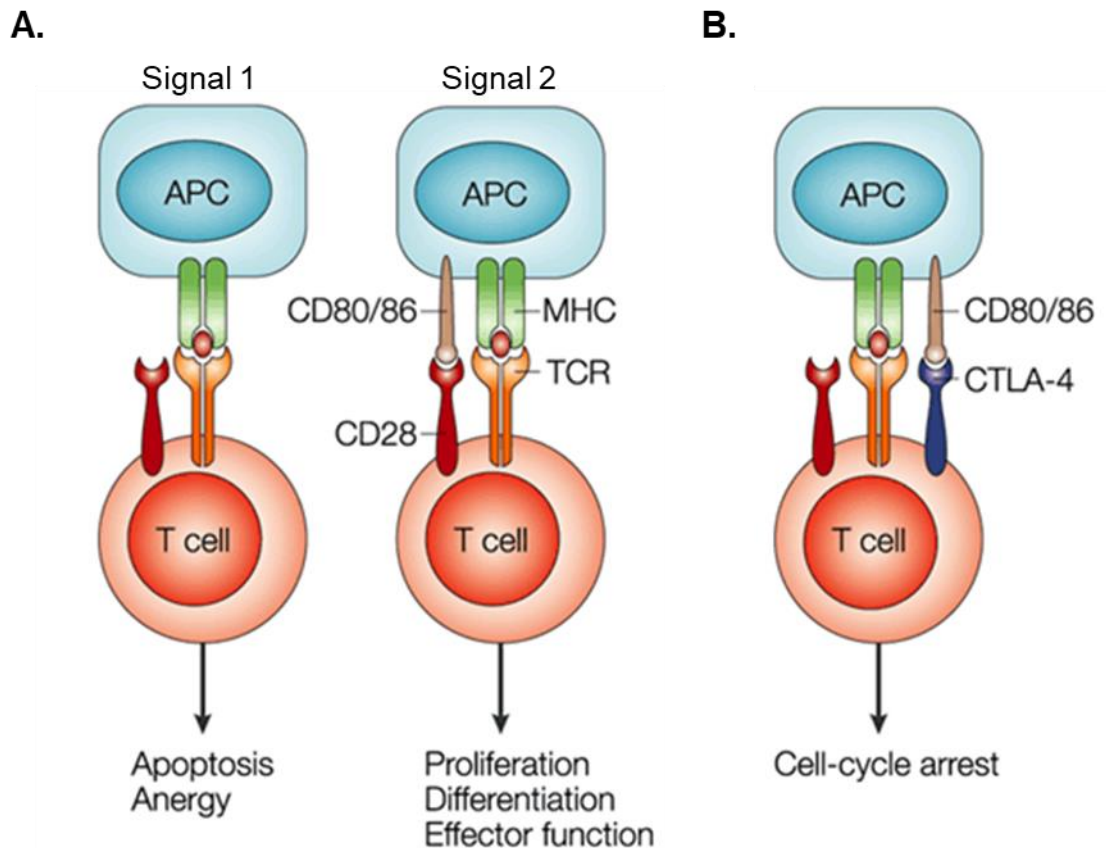
Figure 1. 1. The two signal model of T cell activation. (A). The TCR on the surface of a T cell recognises peptide-MHC complexes on the surface of an antigen presenting cell (APC) (Signal 1). In the absence of co-stimulation, T cells become anergic or undergo apoptosis. For activation, T cells require a second signal provided by CD28 binding to ligands CD80 or CD86 on the surface of an APC (signal 2).**(B).** Following activation, T cells upregulate CTLA4 which binds CD80 and CD86 with higher affinity than CD28, and inhibits T cell responses. (Alegre et al., 2001).

1.1.5. Co-receptors and peripheral tolerance

Despite the process of negative selection in the thymus, a large number of self-reactive T cells are readily detectable in the periphery of healthy people (Kronenberg and Rudensky, 2005). As such, central tolerance is not completely effective, partly because not all self-antigens are expressed in the thymus and partly because if negative selection was too stringent, you risk narrowing the T cell repertoire available for foreign antigen recognition. Therefore, the requirement of CD28 co-stimulation, is a key mechanism of intrinsic peripheral tolerance. Anergy is also regulated by DCs, where mature DCs capable of antigen presentation concurrently express high levels of the CD28-ligands, CD80 and CD86, can easily convert to tolerogenic DCs, characterised by low expression of co-stimulatory ligands (Kryczanowsky et al., 2016; Raker et al., 2015). Intriguingly, anergy from lack of co-stimulation on CD4+ naïve T cells with cognate TCRs for food antigens results in expansion, but lack of differentiation into inflammatory Th cells, and instead promotes Treg generation permitting potential immune suppression (Hong et al., 2022). Thus, anergy is a key mechanism to allow tolerance to foreign proteins in food (Hong et al., 2022). As well as CD28, several other co-stimulatory receptors have been identified including ICOS, CD226, OX40 and 4-1BB (Sharpe, 2009). Equally, anergy can be actively induced by expression of co-inhibitory receptors e.g. cytotoxic T-lymphocyte-associated protein 4 (CTLA4) or programmed cell death 1 (PD-1) receptors, upregulated following T cell activation (**Figure 1.1B**) (Greenwald, 2001; Parekh et al., 2009; Tsushima et al., 2007).

Other mechanisms of peripheral tolerance include immune ignorance, whereby self-antigens are in sites with low immunogenicity and are therefore

anatomically separated from immune effectors, or the low TCR avidity which allowed thymic escape is too low for response and therefore autoreactive T cells ignore cognate antigens (Xing and Hogquist, 2012). Additionally, there is activation-induced cell death, whereby self-activated T cells upregulate death receptors (e.g. Fas) leading to T cell apoptosis, thereby ending the immune response and restoring immune homeostasis (Green et al., 2003). Together, cell-intrinsic mechanisms of immune tolerance permit release of self-reactive T cells into the periphery, without resulting in autoimmunity.

1.1.6. The role of regulatory T cells in adaptive immunity

As well as intrinsic mechanisms, the Treg subset of CD4+ T cells are central to the extrinsic control of T cell tolerance. Identified in the 1990s, Tregs target numerous cell populations to elicit potent immunosuppression, shown by loss of Tregs resulting in catastrophic immune system over-activation (Itoh et al., 1999; Sakaguchi, 1995). Tregs are defined by expression of CTLA4, IL-2 receptor subunit CD25, low levels of IL-7 receptor CD127, and most crucially, the lineage marker forkhead box protein 3 (FoxP3). FoxP3 is fundamental for Treg development, maintenance, and function (Fontenot et al., 2003; Hori et al., 2003; Liu et al., 2006). Indeed, mutations of *FOXP3* lead to scurfy in mice, and development of immunodysregulation, polyendocrinopathy and enteropathy, X-linked (IPEX) syndrome in humans, a profound autoimmune disease characterised by loss of functional Tregs, again demonstrating the importance of Tregs in the maintenance of peripheral tolerance (Brunkow et al., 2001; Craig L. Bennett et al., 2001; Wildin et al., 2001). In addition to FoxP3, IL-2 is indispensable for Treg function and survival. High production of IL-2 from activated CD4+ Teff binds to the high-affinity IL-2 receptor abundantly expressed

on Tregs, composed of the CD25 (IL-2Rα) subunit, inducing FoxP3 expression and Treg cell differentiation. Tregs themselves are unable to produce IL-2, and thus IL-2 consumption by Tregs has potential biological significance in limiting extracellular IL-2 concentrations and maintaining an IL-2 based Treg-Teff cell regulatory loop for immune homeostasis (Cheng et al., 2011; Chinen et al., 2016). Consistently, IL-2 or CD25 deficiency leads to lymphoproliferative autoimmune disorders in mice, and a clinical phenotype highly overlapping IPEX syndrome in humans (Hünig and Schimpl, 1998; Roifman, 2000).

Tregs are divided into two main categories; naturally occurring thymic Tregs (tTregs), generated in the thymus following high-avidity interactions between MHC class II molecules and the TCR, and induced Tregs (iTregs), which differentiate from mature conventional CD4+ cells in the periphery. Whilst the mechanisms of action of iTreg compared to tTreg mediated suppression are not clearly defined, it is likely they have synergistic functions whereby both populations are required for sufficient immune regulation (Shevach and Thornton, 2014). Due to their origin in the thymus, tTregs respond to self-antigens to balance peripheral tolerance. In contrast, iTregs likely respond to exogenous antigens, acting to terminate T cell activation. tTregs are best characterised, eliciting suppression via multiple mechanisms. This includes release of classical inhibitory cytokines IL-10, TGFβ and IL-35, shown to be crucial in prevention of colitis in mouse models of inflammatory bowel disease (IBD), suppression of allergic responses and play a limiting role in anti-tumour immunity (Akbari et al., 2002; Liu et al., 2003; Marie et al., 2005; Ohue and Nishikawa, 2019; Pontoux et al., 2002; Whitehead et al., 2012). Tregs are also known to secrete granzymes and perforin, mediating Treg-induced cytolysis in a manner canonical to CD8+ T cells (Cao et al., 2007). Tregs also modulate the function of APCs, specifically

DCs, to attenuate Teff activation. This mechanism is linked to both conditioning of DCs to express regulatory molecules such as indoleamine 2,3- dioxygenase (IDO), as well as modulating the expression levels of co-stimulatory ligands required for T cell activation (Fallarino et al., 2002; Paust et al., 2004). Importantly, Tregs constitutively express high levels of inhibitory receptor CTLA4, with overwhelming evidence supporting a role for CTLA4 in the extrinsic function of Tregs *in vivo* (Hori et al., 2017; Walker, 2013). Specifically, our group demonstrated that CTLA4 can bind to co-stimulatory ligands CD80 and CD86 on the surface of an APC and physically remove them by a process of transendocytosis, limiting T cell activation by preventing CD28 co-stimulation (Qureshi et al., 2011). Importantly, the convergence of Treg and CTLA4 research has identified that Tregs rely heavily on CTLA4 for regulatory function. Likewise, although CTLA4 is upregulated on Teffs following activation, it is considered its main regulatory function is due to its constitutive expression on Tregs (see **section 1.5**). Recent advances seek to harness the potent regulatory function of Tregs, with cellular therapies using Tregs undergoing clinical trials in graft-versus-host disease and transplant rejection (Hefazi et al., 2021; Raffin et al., 2020; Tang and Vincenti, 2017). Due to identification of this potential, how Tregs work to dampen effector responses and balance immunity is currently a key focus of many research efforts.

1.2. The CTLA4:CD28 pathway

1.2.1. The receptors: CTLA4 and CD28

Ligation of co-stimulatory receptor CD28 results in powerful T cell activation, which if misguided could result in fatal autoimmune responses, and thus warrants effective control. This control is provided by the inhibitory receptor

CTLA4. CTLA4, like CD28, belongs to the IgSF and is located next to the CD28 gene on human chromosome 2q33 (Ling et al., 2001). CTLA4 is a 45-50 kDa glycoprotein and is a constitutive homodimer due to a disulphide linkage by a cysteine residue at position 157 (Lindsten et al., 1993). CTLA4 also contains a short (36aa) cytoplasmic tail and shares ~30% sequence homology with CD28, supporting the notion that these genes arose due to a genetic duplication event but have since diverged (Harper et al., 1991). This homology includes a conserved 'MYPPPY' motif responsible for binding their shared ligands, CD80 and CD86. However, differences in residues which contribute to ligand binding means CTLA4 has higher affinity for both CD80 and CD86 than does CD28, and therefore can act to out-compete CD28 for ligand binding when both ligands are co-expressed (Van Der Merwe et al., 1997; Collins et al., 2002a).

CD28 and CTLA4 are widely accepted to have opposing functions on T cells (Krummel and Allison, 1995). Whilst CD28 amplifies TCR mediated responses resulting in T cell activation, CTLA4 dampens responses in a manner which maintains tolerance and protects against autoimmune disease. In addition, whilst CD28 is near constitutively expressed on resting and activated T cells, CTLA4 is restricted to activated T cells. The exception is in Tregs, where constitutive expression of CTLA4 at high levels is vital for their regulatory function (Takahashi et al., 2000). In Teffs, CTLA4 expression is induced by TCR ligation, with evidence of synergistic CD28 and IL-2 regulation (Finn et al., 1997; Linsley et al., 1996). This induction occurs early, with CTLA4 mRNA levels detected 1-hour post-activation,with peak expression after 24-36 hours. In this way, CTLA4 prevents chronic activation by CD28, acting as a gatekeeper of T cell responses and earning its identification as an 'immune checkpoint'.

The CTLA4:CD28 interplay is clear in the phenotypes of knock-out mice, where CTLA4-deficient (Ctla4-/-) mice develop a T cell-mediated lymphoproliferative disease, show a lethal phenotype caused my mass lymphoproliferation, tissue infiltration and organ destruction (Chambers et al., 1997; Khattri et al., 1999; Waterhouse et al., 1995). Strikingly, this phenotype is reversed in mice by concurrent deletion of CD28, with dual knock-out mice resistant to this disorder (Tai et al., 2007), providing the clearest evidence that CTLA4 is present to directly control CD28 co-stimulation. In addition, the importance of CTLA4 in controlling autoimmune responses is also evident in humans. Homozygous mutations in *CTLA4* in humans has not yet been identified, most likely due to predicted early lethality. However, Individuals with heterozygous germline mutations in *CTLA4* as well as those with deficiency of lipopolysaccharide-responsive and beige-like anchor protein (LRBA), key for CTLA4 trafficking, present with complex immune dysregulation and autoimmunity (Lopez-Herrera et al., 2012; Verma et al., 2017).

1.2.2. The ligands: CD80 and CD86

CD28 and CTLA4 share two ligands, CD80 and CD86. CD80 and CD86 are commonly considered to have overlapping functions *in vivo* and are thought to work in tandem to regulate a diverse range of functions (Sansom, 2000). This perception is based on the knowledge that both ligands can co-stimulate T cells via CD28 ligation, as well as be controlled by CTLA4. Attempts to delineate the individual roles of CD80 and CD86 have been complicated by their mice KO phenotypes indicating functional redundancy. Whilst mice lacking both CD80 and CD86 exhibit a phenotype reminiscent of a CD28$^{-/-}$ phenotype, single gene

deletion of CD80 or CD86 only results in a mild reduction of CD28 dependent responses (Mandelbrot et al., 1998; Salomon et al., 2000b) .

Despite this, CD80 and CD86 are known to differ regarding both their structure, as well as their cellular and kinetic expression profiles. CD80 and CD86 are both membrane bound type I glycoproteins, containing two extracellular Ig-like domains (a membrane distal IgV and membrane proximal IgC), linked to a transmembrane region and short cytoplasmic tail (Collins et al., 2005; Hansen et al., 2009). However, CD80 and CD86 only possess ~26% sequence homology, with evidence of considerable evolutionary diversion correlating with mammal complexity (Freeman et al., 1993). Importantly, CD80 has higher affinity for both CD28 and CTLA4 than CD86 (**see section 1.2.3**) (**Figure 1.2**). An additional difference key to this thesis is that whilst CD86 exists only as a monomer, CD80 forms non-covalent dimers at the cell surface (Bhatia et al., 2005). Whilst CD28 and CTLA4 binding maps to overlapping sites on the GFCC'C'' β-sheet of both CD80 and CD86 – albeit involving different residues – only the alternate face of the CD80 IgV domain contains multiple hydrophobic residues (Ikemizu et al., 2000; Peach et al., 1995). These resides form a hydrophobic pocket in CD80, supporting a dimeric interaction, that is absent for CD86. Furthermore, residue differences in ligand transmembrane regions and cytoplasmic tails support differential cytoskeletal recruitment, internalisation rates and ubiquitin ligase association of both CD80 and CD86. For example, the CD86 cytosolic domain contains a lysine rich motif, linked to binding and rapid internalisation by MARCH1 (Corcoran et al., 2011).

In addition to structural differences, CD80 and CD86 have different expression patterns. Multiple lines of evidence indicate CD86 is essentially
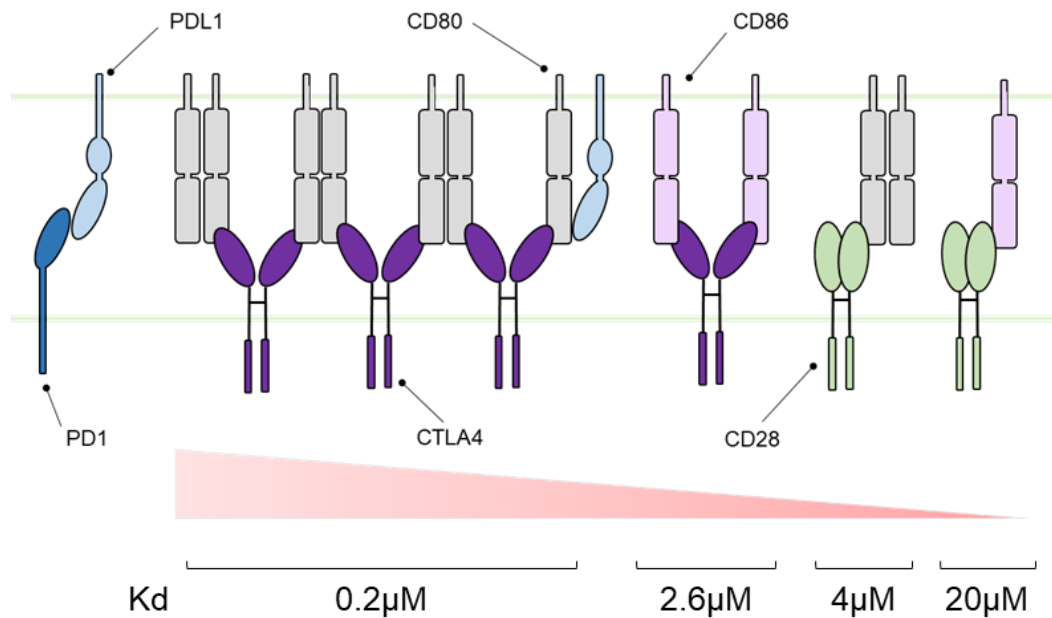
Figure 1. 2. Summary of CTLA4, CD28, CD80 and CD86 interactions with PDL1 crosstalk. Schematic representation showing receptor:ligand pairings and reported monovalent affinities (Kd) (adapted from Collins et al., 2002). CD28, CTLA-4 and CD80 are dimers, whilst CD86 is a monomer. CTLA4 binds bivalently, forming higher order lattice structures with CD80. CD28 binds monovalently to both CD80 and CD86. PDL1, ligand for receptor PD1, binds in *cis* to CD80, likely at the site required for CD80 homodimerization.

constitutively expressed on activated APCs including monocytes, DCs and B cells due to rapid upregulation downstream of TLRs or inflammatory cytokine receptor activation, such as IL-5 (Hathcock et al., 1994; Takatsu, 2006). In contrast, whilst CD80 is also expressed on these APCs following activation, delayed upregulation compared to CD86 is commonly observed *in vitro*. In this way, CD86 is thought to be responsible for initiation of T cell responses, with CD80 responsible for later response stages. Whilst there are exceptions, e.g. on certain cell type such a mTECs and memory B cell subsets CD80 is the solitary ligand (Derbinski et al., 2005; Zuccarino-Catania et al., 2014), it supports the currently emerging concept that CD86 is the more important CD28 ligand, responsible for co-stimulation. Indeed, CD86 is shown to recruit CD28 to the IS, whereas CD80 is more important for recruitment of CTLA4 (Pentcheva-Hoang et al., 2004a). Although redundancy is seen in KO mice models, CD86$^{-/-}$ mice show impaired germinal centre formation, and T cell responses following viral infection whereas CD80$^{-/-}$ mice are less affected (Borriello et al., 1997; Santra et al., 2000). Although expression patterns and biophysical characteristics suggest implicit differences, a full understanding of the differential function of these ligands remains elusive.

1.2.3. Receptor-ligand interactions: affinity, avidity, and valency contributions

Undoubtably key to their differential roles *in vivo* is the different binding properties of CD80 and CD86. CD80 binds both CTLA4 and CD28 with higher affinity (0.2µM and 4µM, respectively) than CD86 (2µM and 20µM, respectively)(Collins et al., 2002). Accordingly, there is a hierarchy of interactions that can occur when a T Cell meets a cell expressing CD80 and CD86 (**Figure**

1.2). However, structural influences add further complexity to the strength of these interactions. CTLA4 is a constitutive dimer able to bind bivalently to CD80 and CD86. Under physiological conditions, CD80 is able to form a dimer in the membrane unlike CD86, which only exists as a monomer (Bhatia et al., 2005a; Girard et al., 2014). Crystallograpy studies support the notion that CTLA4 and CD80 are therefore able to form higher-order lattice or 'zipper' structures, providing an avidity advantage for CD80 over CD86 (Schwartz et al., 2001; Stamper et al., 2001). As such, the influence of avidity on the CTLA4:CD80 interaction is estimated to increase the overall binding strength by several orders of magnitude over the reported affinity. Whilst limited studies exist that consider the impact of avidity on the function of this system, the theoretical implications suggest interesting consequences for T cell responses (Jansson et al., 2005). Indeed, our group recently reported the strong bias of CD80 reduces its function as a CD28 ligand when CTLA4 is co-expressed, supporting CD86 as the dominant CD28 ligand despite its overall low affinity/avidity (Halliday et al., 2020).

Despite also being dimeric, CD28 is proposed to bind CD80 and CD86 monovalently due to steric hindrance (Evans et al., 2005). However, this model has recently been challenged, with evidence of bivalent interaction due to rapid re-orientation of the cytosolic tail of CD28 following TCR ligation (Ganesan et al., 2018; Sanchez-Lockhart et al., 2014). Whilst the valency of CD28 warrants further investigation, considering valency, avidity and affinity together supports the possibility of multiple different outcomes resulting from ligand-receptor interactions and is an area of CD28:CTLA4 biology that is not currently well understood.

1.2.4. CD80 crosstalk with the PD1:PDL1 pathway

Adding further complexity to this system is the recent observation that CD80 binds in *cis* to PDL1, the ligand for PD1 (Chaudhri et al., 2018). PD1 is known for its function as an inhibitory T cell receptor and as a key immune checkpoint which, when targeted alongside CTLA4, pioneered the field of cancer immunotherapy (Buchbinder and Desai, 2015; Curran et al., 2010). PD1 is inducibly expressed on activated T cells, with expression persisting in a manner dependent on whether the response is due to acute or chronic infection. In situations of continuous antigen burden leading to chronic stimulation, PD1 expression correlates with T cell dysfunction where unresponsive T cells are said to be 'exhausted' (Wherry et al., 2015). Engagement of PD1 initiates downstream signalling events, with multiple mechanisms of inhibition suggested. For example, PDL1 binding to PD1 leads to cytoplasmic tail phosphorylation and recruitment of PTP SHP-2, which in turn reduces phosphorylation of the Zap70/CD3ζ signalosome downstream of the TCR (Marasco et al., 2020; Sheppard et al., 2004). Additionally, PD1 ligation has been linked to attenuation of downstream signalling of CD28, e.g. PI3K, thus providing further crosstalk between the CTLA4 and PD1 pathways of T cell inhibition at a molecular level (Parry et al., 2005).

Whilst limited research has directly investigated the functional role of the CD80:PDL1 interaction, reports show that this *cis* interaction prevents PDL1 binding to its receptor, PD1 (Garrett-Thomson et al., 2020; Sugiura et al., 2019; Zhao et al., 2019) . This indicates a new role for CD80 as a regulator of the PD1 pathway. Conversely, how this interaction impacts CD80 binding to CD28 and CTLA4 remains contentious. Zhao et al., report CTLA4 binding is inhibited by the CD80:PDL1 *cis* interaction, whilst CD28 co-stimulation remains unaffected (Zhao

et al., 2019). However, other studies contest this observation, since PDL1 binding to CD80 is on the opposite face of the molecule that is required for receptor binding, and thus the ability of CD80 to bind its receptors remains unaffected in principle (Sansom and Walker, 2019). Indeed, structural studies report this CD80:PDL1 *cis* interaction occurs at the face required for CD80 homodimerisation, raising the possibility of altered valency of CD80 binding to CD28/CTLA4 when PDL1 is co-expressed (Sugiura et al., 2019b). In support, we recently demonstrated CTLA4 can still remove CD80 via transendocytosis when co-expressed with PDL1 on an APC (Kennedy et al., 2022), supporting the notion that the CTLA4 binding site is not restricted. Nevertheless, functional impacts of this interaction remain enigmatic. Considering the complex roles of PD1, CTLA4 and CD28 and the power of targeting these receptors in immunotherapy, a full understanding of this interplay will have significant implications for the field of immunology.

1.3. CTLA4 mechanism of action

It is not under dispute that CTLA4 acts to inhibit T cell activation, however the precise mechanism of how it can exert inhibitory responses is not clearly defined and has been widely debated. In the simplest model, the superior affinity/avidity of CTLA4 for both CD80 and CD86 suggests CTLA4 out-competes CD28 for ligand binding and therefore limits CD28 co-stimulation. However, what happens following CTLA4 ligation, specifically, whether CTLA4 can deliver cell-intrinsic negative signals via canonical signalling pathways has long been under dispute (Walker et al., 2015; Rowshanravan et al., 2018; Sobhani et al., 2021).

1.3.1. CTLA4 cell biology

Internalisation

Key to its function as an inhibitory receptor is the unique cellular distribution of CTLA4. Whilst CTLA4 is trafficked to the plasma membrane to allow ligand binding, the majority of CTLA4 is found intracellularly with only ~20% of the total pool of CTLA4 expressed on the cell surface. To maintain this distribution, CTLA4 undergoes constitutive, rapid endocytosis with ~half of total CTLA4 being internalised within 5 minutes (Qureshi et al., 2012a). Specifically, CTLA4 is internalised by clathrin-mediated endocytosis (CME), a well-understood mechanism for regulating cell surface trafficking (Qureshi et al., 2012b). For CME, clathrin is recruited to the plasma membrane and forms clathrin-coated pits, which bud off the membrane into receptor-containing vesicles. In the case of CTLA4, CME is dependent on CTLA4 binding to the µ2 subunit of clathrin adaptor protein AP2, which binds to a conserved tyrosine motif 'YxxM' present with the C-terminal CTLA4 tail (Schneider and Rudd, 2014; Shiratori et al., 1997; Zhang and Allison, 1997). Indeed, the C-terminal tail of CTLA4 contains multiple motifs highly conserved through evolution, suggesting their functional importance even though their precise role is not fully understood (Leung et al., 1995). For example, whilst mammals and birds have the key 'YVKM' motif required for CME, this is absent in trout, implying the higher affinity of CTLA4>CD28 may be enough for immune regulation in some species and endocytosis of CTLA4 is one that has evolved due to the need for more complex immune regulation (Kaur et al., 2013; Schneider et al., 2001).

CTLA4 Recycling

Despite knowledge of the cellular distribution and internalisation patterns, the trafficking itinerary of CTLA4 is yet to be delineated. Following internalisation, CTLA4 has two fates; it can either be recycled to the plasma membrane or trafficked to lysosomes for degradation (Khailaie et al., 2018; Sansom, 2015), a pattern of trafficking also observed for other recycling receptors, including the transferrin receptor (TfR) and the epidermal growth factor receptor (EGFR) (Ciechanover et al., 1983; Watts, 1985). Further, our group recently studied the role of the Rab family of GTPases in orchestrating CTLA4, demonstrating dominant-negative mutations in Rab5 increased surface CTLA4 expression, whereas Rab11 increased degradation (Janman et al., 2021). Whilst Rab5 is a marker for early endosomes, Rab11 marks recycling endosomes, thus indicating CTLA4 fate maps to canonical pathways following CME.

The importance of CTLA4 recycling for its inhibitory function gained traction following the observation that patients with heterozygous mutations in LRBA exhibit autoimmunity coupled with immunodeficiency due to reduced surface CTLA4 expression (Lopez-Herrera et al., 2012). Later studies confirmed increased CTLA4 degradation following LRBA deficiency, alongside co-localisation of LRBA, CTLA4 and Rab11 which together support a key role for LRBA in the regulation of CTLA4 recycling (Burnett et al., 2017; Lo et al., 2015a). Recently, another protein found to be mutated in patients with systemic autoimmunity, differentially expressed in FDCP6 homolog (DEF6), has also been linked to impaired surface regulation of CTLA4, providing further support for a key role of trafficking in CTLA4 function (Serwas et al., 2019).

CTLA4 lysosomal degradation

The alternate fate for CTLA4 is trafficking to lysosomes for degradation. CTLA4 has a short half-like of ~3 hours, with clathrin-adaptor AP-1 linked to this process (Schneider et al., 1999). Receptor degradation is a key mechanism for controlling cell responses, with many receptors, including PD1, using lysosomal degradation as a mechanism to downregulate the receptor and terminate the resultant downstream signal. Importantly, the rate of degradation varies greatly dependent on the receptor function, with recycling cell surface proteins exhibiting a shorter half-life (1/2-20hrs) when compared with standard cell surface proteins (Cohen et al., 2013).

Classically, trafficking to lysosomes follows protein post-translational modification in the form of ubiquitination. Ubiquitin molecules attached to ubiquitin-conjugating (E2) enzymes are transferred to lysine resides on substrate proteins by interaction with an E3 ubiquitin ligase. Different E2/E3 subtypes confer the type of chain linkage, with the ability of ubiquitin to form different chains underlying its facilitation in diverse cellular outcomes in addition to degradation (Staub and Rotin, 2006). Typically, ubiquitin linkages at K48 direct degradation, sorting substrate proteins into multivesicular bodies by members of the endosomal sorting complexes required for transport (ESCRT) complexes, on the surface of late endosomes. ESCRT complexes then direct ubiquitinated cargo to lysosomes, enabling endo-lysosome fusion and subsequent destruction (Migliano et al., 2018). Whilst this pathway has been clearly linked to lysosomal trafficking of the archetypal recycling receptor EGFR, no such involvement has yet been found for CTLA4 (Raiborg and Stenmark, 2009; Roepstorff et al., 2009). Our group recently demonstrated the lysine-rich intracellular tail of CTLA4 was

ubiquitinated following ligation of CD80, but not CD86 (Kennedy et al., 2022). This observation not only uncovered a crucial difference between CD80 and CD86, but also demonstrated a major role for ubiquitination of the CTLA4 tail in controlling CTLA4 cellular localisation and lysosomal trafficking. To date, the E3 ligase responsible for CTLA4 ubiquitination remains unknown.

1.3.2. Cell-intrinsic models of CTLA4 function

An early view of CTLA4 biology was that CTLA4 ligation initiates downstream signalling cascades which act to antagonise the CD28 pathway and actively inhibit T cell activation. This cell-intrinsic model of CTLA4 function was based on the observation that anti-CTLA4 antibodies inhibited T cell activation, and were therefore considered to be agonistic, activating an inhibitory pathway (Krummel and Allison, 1996; Walunas et al., 1996). Multiple studies have since used anti-CTLA4 antibodies in an attempt to delineate a negative signalling pathway, although this method has provided conflicting data. Some studies report CTLA4 signals via recruitment of PI3K and PKCδ following phosphorylation of the CTLA4 tail by SRC family kinases, demonstrating PI3K mediated phosphorylation of protein kinase B (PKB/AKT) induces T cell anergy by inhibiting activation of pro-apoptotic BAD(Hu et al., 2001; Schneider et al., 2008, 1998). PI3K activation downstream of CTLA4 has also been shown to initiate Th cell migration to inflamed tissues (Ruocco et al., 2012). Alternatively, ligation of CTLA4 has been proposed to recruit phosphatases SHP-2 and PP2A, acting to inhibit inflammatory signals downstream of the TCR such as CD3ζ and linker for activation of T cells (LAT) (Choi et al., 2008; Calvo et al., 1997). CTLA4 activation has also been linked to PKC-η signalling, upregulating factors which prevent activation-induced cell death as well as being linked to inhibition of lipid raft formation and

recruitment of ZAP70 (Guntermann et al., 2002; Rudd et al., 2009, Kong et al., 2014). However, other groups have reported conflicting evidence that does not support these observations, for example CTLA4 has also been reported to have no effect on ZAP70 phosphorylation (Calvo et al., 1997). Thus, although an overwhelming number of studies have investigated the negative signalling cascade activated by CTLA4, a cohesive pathway has not yet been identified. Nevertheless, CTLA4 is still commonly considered to act via cell-intrinsic mechanisms to exert inhibitory function. For example, cross-linking of CTLA4 by clinical anti-CTLA4 antibodies has been proposed to induce PD-L1 expression in non-small cell lung cancer cells following downstream phosphorylation of MEK and ERK (Zhang et al., 2019).

Overall, how CTLA4 acts in a cell-intrinsic manner to regulate T-cell responses has not been elucidated, despite thorough investigation. Moreover, proposals of intrinsic molecular mechanisms commonly do not consider the nature of CTLA4 as a mainly intracellular, recycling protein. As a receptor with such clear biology, it is likely this contributes to its function.

1.3.3. Transendocytosis; a cell-extrinsic function of CTLA4

Alternatively, evidence that CTLA4 acts in a cell-extrinsic manner to regulate CD28 came from bone marrow chimera mice. Whilst CTLA4-/- mice exhibit a lethal phenotype due to mass lymphoproliferation and multi-organ infiltration, mice that contain a mix of CTLA4 WT and CTLA4-/- cells develop normal immune systems, with no evidence of spontaneous over-activation of the CTLA4-/- cells (Bachmann et al., 2001, 1999). This replicable finding is also demonstrated in adoptive-transfer models, as well as post-infection. For example, following lymphocytic choriomeningitis virus (LCMV) infection in mixed mouse

models, CTLA4-/- cells expand, differentiate, and respond in a manner indistinguishable from WT cells (Corse and Allison, 2012; Homann et al., 2006; Tivol and Gorski, 2002). These findings, alongside multiple other studies demonstrate CTLA4 acts extrinsically to control autoimmunity.

Despite these *in vivo* observations, the molecular mechanism utilised by CTLA4 has not been clear. An review by Walker et al., provided a comprehensive overview of potential cell-extrinsic models (Walker and Sansom, 2011). Initially, CTLA4 was proposed to provide a 'reverse-signal' to DCs. This model is based on the induction of Indoleamine 2,3-dioxygenase (IDO) following ligation of CD80 and CD86, an enzyme which catabolizes Tryptophan, a key amino acid for T cell proliferation (Fallarino et al., 2002; Koorella et al., 2014). This model provides the basis behind ongoing trials for combination therapies which combine CTLA4 and IDO blockade (Brown et al., 2018; Speeckaert et al., 2017). Whilst an interplay between CTLA4 and IDO is evident, the lack of classical signalling motifs in the short cytoplasmic tails of CD80 and CD86 as well as contradictory evidence using CTLA4-Igs suggests this model is not the primary function of CTLA4. Alternatively, the *in vivo* observations which could only be explained by an extrinsic model were suggested to be a result of CTLA4-mediated stimulation of Treg inhibitory cytokine production. Indeed, TGFβ production has been linked to CTLA4-Ig binding to CD80/CD86 on APCs (Deppong et al., 2013). However, a direct link between TGFβ production and CTLA4 ligation has been difficult to discern, with this model relying on a cell-intrinsic signal mediated by CTLA4.

Progress in understanding was made by our group over a decade ago where we showed that CTLA4 can bind and physically remove both CD80 and CD86 from the surface of an APC in a process called transendocytosis,
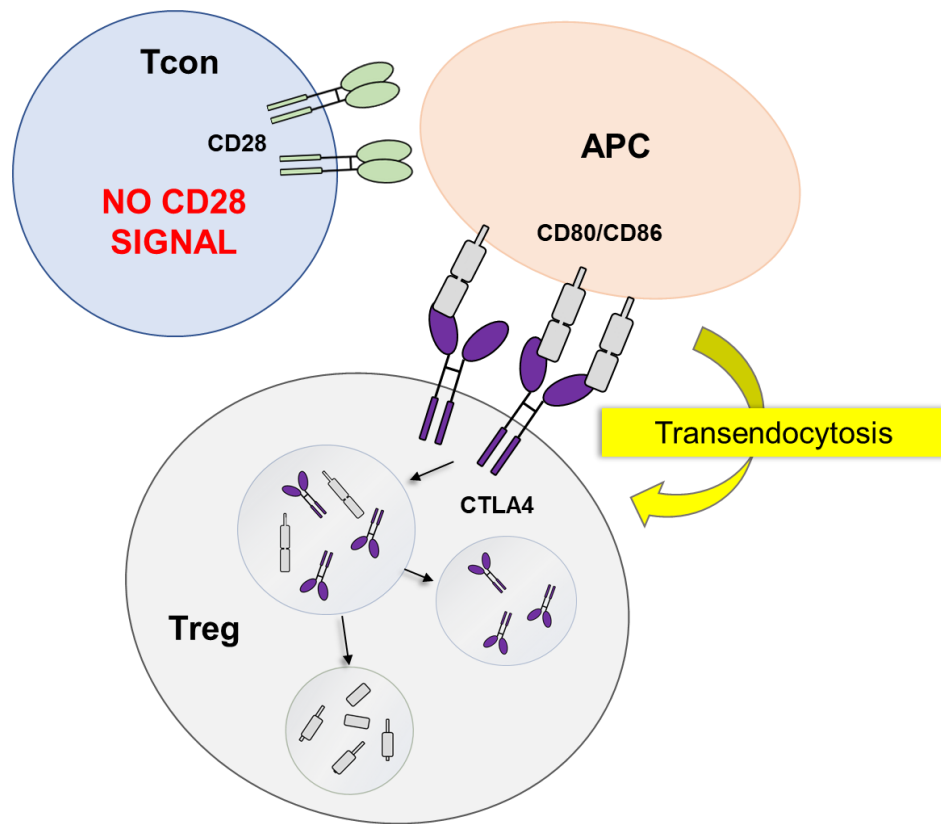
Figure 1.3 Transendocytosis as a cell-extrinsic mechanism of CTLA4 function. CTLA4 binds CD80 and CD86 on the surface of an antigen-presenting cell and internalizes the molecule, destroying captured ligands in lysosomes. This limits the availability of ligand for CD28 mediated co-stimulation (adapted from Walker and Sansom, 2011).

destroying captured ligands in lysosomes. As a result, CTLA4 limits the availability of the ligands required for CD28 co-stimulation (**Figure 1.3**) (Qureshi et al., 2011). This finding explained prior confounding observations such as the ability of Tregs to impair the ability of DCs to co-stimulate *in vitro*, and the ability to down-regulate CD80 and CD86 but leave expression levels of other molecules (e.g. CD40, MHC Class II) unchanged (Cederbom et al., 2000; Misra et al., 2004; Oderup et al., 2006). Moreover, the dynamic intracellular trafficking of CTLA4 as a result of CME and its predominantly intracellular vesicular location support this model (Qureshi et al., 2012a). CTLA4 mediated transendocytosis has since been corroborated by other studies, providing further insight into the mechanism of clinical anti-CTLA4 antibodies as well as being harnessed as a functional readout for patient *CTLA4* mutations (Altman et al., 2019; Westermann-Clark et al., 2022). Further, transendocytosis has been shown to occur most prominently between Tregs and migratory DCs *in vivo*, adding insight into how this process contributes to adaptive immunity (Ovcinnikovs et al., 2019).

Until recently however, there were still fundamental aspects of this system which were not understood. Namely, why does this system require two ligands with such contrasting properties? Work presented in this thesis, and recently published by our group begins to address this question, revealing that transendocytosis of CD80 and CD86 results in markedly different fates for CTLA4. Following transendocytosis of CD80, CTLA4 and CD80 remain bound, undergo post-translational modification in the form of ubiquitination and the high-avidity complex gets trafficked to late endosomes. In contrast, transendocytosis of weaker affinity CD86 permits CTLA4 dissociation and re-entry back into the LRBA-dependent recycling pathway (**Figure 1.4**). In this model, CD80 is therefore proposed to negatively regulate CTLA4, protecting CD86 from

transendocytosis and promoting CD86:CD28 mediated co-stimulation (Kennedy et al., 2022). As a result, this model supports the emerging body of work which places CD86 as the major stimulatory ligand for CD28. Indeed, our we identified mutations of *CTLA4* in patients with autoimmune disease which exhibit a selective loss of CD86 binding (Kennedy et al., 2022).

Despite this advance, a clear understanding of the biophysical properties of receptor-ligand interactions that enable this differential CTLA4 fate is still lacking. Specifically, it is unknown how affinity differences influence these outcomes, or how integral the avidity influence, resulting from the ability of CTLA4:CD80 to form higher-order lattice structures, is for this divergence in fate. Intriguingly, in our recent study, a mutant version of CTLA4, CTLA4 R70Q, exhibited lower affinity binding to CD80 than did CTLA4 WT, but was able to compensate by an increased propensity to dissociate and recycle in a CD86-like manner. Moreover, considering the crosstalk between the CTLA4 and PD1 pathways due to the recently identified *cis* interaction of CD80 and PDL1 proposed to prevent CD80 homo-dimerisation, how valency contributes to this model has implications when understanding this mechanism, and thus designing therapies which target this axis.
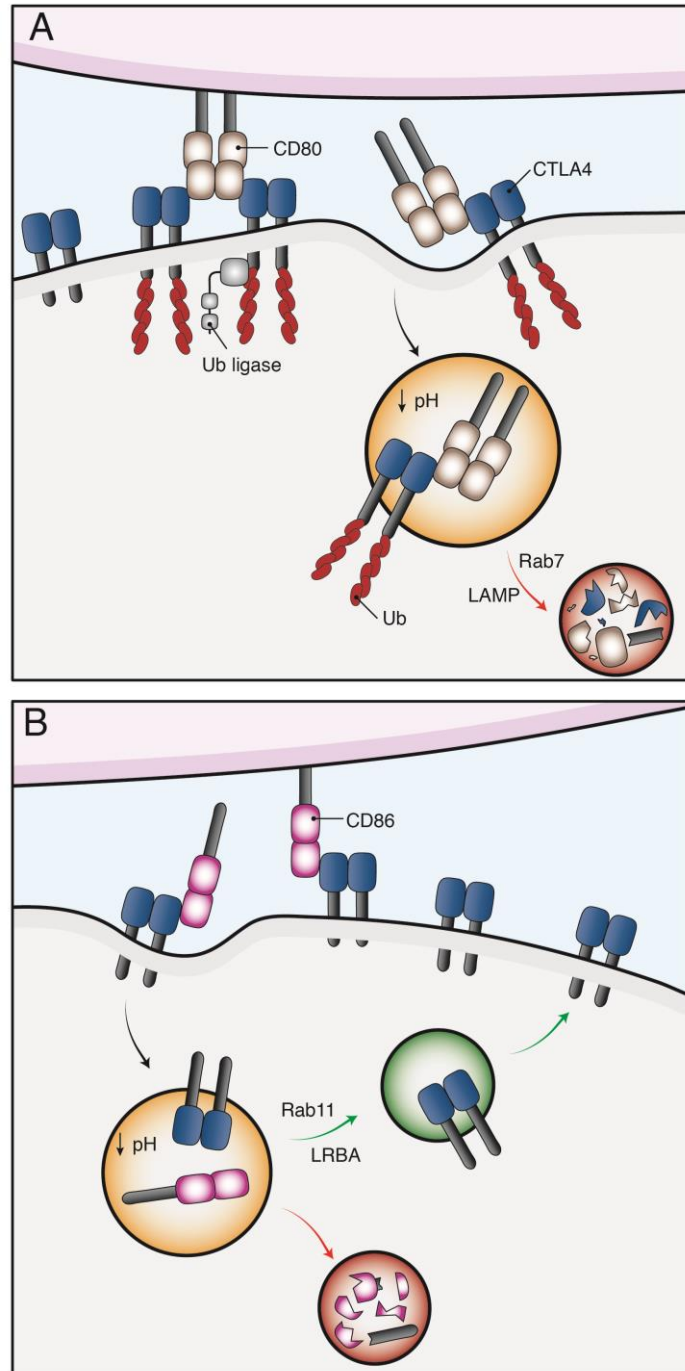
Figure 1.4 Differential fate of CTLA4 following CD80 or CD86 transendocytosis. A. CTLA4:CD80 lattice formation permits high avidity binding, directing CTLA4 ubiquitination, complex survival in low pH compartments and trafficking to late endosomes/lysosomes marked by Rab7 and LAMP3. B. Low affinity CTLA4:CD86 interaction does not cause CTLA4 ubiquitination. Complex dissociation in low pH compartments allows CTLA4 recycling via a LRBA and Rab11 dependent pathway, with CD86 destroyed in lysosomes.

1.4. Project Aims

How the complex relationship of receptor-ligand interactions and higher-order structure formation contributes mechanistically to CTLA4 transendocytosis and CD28 function is unclear. We theorised that disrupting the characteristics of CTLA4/CD28-CD80/CD86 binding will increase our understanding of how they cooperate to influence T cell responses under normal conditions. Therefore, we aimed to remove the avidity influence on receptor-ligand interactions by creating mutants unable to form functional dimers, establishing methods to assess dimerisation such as split-luciferase systems and Bioluminescence Resonance Energy Transfer (BRET). By doing this, we can exploit monomeric receptor-ligand interactions to study the impact of loss of avidity in the context of CTLA4 transendocytosis and CTLA4-regulated CD28 co-stimulatory responses *in vitro*. Moreover, we aimed to use our established methods to investigate the *cis* CD80:PDL1 heterodimer and its influence on the ability of CD80 to homodimerize, as well as prevent CD80:CTLA4 lattice formation. From this, we aimed to explore how PDL1 may regulate CTLA4 by controlling its fate following transendocytosis of CD80.

Finally, qualitative, and quantitative characterisation of CTLA4 transendocytosis allowed identification of several features of CTLA4 biology integral to this mechanism, but an assay using primary Tregs *in vitro* is currently lacking. We therefore aimed to develop a method of Treg isolation and expansion to study the molecular detail of transendocytosis in a physiologically relevant cell type.

1.4.1. Specific project objectives

- Generate mutant versions of CTLA4 and CD80 impaired in dimerization, confirming disruption following optimisation of methodologies such as BRET.

- Use mutant constructs to elucidate how affinity, avidity, and valency contributions within CTLA4-CD80/CD86 interactions collectively influence the differential fate of CTLA4 following transendocytosis.

- Investigate why CD80 exists as a non-covalent dimer.

- Investigate how the *cis* interaction between CD80 and PDL1 influences CTLA4 binding and the outcome of transendocytosis.

- Develop a primary Treg model to study transendocytosis *in vitro* and study our proposed model in a physiologically relevant system.

Chapter 2: Materials and Methods

2.1. Cell Line Culture

Chinese hamster ovary (CHO) cells were cultured in Dulbecco's modified Eagle media (DMEM) (Invitrogen) supplemented with 10% (v/v) fetal calf serum (FCS, Sigma-Aldrich), 2 mM L-glutamine (Sigma-Aldrich) and 1% Penicillin-Streptomycin (Invitrogen), hereon referred to as complete DMEM. Cells were cultured at 37ºC in a humidified 5% CO_2 environment. CHO cells expressing C-terminal green fluorescent protein (GFP) tagged CD80 and CD86, untagged and mCherry tagged PDL1 either alone or in combination, and CTLA4 WT and Kless were kindly provided by Dr. Alan Kennedy. CTLA4 C157A expressing CHO cells, GFP tagged CD80I2R CHO cells, or GFP tagged CD80I2R CHO cells expressing mCherry tagged PDL1 were generated by retroviral transduction. Cells were passaged 2-3 times per week following trypsinization. Purity and expression levels were routinely checked.

Jurkat and DG75 B cells were cultured in Roslin Park Memorial Institute media (RPMI) (Invitrogen) supplemented with 2mM L-glutamine (Sigma-Aldrich). Media was further supplemented with 10% (v/v) FCS (Lab Tech) and 1% Penicillin-Streptomycin (Invitrogen), referred hereafter as complete RPMI. Jurkat and DG75 were cultured at 37ºC in a humidified 5% CO_2 environment in vented tissue cultured flasks. Cells and were passaged 3 times a week by removing 4/5th cell suspension and replacing with fresh RPMI. Jurkat expressed endogenous CD28 and CD3 but were transduced with CTLA4, or CTLA4 Kless. CD80 and CD86 endogenous to DG75 B cells was targeted by CRISPR-Cas9 to generate CD80/CD86 KO DG75 lines by Dr Alan Kennedy. CD80-GFP/ mCherry or CD86-GFP/ mCherry, CD80I2R-GFP/mCherry or PDL1-mCherry were subsequently

transduced to generate tagged ligand expressing DG75 lines. Purity and expression were routinely checked by flow cytometry.

Phoenix cells were grown in Iscove's modified Dulbecco's medium (IMDM) (Thermo Fisher, Loughborough, UK) supplemented with 10% (v/v) FBS, 2mM L glutamine, and 100U/ml penicillin and streptomycin (referred to from now on as complete IMDM) in a humidified 5% CO_2 environment. Cells were passaged 2-3 times a week by trypsinisation to avoid overgrowth.

2.2. Isolation and expansion of primary human cells

2.2.1. Isolation of PBMCs

Leukocyte reduction system (LRS) cones were purchased from NHS Blood and Transport (London, UK). Whole blood from LRS cones was diluted 1:4 with phosphate buffered saline (PBS) and layered onto Ficoll-Paque PLUS (GE healthcare) before being centrifuged for 25 minutes at 1060g with no brake. For fresh blood, blood was diluted 1:1 in PBS, before layering onto Ficoll-Paque PLUS and centrifuged for 10 mins, 1200g with brake '9'. Peripheral blood mononuclear cells (PBMCs) were collected using a Pasteur pipette. Cells were washed with PBS by centrifugation for 10 minutes at 1060g, followed by 5 minutes at 260g. PBMCs were then washed twice in magnetic activated cell sorting (MACS) buffer (2 mM ethylenediamine tetra-acetic acid (EDTA), 0.5% bovine serum albumin (BSA) in PBS) for 5 minutes at 490g. PBMCs were then re-suspended in MACs buffer at 100×10^6 cells/ml.

2.2.2. Isolation of Memory CD4+CD45RO+CD25- T cells

PBMCs were isolated as previously described. Memory CD4+CD45RO+ T cells were isolated by immunomagnetic negative selection by addition of

61

EasySep Human memory CD4+ T Cell enrichment antibody cocktail (targeting non-memory CD4+ T cells) to PBMCs followed by incubation for 10 minutes at room temperature. Cells were then incubated with EasySep D magnetic particles at a volume recommended by the manufacturer for 5 minutes at room temperature. Cell and bead suspensions were placed in EasySep magnets for 2.5 minutes before pouring off the liquid containing purified memory CD4+ T cells into a fresh falcon tube. Isolated cells were centrifuged for 5 minutes at 260g and washed in PBS for 5 minutes at 490g. Purity was confirmed by flow cytometry and was typically above 80%.

2.2.3. Isolation of Tregs

For Treg isolation, CD4+ T cells were enriched by dilution of leukocyte cones 1:2 with phosphate buffered saline (PBS), prior to addition of RosetteSep™ Human CD4+ T Cell Enrichment Cocktail (Stemcell Technologies) for 20 minutes at room temperature, as per manufacturer's instructions. Blood was layered over Ficoll-Paque PLUS (GE Healthcare) and centrifuged at 1200g for 25 minutes with slow acceleration and no brake. The CD4 enriched layer was collected and washed twice in PBS by centrifugation for 10 minutes at 300g with gentle brake, followed by centrifugation for 5 minutes at 490g with brake '9'.

CD4+CD25+ cells were then isolated by immunomagnetic positive selection using human CD25 MicroBeads II (Miltenyi Biotec). 10µl of beads were added per 100 million cells and incubated at 4ºC for 15 min. Cell and bead suspensions were topped up to 50 ml of MACs buffer and centrifuged for 10 minutes at 300g. The supernatant was discarded, and cell pellets were resuspended in 3 ml of MACs buffer. LS columns (Miltenyi) were placed on midi MACS magnets (Miltenyi). LS columns were washed once with MACS buffer

before addition of labelled cells. Unlabelled (CD4+CD25-) cells passed through the column whilst magnetically labelled CD4+CD25+ cells remained in the column due to positive selection. LS columns were washed 3 times and elute collected, before removing from the magnet and collecting CD4+CD25+ Treg cells by addition of 5 ml of MACs buffer and using a plunger.

Enriched CD4+CD25+ cells (and eluted CD4+CD25- cells) were stained using an antibody cocktail (Anti-CD4 (RPA-T4), anti-CD25 (3G10) and anti-CD127 (A019D5)) (see **section 2.6.4** for FACS staining protocol). Fluorescence-activated cell sorting (FACS) on a FACSAria was used to sort CD4+CD25+CD127lo Tregs.

2.2.4. *In vitro* expansion of Human Tregs

For Treg expansion, DG75 B cell lines stably expressing CD80-GFP or CD86-GFP were irradiated at 7500rads. Sorted Treg populations were plated at a 1:1 ratios with irradiated DG75, with 1000ng/mL of anti-human-CD3 (OKT3, Biolegend) and 1000 IU/ml IL2 (PeproTech) in a 96-well round bottom plate.

All Treg lines were maintained in complete OpTimizer Medium, supplemented with OpTimizer T-Cell Expansion Supplement, 10% FBS, 2mM L-Glutamine, 100 U/ml penicillin, and 100 mg/ml streptomycin (all from Life Technologies, Gibco). IL2 was replenished every 2 days, and Treg were restimulated every 7 days.

2.3. Molecular Biology

2.3.1. Generation of CTLA4 and CD80 mutants by site directed mutagenesis

ApE DNA software was used to design non-overlapping primer sets to introduce CTLA4 and CD80 point mutations, using full-length hCTLA4 and hCD80 as templates (table 2.1). Primer sets were used in the Q5 Site-Directed Mutagenesis kit (NEB) using pMP71-CTLA4 or pMP71-CD80-GFP retroviral vectors previously generated in the lab as template DNA. Site-Directed Mutagenesis was performed according to manufacturer's protocol (NEB). Briefly, 25ng of template DNA was mixed with 10µM of Forward primer, 10µM Reverse Primer and Q5 Hot Start High-Fidelity 2X Master Mix, with Nuclease-free water added to a final volume of 25µL in a PCR tube. PCR was performed by pre-denaturation at 98ºC for 30 seconds, followed by 25 cycles at 98ºC for 10 seconds, annealing at 55ºC and extension at 72ºC for 2 minutes, prior to cooling at 4ºC. 1µL of PCR product was then mixed with 2X KLD Reaction Buffer, 10X KLD Enzyme Mix and nuclease-free water to a final volume of 10µL.and incubated for 5 minutes at room temperature, before progressing to bacterial transformation (**See section 2.3.3**). 5-8 bacterial colonies were selected and cultured before plasmid isolation by DNA miniprep (see **section 2.3.4.1**).

Construct	Plasmid DNA	Primers	Product Length
CTLA4 C157A	CTLA4	[F]GAACCGgccCCAGATTCT [R]TGGATCAATTACATAAATC	5264bp
CD80I2R	CD80	I92R and I95R [F]ACAAGAACCGGACCcgcTTTGATcgcACTAATAACC	6325bp

Table 2. 1. Forward and reverse primer sequences used for site-directed-mutagenesis. [F], Forward; [R], Reverse; bp, base pair.

Plasmids were then sequenced to screen for DNA with the mutation successfully incorporated.

2.3.2. Generation of NanoBiT and NanoBRET constructs using the FlexiVector System

1.3.2.1. Generation of pF4A FlexiVectors

NanoBiT and NanoBRET constucts were generated by first cloning into pF4A CMV Flexi Vector (**Figure 2.1**). As multiple tags for multiple protein coding regions were required, use of the Flexi Vector System reduced cloning burden by allowing transfer of protein-coding regions between vectors based on antibiotic resistance genes. A technical manual giving a detailed explanation of the Flexi Vector system is available (FlexiVector Systems, Promega 2021).
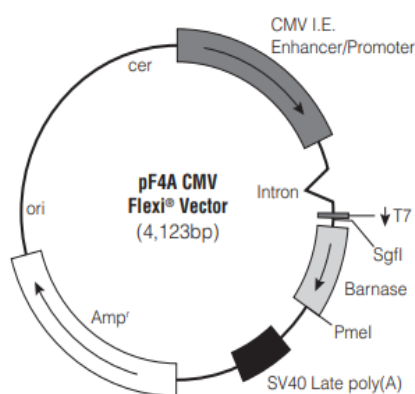
Figure 2. 1. pF4A CMV Flexi® Vector map and sequence reference points

First, ApE software was used to design primer sets to amplify desired protein-coding regions, incorporating a SgfI site in the amino-terminal PCR primer, and a PmeI site in the carboxy-terminal PCR primer (**Table 2.2**). The protein-coding regions were subsequently amplified by PCR. Following PCR

amplification, PCR products were purified using the Wizard SV Gel and PCR Clean-Up System (Promega), as per manufacturer's instructions.

Subsequently, restriction digest was performed to generate sticky ends required for cloning for both the amplified PCR product and the pF4A CMV Acceptor Flexi Vector. For this, 500ng of PCR product was incubated with 4µL of 5X Flexi Digest Buffer and 4µL Flexi Enzyme blend, with Nuclease-Free Water up to a final volume of 20µL. The Acceptor FlexiVector possesses the SgfI and PmeI restriction sites flanking a lethal barnase gene, allowing high-efficiency transfer as clones still containing this gene will not survive. For digestion of the Acceptor Vector, 2µL of vector was mixed with 4µL of 5X Flexi Digest Buffer, 2µL of Flexi Enzyme blend (SgfI and PmeI) and 12µL of Nuclease-Free Water. Both reactions were then incubated at 37ºC for 30 minutes, before incubating at 65ºC for 20 minutes to inactivate the restriction enzymes. Reactions were then stored on ice, before being purified using the Wizard SV Gel and PCR Clean-Up System (Promega), as per manufacturer's instructions.

Following digestion, the cut PCR product and Acceptor Flexi Vector were ligated, by mixing 5µL of digested Acceptor FlexiVector, 200ng of PCR product and 1µL of T4 DNA Ligase (20u/µL) with Nuclease-Free Water up to a final volume of 20µL. Ligation mixtures were then incubated for 1 hour at room temperature before continuing with transformation (see **section 2.3.3**). 5 bacterial colonies were selected and cultured before plasmid isolation by DNA miniprep. Colonies were screened by restriction digest using SgfI and PmeI.

Protein Coding Region	Template DNA	Primers	Product Length
CD80	pMP71-EGFPCD80	[F]CGCG==GCGATCGC==CATGGGCCACACACGGAGGCA	888bp
CD80I2R	pMP71-EGFPCD80I2R	[R]GGGG==GTTTAAAC==TACAGGGCGTACACTTTCCCTTCTCAATCT	888bp
CD86	pMP71-EGFPCD86	[F]AGGA==GCGATCGC==CATGGATCCCCAGTGCACTAT [R]TTGT==GTTTAAAC==AAAACATGTATCACTTTTGTCGC	1012bp

Table 2. 2. Forward and reverse primer sequences used to incorporate Sgf1 (highlighted blue) and PmeI (highlighted green) restrictions sites. CD80 and CD80I2R used the same primer pair. [F], Forward; [R], Reverse; bp, base pair.

2.3.2.2. Transfer of Protein-Coding Regions between FlexiVectors

pF4A FlexiVectors expressing CD80, CD86 or PDL1, generated as described (**See section 2.3.2.1**), were then used to transfer protein-coding regions into FlexiVectors containing C-terminal-tags (e.g. NanoLuc). Transfer was based on antibiotic selection, as the pF4A vector is Ampicillin-resistant, whereas acceptor FlexiVectors are Kanamycin-resistant. Note that Ampicillin-resistant vectors will have names ending in "A", and Kanamycin-resistant with "K".

The FlexiVectors used as Acceptors for NanoBiT applications were the pFC34K LgBiT TK-Neo FlexiVector and the pFC36K SmBiT TK-Neo Flexi® Vector (**Figure 2.2**). For NanoBRET applications, the pFC32K Nluc CMV-neo Flexi® Vector and the pFC14K HaloTag CMV Vector (**Figure 2.3**) were used. These vectors contain a lethal gene (barnase) flanked by SgfI and EcoICRI restriction enzyme sites, which must be replaced for a bacterial clone for survival.

For transfer, donor pF4A FlexiVectors were digested by assembling 2µL of 5X Flexi Digest Buffer, 100ng of Donor Flexi Vector, 1µL of Flexi Enzyme Blend (SgfI & PmeI) with Nuclease-Free Water up to a final volume of 10µL. In a separate tube, acceptor C-terminal FlexiVectors were digested by assembling 2µL of 5X Flexi Digest Buffer, 100ng (1µL) of Donor Flexi Vector, 1µL of Carboxy Flexi Enzyme Blend (SgfI & EcoICRI). Both reactions were then incubated at 37ºC for 30 minutes, before incubating at 65ºC for 20 minutes to inactive the restriction enzymes. Following digestion, the Donor and Acceptor Flexi Vector were ligated, by mixing 10µL of 2X Flexi Ligase Buffer, 5µL (~50ng) of digested donor FlexiVector, 5µL (~50ng) of digested acceptor FlexiVector and 1µL T4 DNA Ligase (HC) prior to incubation at room temperature for 1 hour before continuing

with transformation (see **section 2.3.3**) Importantly, transformed bacteria was spread onto Kanamycin-resistant agar plates and grown overnight, to permit growth of only vectors containing protein-coding regions with C-terminal tags (**Figure 2.2 and 2.3**). <8 bacterial colonies were selected and cultured before plasmid isolation by DNA miniprep (**see section 2.3.4.1**). Colonies were screened by restriction digest using SgfI and EcoICRI.
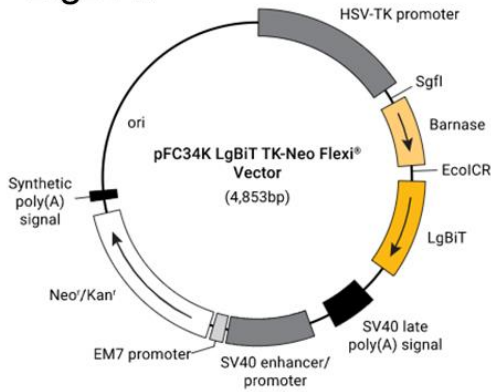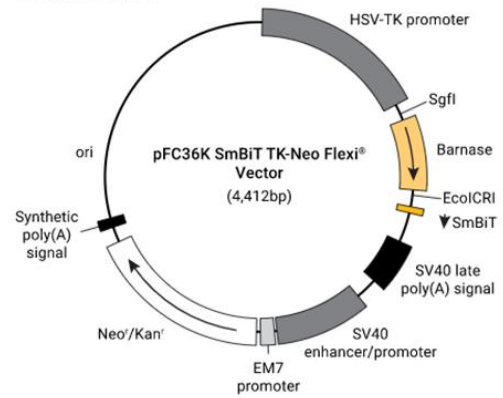
Figure 2. 3. NanoBiT Vector circle maps and sequence reference points
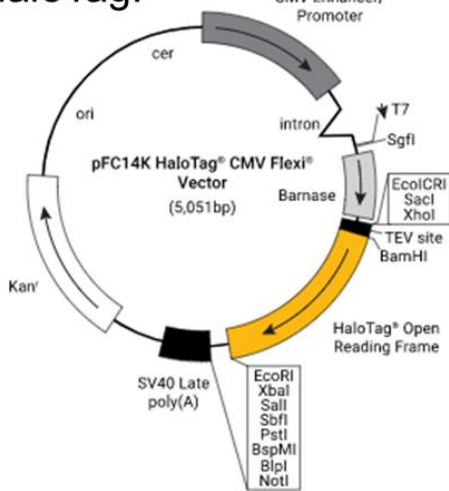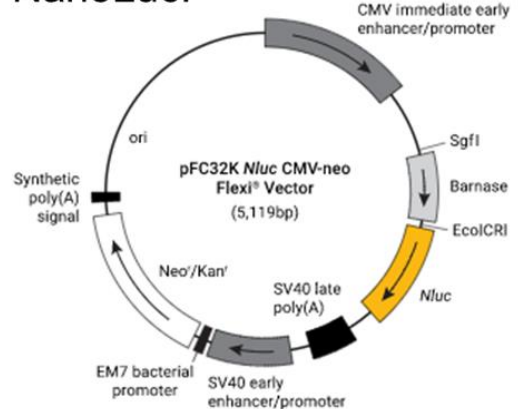
Figure 2. 2. NanoBRET Vector circle maps and sequence reference points

2.3.3. Bacterial Transformation

For bacterial transformation, 1 vial of NEB 5-alpha Competent *E. coli* cells per transformation was thawed on ice for 10 minutes. 1-5µL (containing ~100 ng) of plasmid DNA was added to 50µL of cells in an Eppendorf before gentle mixing, and incubation on ice for 30 minutes. Bacteria was heat-shocked by placing the Eppendorf in a heat-block at 42ºC for exactly 30 seconds, before being moved to ice for 5 minutes. 950µL of Super Optimal broth with Catabolite repression (SOC) media was added, before cells were shaken vigorously (>250rpm) for 1 hour at 37ºC. 50-100µL of bacteria was spread onto 10cm plates containing 20ml of Luria-Bertani (LB) agar supplemented with 100µg /ml ampicillin or 25µg /ml kanamycin (dependant on vector transformed), and incubated overnight at 37ºC.

2.3.4. Plasmid Preparations

2.3.4.1. Mini Plasmid Preparations

Individual colonies from **section 1.3** were picked and grown overnight in 5ml of antibiotic containing LB broth, by incubation for 8-12 hours at 37ºC in a shaking incubator (>250rpm). Plasmid DNA extraction was then performed using the QIAGEN plasmid mini kit, as per manufacturer's instructions. Briefly, 1ml of culture was pelleted, resuspended in 250µL of Buffer P1 and transferred to a microcentrifuge tube. 250µL of Buffer P2 was added for cell lysis before addition of 350µL of Buffer N3. Reactions were centrifuged for 10 minutes at 1600rpm, and the supernatant was added to a QIAprep spin column attached to a collection tube. The spin column containing bound DNA was washed once with 750µL of ethanol containing wash buffer PE by centrifugation at maximum speed for 30-60 seconds. This step was repeated with no wash buffer to remove residual ethanol.

The column was then transferred to a fresh Eppendorf, and DNA was eluted by addition of 50µL of elution buffer EB and centrifugation at maximum speed for 30-60 seconds. Plasmid DNA was stored at 4ºC until required. Remaining cultures were stored at 4ºC for large-scale preparations of DNA if required.

2.3.4.1. Maxi Plasmid Preparations

For large-scale plasmid preparations, 100µL of small-scale cultures were added to 200 mL of antibiotic containing LB broth in a conical flask and grown by incubation for 8-12 hours at 37ºC in a shaking incubator (>250rpm). Plasmid DNA extraction was then performed using the QIAGEN plasmid maxi kit, as per manufacturer's instructions. Briefly, 200ml of culture was pelleted by centrifugation for 15 minutes at 6000 x g at 4ºC. Pellets were resuspended in 10ml of Buffer P1, before addition of Buffer P2 (for lysis) and incubation at room temperature for 5 minutes. 10ml of neutralisation Buffer P3 was added, prior to incubation for 10 minutes at room temperature.

2.3.5. Cell Line Engineering

For generation of stable cell lines, 1×10^6 Phoenix-Amphoteric packaging cells were plated in T25 flasks in 5mL of complete IMDM and incubated overnight at 37ºC with 5% CO_2. For viral transfection, 3.5µg of wild-type or mutant receptor and GFP-tagged ligand MP71 retroviral vectors were diluted in 100µL of Opti-MEM alongside 1.5ug VSVg. Diluted DNA was mixed with 100µL of Opti-MEM containing FuGENE HD transfection reagent (Promega) and left at room temperature for 20 minutes, before dripping onto Phoenix-Amphoteric packaging cells. Cells were then incubated for 48 hours, with the media replaced after 12 hours. For transduction, 0.5×10^6 cells were plated per well of a retronectin coated

24-well plate, with 1ml of retroviral supernatant from transfected cells and 2ug of polybrene. Cells were spinoculated for 90 minutes at 2000rpm at 32ºC with no centrifugal brake. Cells were analysed by flow cytometry for transduction efficiency ~72 hours later.

2.4. NanoLuc® Binary Technology (NanoBiT) assays

For NanoBiT assays, 4×10^4 CHO cells were plated per well of a white 96-well tissue culture plate in a volume of 100µL of Opti-MEM without Phenol red and FCS and incubated for 6 hours to allow cell attachment. Lrg-BiT and Sml-BiT tagged vectors were diluted in Opti-MEM to 6.25ng/µL, before addition of a 3:1 ratio of FuGENE HD transfection reagent. DNA-lipid mixtures were incubated at room temperature for 15 minutes, before 8µL of transfection mixes are added to relevant wells, for a total of 50ng/well. Plates were incubated at 37ºC, 5% CO_2, for 24 hours. Following incubation, medium was exchanged for 100µL of fresh Opti-MEM with no Phenol red and 4% FCS.

For luminescence readout, Nano-Glo Live Cell Substrate (containing Fumarizine) was diluted 1:20 with Nano-Glo LCS Dilution Buffer and kept at 4ºC. 25µL of Nano-Glo substrate was added to each well, and the plate was mixed by gentle orbital shaking (15s at 300-500rpm). Wells were allowed to equilibrate by incubation at 37ºC for 20 minutes, prior to luminescence measurement. For experiments where CTLA4-Ig was added, 25µL of Opti-MEM containing 50µg/ml CTLA4-Ig was added to each well (10µg/ml final). Luminescence was read on a BioTek Synergy H1 plate reader either at a defined end-point, or once every minute for kinetic traces.

2.5. NanoLuc® Bioluminescence Resonance Energy Transfer (NanoBRET) assays

For end-point NanoBRET read-out assays, 0.8×10^6 CHO cells were plated per well of 6-well tissue culture plate in a volume of 2mL of Opti-MEM with no Phenol red and 5% FCS, and incubated at 37°C, 5% CO_2 for 6 hours to allow cell attachment. 2µg of HaloTag Plasmid was mixed with 0.2µg of NanoLuc plasmid diluted in 100µl of Opi-MEM, per well for each combination being tested. 6µl of FuGENE® HD Transfection Reagent was added to each DNA mixture, and DNA-lipid mixtures were incubated at room temperature for 15 minutes. Mixtures were then added to each well of cells and left to express for 20 hours.

For the donor saturation assay, 0.4×10^6 CHO cells were plated per well of a 12-well tissue culture plate in a volume of 1mL of Opti-MEM with no Phenol red and 5% FCS, and incubated at 37°C, 5% CO_2 for 6 hours to allow cell attachment. HaloTag acceptor DNA was diluted by performing a 1:3 serial dilution, creating concentration ranges from 1,000-0.46ng/µL (8 dilutions). 10ng of NanoLuc plasmid DNA was added to each dilution and made up to 46µl by addition of Opti-MEM with no FCS. 4µl of FuGENE® HD Transfection Reagent was added to each DNA mixture, and DNA-lipid mixtures were incubated at room temperature for 15 minutes. Mixtures were then added to each well of cells and left to express for 20 hours.

For the type-1 BRET assay (Felce et al., 2012), 0.4×10^6 CHO cells were plated per well of a 12-well tissue culture plate in a volume of 1mL of Opti-MEM with no Phenol red and 5% FCS, and incubated at 37°C, 5% CO_2 for 6 hours to allow cell attachment. HaloTag acceptor and NanoLuc DNA was diluted by performing a 1:3 serial dilution, creating concentration ranges from 1,000-

0.46ng/μL (8 dilutions). HaloTag and NanoLuc DNAs were combined to create acceptor-to-donor ratios of 100-0.046 with a total of 1,000ng of DNA in each condition. 4μl of FuGENE® HD Transfection Reagent was added to each DNA mixture, and DNA-lipid mixtures were incubated at room temperature for 15 minutes. Mixtures were then added to each well of cells and left to express for 20 hours.

Following the 20-hour incubation, medium was removed from the transfected CHO cell monolayers. Cells were washed once in PBS, before addition of 0.5ml of 0.05% trypsin-EDTA for 5 minutes at room temperature until cells easily lifted from the plate. 2ml of Opti-MEM containing 5% FBS was added to each well, before cells were removed and added to 15 ml falcon tubes. Cells were then counted and resuspended at 2×10^5 cells/ml. Cells were then divided into 2 pools. To one pool, 1μl/ml of HaloTag NanoBRET 618 Ligand was added. No ligand was added to the other pool. Where CTLA4-Ig was used, it was added to a final concentration of 10μg/ml. 100μl of cells with or without ligand were added per well of a white 96-well tissue culture plate and incubated overnight at 37ºC with 5% CO_2.

The following day, a 5X solution of NanoBRET Nano-Glo Substrate was made by performing a 1:100 dilution in Opti-MEM Reduced Serum Medium, with no phenol red. For NanoBRET Measurement, 25μL of diluted reagent was added per well of a 96-well plate containing cells in 100uL and mixed by gentle orbital shaking (15s at 300-500rpm). Donor emission (460nm) and acceptor emission (618nm) was read within 10 minutes of substrate addition on a BioTek Synergy H1 plate reader with custom NanoBRET filter cubes.

2.6. Flow Cytometry

Flow cytometry was carried out using a BD™ Fortessa flow cytometer (BD Biosciences) and acquired using BD FACSDiva™ software. Analysis was performed using FlowJo (TreeStar). All Flow cytometry assay data are from at least 3 independent experiments unless otherwise stated. All antibodies are listed in **Table 2.3**.

2.6.1. CTLA4 Recycling Assay

0.2×10^6 cells CHO CTLA4 WT or C157A per condition were added to FACs tubes containing 20ug/ml α-CTLA-4 monoclonal antibody (Tremelimumab) in complete DMEM for 60 minutes at 37°C, to label the pool of cycling CTLA4. Tubes were then washed twice in PBS and transferred to ice. A 1:1000 dilution of α-huFc-AF647 conjugated antibody in complete DMEM, or DMEM containing 20mM ammonium chloride was added for 10 minutes. Tubes were then transferred to 37°C for 0-60 minutes to resume CTLA4 trafficking before being returned to ice. All samples were fixed in 4% PFA for 15 minutes, then washed twice prior to resuspension in 200µL PBS for FACs analysis.

2.6.2. Ligand-IgG Binding Assays

To determine ligand binding, 0.2×10^6 cells CHO CTLA4 WT or C157A per condition underwent two differing staining procedures. Cells were either fixed in 4% paraformaldehyde in PBS and permeabilized in 0.1% saponin prior to staining with 1µg/ml CD80-Ig (R&D Systems), CD86-Ig (R&D Systems) or an Ig-IgG control at 4°C for 45 minutes. Alternatively, cells were incubated with 1µg/ml CD80-Ig (R&D Systems), CD86-Ig (R&D Systems) or an Ig-IgG control at 37°C for 90 minutes in the presence or absence of 20mM ammonium chloride prior to

fixation and permeabilization, allowing measurement of ligand uptake. Following both protocols of ligand-IgG binding, cells were washed twice in PBS then stained with a rabbit α-huFc-PE conjugated antibody and directly conjugated C-terminal α-CTLA4 antibody (C19-AF647) to normalize to total CTLA4 expression.

2.6.3. Transendocytosis Assays

For transendocytosis assays by flow cytometry, CHO or DG-75 cells expressing tagged ligand constructs were labelled with $1\mu g/ml$ CellTrace Violet labelling kit (ThermoFisher Scientific). CTV+ 'donor' cells were then incubated with wild-type or mutant 'ripper' CTLA4 expressing cells, or CHO or Jurkat cells with no ligand or receptor, in round bottom 96-well plates at 37°C for 0-6 hours. Each well contained a total of 0.2×10^6 cells permitting the ratio of donor: ripper cells to be dictated, with ratio used stated. Ammonium Chloride was added in complete DMEM as appropriate at 20mM final concentration. Bafilomycin A was added in complete RPMI as appropriate at 50nM final concentration. Cells were then transferred to FACs tubes and placed on ice prior to immediately running on the flow cytometer.

2.6.4. Flow Cytometry staining

2.6.4.1. Surface Staining

For surface staining, cells were washed in PBS by centrifugation at 4°C at 490 x g twice. Cell pellets were resuspended in appropriate volume of antibody containing FACS buffer (2% fetal calf serum in PBS). For primary cells, antibody master-mixes were made with Brilliant Stain Buffer (BD Biosciences). Cell-antibody mixtures were incubated at 4°C for 30 minutes. Cells were then washed twice and resuspended in 200 μl of PBS.

2.6.4.2. Intracellular Staining

For intracellular staining, surface staining was performed as above. Then, cells were centrifuged at 4°C at 490 x g and pellets were resuspended in 4% paraformaldehyde in PBS for 10 mins on ice. Cells were then washed twice by centrifugation and resuspended in perm buffer (PBS containing 0.1% saponin and 2% BSA) at room temperature for 10 minutes. Cells were then centrifuged at 4°C at 490 x g, and pellets were resuspended in an appropriate volume of perm buffer containing appropriate antibodies for 1 hour at 4°C. For Tregs, cells were stained as outlined in **section 2.2.3**. Cells were washed once in perm buffer, then once in PBS at 4°C at 490 g. For all cell types, cells were resuspended in 200μL for acquisition.

Flow Cytometry				
Target antigen	Flourophore	Clone	Dilution	Supplier
Cell trace violet			1 in 1000	Thermo Fisher
Near infrared viability dye			2 in 1000	Thermo Fisher
CD4	AF700	RPA-T4	1 in 100	BD Biosciences
CTLA4	PE	BNI3	1 in 100	BD Biosciences
	BV786	BNI3	3 in 100	BD Biosciences
	AF647	F8	1 in 100	BD Biosciences
	PE	F8	1 in 100	Santa Cruz
ICOS	BUV395	DX29	3 in 100	BD Biosciences
Fox P3	PE-Cy7	236A/E7	3 in 100	Invitrogen
CD127	BV421	HIL-7R-M21	2 in 100	BD Biosciences
CD25	BV605	BC96	3 in 100	BD Biosciences
Ki67	FITC	2A3	3 in 100	BD Biosciences
PD1	PE-Cy7	EH12.1	1 in 100	BD Biosciences
CD80	AF700	16-10A1	1 in 100	Invitrogen
	PE	L307	2 in 100	BD Biosciences
GFP	APC	1A12-6-18	1 in 100	BD Biosciences
CD86	BV510	FUN-1	3 in 100	BD Biosciences
a-human-Fc	AF488	M1310G05		Biolegend
Western Blot / Confocal Microscopy				
Target antigen		Clone	Dilution	Supplier
CTLA4		C19	1 in 1000	Thermofisher - discontinued
		EPR1972	1 in 1000	Abcam
GFP		4B10	1 in 1000:WI	Cell Signaling
Ubiquitin		PD41	1 in 1000	Cell Signaling
Tubulin		DM1A	1 in 1000	Cell Signaling
a-goat-HRP		-	1 in 1000	Cell Signaling
a-mouse-HRP		-	1 in 1000	Cell Signaling
a-rabbit-HRP		-	1 in 1000	Cell Signaling

Table 2. 3. List of Antibodies and reagents used for flow cytometry.

Antibody names, clones, suppliers, and dilutions are shown. All flow cytometry and primary western antibodies react to human antigens.

2.7. Confocal Microscopy

2.7.1. Transendocytosis assays

For transendocytosis assays via confocal microscopy, CHO cells expressing WT or mutant CTLA-4 were plated onto 13mm diameter glass coverslips with CHO cells expressing GFP tagged ligand at a 1:1 ratio for a total of 0.2×10^6 cells per condition and left for 18 hrs to permit adhesion and TE. Cells were then washed twice in PBS and then fixed and permeabilised in methanol for 10 minutes at -20°C. Cells were then stained with 1:500 unconjugated goat α-human CTLA4 (C-19) antibody for one hour with gentle rocking, before staining with 1:250 donkey α-goat-Fc-AlexaFluor546 secondary antibody for one hour in the dark at room temperature. Coverslips were washed twice in PBS, before mounting onto glass confocal slides using DAPI containing mounting medium, to provide a nuclear stain. Images were acquired on confocal settings using an inverted Nikon Eclipse Ti-E equipped with a 60X oil immersion objective.

All images were processed using Fiji image processing software. For quantification, pipelines were created using CellProfiler software, with at least 5 images run through the pipeline per condition for each experiment.

2.7.2. Proximity Ligation Assays

Proximity ligation assays use DNA linked antibodies to allow an amplification reaction between two antibodies which are in proximity of < 40nm (Alum, 2018). CHO cells were set up for transendocytosis via confocal microscopy as described previously but underwent a different staining procedure using the Duolink® PLA reagents supplied in the *In Situ* Red Starter Kit for Mouse/Goat antibodies, according to the manufacturer's protocol (Promega). In

brief, cells were fixed and permeabilised in methanol for 10 minutes at -20°C and washed in PBS three times and blocked in blocking buffer at room temperature for 1 hour. Cells were stained with primary antibodies against CTLA-4 (C-19, Santa Cruz) and mouse monoclonal α-GFP (clones 7.1 and 13.1, Sigma-Aldrich) diluted in Duolink® antibody diluent at a 1:500. Coverslips were washed and incubated with PLA PLUS and MINUS probes against mouse and goat antibodies, respectively for 1 hour at 37°C. The oligonucleotides conjugated within the probes were ligated for 30 minutes at 37°C using Duolink® ligase and amplified for 100 minutes at 37°C with Duolink® polymerase, which encodes a red fluorophore permitting visualisation of the PLA signal. The PLA signal should be limited to where the primary antibodies are within 40nm proximity. Coverslips were washed twice in Duolink® wash buffer B prior to mounting onto slides using Duolink® In Situ Mounting Media with DAPI and left for at least 15 minutes prior to analysis by confocal microscopy.

2.8. Western Blotting and Immunoprecipitation

For all western blot and immunoprecipitation experiments, whole cell lysates (WCL) were prepared by resuspending cells in lysis buffer (20mM Tris-HCl, 1% Triton-X, 0.5% CHAPs, 150mM NaCl and 2mM EDTA) and incubating on ice for 20 minutes with regular vortexing. All proteins were separated by SDS-page, electrophoretically transferred onto polyvinylidene difluoride (PVDF) membranes for blot of CTLA4, GFP, tubulin and mCherry, or nitrocellulose for blot of ubiquitin. Membranes were then blocked for >1 hour in tris-buffered saline + 1% Tween-20 (TBST) containing 5% milk, before primary antibody incubation overnight at 4°C. Following primary antibody incubation, membranes were washed 3 times for 10 minutes in TBST with gentle agitation. Membranes were

then incubated with HRP-conjugated secondary antibodies for 1 hour at room temperature. Secondary antibodies were removed by repeating 3x 10 minutes wash steps. All primary and secondary antibodies were used at a 1:1000 dilution. For visualization, membranes were incubated with Clarity western ECL HRP-substrate (Bio-Rad) and visualised on the ChemiDoc Touch system (Biorad).

For dimerisation analysis, $2x10^6$ CHO cells expressing CTLA4 WT or CTLA4 C157A were lysed and denatured at 100°C for 10 mins in NuPAGE LDS sample buffer (Invitrogen) in the presence or absence of 1mM Dithiothreitol (DTT) to reduce disulphide bonds. Denatured WCL underwent SDS-page and transfer to polyvinylidene difluoride (PVDF) membranes, before staining membranes with rabbit N-terminal α-CTLA4 antibody (EPR1476) (Abcam) and anti-rabbit IgG HRP-linked (cell signalling) secondary antibody.

For immunoprecipitation assays, $4x10^6$ CHO cells expressing receptors and $4x10^6$ CHO cells ligands from indicated conditions were mixed in universals and incubated for 5 hours at 37°C, permitting transendocytosis. Cells were lysed in lysis buffer with an additional 100µM of deubiquitinase inhibitors Iodoacetamine and 50µM N-ethylmaleimide, to prevent de-ubiquitination. This gave >1mg of protein per condition. GFP-Trap (Chromotek) or Ubiquitin-Trap beads (Cytoskeleton) were washed 5 times for 1 minute with lysis buffer. 0.5-1mg of protein were incubated with 20µL of bead slurry per condition for >2 hours at 4°C with gentle rotation. For GFP-trap, beads were then washed again and resuspended in NuPAGE LDS sample buffer (ThermoFisher) plus NuPAGE sample reducing agent (ThermoFisher) for 10 minutes at 100°C, before being spun at 17,000 x g for 1 minute at 4°C. For Ubiquitin-Trap, beads were resuspended in just NuPAGE LDS sample buffer before spinning. Supernatants

were collected and run via SDS-page. Membranes were stained with goat C-terminal α-CTLA4 antibody (C19), mouse pan α-ubiquitin antibody (P4D1, Santa Cruz), mouse α-GFP antibody (clones 7.1 and 13.1, Sigma-Aldrich) or mouse α-alpha tubulin (DM132).

2.9. Statistical Analysis

Statistical analysis was performed using GraphPad prism (GraphPad Software, Inc., CA, USA). P values <0.05 were considered significant.

Chapter 3: Developing cell line model systems to study dimerisation in the CTLA4:CD28 system

3.1. Introduction

Despite directly opposing functions, CD28 and CTLA4 share two ligands, CD80 and CD86. The differential function of these ligands remains elusive, although expression patterns and biophysical characteristics suggest implicit differences (Sansom et al., 2003). For example, CD80 binds both CTLA4 and CD28 with higher affinity (0.2μM and 4μM, respectively) than CD86 (2μM and 20μM, respectively) (Collins et al., 2002). Accordingly, there is a hierarchy of interactions that can occur when a T Cell engages a cell expressing CD80 and CD86.

Affinity differences suggest that CTLA4 regulates CD28 co-stimulation by out-competing for ligand binding. However, structural influences add complexity to these interactions. CTLA4 is a constitutive dimer, able to bind bivalently to CD80 and CD86. Under physiological conditions, CD80 is able to form a non-covalent dimer in the membrane unlike CD86, which only exists as a monomer (Bhatia et al., 2005; Collins et al., 2002; Girard et al., 2014). Crystallisation studies support that CTLA4 and CD80 are therefore able to form higher-order lattice or 'zipper' structures, providing an avidity advantage for CD80 over CD86 (Stamper et al., 2001, Schwartz et al., 2001). Considering valency, avidity and affinity together supports the possibility of multiple different outcomes resulting from ligand-receptor interactions.

Recently, a further interaction between CD80 and PDL-1, a ligand for inhibitory checkpoint PD-1, has been identified (Chaudhri et al., 2018).

Interestingly, this interaction appears to occur at the CD80 dimer interface and therefore disrupts CD80 homo-dimer formation (Sansom and Walker, 2019). The impact of this *cis-* interaction on the ability of these ligands to interact with their receptors is yet to be fully understood.

In this Chapter, we aimed to remove the avidity influence on receptor-ligand interactions by creating mutants unable to form functional dimers. Moreover, we sought to establish methods to assess protein-protein interaction at a cell membrane such as NanoLuc Binary Technology (NanoBiT) and Nano Bioluminescence Resonance Energy Transfer (NanoBRET), to confirm dimerisation status and valency properties of our mutants.

Using of these assays we confirmed disruption of CTLA4 dimerisation by a C157A mutation, and CD80 dimerisation by two isoleucine mutations, as well as by co-expression of PDL1. We then tested monovalent receptor-ligand interactions resulting from our mutants to study the impact of loss of avidity in the context of CTLA4 transendocytosis and CTLA4 regulated CD28 co-stimulatory responses *in vitro*.

3.2. Results

3.2.1. Mutation of cysteine 157 disrupts CTLA4 dimerization

Sequence and biochemical analysis of the CTLA4 ectodomain confirm CTLA4 is a disulphide linked homodimer through a cysteine residue at position C157 (Linsley et al., 1995). To study the impact of this bivalent homodimer, we used site-directed mutagenesis to introduce a single cysteine to alanine mutation at position 157 (CTLA4 C157A), hypothesizing mutation of this residue will prevent dimerisation, as shown schematically in **Figure 3.1A.** A cysteine to alanine mutation is commonly used to disrupt intermolecular disulfide bonds as it is thought to be less destabilizing due to lack of potential to introduce extra side-chain intramolecular effects (Chakrabarti and Pal, 2001). We then used resultant constructs to generate stably transduced CTLA4 wild-type (WT) and CTLA4 C157A expressing CHO and Jurkat cell lines, having previously established them as suitable models for studying CTLA4 biology (Qureshi et al., 2011).

To confirm this mutation prevented CTLA4 dimerisation, we performed Western blot analysis under reducing (+DTT) and non-reducing (-DTT) conditions of Jurkat CTLA4 WT or C157A expressing lines (**Figure 3.1B**). We observed that in non-reducing conditions CTLA4 WT had a band at ~50kDa, representative of a dimeric form of CTLA4, which was reduced to ~25kDa in the presence of DTT. CTLA4 C157A did not show a band at 50kDa and instead ran at 25kDa even in non-reducing conditions, suggesting mutation of C157 alone prevented CTLA4 dimerisation. This is unlike previously reported data, where it was suggested that asparagine residues at positions N113 and N145 could stabilize CTLA4 dimers in the absence of an intermolecular disulphide bond (Darlington et al., 2005).

We also observed that under reducing conditions, whilst CTLA4 WT ran as one band at 25kDa, CTLA4 C157 ran as two bands around the 25kDa mark, indicative of altered post-translational modification. We hypothesized that since CTLA4 is a heavily glycosylated protein, monomeric CTLA4 may have additional exposed sites able to undergo glycosylation. To test this, we performed analysis by western blotting following treatment with or without PNGase F, which removes N-linked oligosaccharides from proteins. As shown in **Figure 3.1C,** treatment with PNGase F revealed the same double bands for both CTLA4 WT and CTLA4 C157A, indicating that the additional C157 forms were due to altered glycosylation.
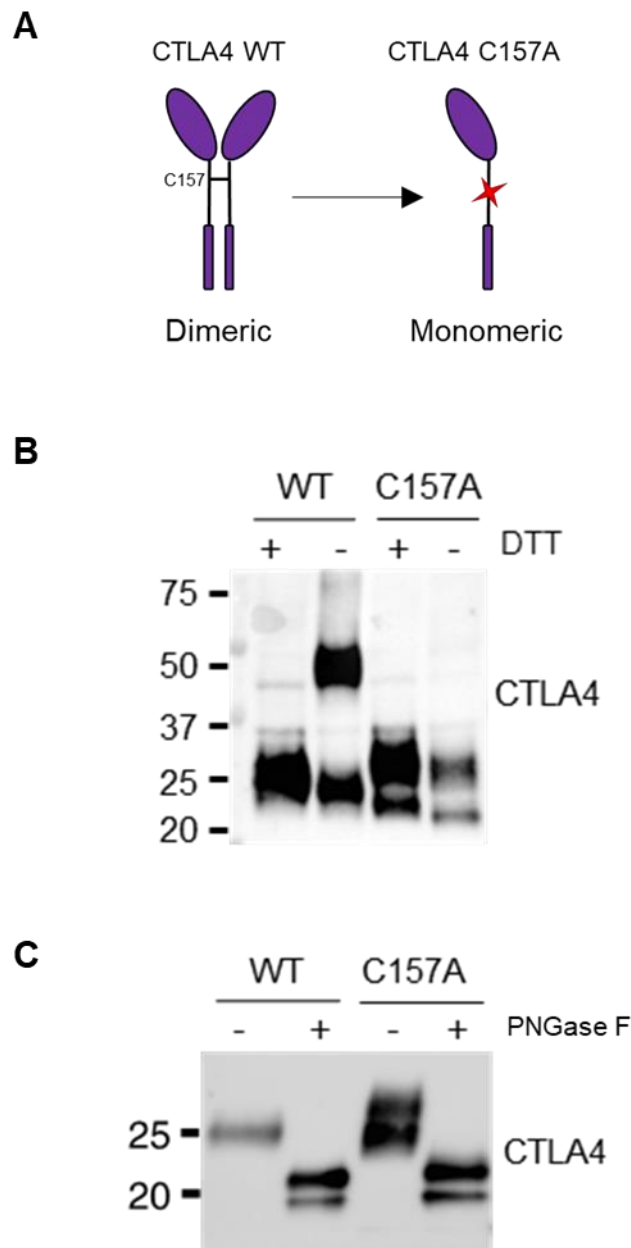
Figure 3.1 CTLA4 dimerisation requires intermolecular disulphide bonding at C157. (A). Cartoon depiction of CTLA4 WT as a dimer due to a disulphide link at C157, and CTLA4 C157A as a monomer. **(B).** Western blot analysis of total lysates from Jurkat cells transduced with CTLA4 WT or CTLA4 C157A lysed with or without Dithiothreitol (DTT), a reducing agent used to disrupt disulphide bonds. Lysates were blotted for anti-CTLA4 (C19). **(C)** Reduced whole cell lysates as in **(B)** were treated +- PNGase F to remove N-linked oligosaccharides, and blotted for CTLA4.

Interestingly, it is known that N-linked glycosylation is important for correct trafficking through the Golgi, protein stability and cell surface expression. To investigate protein localization of CTLA4 C157A, we stained surface CTLA4 with an N-terminal anti-CTLA4 antibody at 4ºC on CTLA4 WT and CTLA4 C157A expressing CHO cell lines, followed by an intracellular stain using a C-terminal anti-CTLA4. We found that the level of surface CTLA4 relative to total CTLA4 was similar for both CTLA4 WT and C157A (**Figure 3.2A**). In addition, confocal microscopy revealed CTLA4 C157A correctly localized in intracellular vesicles - a key feature that underlies the ability of CTLA4 to rapidly recycle to the cell surface - and was again similar to CTLA4 WT (**Figure 3.2B**).

To test if glycosylation was required for the correct protein localization of C157, we created additional N113A and N145A mutations in the CTLA4 protein, as previously reported (CTLA4 NNC) (Darlington et al., 2005)., We stained CHO cells with anti-CTLA4 antibody live at 37ºC, as at this temperature only CTLA4 that traffics via the plasma membrane can be detected, or after fixation and permeabilization, before analysis by confocal microscopy. We observed that whilst anti-CTLA4 accumulated in intracellular vesicles in CTLA4 WT cells, antibody staining was impaired in CTLA4 NNC cells, suggesting limited cell surface expression and/or CTLA4 cycling (**Figure 3.3, top panel**). Fixation and permeabilization prior to staining revealed that CTLA4 NNC did not show vesicular expression, and localisation suggested a defect in protein folding or trafficking causing retention in the endoplasmic reticulum (**Figure 3.3, lower panel**).

Overall, we concluded that the CTLA4 C157A mutation was sufficient to prevent disulphide bond formation and therefore homodimerization of the CTLA4

protein, and that its altered glycosylation did not prevent functional trafficking of the receptor. Therefore, CTLA4 C157A could be used as monomeric CTLA4 protein to model the impact of valency in our system.

A

B
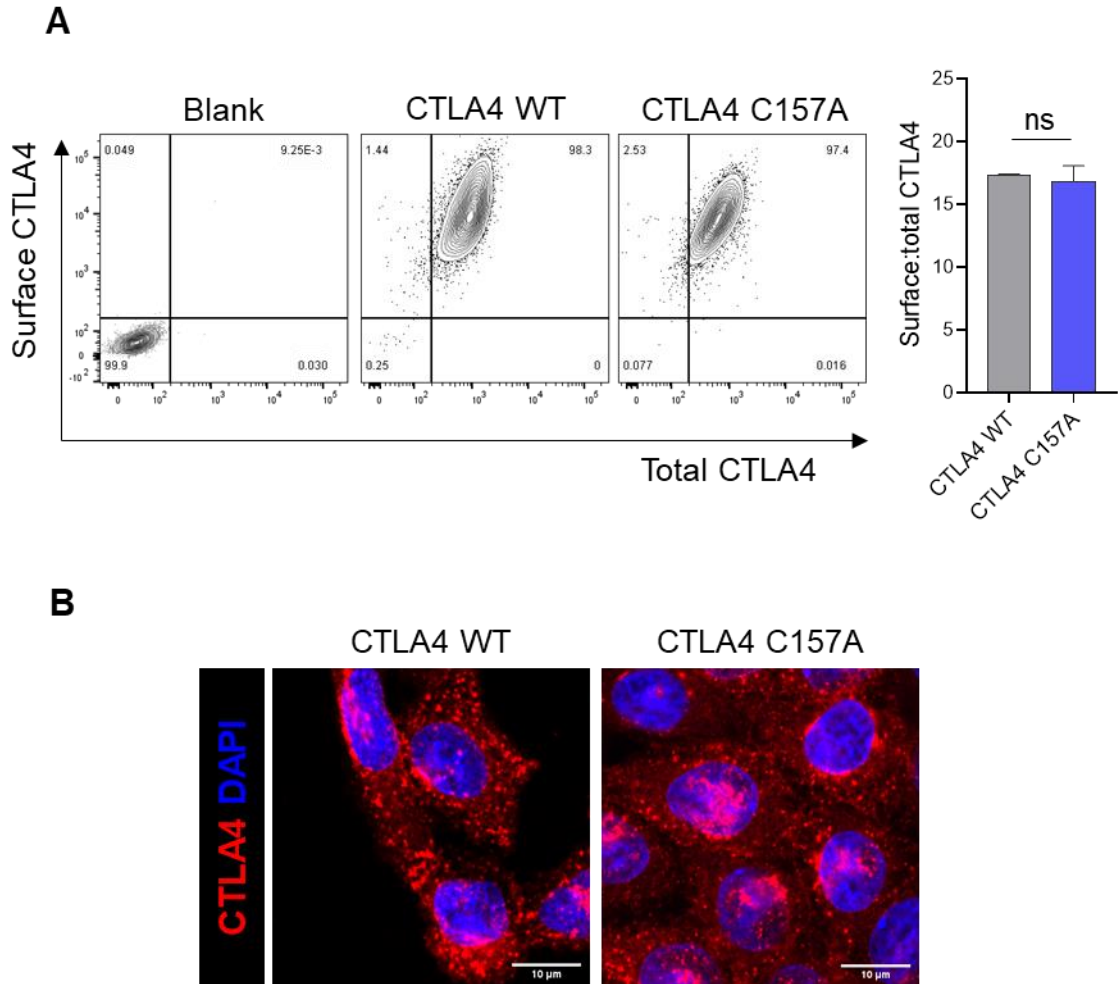
Figure 3. 2 Cysteine to Alanine mutation at position 157 of CTLA4 does not alter surface expression. (A) CHO cells expressing human CTLA4 wildtype (WT) or CTLA4 C157A were stained for surface expression using an ectodomain antibody at 4°C, then fixed and permeabilised prior to staining for total CTLA4 expression. Graph shows surface staining relative to total CTLA4 from 3 technical repeats +- SD. **(B)** CHO cells from A were seeded onto glass coverslips overnight before staining for CTLA4 (red) and DAPI (blue). Scale bar of 10μM.
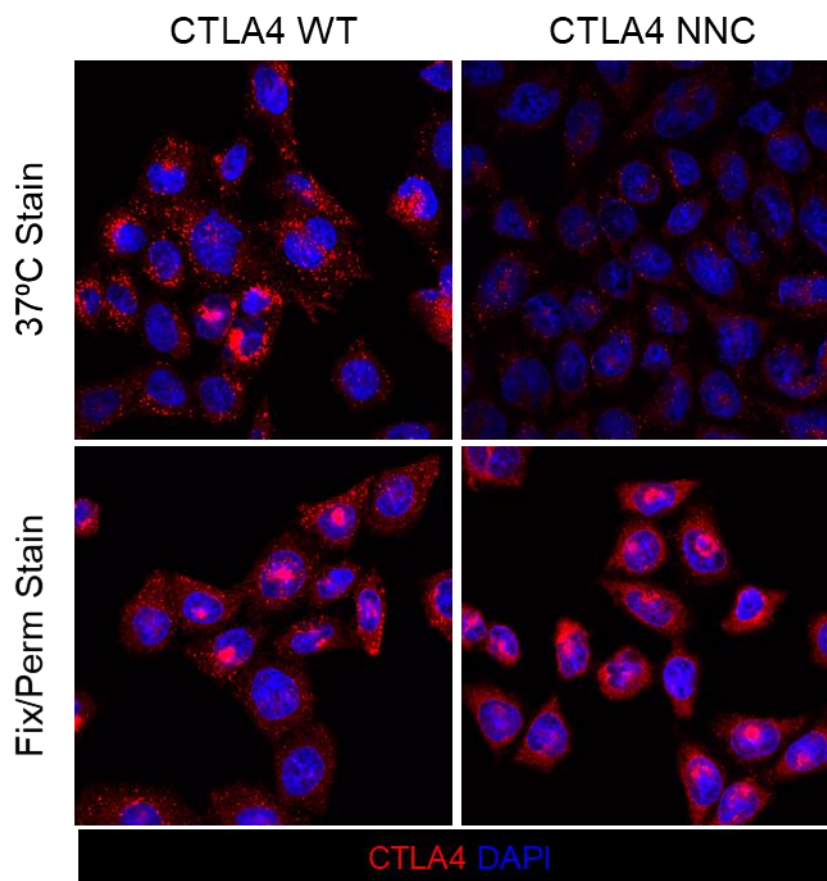
Figure 3. 3 CTLA4 NNC is aberrantly glycosylated and affects trafficking and expression. CHO cells expressing CTLA4 WT or CTLA4 with C157A and two additional asparagine mutations (N) (CTLA4 NNC) were grown on coverslips, before addition of anti-CTLA4 antibody for 1 hour at 37ºC (top panel), or fixed and permeabilized before 1 hour anti-CTLA4 staining (bottom panel) and analyzed by confocal microscopy (red). DAPI was used for nuclear staining (blue). Data shown is representative of 2 individual experiments**.**

3.2.2. Isoleucines in hydrophobic domain of CD80 are identified as key dimer contact residues

Having successfully generated a monomeric CTLA4 protein, we then sought to disrupt dimerisation of the high affinity CTLA4 ligand, CD80. Structural, fluorescent, and bioluminescent resonance energy transfer (FRET/BRET) studies previously confirmed that CD80 exists as a non-covalent dimer in the membrane with a relatively weak (~50µM) interaction (Ikemizu et al., 2000). Whilst CTLA4 was easily disrupted by targeting of the disulphide bond, disrupting CD80 required knowledge of the residues within the dimer interface. Modelling of the known crystallographic structure of the CD80 membrane distal IgV domain was used to highlight key residues in the hydrophobic interface predicted to stabilize the CD80 homodimer. This analysis identified two isoleucine residues at positions 58 and 61, shown in red (**Figure 3.4A).** Therefore, we introduced two isoleucine to arginine point mutations to generate a potentially monomeric mutant termed CD80I2R, show schematically in **Figure 3.4B.**
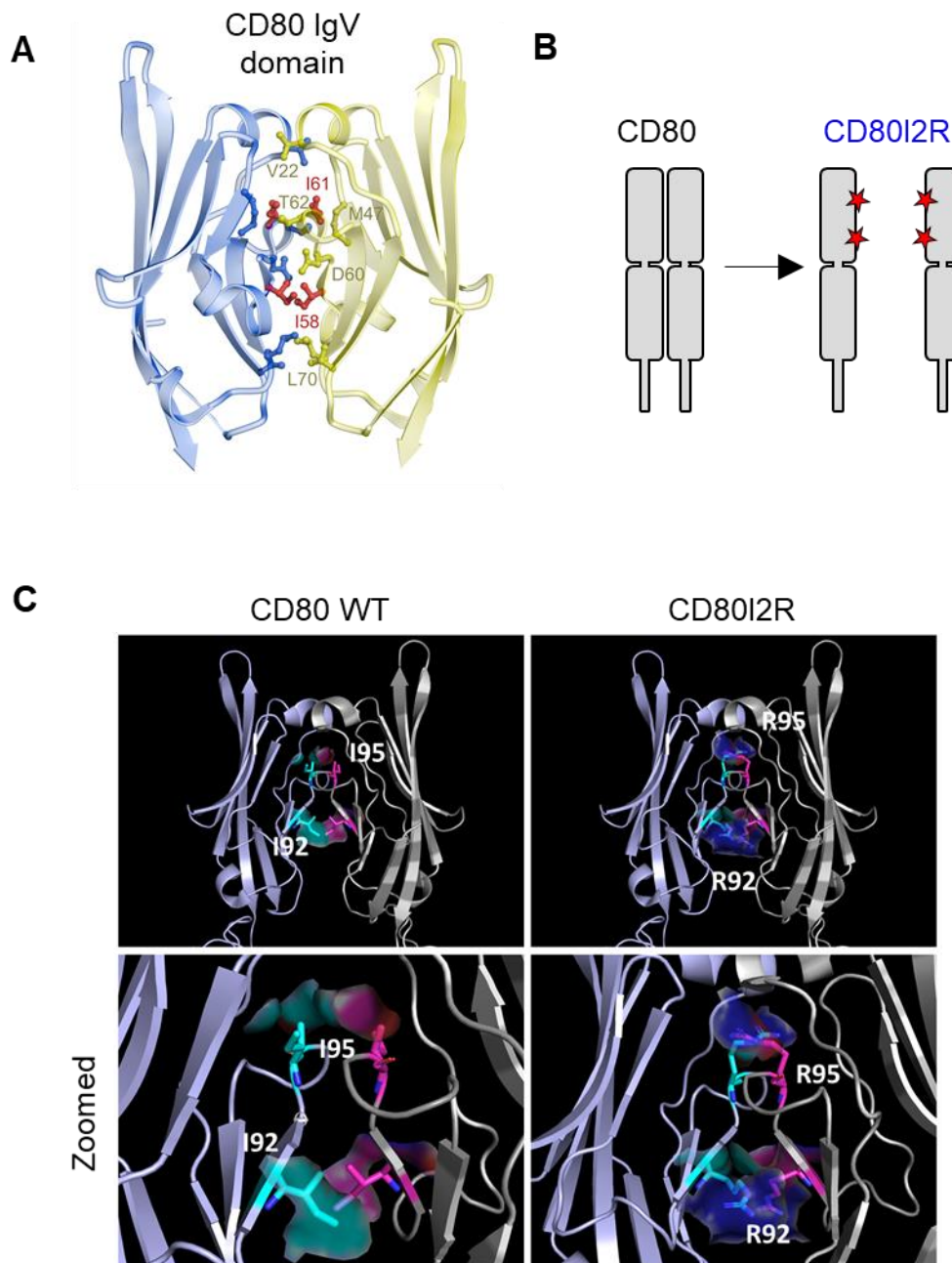
Figure 3. 4 Isoleucines 58 and 61 in membrane distal CD80 domain are dimer contact residues. (A). Crystal structure of two CD80 IgV domains (blue and yellow) with dimer contact residues highlighted. Isoleucines highlighted in red**. (B).** Cartoon prediction of CD80 WT as a non-covalent dimer and CD80 with isoleucines mutated to arginines (CD80I2R) as a monomer.

D

Wildtype CD80 I95 — Mutant CD80 R95

FRONT ON / ANGLED

E

Wildtype CD80 I92 — Mutant CD80 R92

FRONT ON / ANGLED
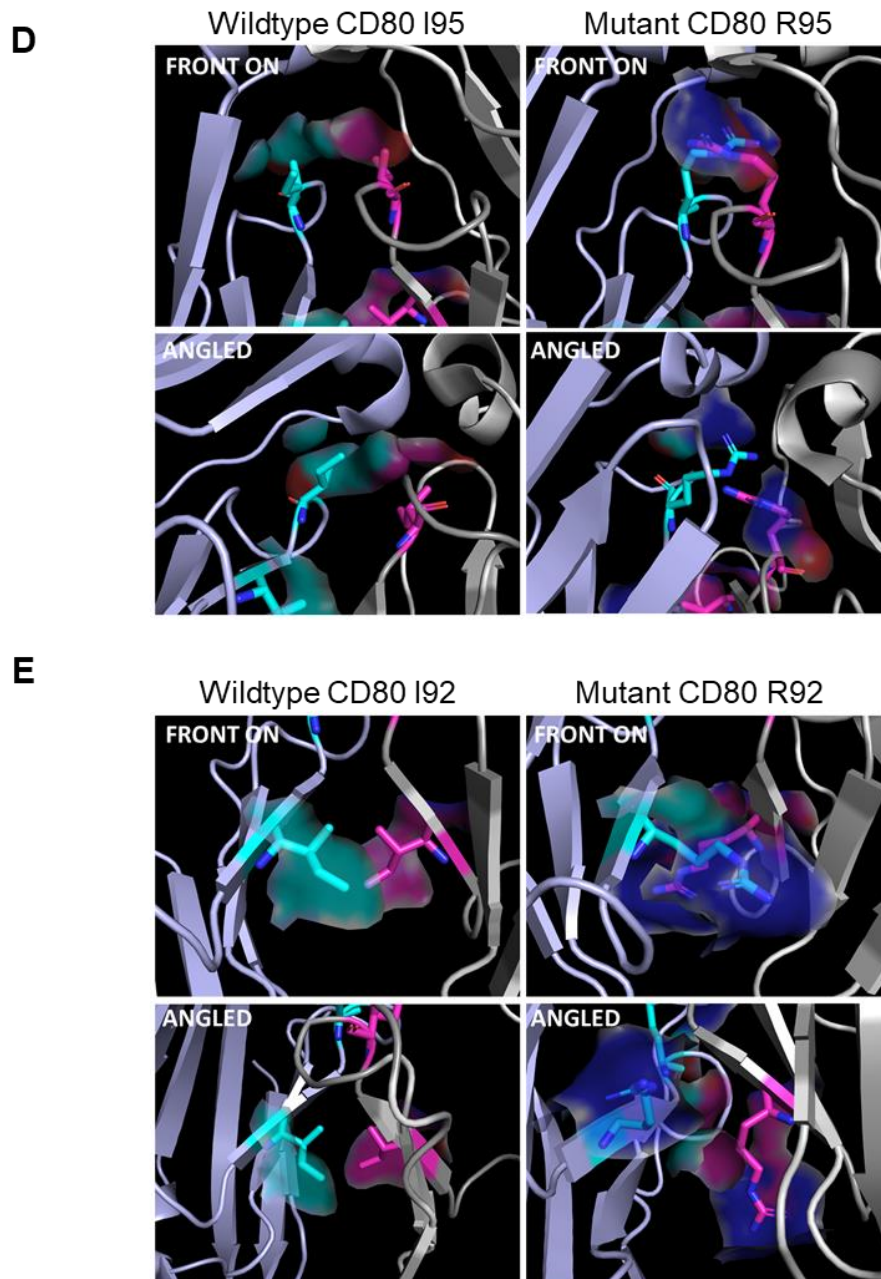
Figure 3.4. Isoleucines 58 and 61 in membrane distal CD80 domain are dimer contact residues. (C, D and E). Interaction of amino-terminal IgV domains of a CD80 WT (left) or CD80I2R (right) dimer. Left monomer coloured light blue, right monomer coloured in grey. Protein is modelled as a 'ribbon structure, except residues 92 and 95 which are modelled as 'sticks' and coloured cyan for the left monomer, and magenta for the right monomer. Basic amino groups ($-NH_2$) are coloured in blue and acidic carboxyl groups (-COOH) are coloured in red. The transparent 'clouds' show how the highlighted residues affect the surface of the dimer. Both residues shown in **(C).** With zoomed on I95 shown in **(D).** and I92 shown in **(E).**

To understand how these mutations may impact CD80 homodimerization, we modelled both CD80 WT and CD80I2R in PyMOL (PyMOL, 2021) **(Figure 3.4.C-E). Figure 3.4C** shows the interactions of a CD80 WT dimer (left panel) and CD80I2R dimer (right panel) modelled as a cartoon. Residues 92 and 95 (note that I58 and I61 are equivalent to I92 and I95, with the difference due to whether the signal peptide is included in the nomenclature) are indicated and modelled as 'sticks', coloured in cyan for the left monomer and magenta for the right monomer. Transparent 'clouds' showed how highlighted residues affect the surface of the dimer.

For CD80 WT, residues 92 and 95 are isoleucine's. Isoleucine is a hydrophobic amino acid with no charge, and therefore we observed that isoleucine residues preferentially 'bury' themselves within the dimer interface, forming hydrophobic Van der Waal interactions with residues on the interacting monomer. In the zoomed image (bottom left **Figure 3.4C, left lower panel**), we observed that CD80 I95 on each monomer are close, causing surfaces to interact and contribute to the dimer interface (cyan and magenta clouds).

In contrast, arginine is a basic amino acid (-NH2 group, indicated as blue) and therefore possesses' an overall positive charge. As such, mutation of isoleucine's to arginine introduced an area of positive charge, indicated by dark blue 'clouds', resulting in repulsion of the residues, as opposed to interaction. This is also shown in zoomed in images at two rotations at residue 95 **(Figure 3.4D)** and residue 92 **(Figure 3.4E),** showing attraction of isoleucine's and repulsion of arginine residues**.** Overall, this modelling supports the hypothesis that mutation of isoleucine's 58 and 61 to arginine's will impact the CD80 homodimer.

Having determined which residues of CD80 to mutate in our study, we first wanted to ensure introducing the I to R mutations did not impair CTLA4 binding. We therefore generated DG75 B cell lines stably expressing CD80, CD86 and CD80I2R constructs, C-terminally tagged with GFP. We then characterized receptor binding by titration of CTLA4-Ig (directly conjugated to APC), and staining for 30 mins at 37ºC. As shown in **Figure 3.5A**, WT CD80 showed a dose-dependent binding curve reaching saturation at ~1µg/ml with a maximum MFI of ~45000, reflecting maximal binding. In contrast, the binding curve for CD86 was shifted to the right, consistent with a lower affinity interaction with the maximal response still not reached by 100 µg/ml CTLA4-Ig. Nonetheless, the CD86 binding curve appeared to approach saturation with a potential maximum response of ~90-100,000 MFI, approximately double that of CD80. This higher maximum could be explained by each CTLA4-Ig being able to bind one CD86 molecule, binding at a 1:1 ratio. In contrast, each CTLA4-Ig might only bind one of CD80 molecule present as a dimer, and thus binds at a 1:2 ratio, thereby reducing detection by ~50%. As such, these observations suggest this assay can provide information on the valency of ligand:receptor binding.

Strikingly, CTLA4-Ig binding to CD80I2R displayed a curve which appeared to bind similarly to CD80 at lower concentrations of CTLA4-Ig (up to ~1ug/ml), but then continued to increase with increased concentrations of CTLA4-Ig, like CD86 (**Figure 3.5A**). This was an unexpected observation, but could potentially be explained if CD80I2R is acting as a weaker dimer, thereby shifting the monomer-dimer equilibrium at steady state. In this scenario, we would predict CTLA4-Ig to bind bivalently i.e. one CTLA4-Ig to two CD80I2R molecules, but at high CTLA4-Ig concentrations, the increased presence of monomers

permits monovalent binding. This explanation is shown schematically in **Figure 3.5B**.

To further test whether CTLA4-Ig binding curves robustly reflected ligand properties, we performed this titration on DG75 lines expressing a high-affinity CD86 variant CD86-H113L. As expected, the binding curve was left-shifted reflecting higher-affinity, but again approached the same maximal response as WT monomeric CD86 **(Figure 3.5C)**. Moreover, introducing a cysteine residue (and therefore making a disulphide linkage) into CD80 and CD86, creating an artificial dimer (CD80/CD86-cys), had no impact on the CTLA4-Ig binding curve of CD80-cys compared to CD80 WT (**Figure 3.5D),** but reduced the maximal binding for CD86-cys compared to CD86 WT (**Figure 3.5E**) supporting the concept that CTLA4-Ig binding curves reflected affinity and valency properties of the ligands.

Taken together, CTLA4-Ig titrations suggest that CD80I2R can bind robustly to CTLA4-Ig with similar affinity to CD80, but with different valency properties that are consistent with impaired dimerisation.
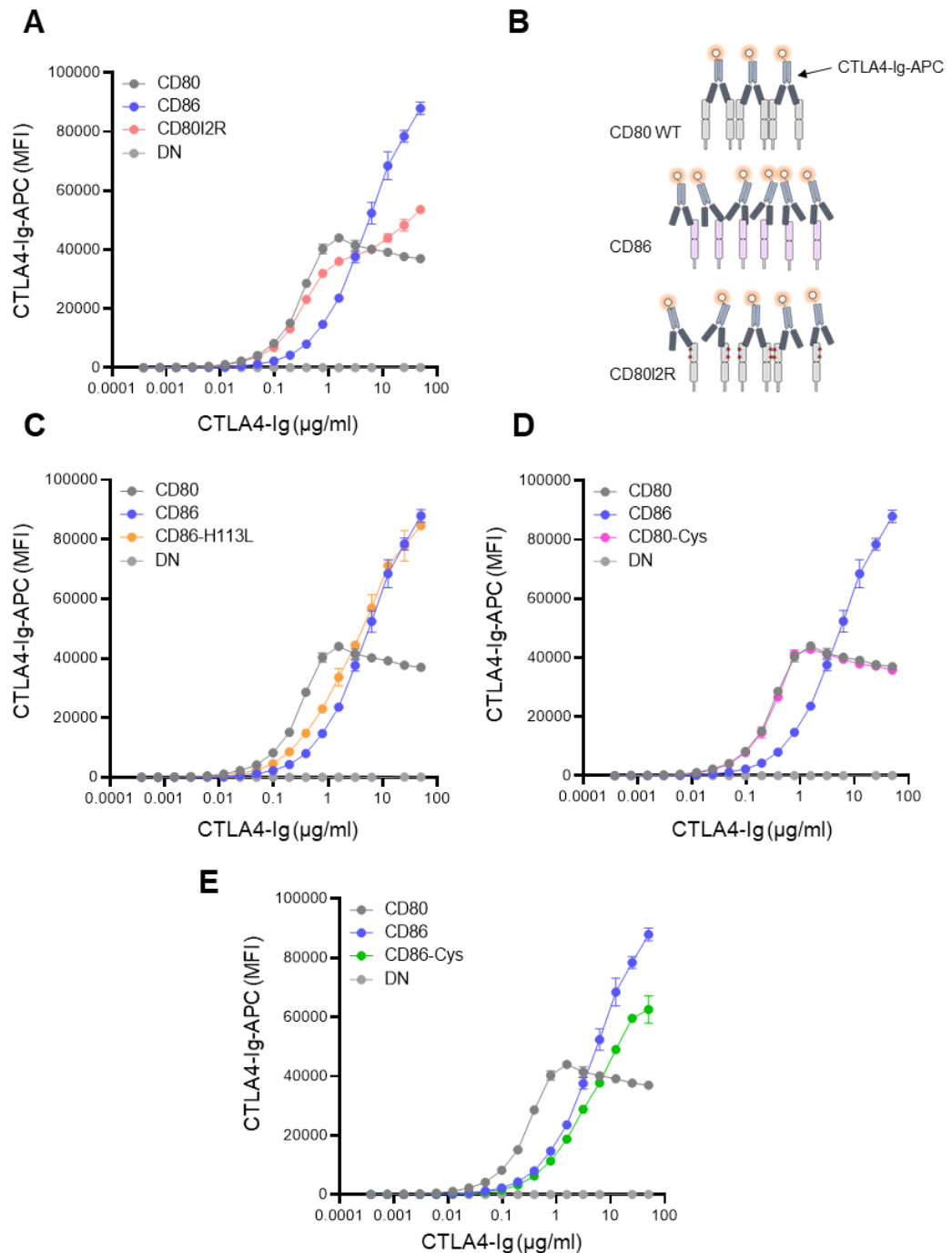
Figure 3. 5. Directly conjugated CTLA4-Ig binding curves reflect different valency properties of ligands. Dose response curves of CTLA4-Ig-APC binding at 37ºC for 60 mins to DG75 cells expressing no ligand (DN), CD80 or CD86, performed by serial 2-fold dilutions starting at 50µg/ml, compared to DG75 cells expressing CD80I2R **(A). (B).** Schematic of CTLA4-Ig-APC binding to CD80 WT dimers, CD86 monomers, and weak dimer CD80I2R. **(C)** As before, with CD86-H113L, CD80-cys **(D),** and CD86-cys **(E).** Data represented as mean ± SD from 2 independent experiments (n=4).

To directly study the dimerisation of CD80I2R compared to CD80, we performed Western blot analysis following treatment with a titration of BS[3] crosslinker under non-reducing conditions (**Figure 3.6A**). BS[3] is a membrane impermeable, amine-to-amine crosslinker of up to 11.4Å length, and is commonly used to study dimer interactions. We observed that in untreated conditions, CD80 and CD80I2R ran at ~75kDa (molecular weight of CD80 plus the GFP tag), and CD86 at ~100kDa. For CD80 WT, we saw a dose dependent increase in a 150kDa band with BS[3] treatment, indicative of stabilization of CD80 dimers. The presence of an increased molecular weight band was also seen for CD80I2R, however the band was much weaker for CD80I2R and similar to that seen for CD86, consistent with the CD80I2R mutation shifting the equilibrium towards monomeric CD80 at a steady state. Quantification of the dimeric band compared to the monomeric band confirmed these observations (**Figure 3.6B**).

A

CD80-GFP CD80I2R-GFP CD86-GFP

0 0.1 0.5 1 0 0.1 0.5 1 0 0.1 0.5 1 BS^3 (mM)

250
150
100
75

GFP

B
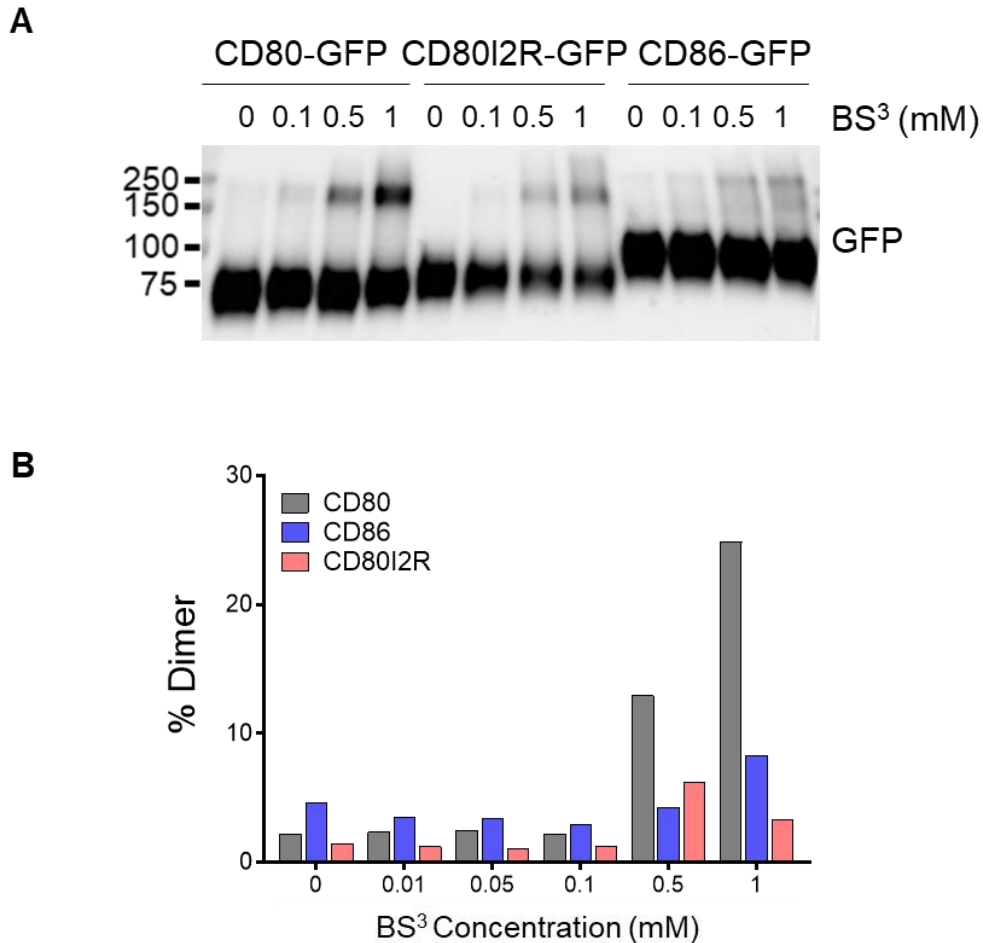
Figure 3.6 BS^3 crosslinking demonstrates CD80I2R mutations weaken CD80 homodimers. (A). CHO cells expressing CD80-, CD80I2R- or CD86-GFP were treated with indicated concentrations (0-1mM) of Bissulfosuccinimidyl suberate (BS3) crosslinker for 1 hr, before cell lysis and analysis by western blotting for GFP, using an anti-GFP antibody (clone 13.1, Sigma-Aldrich). **(B).** GFP bands in (A). were quantified for the dimeric band (150kDa) relative to monomeric band (75kDa) using ImageLab and expressed as % dimer (n=1).

3.2.3. Analysis of CD80I2R dimer interactions using NanoLuc Binary Technology

Despite supportive results from the cross-linking experiments, dimerisation of WT CD80 was only strongly observed at high-concentrations of crosslinker and complete dimer formation was not seen. To further evaluate our conclusions of impaired dimerisation of CD80I2R, we employed the NanoLuc Binary Technology (NanoBiT) system for analysis of protein-protein interactions in live cells.

NanoBiT is a novel protein-fragment complementation technique based on the engineered luciferase NanoLuc, composed of a large fragment (LgBit ~18kDa) and a small fragment (SmBit 11aa) which have weak association for each other. When fused to interacting proteins, the fragments can associate producing a strong and specific luciferase complex that upon substrate addition, produces luminescence. Since being established, NanoBiT has been widely applied to study receptor and ligand interactions, and dimerization/ oligomerization states of various proteins (Norisada et al., 2018; Oh-Hashi et al., 2016). Therefore, we constructed CD80 and CD80I2R C-terminally tagged with LgBit or SmBit, shown schematically in **Figure 3.7A** and expressed these constructs in CHO cells. 48 hours post-transfection, flow cytometry analysis confirmed LgBiT and SmBiT- tagged proteins were expressed and detectable by surface CD80 antibody staining (**Figure 3.7B),** suggesting proteins were correctly folded and suitable for use in a NanoBiT assay. Importantly, whilst CD80 and CD80I2R constructs were consistently expressed at similar percentages per transfection, the level itself was somewhat variable.
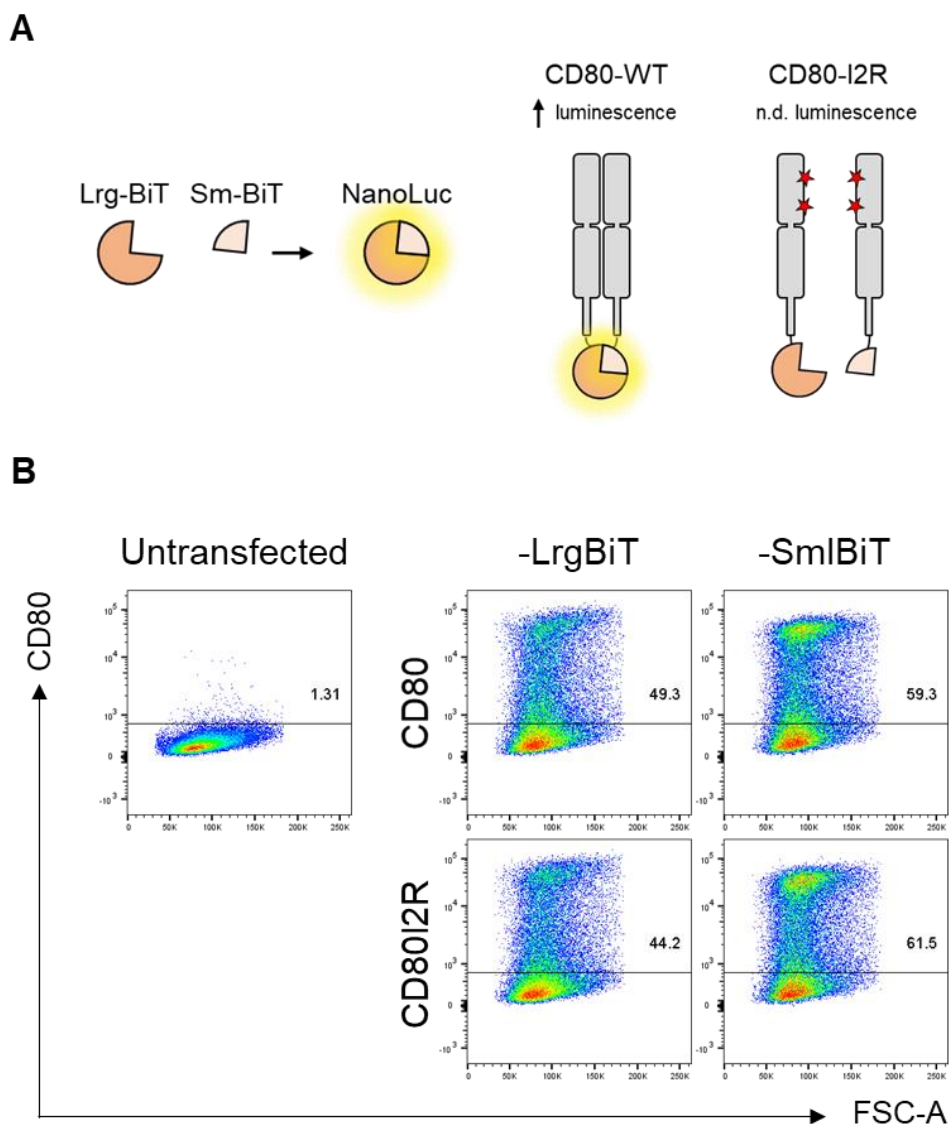
Figure 3. 7. NanoLuc® Binary Technology (NanoBiT) System to assess CD80 dimerisation. (A). Schematic of the NanoBiT structural complementation system based on NanoLuciferase showing Lrg-BiT and Sm-BiT (fragments of Nano Luciferase) as tags for CD80 WT and CD80I2R (mutations depicted by red stars). Lrg-BiT and Sml-BiT combine to form full a full NanoLuciferase (NanoLuc) when in close-proximity (<100nm), generating luminenscence following substrate addition. **(B).** CHO cells were transfected with LrgBiT and Sml-BiT tagged plasmid constructs (50ng) of CD80 and CD80I2R-. 48 hours post-transfection, cells were stained for surface expression using an anti-CD80-PE antibody and analyzed by flow-cytometry. Data shown is representative of n=8 separate transfections.

We then determined the luminescent signal produced by the NanoBiT ligand tagged constructs by co-transfecting -LrgBiT tagged constructs at a 1:1 ratio with -SmlBiT constructs and measuring luminescence 48 hours post-transfection following addition of NanoLuc substrate, fumarizine. Luminescence for indicated LrgBiT:SmlBiT combinations are shown in **Figure 3.8A**. The NanoBiT-tagged WT CD80 pair showed high luminescence when compared to a CD80-LrgBit:HaloTag-SmlBit control pair, confirming homodimeric interaction of WT CD80 is detectable in this system. Conversely, the CD80I2R-LrgBiT:SmlBiT pair showed significantly reduced luminescence. Moreover, heteromers of CD80 WT and CD80I2R NanoBiT pairs also showed decreased luminescence compared to CD80 homodimers, but above that of negative control combinations.

An important caveat of this system is that the detected luminescent signal will be largely dependent on transfection level and cell number and thus can be highly variable, reflected by the large spread of data. Nevertheless, pairing data from CD80 and CD80I2R per transfection strengthened statistical significance and showed that the luminescent signal was significantly impaired for CD80I2R, regardless of transfection efficiency (**Figure 3.8B),** again supporting the conclusion that CD80I2R is impaired in dimer formation.

A

CD80-LrgBiT	X		X		X		X		
CD80-SmlBiT	X			X		X		X	
CD80I2R-LrgBiT		X		X	X				X
CD80I2R-SmlBiT	X	X				X			X
HaloTag-SmlBiT						X	X	X	X

B
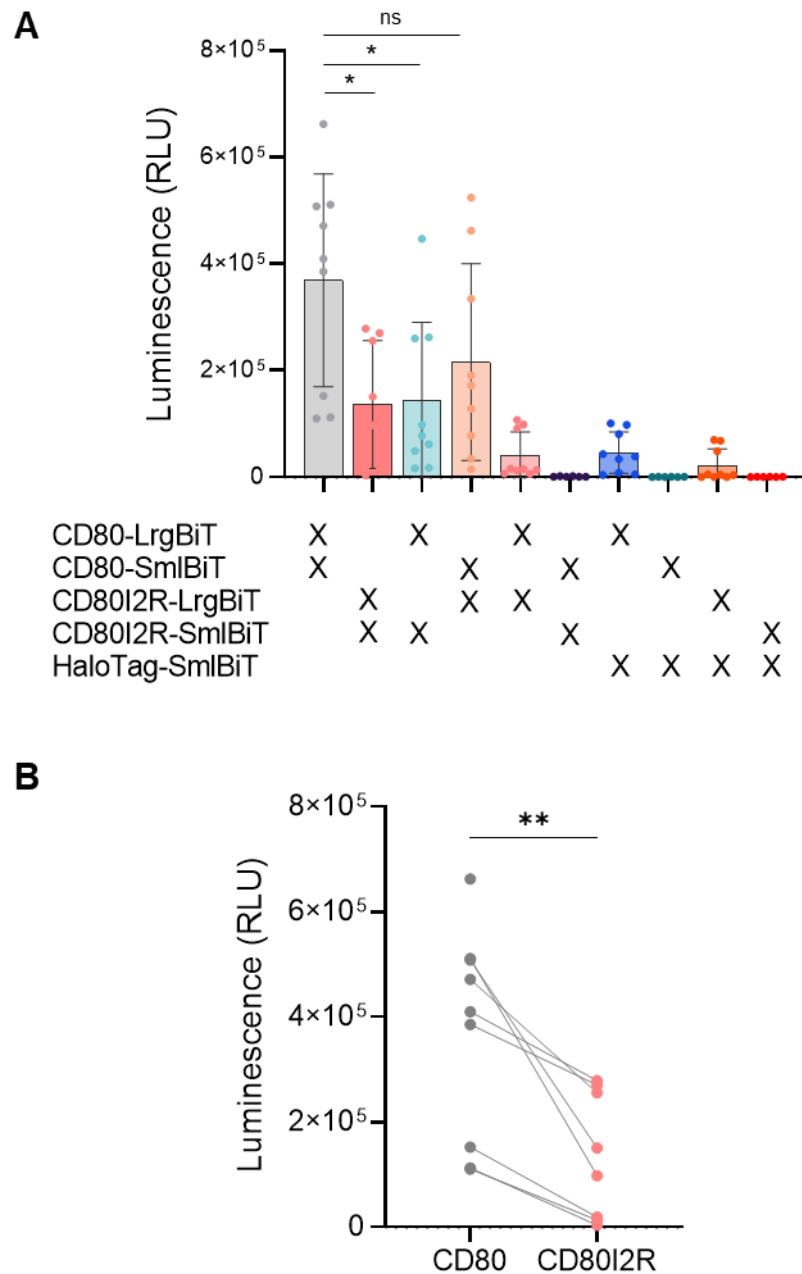
Figure 3. 8. Mutation of Isoleucines 58 and 61 disrupt CD80 homodimerization. (A). NanoBiT (Lrg-BiT and Sml-BiT) split luciferase tagged CD80 and CD80I2R constructs were transfected into CHO cells at a 1:1 ratio for indicated conditions. 24 hours later, luminescence was measured using a Synergy H1 plate reader (BioTek) following addition of luminescent substrate fumarizine. Data shown from 2-3 technical repeats from 3 individual transfections. **(B).** Luminescence expressed as paired data from CD80-LrgBiTSmlBiT and CD80I2R-LrgBiTSmlBiT conditions (n=8-9), analysed by paired T-test *p≤0.05, **p≤0.01,***p≤0.001, ****p≤0.0001.

Having demonstrated that NanoBiT technology could be used to assess dimerisation, we then investigated whether CTLA4 binding could alter CD80 dimerisation status. For this, we measured the luminescent signal from CD80 or CD80I2R NanoBiT pairs, (or a CD80/CD80I2R-LrgBiT:HaloTag control pair) for 10 minutes, prior to addition of 10µg of CTLA4-Ig. As shown in **Figure 3.9A,** before CTLA4-Ig addition CD80I2R showed a low level of luminescence compared to CD80, consistent with the previous experiment and suggesting impaired dimerisation. However, following CTLA4-Ig addition the luminescent signal resulting from CD80I2R was rapidly increased, implying CTLA4 may bring two CD80I2R monomers into close enough proximity to result in a NanoBiT interaction. Likewise, CD80 luminescence also increased in comparison to the no CTLA4-Ig control wells, again suggesting CTLA4 can stabilize CD80 dimers or promote sufficient proximity between monomers or dimers.

Notably, quantification of the fold change pre- and post- CTLA4 Ig treatment revealed that the change associated with CD80I2R was consistently larger (**Figure 3.9B),** implying a monomer:dimer equilibrium shifted toward monomers at the steady state for the CD80I2R pair, compared to CD80. Taken together, these results suggest that CTLA4 can bind bivalently to both CD80 and CD80I2R, but maintains the conclusion that CD80I2R is a weaker dimer.

A

- CD80 + Halotag (control)
- CD80I2R + Halotag (control)
- CD80 NanoBiT pair + CTLA4-Ig
- CD80 NanoBiT pair - CTLA4-Ig
- CD80I2R NanoBiT pair + CTLA4-Ig
- CD80I2R NanoBiT pair - CTLA4-Ig

B
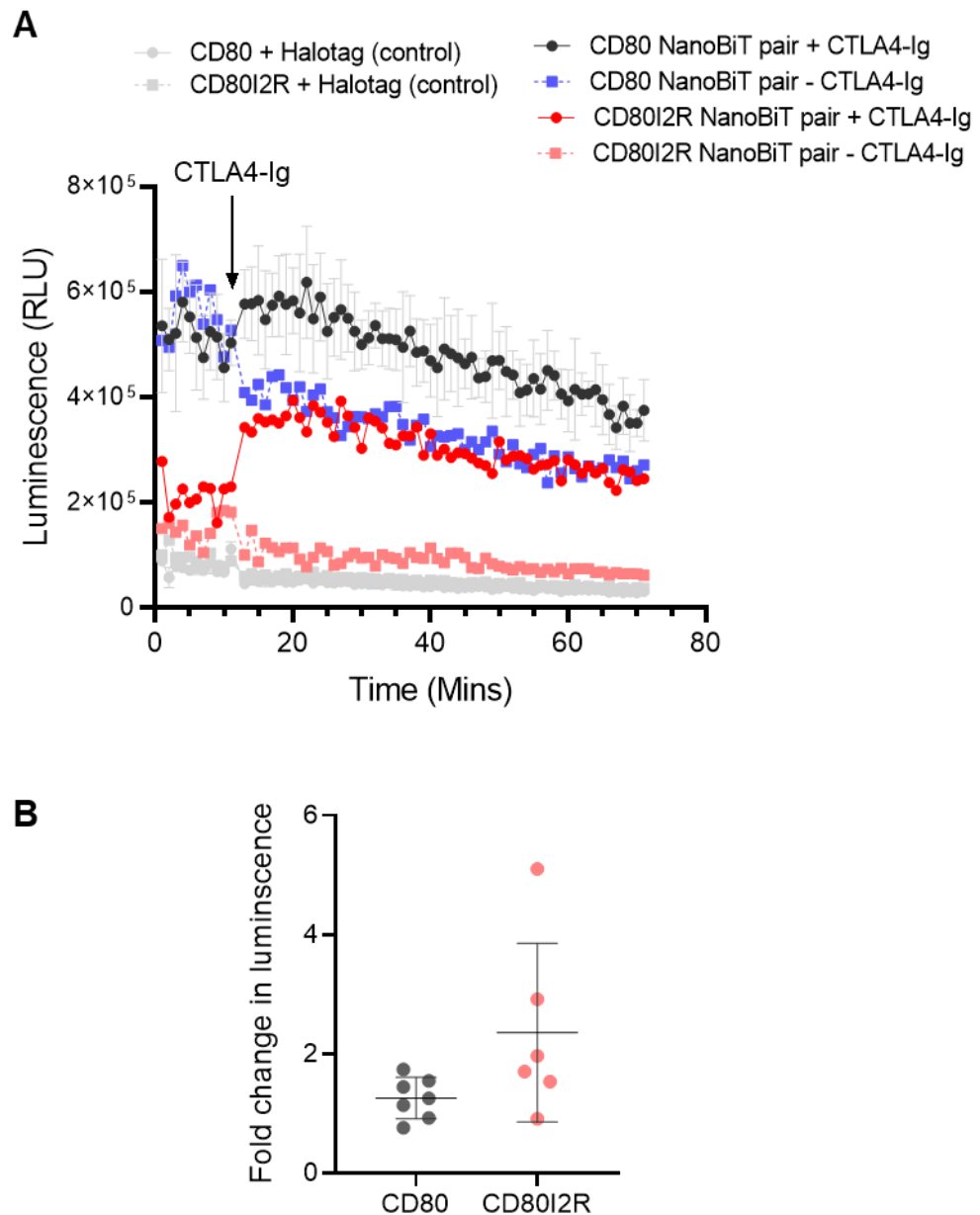
Figure 3. 9. CTLA4-Ig binding modulates dimerisation of CD80I2R using NanoBiT. (A). CHO cells were transfected at a 1:1 ratio with either CD80-LrgBiT/SmlBiT NanoBiT pair or CD80I2R-LrgBiT/SmlBiT NanoBiT pair constructs. Following addition of luciferase substrate, luminescence was measured for 10 minutes before addition of 10µg/ml CTLA4-Ig (Abatacept). Luminescence was recorded for a further hour. **(B).** Collated data from 6 independent transfections showing fold change in luminescence following CTLA4-Ig addition for CD80 and CD80I2R conditions.

107

3.2.4. PDL1 binds at the CD80 dimer interface, acting as an endogenous regulator of CD80 homo-dimerisation

It has been recently reported that PDL1 can bind in *cis* to CD80 in a manner that disrupts PDL1 binding to PD1, but not CD80 binding to CTLA4. This is thought to be because the PDL1 binding site is at the opposite face of the CD80 molecule to the CTLA4 binding site (Sugiura et al., 2019), and therefore overlaps with the CD80 homodimer interface. As such, PDL1 binding not only disrupts PD1 binding but also CD80 homodimer formation. Recently, our group has generated data in support of these observations, showing *cis* expression of CD80 and PDL1 prevents detection of PDL1 by anti-PDL1 antibodies (Kennedy et al., EMBO.J. in press).

Considering this interaction, we sought to determine whether CD80I2R could bind to PDL1. We stained for PDL1 using 3 different anti-PDL1 ectodomain antibodies on cell lines which expressed PDL1 (carrying a cytoplasmic mCherry tag), along with either CD80-GFP, CD86-GFP or CD80I2R-GFP. **Figure 3.10A** shows expression levels of -GFP and -mCherry, confirming co-expression of indicated ligand pairs. Whilst PDL1-mCherry levels were equal in CD80-GFP and CD86-GFP lines, PDL1-mCherry levels were unfortunately higher in CD80I2R-GFP lines as PDL1-mCherry, was transduced into this line, complicating analysis.

Strikingly, co-expression of CD80 completely prevented anti-PDL1 binding of all antibodies, as previously reported. In contrast, anti-PDL1 binding was readily detectable when PDL1 was co-expressed with CD86. When co-expressed with CD80I2R, PD-L1 was again readily detectable (**Figure 3.10B)** suggesting that the two isoleucine residues of CD80 are also critical for PDL1 binding., Due to the high level of PD-L1 expression in the CD80I2R lines it was

possible visible staining was due to presence of PDL1 not in a heterodimer. However, it was clear CD80I2R did not affect PDL1 staining in these cells. This provides further evidence that PDL1 binds at the hydrophobic dimer interface of CD80 and that CD80I2R is therefore an impaired dimerisation mutant, which likely affects interactions with PD-L1.

Figure 3. 10. PDL1 co-expression with CD80, but not CD80I2R, inhibits PDL1 detection. **(A)** Expression levels of GFP and mCherry on DG75 cells co-expressing either CD80-, CD86- or CD80I2R-GFP with PDL1-mCherry, compared to untransduced DG75 lines (blank) **(B).** DG75 lines in **(A)** were stained with anti-PDL1 clones MIH1, MIH3 or 29E.2A3 as indicated for 30 min at 37ºC, with representative flow cytometry plots from 2 technical repeats showing staining against total PD-L1-mCherry levels.

To further study PDL1 effects on CD80 homodimers, we used the CD80LrgBiT:CD80SmlBiT pair transfected into both CHO blank cells and CHO PDL1 containing cells in a NanoBiT luminescence assay. We hypothesized that presence of PDL1 should reduce luminescence, shown schematically in **Figure 3.11A**. This experiment revealed that luminescence was significantly reduced in PDL1 expressing CHO lines (**Figure 3.11B)** due to disruption of CD80 dimerisation.

Interestingly, treatment with Atezolimumab, an anti-PDL1 antibody that has been suggested to be able to disrupt CD80:PDL1 homodimers (Zhao et al., 2019) showed no revival of the NanoBiT signal. However, this may be due to the overexpression of PDL1 not in a heterodimer with CD80 capturing the antibody first. In contrast, treatment with anti-CTLA4-Ig increased the luminescence, although not statistically significantly, in both CHO blank and CHO PDL1 conditions, again suggesting CTLA4, at least in its Ig-chimera form, can stabilize CD80 dimers.

Taken together, these results indicate that isoleucine's in the hydrophobic pocket of the extracellular domain of CD80 are required for homodimerization, and the CD80I2R mutant, or CD80 expressed in *cis* with PDL1, can be exploited to investigate the functional role of CD80 dimers in the CTLA4 system.
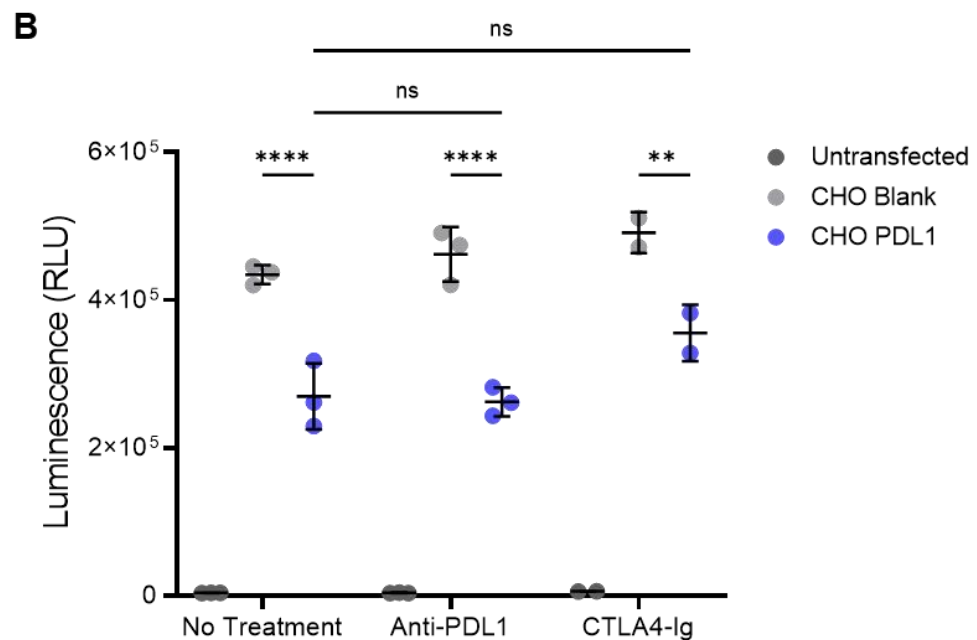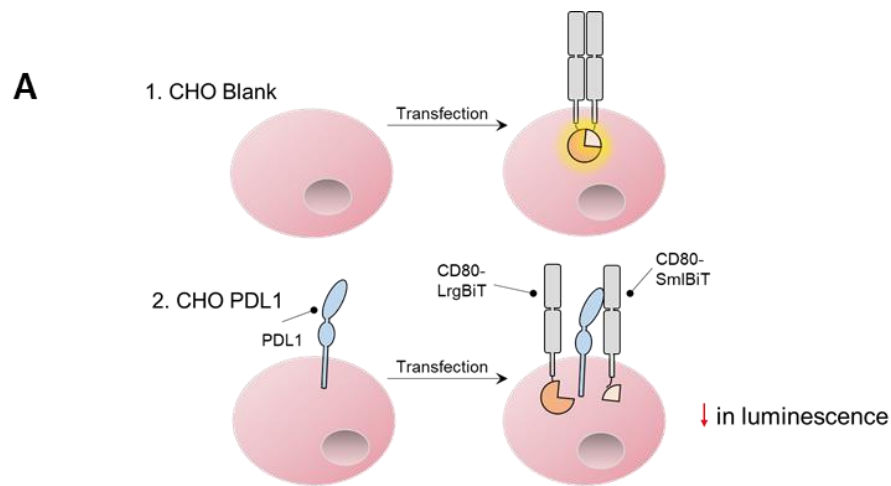
Figure 3. 11. PDL1 *cis* **expression with CD80 disrupts CD80 homodimers.** Untransduced CHO cells, or CHO cells stably expressing PDL1 were transfected with CD80-LrgBiT and CD80-SmlBiT at a 1:1 ratio. A decrease in NanoLuc luminescence was predicted in the presence of PDL1 as depicted in **(A). (B).** Assay in **(A).** was performed. 48 hours post-transfection, cells were treated with 20μg/ml of anti-PDL1 (Atezolimumab), 20μg/ml of CTLA4-Ig or received no treatment for 2 hours at 37ºC. NanoLuc substrate was added and luminescence was read following 30 minute incubation at 37ºC. Data from 3 wells from 1 independent repeat, and analysed by 2-Way ANOVA (*p≤0.05, **p≤0.01,***p≤0.001, ****p≤0.0001).

3.2.5. Disruption of CD80 dimerisation by I2R mutations and co-expression of PDL1 confirmed using NanoBRET technology

Whilst use of the NanoBiT system allowed us to draw some conclusions on the dimerisation status of CD80 vs CD80I2R, limitations of the technology, specifically regarding the inability to control for transfection efficiency and cell number, hindered robust interpretation and resulted in inability to compare across conditions.

Therefore, we opted to develop NanoBRET (Bioluminescence Resonance Energy Transfer) technology, depicted schematically in **Figure 3.12A**. Whilst BRET has been an established method for studies of protein interactions for many years (Harikumar et al., 2017), NanoBRET uses the same principle, but with the smaller (19 kDa), brighter and more stable NanoLuc (NLuc) tag. NanoBRET utilises NLuc fused to one protein as an energy donor, and a fluorescent acceptor fused to another protein. If these two proteins are within 10nm proximity, this results in an energy transfer detectable as a quantifiable BRET signal. In fact, the efficacy of energy transfer is inversely proportional to the distance between donor and acceptor. Therefore, NanoBRET is a measure of the proximity of protein pairs, in contrast to NanoBiT, which only measures a physical interaction of the NanoBiT tags.

In addition, we opted to develop NanoBRET with a HaloTag acceptor. HaloTag technology is based on a HaloTag protein (33kDa) being fused to a protein of interest, which is able to form a covalent bond with a fluorescent HaloTag ligand of choice. As such, HaloTag technology allows labelling of a specific pool of protein and permits measurement of background NanoBRET signal in the absence of ligand addition. NanoBRET was optimized using the

HaloTag 618 ligand, a red-shifted fluorophore giving maximal spectral separation and minimal background signal **(Figure 3.12B).** By measuring luminescent signals from acceptor and donor emission wavelengths, a BRET ratio can be calculated **(Figure 3.12B, inset)** which allows correction for well-to-well variation and overcomes limitations encountered by NanoBiT technology.

To set up the NanoBRET assay, we first generated CD80 and CD86 constructs C-terminally tagged with either NLuc donor tag or HaloTag acceptor tags. For the initial screen, we transfected CHO cells at a 1:100 ratio of NLuc to HaloTag, with the CD80 or CD86 NanoBRET pair, or for a CD80NLuc:CD86HaloTag pair for use as a negative control. 24 hours post-transfection, cells were treated with or without HaloTag 618 ligand to allow measurement of background donor signal. Raw luminescence resulting from donor emissions are measured using 460nm luminescent filters, and control for transfection efficiency of NLuc constructs (**Figure 3.12C). Figure 3.12D** shows representative acceptor emissions, measured using 610nm filters, and represent the energy transfer from the NLuc donor to the HaloTag acceptor. This revealed these emissions were highest for the CD80 NanoBRET pair, as expected for the CD80 homodimer interaction. The no-ligand control samples representing bleed-through of the donor show minimal signal across all NanoBRET combinations suggesting our plate reader band pass filter is optimal for selectively measuring donor signal.

Calculation of the resultant BRET ratios demonstrated that the CD80 NanoBRET pair resulted in a strong signal, indicative of CD80 homodimeristion which was absent in the known monomer CD86 (**Figure 3.12E).** As a result, we

concluded we were able to set up a NanoBRET assay to study protein:protein interactions and that NanoBRET was able to observe protein dimerisation.

We then extended this assay by generating CD80I2R NanoBRET constructs and comparing resultant NanoBRET signals to CD80 and CD86 BRET pairs (**Figure 3.13).** We observed that CD80 WT resulted in the strongest BRET signal, whilst CD80I2R BRET pairs showed a significant reduction in energy transfer, although still markedly above that observed for CD86. Together, this suggests reduced interaction of CD80I2R monomers at steady state, but not complete monomerization.

.
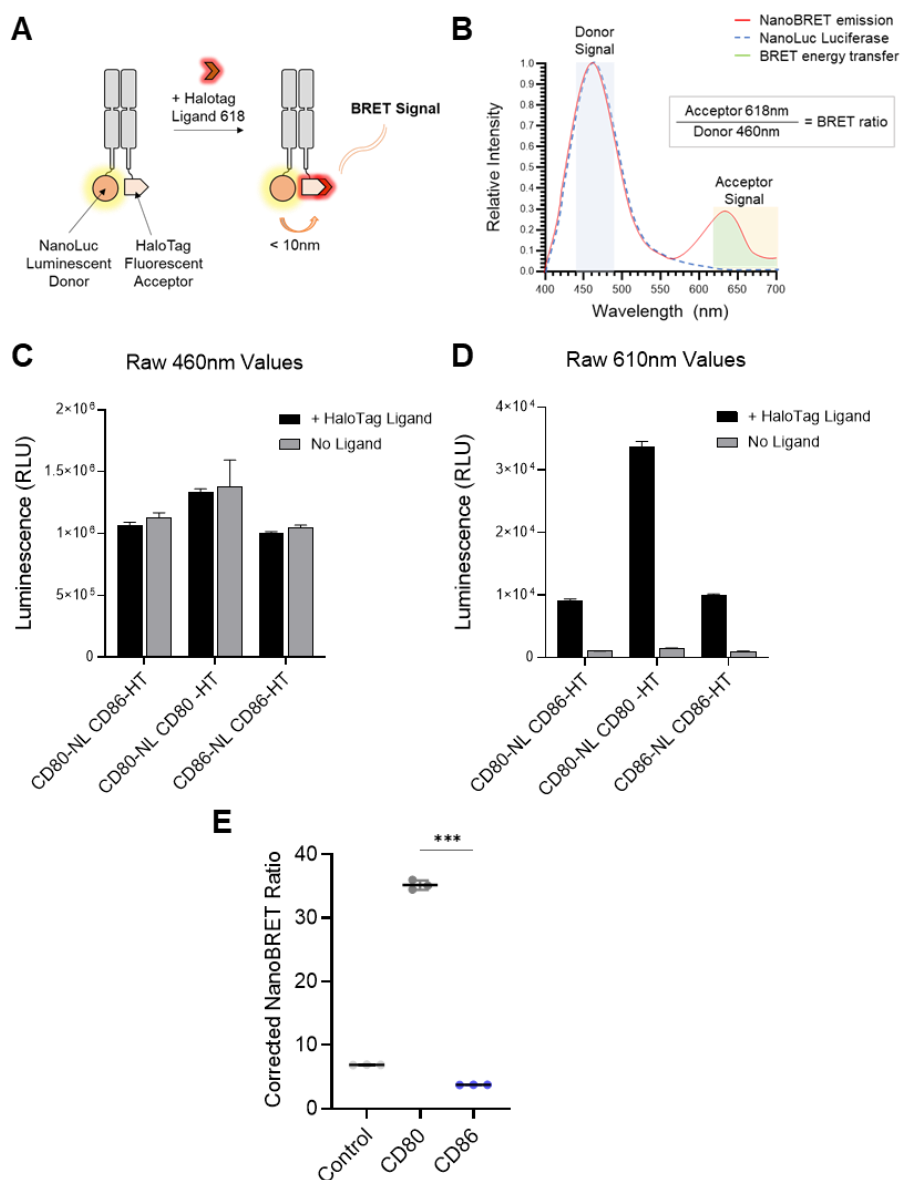
Figure 3.12. NanoBRET system reduces variability by correcting for transfection level, and successfully confirms CD80 and CD86 dimerisation states. (A). Schematic of NanoBRET assay depicting NanoLuciferase luminescent donor and HaloTag Acceptor, which becomes fluorescent following addition of HaloTag ligand 618. (B). Donor (460nm) and Acceptor (618nm) spectral separation and equation for calculation of NanoBRET ratio, adapted from (Dale et al., 2019).(C). Raw donor values in relative light units measured from the 460nm filter. (D). Raw acceptor values from the 610- long pass filter representing energy transfer from donor to acceptor. Conditions with no ligand represented as a control (No ligand). (E). Corrected BRET ratios calculated as Acceptor/Donor emissions (BRET ratio) minus BRET ratio from No Ligand conditions. Data from 3 wells from 1 independent repeat, representative from 3 independent repeats, analysed by Brown-Forsythe and Welch ANOVA test (***p≤0.001)
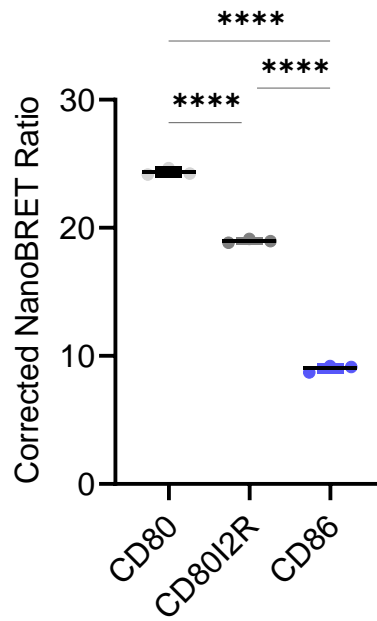
Figure 3. 13. Mutation of isoleucine residues reduces NanoBRET signal of CD80 homodimers. CD80, CD86 and CD80I2R-NanoLuc (donor) and HaloTag (acceptor) constructs were transfected at a 1:100 donor to acceptor ratio into CHO cells. 24 hours post-transfection, HaloTag 618 ligand was added, before reading donor (460nm) and acceptor (618nm) luminescence 24 hours later. Corrected NanoBRET ratios were calculated as Acceptor/Donor emissions (BRET ratio) minus BRET ratio from No Ligand conditions. Data from 3 wells from 1 independent repeat, representative from 3 independent repeats, analysed by ordinary one-way ANOVA, *p≤0.05, **p≤0.01,***p≤0.001, ****p≤0.0001.

Despite successfully generating a working NanoBRET system to study CD80 dimers, an important caveat is that a single endpoint measurement of BRET ratio does not confirm homodimerization itself, as it doesn't exclude the possibility of energy transfer resulting solely from random, non-specific protein interactions due to protein overexpression. Therefore, we sought to validate that the interactions observed were specific by performing a donor saturation assay (DSA).

The principle of the DSA is depicted in **Figure 3.14A.** Here, we transfect a fixed amount of donor (-NLuc tagged protein) with a gradually increasing concentration of HaloTagged acceptor protein. Theoretically, BRET will increase in a hyperbolic fashion if the two proteins specifically interact, eventually reaching a plateau indicating saturation when all the donors are bound with acceptor molecules. Conversely, non-specific BRET will increase linearly with increasing concentrations of acceptor due to the increased possibility of random BRET pair interactions.

We carried out the DSA for our 3 ligand NanoBRET pairs. **Figure 3.14B** shows the 460nm luminescence (measuring total -NLuc expression) for CD80, CD86 and CD80I2R NanoBRET pairs. Unexpectedly, donor luminescence signal was variable across all transfected ratios for all ligand pairs, despite the amount of donor DNA being held constant. This disparity may be due to variation of total DNA in each condition where the amounts of acceptor DNA alter overall transfection efficiency.

Nevertheless, BRET ratios (amount of acceptor signal corrected for amount of donor luminescence) showed that as expected, both CD80 and CD80I2R NanoBRET pairs gave a hyperbolic curve, strongly deviating from a

118

hypothetical linear fit (dashed lines), indicating a specific interaction (**Figure 3.14C).** Moreover, the energy transfer from CD80 NanoBRET pairs was consistently above that of CD80I2R, in line with our theory that the dynamic equilibrium between monomers and dimers is shifted towards monomers for CD80I2R. Additionally, whilst CD86 could be fitted to a hyperbolic curve, the increase in BRET ratios best fitted a simple linear regression supporting a non-specific interaction. However, this experiment showed at the acceptor and donor concentrations tested, saturation was not reached. Indeed, graphs did not appear to be approaching saturation, reflecting the caveat of unequal donor expression.
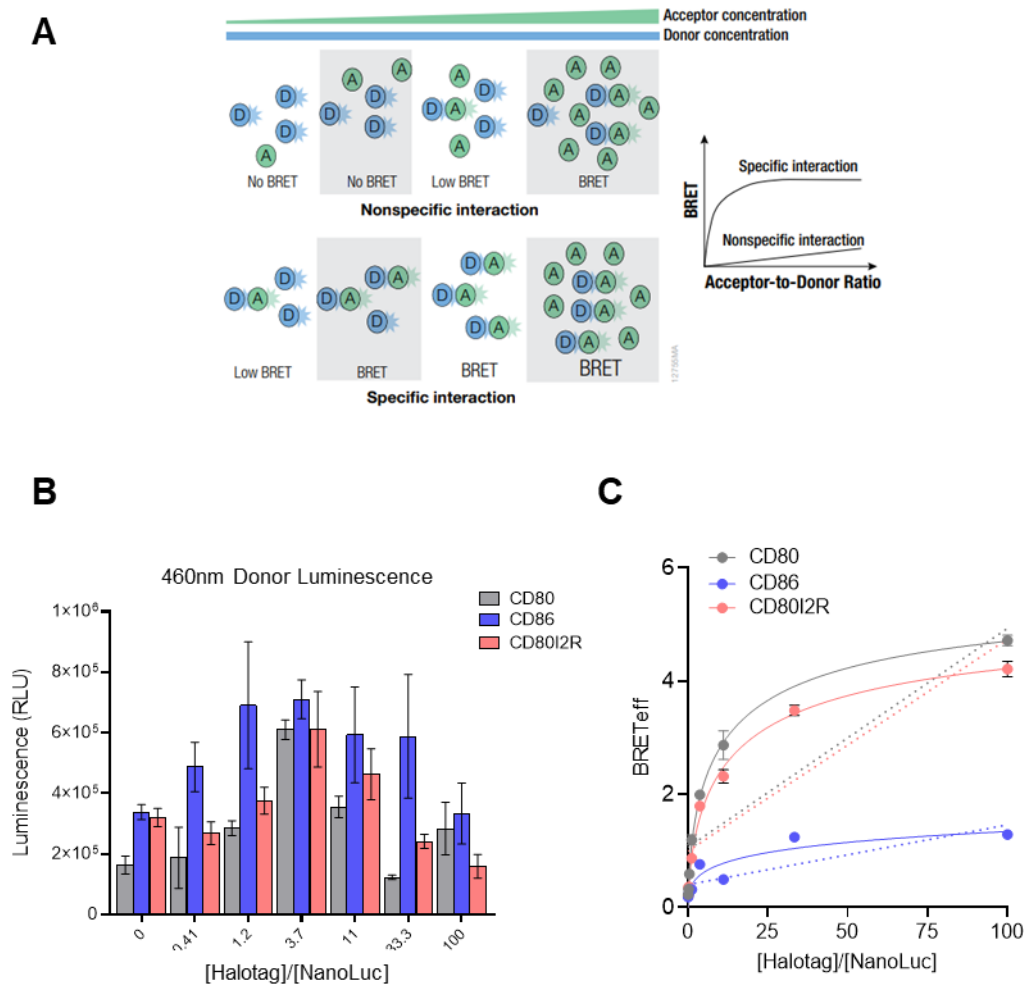
Figure 3. 14. Donor Saturation Assay shows specific interaction of CD80I2R monomers, and highlights need for assay optimization. (A). Principle of a donor saturation assay (taken from Wade et al., 2004). NanoBRET donor concentration is kept the same, but NanoBRET acceptor is increased. For specific interactions, resultant BRET with increase as a hyperbolic curve. For non-specific interactions, BRET will increase linearly. **(B and C).** CD80, CD86 and CD80I2R-NanoLuc (donor) and HaloTag (acceptor) NanoBRET pairs were used in a DSA. Raw donor values (460nm) shown in **(B)** and corrected BRET ratios calculated as Acceptor/Donor emissions (BRETeff) minus BRET ratio from No Ligand conditions shown in **(C).** Data fit to hyperbolic (full lines) or linear (dashed lines) relationships. Data from 3 wells from 1 independent repeat, representative from 3 independent repeats.

To overcome the issue of inconsistent DNA amounts, we decided to test our constructs in a 'type-1' BRET assay, developed specifically to detect protein oligomerization and previously reported to identify CD80 dimers and CD86 monomers (Felce and Davis, 2012).

In a 'type-1' experiment, the total amount of DNA transfected, and therefore protein expressed, is held constant but the ratio of acceptors/donors (-HaloTag/-NLuc) Is varied. The theoretical model for a type-1 BRET assay is depicted in **Figure 3.15A**, adapted from (Felce and Davis, 2012). This model shows that when density is kept the same, but acceptor/donor ratio is increased, efficiency of BRET ($BRET_{eff}$) for a monomeric protein will not change.

In contrast, when density is kept the same, but acceptor/donor ratio is increased, $BRET_{eff}$ for a dimeric protein will continue to increase. This is since, following an increase in the acceptor/donor ratio, a donor:donor interaction will be replaced by a donor:acceptor interaction, resulting in BRET. Therefore, the dependance of $BRET_{eff}$ on acceptor/donor ratio when proteins are expressed at a constant density can give insight into the dimerisation status of proteins, and so we used the 'type-1' assay to study the CD80I2R mutant.

As shown in **Figure 3.15B**, as expected there was a ratio-dependent decrease in luminescence arising from the -NLuc donor protein as the amount of NLuc was reduced, for CD80, CD86 and CD80I2R. Resultant $NanoBRET_{eff}$ for the three NanoBRET pairs are shown in **Figure 3.15C.** Strikingly, monomeric CD86 showed that after an acceptor/donor ratio of ~10/1, $BRET_{eff}$ remained constant at a $BRET_{eff}$ maxima of ~5. This result was in line with the assays theoretical predictions for monomeric proteins and aligned with published data (Felce and Davis, 2012). Similarly, $BRET_{eff}$ curves for CD80 WT NanoBRET pairs

were also in full accord with theoretical predications and previously published observations, showing an increase in $BRET_{eff}$ that was dependent on acceptor/donor ratios. Interestingly, whilst CD80I2R showed a hyperbolic curve and thus best fit the model of a dimeric interaction, the asymptote was again significantly lower than for CD80. This observation was consistent with CD80I2R being a weaker dimer than CD80, with $BRET_{eff}$ reflecting the steady state monomer-dimer equilibrium.
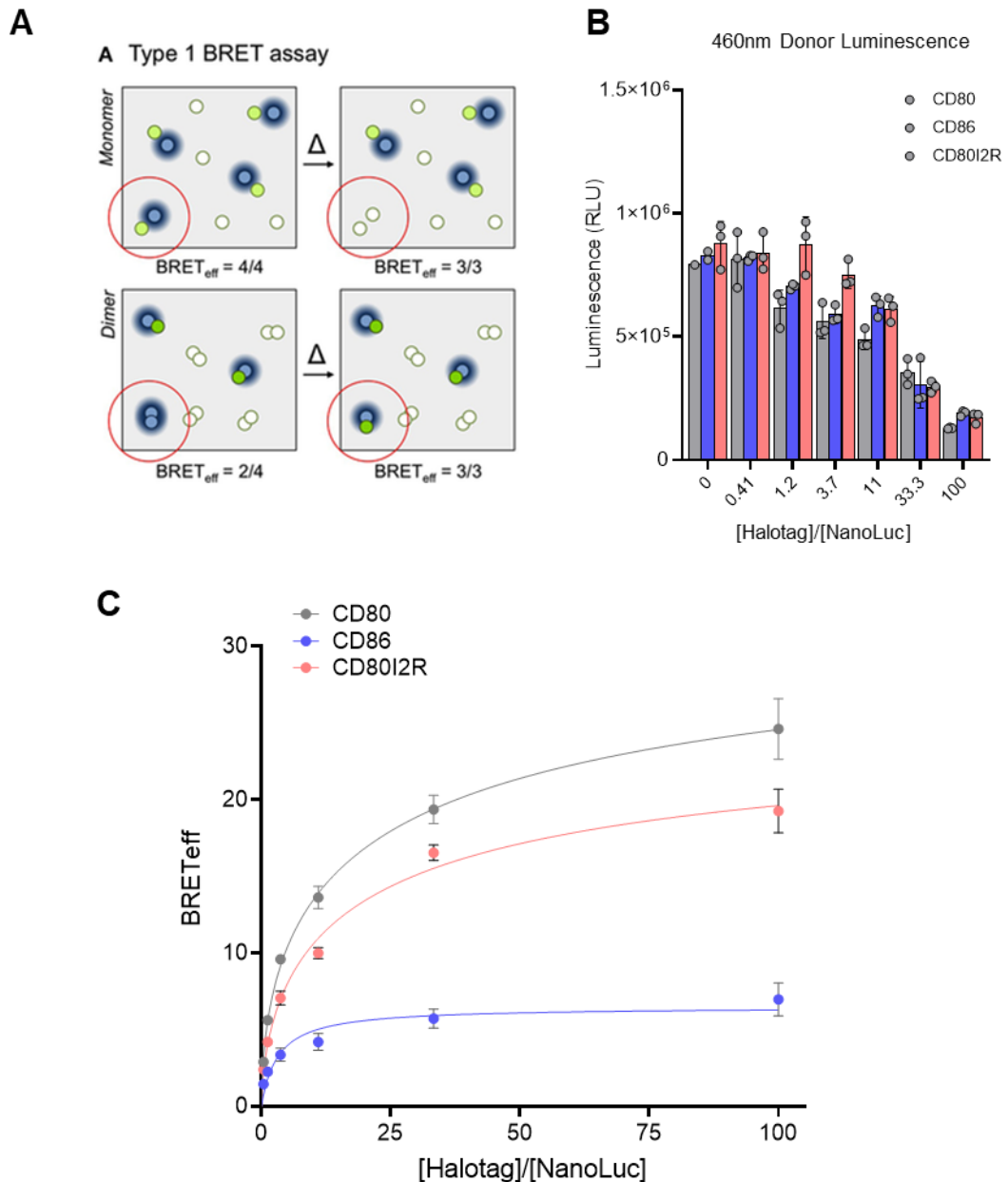
Figure 3. 15. Type 1 BRET assay: CD80I2R is impaired in dimerisation. (A).
Principle of a Type 1 BRET assay, taken from Felce et al., 2012. NanoBRET
donor and acceptor concentrations are varied, keeping total protein concentration
the same. For a monomer, $BRET_{eff}$ is unaffected by an increase in acceptor. For
a dimer, $BRET_{eff}$ is sensitive to changes in acceptor/donor ratio. Blue circles =
Luciferase Donor; Full Green Circles = Excited Fluorescent Donor; White Circles
= Unexcited Fluorescent Donor **(B and C).** CD80, CD86 and CD80I2R-NanoLuc
(donor) and HaloTag (acceptor) NanoBRET pairs were used in a Type 1 BRET
assay. Raw donor values (460nm) shown in **(B)** are used to normalize
expression, and corrected BRET ratios calculated as Acceptor/Donor emissions
(BRET ratio) minus BRET ratio from No Ligand conditions shown in **(C).** Data fit
to hyperbolic relationships. Data from 3 wells from 1 independent repeat,
representative from 3 independent repeats.

Previous results from the NanoBiT assays suggested that CTLA4-Ig binding could stabilize CD80 and CD80I2R dimers. Therefore, we wanted to see if we could observe the same effect in our NanoBRET 'type-1' assay. For this, we performed the 'Type-1' assay as described above, but incubated transfected cells with or without CTLA4-Ig for 1 hour prior to addition of the luciferase substrate. As shown in **Figure 3.16,** addition of CTLA4-Ig strongly enhanced $BRET_{eff}$ calculated from CD80, supporting stabilization of CD80 dimers, but had no effect on CD86 BRET ratio. Surprisingly, addition of CTLA4-Ig had a minimal, non-significant effect on the $BRET_{eff}$ resulting from CD80I2R NanoBRET pairs, suggesting CTLA4-Ig cannot promote dimer assembly.

Finally, we used NanoBRET to further characterize the impact of PDL1 on CD80 homo-dimerisation and the influence of CTLA4 binding on these interactions. In this experiment, we used PDL1-NLuc as the donor, and co-transfected CD80-, CD86- or CD80I2R-HaloTag as the acceptor, or an empty vector control, at a 1:100 donor to acceptor ratio as this gave maximal $BRET_{eff},$ as above. As shown in **Figure 3.17**, CD80 homodimers showed a strong BRET ratio that was significantly enhanced by binding of CTLA4-Ig. $BRET_{eff}$ of PDL1:CD80 heterodimers was very similar to that of CD80 homodimers, reflecting their ability to interact in *cis*. Interestingly, binding of CTLA4-Ig did not significantly reduce $BRET_{eff}$ for the CD80:PDL1 interaction, suggest CTLA4-Ig binding does not disrupt CD80:PDL1 heterodimers. Moreover, $BRET_{eff}$ for PDL1:CD80I2R BRET pairs was above that of negative controls, but not as high as CD80:PDL1 heterodimers. Despite not reaching significance due to lack of power, this trend was in support of the CD80I2R mutations disrupting the ability to bind PDL1 in *cis* and overall supporting that this binding takes place in the hydrophobic dimer interface of CD80.

Overall, application of NanoBRET in the various assays described consistently revealed a reduction in $BRET_{eff}$ for CD80I2R than CD80, consistent with the notion that CD80I2R exists as a lower affinity/impaired dimer. Moreover, considering results from CTLA4-Ig binding curves and the minimal effect on NanoBRET ratio in the 'type-1' assay, we concluded that CD80I2R preferentially binds as a monovalent interaction to CTLA4. As such, CD80I2R can be used to model decreased ligand valency within the CTLA4 system. Likewise, NanoBiT studies supported PDL1 co-expression disrupting CD80 homodimer formation and therefore we can use PDL1 as an endogenous tool to study the impact of loss of dimerisation.

A summary of the predicted interactions between all CTLA4:ligand combinations is shown in **Figure 3.18**, with all of the altered biophysical properties as a result of mutations depicted.
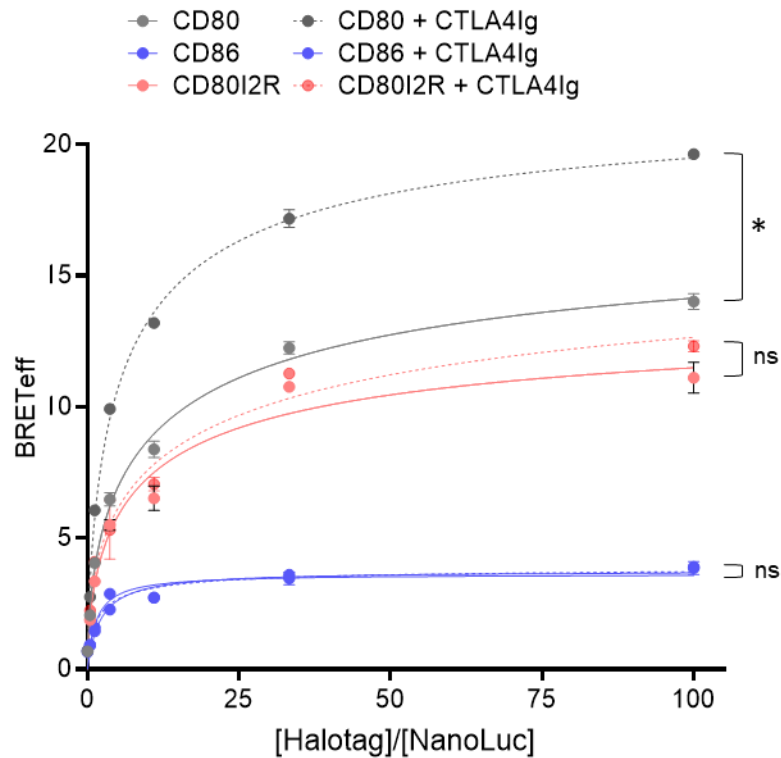
Figure 3. 16. CTLA4-Ig binding cannot stabilize CD80I2R dimers. CD80, CD86 and CD80I2R-NanoLuc (donor) and HaloTag (acceptor) NanoBRET pairs were used in a Type 1 BRET assay. 48 hours post-transfection, 10µg/ml of CTLA4-Ig (Abatacept) was added for 1 hour at 37ºC before addition of luminescent substrate. Corrected BRET ratios calculated as Acceptor/Donor emissions minus BRET ratio from No Ligand conditions (BRETeff). Data fit to hyperbolic relationships –CTLA4 Ig (full lines) or + CTLA4 Ig (dashed lines). Data shown from 3 wells from 1 independent repeat, representative from 3 independent repeats, analysed by two-way ANOVA (*p≤0.05, **p≤0.01,***p≤0.001, ****p≤0.0001).
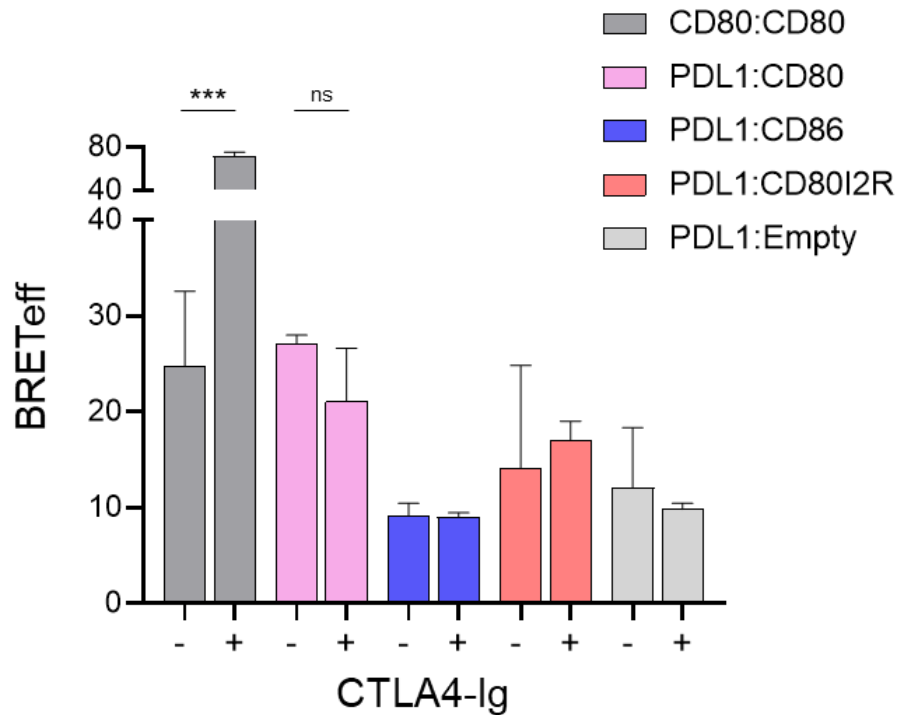
Figure 3. 17. *Cis* **interaction of PDL1 and CD80 is detectable by NanoBRET and disrupted by CD80I2R mutation.** CD80, and PDL1-Nluc (donor) and CD80-, CD86- and CD80I2R-HaloTag (acceptor) constructs (or empty vector control) were transfected at a 1:100 donor to acceptor ratio into CHO cells. 24 hours post-transfection, HaloTag 618 ligand was added, before reading donor (460nm) and acceptor (618nm) luminescence 24 hours later. 1 hour before luminescence readout, 10µg/ml of CTLA4-Ig was added at 37ºC, or DMSO control. Corrected NanoBRET ratios were calculated as Acceptor/Donor emissions (BRET ratio) minus BRET ratio from No Ligand conditions. Data from 3 wells from 1 independent repeat. Data analysed by 2-way ANOVA, *p≤0.05, **p≤0.01,***p≤0.001, ****p≤0.0001.
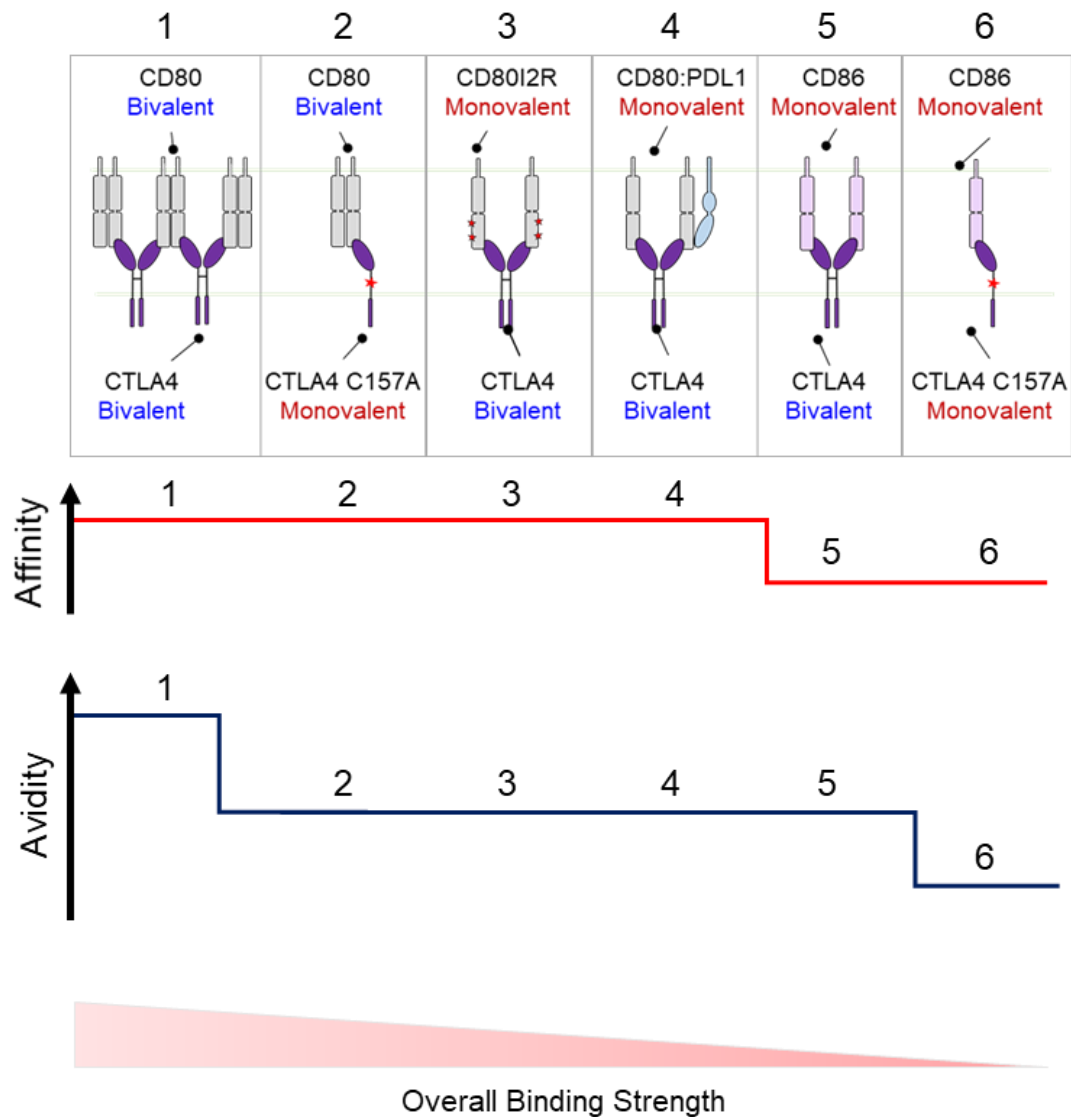
Figure 3. 18. Summary of biophysical characteristics of wild-type and mutant receptor:ligand interactions used to study dimerisation in the CTLA4 system. Cartoon depiction of predicted wild-type and mutant receptor: ligand interactions in order from strongest to weakest overall binding strength: 1. CTLA4 dimers show bivalent binding to also bivalent CD80 homodimers, forming lattices with high affinity and high avidity. 2. Mutant CTLA4 C157A is a monomer showing monovalent binding CD80 dimers with equal affinity but loss of avidity. 3. Mutant CD80I2R shows monovalent binding to bivalent CTLA4, again reducing avidity. 4. CD80:PDL1 *cis* binding inhibits CD80 dimerisation, making CD80 a monovalent binder to CTLA4, reducing avidity. 5. Native monomer CD86 is monovalent, binding bivalent CTLA4 with lower affinity. 6. Monovalent CD86 binds mutant monovalent CTLA4 C157A with weakest affinity and avidity.

3.3. Discussion

The potential of proteins to self-associate to form dimers or higher-order oligomers is fundamental to a wide range of biological mechanisms including enzymes, transcription factors and immunoglobulins. Broadly, dimer/oligomerization of a protein acts to increase the avidity of an interaction and is therefore a key property, in addition to affinity, that defines the overall strength of a ligand-receptor interaction. Moreover, whether proteins form stable or transient, homo or hetero-oligomeric complexes underpins physiological activity of an extensive number of processes, such as regulating GPCR mediated signalling complexes (Milligan et al., 2019). Increasingly, the delineation between affinity and avidity is proving its importance by therapeutic development of protein-protein interaction (PPI) inhibitors, a class of molecule which act to modulate homodimer formation and regulate downstream functions.

Although it is known that CD80 is a non-covalent dimer that can form avid lattice structures with CTLA4, and this is a fundamental difference to monomeric CD86, the relevance of this oligomerization is not understood. Given the extensive evidence demonstrating evolution of homodimers due to the need for intricate immune regulation, it is likely this property has implications for CTLA4 function. In this chapter, we aimed to remove the avidity influence on receptor-ligand interactions by creating mutants unable to form functional dimers. By doing this, we could exploit monomeric receptor-ligand interactions to study the impact of loss of avidity in the context of CTLA4 transendocytosis and CTLA4 regulated CD28 co-stimulatory responses *in vitro*.

3.3.1. Mutation at position C157 prevents CTLA4 dimerisation

The ability of CTLA4 to form homodimers underlies its ability to bind bivalently to both CD80 and CD86 (Linsley et al., 1994). Therefore, preventing CTLA4 dimerisation will create a monovalent CTLA4. Here, we were able to successfully generate monomeric CTLA4 by site-directed mutagenesis at position C157. Moreover, we show that CTLA4 C157A has still localized within intracellular vesicles and exhibited the same cell surface localization profile as CTLA4 WT. The generation of monomeric CTLA4 by a C157 mutation has been previously used to study the relevance of lattice formation in the context of localization within lipid rafts at the cSMAC. Intriguingly, these studies reported no defect of monomeric CTLA4 in IS localization or subsequent T cell inhibition (Darlington et al., 2005; Yokosuka et al., 2010). This is surprising, as we would predict a loss in bivalency would impair binding strength due to loss of avidity influence, and would therefore have implications for the ability of CTLA-4 to control CD28-ligand interactions. This concept is explored further in **Chapter 4,** using functional assays.

Despite these previous studies demonstrating additional glycosylation mutations were required to inhibit dimerisation, we observed a defect in trafficking and antibody uptake with our CTLA4 NNC mutant. Importantly, regulation of surface CTLA-4 expression has been closely linked to N-glycan-branching pathways downstream of TCR signalling, as a mechanism to promote surface retention of CTLA4 in activated T cells (Lau et al., 2007). Moreover, glycosylation is thought to be vital for correct protein folding, vesicular formation, and endocytic trafficking (Fisher et al., 2016; Shental-Bechor et al., 2008). Rapid internalization by CME and membrane recycling via endosomes is crucial to CTLA4 function in

transendocytosis (Qureshi et al., 2012) and therefore we concluded that CTLA4 C157A is acceptable as a monomeric mutant to study loss of bivalency, without obvious caveats of altered surface expression.

3.3.2. Mutations within the CD80 hydrophobic interface impair homodimer formation

It is widely accepted that CD80 forms non-covalent homodimers at the cell surface. Early studies by Ikemizu et al., solving the crystal structure of the CD80 homodimer identified hydrophobic residues responsible for this intermolecular contact, including the I58 and I62 residues modelled in this study (Ikemizu et al., 2000). In keeping with these ideas, we show modelling of these residues, confirming I58 and I62s contribution to the CD80 homodimer interface. Indeed, hydrophobic residues are often predominant at the interface of non-covalent homodimers (Zhanhua et al., 2005), with I68 also confirmed in FRET studies to disrupt dimerisation of CD80 (Bhatia et al., 2005). Moreover, we demonstrate that when substituted for arginine, homodimer formation is disrupted, likely due to the presence of large and highly charged residues causing electrostatic repulsion. Our results from both NanoBiT and NanoBRET assays support this modelling, showing CD80I2R is impaired in dimer formation. Surprisingly, given insertion of two highly charged arginine residues into the interface, our data also suggests CD80I2R was not completely disrupted, as NanoBRET experiments showed increased energy transfer compared to *bona fide* monomer, CD86. Together these data suggest, CD80I2R is likely impaired in dimerisation, rather than completely monomeric as is the case for CD86.

As predicted, we found that CD86 exists as a monomer, and displays weak, non-specific interactions via NanoBRET assays. Since analytical

ultracentrifugation experiments revealed that CD86 does not self-associate (Collins et al., 2002), CD86 expression as a monomeric protein has been widely accepted without much debate. However, prior to this key work, the prevailing view was both CD80 and CD86 had similar structures and binding capabilities for CTLA4 and CD28 (Linsley et al., 1994) with differences between ligands were mainly in regard to cellular and temporal expression (Collins et al., 2005; Sharpe et al., 2002). Similarities were further acknowledged based on structural data, demonstrating CTLA4 interacts orthogonally with both CD80 and CD86 in lattice-arrays (Schwartz et al., 2001), which whilst now conclusive for CD80, has been refuted for CD86 (Collins et al., 2002). Indeed, publication of such ideas influenced the field to the point in which CD80 and CD86 are still commonly referred to as 'CD80/CD86' or 'B7', over 20 years later. This nomenclature has been retained based on their predominant similarity being binding to both CTLA4 and CD28, with differential functions being famously hard to delineate. This is evident in CD80 and CD86 knock-out mice showing no clear phenotype, indicating the overall CD28-CTLA-4 system can still function using a single ligand. Nonetheless, experiments carried out using single knockout mice are very limited to date. Despite this original view, CD86 is accepted to not form dimers, and as such cannot form lattices with CTLA4 (Collins et al., 2002).

In contrast, CD80 does self-associate, and is in a dynamic equilibrium between a monomeric and dimeric form, with a K_d of 20-50µM and rapid rate of dissociation (10^{-2} s^{-1}) (Ikemizu et al., 2000). Importantly, this is regarded in pharmacological terms as a very low affinity interaction. Therefore, rather than completely impairing dimerisation it is plausible our Ile → Arg mutations shift this equilibrium further towards the monomeric state through reduction in homodimer affinity. As such, at steady state, the proportion of dimers to monomers will be

shifted towards monomers for a lower affinity homodimer interaction, like that for CD80I2R.

In accordance with this idea, we demonstrate a reduction in luminescence resulting from our NanoBiT assay for the CD80I2R NanoBiT pair, compared to CD80 WT. Moreover, we observe a reduction in NanoBRET from the CD80I2R BRET pair at both end-point readouts and the 'type-1' BRET assay, specifically designed to characterize dimeric interaction. Indeed, previous studies using CD80 and CD86 BRET pairs in the 'type-1' assay showed similar results to those presented here (Felce et al., 2012), whereby CD80 showed a hyperbolic curve, whilst CD86 saturates at a low BRET efficiency. Moreover, the study by Felce et al., discusses the theory behind the assay, maintaining that the observed asymptote reflects steady state dimer interactions and demonstrating an increase in asymptote for constitutive dimers e.g., CTLA4 and CD28 (Felce and Davis, 2012). This group have also published BRET-based assays which allow quantitative interpretation of dimer equilibriums, more commonly used in GPCR studies (Kufareva et al., 2013; Salahpour et al., 2012). Whilst our data show CD80I2R shows weaker dimer interaction, due to a decrease in asymptote via NanoBRET, it would be of great interest to use further BRET based assays alongside classic SPR studies to quantify the affinity of the CD80I2R interaction.

3.3.3. Valency of ligand:CTLA4 interaction is revealed by CTLA4-Ig treatment in BRET assays

From our results, we conclude that CD80I2R binds monovalently to CTLA4 as no increase in nanoBRET signal is observed following CTLA4-Ig binding. In contrast, we show that CTLA4-Ig binding can stabilize CD80 WT homodimers, revealed by an increase in NanoBRET efficiency for CD80 BRET pairs that was

not seen for CD80I2R, or monovalent CD86. Indeed, the CD80 dimer interface is on the opposite face of the CTLA4 binding domain, supporting CD80 as a bivalent, homodimeric molecule and providing structural support for lattice formation. As the CD80I2R mutant likely exhibits monovalent binding to CTLA4-Ig, lattice formation is inhibited, despite being able to weakly dimerise. The concept that dimerisation doesn't automatically generate bivalency is nicely demonstrated by CD28 - a covalent homodimer only able to bind monovalently to both CD80 and CD86 (discussed further in *Chapter 6*). Notably, original SPR studies reporting the affinity of CD80 to CTLA4 were based on monovalent interactions, with soluble CD80 ran over immobilized dimeric CTLA4-Ig at a Kd of 0.38μM (Linsley et al., 1994). However, as structural data suggests CD80 binds bivalently, the actual binding strength is likely to be several-fold higher. Indeed, earlier studies estimated lower Kd values (~12 nM) when performed with dimeric CD80-Igs, indicating an avidity enhancement. Moreover, reverse experiments whereby dimeric CTLA4Fc was injected over immobilized CD80 bound with higher avidity, demonstrated by a 100-fold increase in the dissociation half-life ($t_{1/2}$ 200s vs ~2s) (Van Der Merwe et al., 1997; Collins et al., 2002). Together, it is sensible to predict CD80 and CD80I2R bind with similar affinities, but altered avidities.

Importantly, CTLA4-Ig (Abatacept) is a disulphide linked dimer through the native disulphide linkage in CTLA4, as IgG1 hinge disulphides were eliminated during construction (**Figure 3.19A**) (Khoury et al., 2017). Therefore, we assume soluble CTLA4-Ig reflects generally cell-bound full length CTLA4 binding, regarding steric effects. As such, data interpretation of results presented in this thesis was initially based on the idea that CTLA4 binding in a manner that cross-links two CD80 homodimers, as opposed to stabilizing one homodimer. However,

two possible binding orientations are shown in **Figure 3.19B** (taken from Izemizu et al., 2000). Izemizu et al., considered these two possibilities, revealing the former is the most sterically favoured for cell bound CTLA4, and coined the avidity model of CTLA4:CD80 lattices. Whether soluble CTLA4-Ig can only bind CD80 in this orientation is unknown and has not been directly studied. One possibility is that in the case of CD80 WT, CTLA4-Ig binding by either mechanism shown in **Figure 3.19B**, where either would result in the increased BRET efficiency we observed. This is because the donor and acceptor tags required for BRET would be bought into closer proximity either by stabilization of one homodimer or bringing together two homodimers if the proximal homodimer units had complementary tags. This explanation for our observations are reasonable, as crystal studies predict that CTLA4:CD80 complexes would have a separation of 105 Å (10.5nm). This is within the distance detectable by NanoBRET, which has been reported to span a chromophore-to-chromophore distance of 12nm (Weihs et al., 2020), despite guidelines suggesting sensitivity is only <10nm.

In contrast to WT CD80, whilst CTLA4 itself can bind to two CD80I2R monomers, supported by our observations with CTLA4-Ig-APC binding curves **(Fig 3.5),** higher order lattice formation is not possible, as seen by an absence in increased NanoBRET signal with the CD80I2R BRET pair.

Using a different system, data showing the addition of CTLA4-Ig did increase luminescence from CD80I2R pairs was observed using the NanoBiT interaction system. However, the contrasting results between NanoBiT and NanoBRET assays can be explained by considering the differences between the two assays used. Whilst NanoBiT relies on a physical association between LrgBiT and SmlBiT subunits, NanoBRET is an energy-transfer based proximity measure.

Indeed, NanoBiT fragments weakly associate with a Kd of ~190µM, with manufactures' guidelines suggesting this system should not be used to study interactions weaker than 10µM. Our data predicts the CD80I2R homodimer affinity is lower than 20-50µM, the affinity of CD80 homodimers (Ikemizu et al., 2003). Therefore, the increase in luminescence observed may result from CTLA4 bivalently binding to two CD80I2R molecules thereby promoting the association of the NanoBiT tags, rather than CD80I2R itself. This would explain why in the proximity based NanoBRET assay you do not see an increased signal, as there is not a sufficient association of the NanoLuc and HaloTag, which have no intrinsic affinity for each other.

Altogether, our findings support that CD80I2R is a weak dimer, that exhibits monovalent binding and thus inability to form highly avid lattices with CTLA4. Therefore, CD80I2R can be used to study the impact of avidity enhancement in our models of CTLA4 transendocytosis and on CD28 co-stimulatory responses.
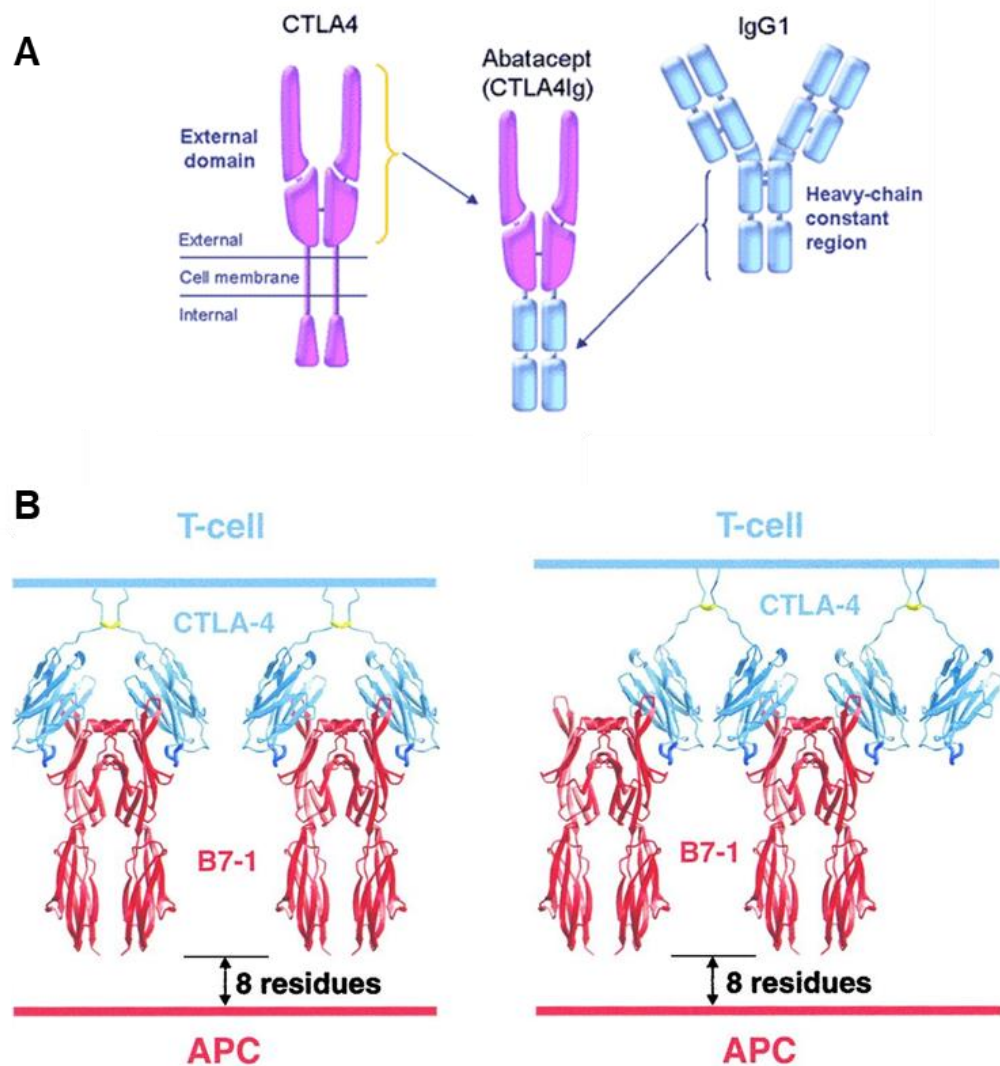
Figure 3. 19. CTLA4:CD80 homodimers could bind in two potential complexes. (A) Structure of Abatacept (CTLA4-Ig), taken from Khoury et al., 2017. **(B)** Taken from Izemizu et al., 2000, Immunity. Crystal structures of CD80 (B7-1) (red) binding at the opposite face of the homodimer interface to CTLA4 homodimers (blue), connected by a disulphide link at C157 (yellow) potentially form two types of complex. (left) paired homodimers or (right) lattice complexes where CTLA4 bridges two CD80 dimers.

3.3.4. Cis expression of PDL1 disrupts CD80 homodimerisation

Since the *cis*-interaction between CD80 and PDL1 was identified (Chaudhri et al., 2018), multiple studies have postulated how this interaction affects CD80 homodimerization. Our data using a competition based NanoBiT assay showed that presence of PDL1 disrupts CD80 homo-dimerisation, as well as observations using the NanoBRET system showing a direct interaction using PDL1-NanoLuc and CD80-HT. Interestingly, CD80 binds with higher affinity to PD-L1(K_D 17.8μM), than to itself (~30-50 μM) (Butte et al., 2008, 2007; Cheng et al., 2013). Garrett-Thompson et al., used mutagenesis to query CD80 residues important for PD-L1 binding, with those identified mapping to the CD80 homodimer interface (Garrett-Thomson et al., 2020). Furthermore, using FRET based assays Zhao et al., demonstrated PD-L1:CD80 cis-heterodimerization disrupts CD80 homodimerization, and theorized this prevented high avidity lattice formation. In contrast, Sugira et al., identified suggested this did not impair CD80 binding to CTLA4 and in keeping with the concept that the CD80-PD-L1 *cis*-interaction occurs at the opposite face to the CTLA4 binding site (Sugiura et al., 2019). Our results using the CD80I2R mutant are in keeping with these ideas, as it both prevents homo-dimerisation, but also PDL1 hetero-dimerisation seen directly by NanoBRET and indirectly by recovery of PDL1 staining when expressed in *cis* with CD80I2R. In line with this, a mutated human CD80-I92E (similar to our I-R mutants) variant was reported to lack *cis*-CD80:PDL1 interactions (Sugiura et al., 2019). Together, multiple studies support our observations that PDL1 *cis* expression disrupts CD80 homodimerization.

How PDL1-CD80 interactions are impacted by CTLA4 binding to CD80 is at present unclear. In this Chapter, we show evidence that the CD80:PDL1

interaction is disrupted by CTLA4-Ig binding, although data did not reach significance. Binding of CD80 to PD-L1 inhibits PD-1 engagement, in agreement with structural studies showing an acute angle of PD-L1 engagement to PD-1 with its binding site on the face of the PD-L1 molecule overlapping with the CD80 interface (Lin et al., 2008; Sansom et al., 2019). Therefore, how this interaction impairs CTLA4 binding remains contentious., Zhao et al., demonstrated PDL1:CD80 cis heteromerization inhibits both CD80 homodimerization and CD80:CTLA4 interactions (Zhao et al., 2019). This is perplexing, as the CD80 dimer interaction is placed on the opposite face of the CTLA4 binding site (Stamper et al., 2001). In addition, this study paradoxically demonstrates that CD28 binding is unimpaired, despite both CTLA4 and CD28 binding CD80 at the highly conserved "MYPPPY" motif. In an opposing view, our group have recently demonstrated that PDL1:CD80 *cis* heteromerization does not inhibit CD80:CTLA4 interactions, as CD80 still undergoes transendocytosis and CTLA-4-Ig can co-precipitate both CD80 and PD-L1. Indeed, we show CD80 transendocytosis results in recovery of PD-L1:PD-1 interactions, thereby revealing an extrinsic crosstalk between inhibitory receptors (Kennedy et al., 2022). However, we also showed that CTLA4-Ig binding to CD80:PDL1 (where transendocytosis is not a consideration) showed very little revival of PD-1-Ig binding, or antibody staining, suggesting CTLA4 binding alone does not free PD-L1 (Kennedy et al., 2022). Therefore, if CTLA4 can bind to CD80-PD-L1 heterodimers, this supports the possibility of altered CD80 binding to CTLA4 and therefore loss of lattice formation when PDL1 is expressed.

3.3.5. Summary

Overall, data presented in this Chapter details the successful generation of CTLA4 and CD80 mutant constructs which are impaired in dimerisation, termed CTLA4 C157A and CD80I2R. We have validated *in vitro* methods to characterize the impact of these mutations by NanoBiT and NanoBRET, confirming CD80I2R is monovalent, and therefore cannot form higher-order lattice structures with CTLA4. Finally, we show that CD80:PDL1 *cis* expression also disrupts the ability of CD80 to dimerize. As CTLA4:CD80 lattices are dependent on a bivalent dimer:dimer interactions, we can therefore use these mutants to look at the dependence of CD80 induced lattice formation on CTLA4 function.

Chapter 4: Dimerisation status and avidity of CTLA4-ligand interactions regulates CTLA4 ubiquitination and transendocytosis efficiency.

4.1. Introduction

Mechanistically, CTLA4 has been shown to physically remove CD80 and CD86 from opposing cells and internalise them in a process termed transendocytosis, destroying captured ligands in lysosomes (Qureshi et al., 2011) thereby limiting ligand availability for CD28 co-stimulation. This exploits the dynamic intracellular trafficking of CTLA4 due to clathrin-mediated endocytosis and provides a rationale for its predominantly intracellular vesicular location (Qureshi et al., 2012a). Moreover, modelling of T cell:APC interactions has suggested that the affinity bias of CTLA4>CD28 is not sufficient to control co-stimulation following low affinity self-antigen presentation to TCR on Teffs, and physical depletion of ligand is likely required to prevent autoimmune responses (Sugár et al., 2017). *In vivo*, transendocytosis by CTLA4 expressing Tregs has been shown to target migratory dendritic cells, providing further support for this extrinsic model (Ovcinnikovs et al., 2019).

However, there are some fundamental aspects of this system which are not understood. Specifically, why there is both a high affinity dimeric ligand, CD80, capable of forming high avidity dimer:dimer interactions, as well as a low affinity monomeric ligand, CD86. Recent work from our lab, together with work presented within this chapter, begins to address this question, revealing that transendocytosis of CD80 and CD86 results in markedly different fates for CTLA4 (Kennedy et al. 2022). Our data shows that following transendocytosis of CD80,

CTLA4 and CD80 remain bound, and CTLA4 undergoes post-translational modification in the form of ubiquitination. In contrast, transendocytosis of the weaker affinity ligand CD86 permits CTLA4 dissociation and re-entry back into the LRBA-dependent recycling pathway. In this model, CD80 is therefore proposed to be a negative regulator of CTLA4, protecting CD86 from transendocytosis and promoting CD86:CD28 mediated co-stimulation. However, understanding of how this relates to the biophysical properties of the interactions, with regards to CD80 homodimer and CTLA4:CD80 lattice formation, for example, is lacking. These properties are of particular interest considering *cis* expression of PDL1 binds to CD80 and prevents this higher-order structure formation (Garrett-Thomson et al., 2020).

In this chapter, we studied how affinity, avidity and valency differences seen in CD80 and CD86 affect CTLA4 fate, using mutants developed in the previous chapter (see **Chapter 3**). Our work reveals that the avid CTLA4:CD80 lattice is a pre-requisite for CTLA4 ubiquitination and sequestration in intracellular compartments. We also show evidence that a monovalent CD80 mutant, or CD80 when co-expressed with PDL1, are more efficient for transendocytosis. We propose this is due to its superior affinity compared to CD86, plus an increased ability to dissociate permitting CTLA4 recycling in a CD86-like manner. Consequently, for CD80, avidity enhancement is counter-productive with regards to optimal ligand removal from and seems to be a mechanism for maintaining CD80-CTLA4 interactions. Overall, this work supports the idea that the efficiency of CTLA4 transendocytosis is a balance between affinity and capacity to recycle, controlled by avidity.

4.2. Results

4.2.1. Dynamic intracellular trafficking of CTLA4 is not altered by C157A mutation

The presence of CTLA4 in intracellular vesicles enables rapid recycling to the cell surface, a likely significant feature for transendocytosis. We initially wanted to characterize the capacity of a monomeric CTLA4 (C157A) to recycle. For this, we developed a flow cytometry assay where CTLA4 was stained with an unconjugated ectodomain primary antibody (Tremelimumab) for 60 minutes at 37°C, allowing labelling of trafficking CTLA4 molecules via the cell surface. Cells were then placed on ice and stained with a fluorophore conjugated α-hu-Fc secondary antibody to give a baseline surface level. Moving cells to 37°C for indicated times (**Figure 4.1**) then allowed CTLA4 trafficking to resume, and the secondary antibody to label any primary antibody recycled back to the cell surface. Both CTLA4 WT and CTLA4 C157A showed the same increase in recycling secondary antibody staining over time (**Figure 4.1**), suggesting dimeric and monomeric CTLA4 have the same propensity to be recycled back to the plasma membrane following internalization. Together with observations in the previous chapter that CTLA4 C157A is also observed in intracellular vesicles (**Figure 3.3**), this data supported monomeric CTLA4 retaining similar characteristics to WT with regard to intracellular expression and controlled cell surface trafficking and internalization.
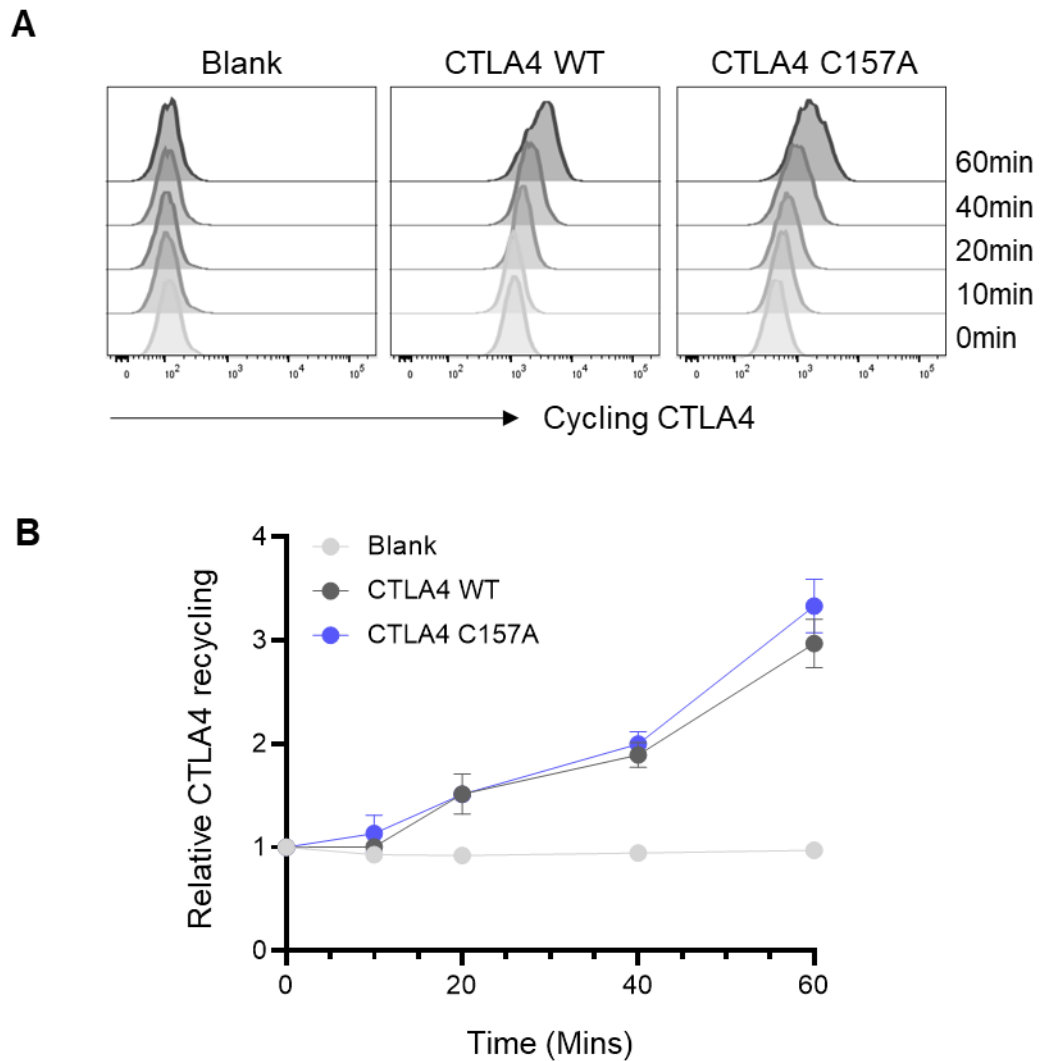
Figure 4. 1. C157A mutation does not affect CTLA4 recycling. Untransduced CHO cells (blank), or CHO cells transduced with CTLA4 WT or CTLA4 C157A were fed with unconjugated anti-CTLA4 (Tremelimumab) for 1 hr. Cells were then moved to ice, and stained with α-human-Fc-AF488 for 10 mins, before moving to 37ºC for indicated time points. Cells were fixed and analysed by flow cytometry, with histograms shown in **(A). (B).** Graph shows cycling CTLA4 relative to time 0. Data from n=3 presented as mean +- SD.

4.2.2. Loss of CTLA4 bivalency significantly impairs CD86 ligand binding compared to CD80

Having confirmed CTLA4 C157A exhibits the same trafficking properties as CTLA4 WT, we then wanted to see whether ligand binding properties were altered. For this, we used soluble CD80-Ig and CD86-Ig chimeras, or an isotype control, to stain for CTLA4 in fixed and permeabilized cells. To normalize ligand binding to total CTLA4 expression we co-stained with a C-terminal antibody. CD80-Ig and CD86-Ig bound robustly to CTLA4 WT, with more CD80-Ig binding reflecting higher affinity relative to CD86-Ig (**Figure 4.2A**). Interestingly, despite theoretical loss of avidity, staining of CTLA4 C157A showed no significant difference than to CTLA4 WT with either ligand **(Figure 4.2B).** Therefore, we concluded that CTLA4 C157A does not possess any structural changes which negatively impact the ligand binding site, and any avidity differences were not detectable under the assay conditions used.

We extended this analysis by looking at staining properties following CD80-Ig and CD86-Ig incubation with CTLA4 WT and C157A for 1 hour 37°C, permitting CTLA4 trafficking (**Figure 4.3**), therefore antibody staining reflects ligand-Ig uptake. CTLA4 C157A showed a non-significant impairment in CD80-Ig staining compared to CTLA4 WT. In contrast, CTLA4 C157A showed significantly reduced staining by CD86-Ig in comparison to CTLA4 WT (**Figure 4.3A, B**). This suggested either a reduced ability to bind and internalize CD86-Ig, or that internalized ligand is more rapidly degraded and thus can no longer be detected.

To distinguish between these possibilities, we used ammonium chloride (NH_4Cl) to neutralize lysosomal pH and prevent protein degradation. Interestingly, NH_4Cl addition normalized the subtle change observed between

CTLA4 WT and CTLA4 C157A CD80-IgG binding, suggesting both variants displayed similar efficiency for CD80-IgG uptake, but soluble ligand might be differentially processed post-internalization. In contrast, NH_4Cl treatment increased CD86-Ig binding to CTLA4 C157A, but it did not fully recover to CTLA4 WT levels. Together, this suggested that CTLA4 C157A is impaired in CD86 uptake, but not CD80 (**Figure 4.3A, B**). However, it is noted that CD86-Ig used in these assays is dimeric in contrast to WT CD86.
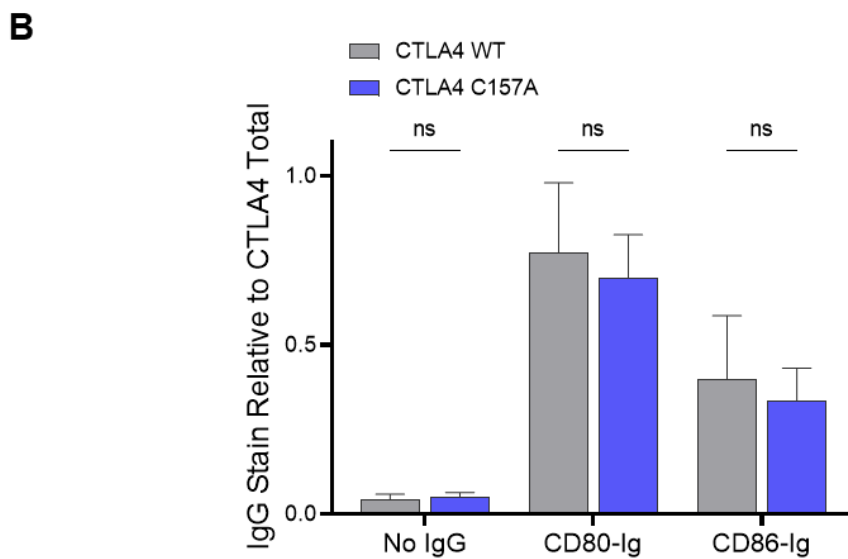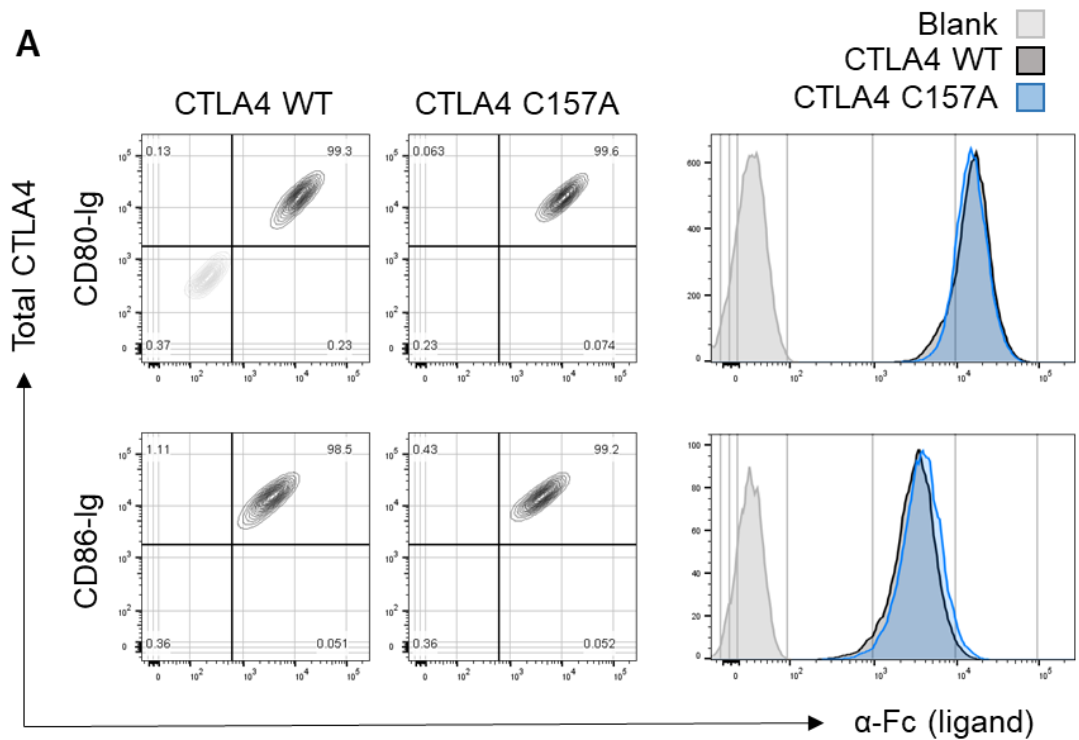
Figure 4.2. C157A mutation does not affect soluble Ig-ligand chimera binding to CTLA4. Untransduced CHO cells (blank), or CHO cells transduced with CTLA4 WT or CTLA4 C157A were fixed, permeabilized and stained with CD80-Ig, CD86-Ig or IgG control followed by α-human-Fc-AF488 before analysis by flow cytometry **(A). (B).** Graph shows CTLA4 C157A IgG stain relative to total CTLA4 stain, relative to CTLA4 WT. Data presented as mean +- SD from 3 independent experiments, analysed by 2-way ANOVA, ns = p>0.05 *p≤0.05, **p≤0.01,***p≤0.001, ****p≤0.0001.
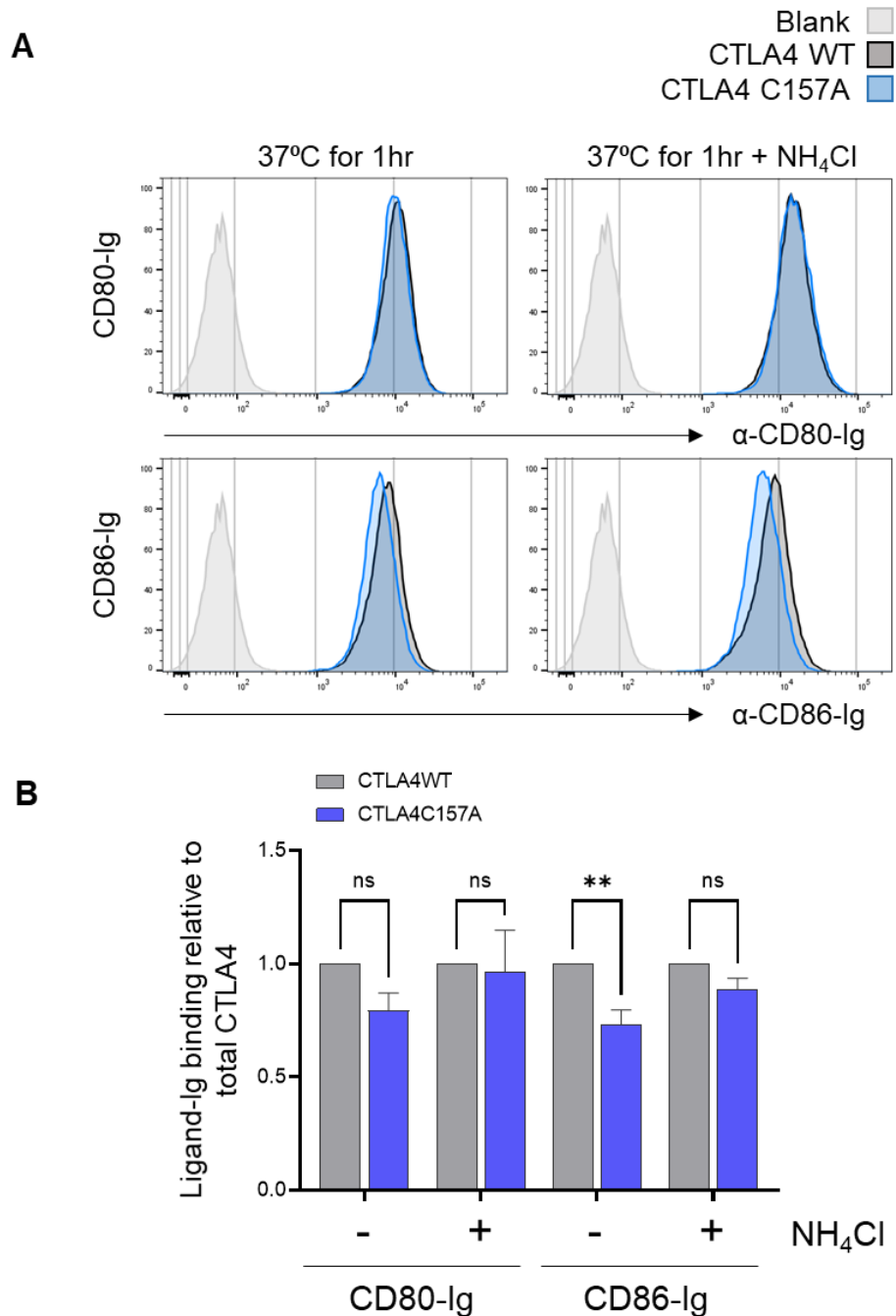
Figure 4. 3. IgG-CD86 chimera uptake is compromised by CTLA4 C157A mutation, but not IgG-CD80. Untransduced CHO cells (blank), or CHO cells transduced with CTLA4 WT or CTLA4 C157A were fed with CD80-Ig, CD86-Ig or IgG control for 60 minutes, with or without 50μM ammonium chloride (NH4Cl). Cells were fixed, permeabilized and stained with α-human-Fc-AF488 before analysis by flow cytometry, with histograms shown in **(A). (B).** Graph shows CTLA4 C157A IgG stain relative to total CTLA4 stain, relative to CTLA4 WT. Data presented as mean +- SD from 3 independent experiments, analysed by 2-way ANOVA, ns = p>0.05 *p≤0.05, **p≤0.01,***p≤0.001, ****p≤0.0001. .

Whilst the use of soluble ligands established that dimeric CTLA4 is not required for ligand binding, it should be noted the soluble proteins are generated from IgG chimeras and are themselves inherently dimeric, which we confirmed via western blot analysis (data not shown). This means that soluble CD86-Ig will have an avidity advantage over monomeric CD86.

To ask whether the cell-expressed membrane ligands showed the same alteration in binding, we co-incubated CD80- and CD86-GFP expressing CHO cells with CTLA4 WT and C157A expressing CHO cells for 3 hours and performed western blot analysis following immunoprecipitation via the GFP-tag, to pull down dimeric and monomeric CTLA4 bound to ligand. As shown in **Figure 4.4A**, precipitations via CD80 effectively pulled down both CTLA4 WT and CTLA4 C157A (**Figure 4.4B**). Precipitations with CD86 recovered ~40% of CTLA4 WT relative to that pulled down via CD80, consistent with weaker affinity. Strikingly, CD86 was never able to recover CTLA4 C157A in this setting, again indicating a decrease in CD86-C157A binding strength (**Figure 4.4B**).

Taken together, this data reveals CTLA4 is not required to be dimeric for binding to CD80 or CD86. Whilst CTLA4 C157A showed no defect in binding to CD80, the most striking differences are in binding to CD86, suggesting CTLA4 dimerisation is more important for maintaining the CD86 interaction. Nonetheless, whilst the data are clear, the reason behind this reduced interaction for the monomeric CD86 is less so.
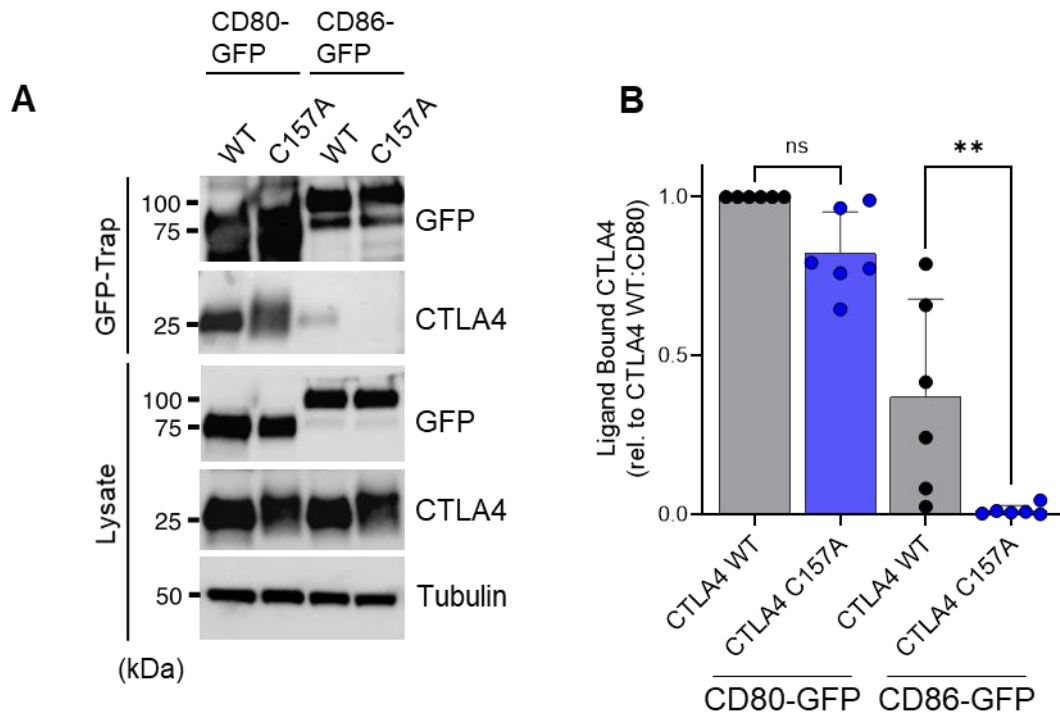
Figure 4. 4. Immunoprecipitation reveals CTLA4 C157A mutation significantly impairs CD86 binding. (A). CHO cells expressing CTLA4 WT or C157A were incubated with CHO cells expressing CD80-GFP or CD86-GFP at a 1:1 ratio for 3 hours. Western blot analysis shows total lysates blotted for CTLA4 (C19), GFP and Tubulin and lysates following 1 hr immunoprecipitation with GFP-Trap beads, blotted for GFP and CTLA4. **(B).** Graph shows quantification of CTLA4 following immunopreciptiation From 6 independent blots, relative to the signal from CTLA4WT and CD80-GFP (lane 1), analysed using ImageJ. Statistics from ordinary one-way ANOVA with multiple comparison analysed by 2-way ANOVA, ns = p>0.05 *p≤0.05, **p≤0.01,***p≤0.001, ****p≤0.0001.

4.2.3. Understanding dynamics of transendocytosis *in vitro*

To investigate how differences in binding properties of WT and monomeric CTLA4 impacted the ability of CTLA4 to transendocytose ligand, we first wanted to understand the dynamics of CTLA4 WT transendocytosis *in vitro*. In this section, we focused on understanding the dynamics of CTLA4 WT. For this, we used a cell-cell based model system of transendocytosis that allows observation of CTLA4 transendocytosis and can reveal differences between CD80 and CD86 localisation (Qureshi et al., 2011). This model uses GFP-tagged ligand stably transduced into CHO cell lines, labelled with a cell dye (CTV+), allowing identification as a distinct 'donor' population by flow cytometry. These cells are then co-incubated with CHO cells stably expressing CTLA4, or un-transduced cells as a control. When CTLA4 is present, transendocytosis is observed as GFP loss from CTV +ve (donor) cells, and GFP uptake into CTV -ve (recipient) CTLA4 expressing cells, as shown in **Figure 4.5A**.

Figure 4.5B shows representative plots following a time course of co-incubation of CTLA4-WT cells at a 1:1 ratio with either CD80-GFP or CD86-GFP cells, expressing ligand at equal levels. As previously reported, a loss of GFP from the donor population was observed with time, demonstrating that transendocytosis is a continuous, active process and thus not due to trogocytosis resulting from cell-cell contact (Kennedy et al., 2022; Qureshi et al., 2012). Interestingly, at 2 hours, ~40% of both CD80 and CD86 had already been removed by CTLA4 expressing cells, suggesting CTLA4 can transendocytose both ligands with similar efficiency. Indeed, kinetic quantification of the MFI of donor cells revealed loss of CD80 and CD86-GFP occurs at a surprisingly similar rate (**Figure 4.5C**), considering their different affinities.

Whilst loss of ligand is a key measure of efficiency of transendocytosis, a second measure quantifiable by this assay is the extent of ligand uptake into CTLA4+ (CTV-ve) cells. As shown in **Figure 4.5B** and quantified in **Figure 4.5D**, acquisition of CD80-GFP was detectable at all time points, with 11.9% GFP+CTV- cells at 6 hours. In contrast, CD86 was only detectable (>5% GFP+CTV-) at early (1-2 hour) time points. This is reflective of the differential degradation processes of the ligands post-internalization and is a distinct phenotypic difference between CD80 and CD86, as recently published (Kennedy et al., 2022).

In order to understand the dependency of transendocytosis on the amount of ligand, we repeated the above experiment at a single 3-hour time-point, but at various donor: recipient ratios (**Figure 4.6A**). Unsurprisingly, as we increased the number of CTLA4 cells (recipients), the extent of ligand loss increased, highlighting that transendocytosis efficiency is dependent on cell number. This is likely due to an increase in the frequency of donor: recipient cell interactions. Likewise, as we decreased the number of ligand-expressing cells (donors), we also decreased detection of ligand inside each recipient cell. Interestingly, both CD80 and CD86 ligand loss is saturated at ratios above 40% recipients (**Figure 4.6B**), demonstrating the remarkable efficiency of CD86 transendocytosis given differences in overall avidity.
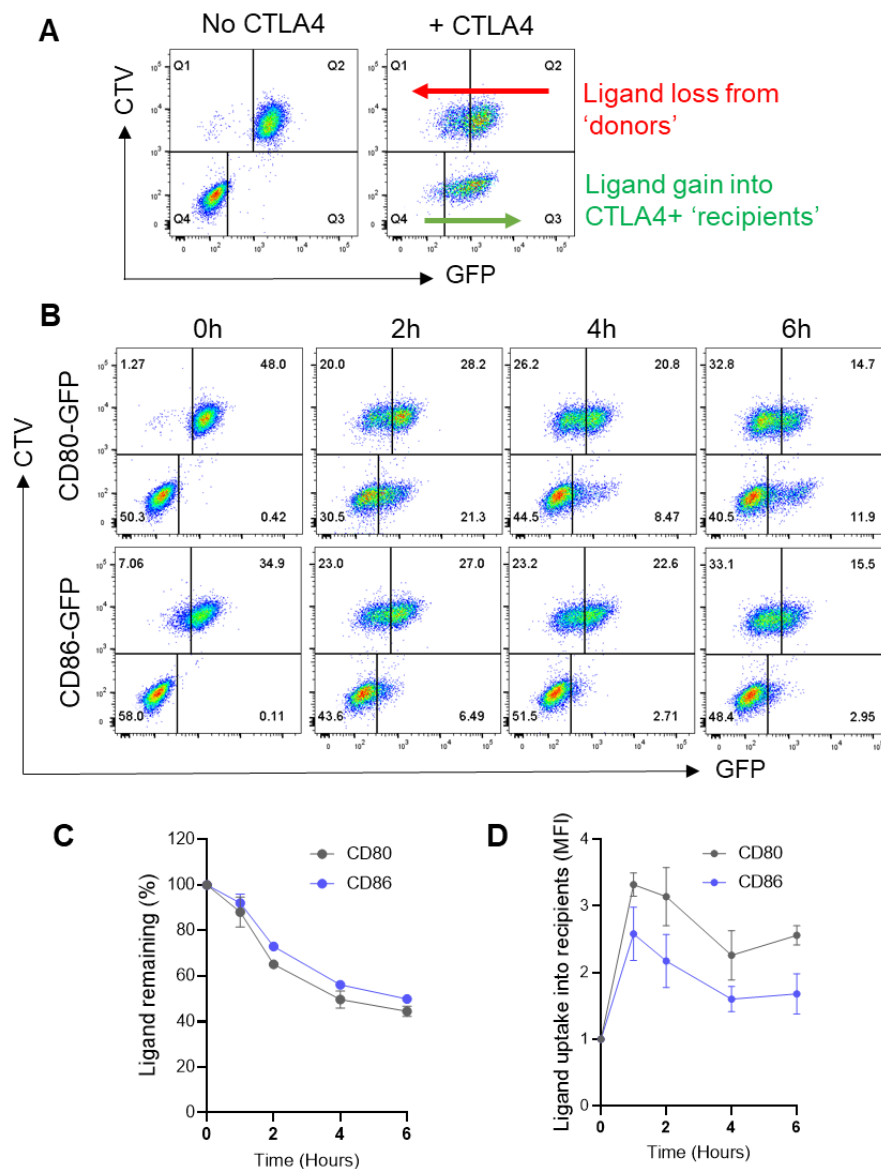
Figure 4. 5. Kinetic analysis of CTLA4 mediated transendocytosis reveals distinct characteristics for CD80 and CD86 ligands. (A). Labelled flow cytometry plots detailing transendocytosis assay. CHO cells expressing GFP tagged ligands are labelled with CellTrace violet (CTV) and mixed with CHO cells with or without CTLA4 before analysis by flow cytometry. During transendocytosis, ligands are removed from CTV+ve cells (Q2 to Q1) and detected in CTV-ve cells (Q4 to Q3). **(B).** CD80-GFP or CD86-GFP expressing CHO cells were incubated at a 1:1 ratio with CTLA4+ CHO cells at indicated times. CTV-ve GFPhigh cells are gated by box in Q3. GFP MFI from Q1 and Q2 were calculated as % change from time 0 **(C).** Or Q3 and Q4 as raw MFI (D). and collated from 3 independent experiments, shown +- SD.
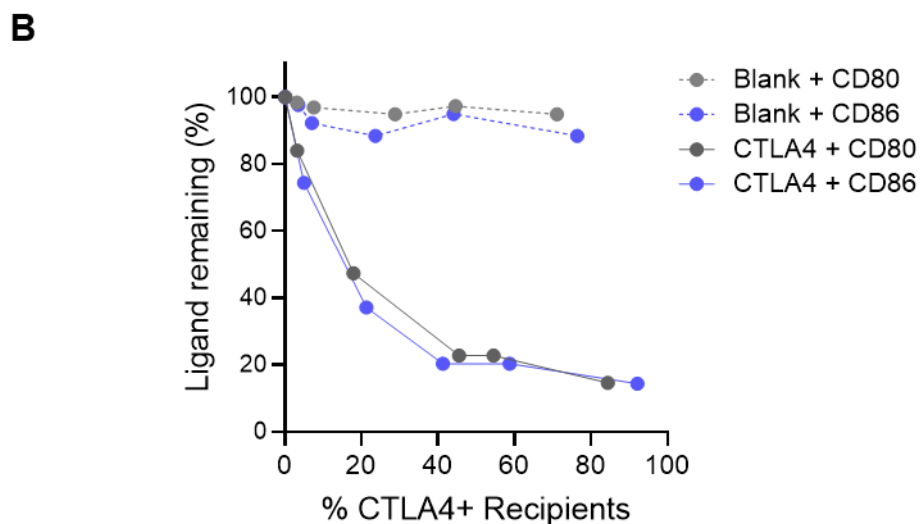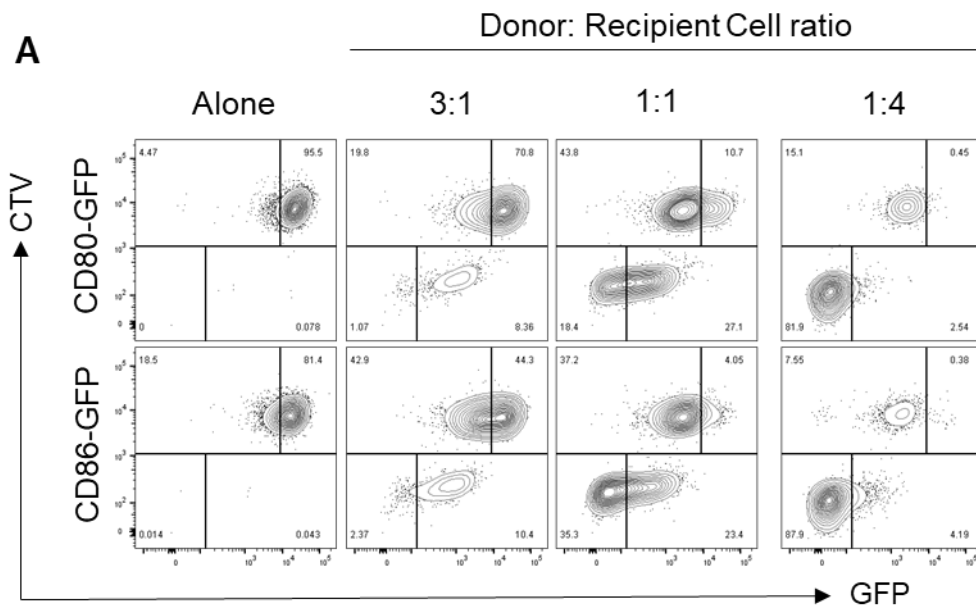
Figure 4. 6. Transendocytosis of CD80 and CD86 is dependent on CTLA4 cell contact. (A). FACs plots of transendocytosis assays with CellTrace Violet (CTV) labelled CD80-GFP or CD86-GFP CHO cells alone, or co-incubated with CHO cells expressing CTLA4 and at indicated ratios for 3 hours. **(B).** Ligand remaining on CTV+ cells following 6 hours transendocytosis vs % CTLA4 cells present, with CHO blank control (no CTLA4, dotted line). Data shown from one experiment, representative of at least 3 independent experiments.

Changing cell ratios revealed how sensitive transendocytosis is to relative CTLA4 and ligand cell numbers, however we also tested how transendocytosis changed when varying expression on a per cell basis. For this, we used clonally expanded CHO cells expressing different levels of ligand-GFP (CD80I2R, although the same trend seen for all ligands (*data not shown*), as measured by GFP MFI (**Figure 4.7A**), co-incubated with CHO cells with or without a fixed expression of CTLA4 for 3 hours at a 3:1 (donor: recipient) ratio. This set-up meant the only independent variable was ligand expression level.

A negative dose-response relationship was observed, with more ligand remaining with increased donor ligand expression (**Figure 4.7B, quantified in Figure 4.7C**). Notably, in settings where there was more ligand on the donor cell, the recipient CTLA-4 cells contained more ligand, albeit that downregulation from the donor cells was more limited. Together, this suggests the trafficking pathways post-transendocytosis can be saturated and emphasizes the continuous nature of ligand degradation post-internalisation.

Likewise, we hypothesized that transendocytosis would also be dependent on CTLA4 expression level and therefore generated Jurkat cell lines expressing varied levels of CTLA4 by FACs (**Figure 4.8A**). Following co-incubation with cells expressing similar levels of CD80 or CD86-GFP for 3 hours, we observed a CTLA4-level-dependent depletion of both ligands **(Figure 4.8B)**. Depletion was equally dependent on CTLA4 expression for both CD80 and CD86, supporting the concept that CTLA4 uses a mechanism which seems to compensate for lower affinity binding of CD86 when carrying out transendocytosis (**Figure 4.8C).**

Overall, we identified that the CTLA4 mediated transendocytosis correlates with ligand and CTLA4 expression levels as well as donor to recipient

cell contacts, establishing the basic parameters affecting transendocytosis. Therefore, we sought to ensure these variables were controlled where possible in experiments comparing wild-type and mutant receptor, and ligands in subsequent transendocytosis assays.
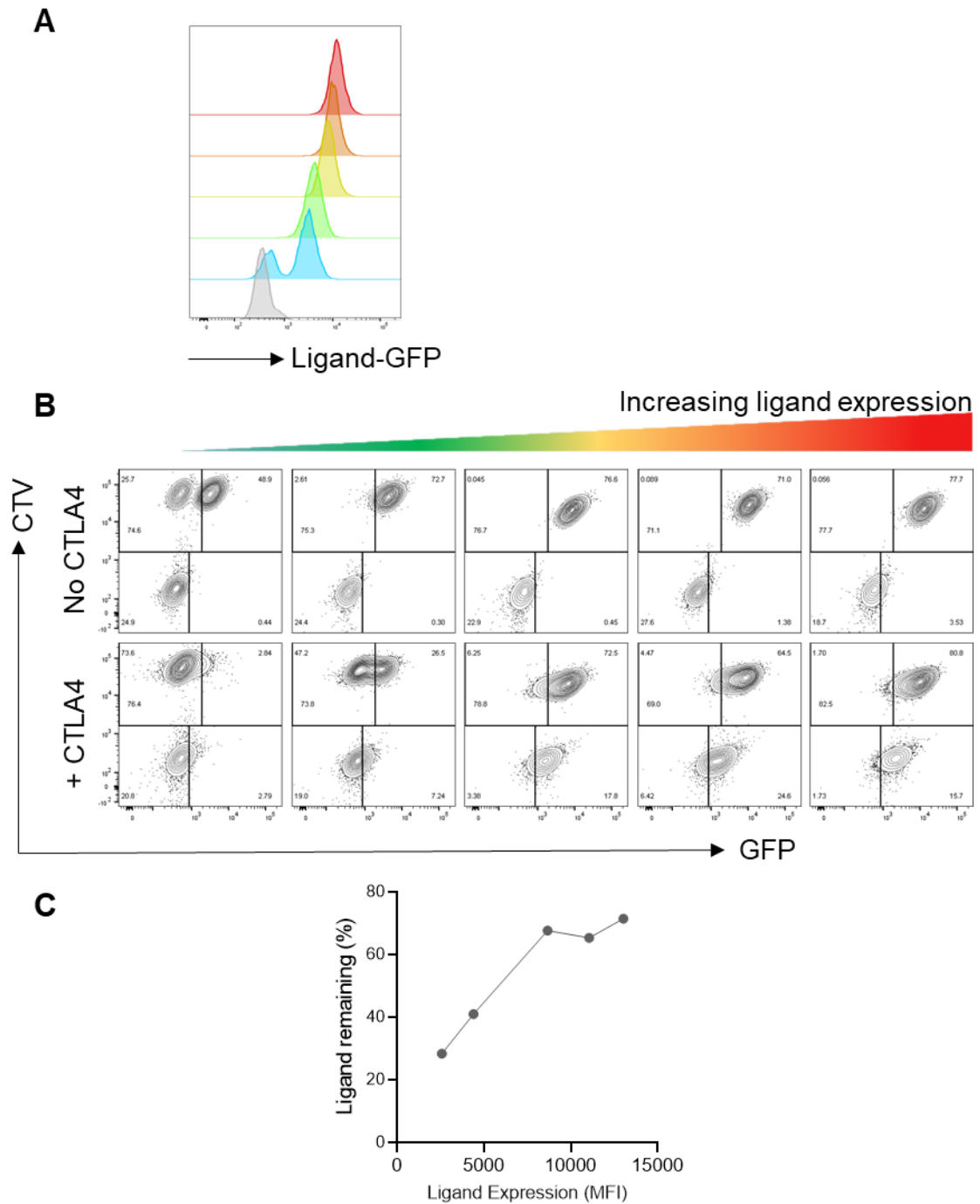
Figure 4. 7. CTLA4 mediated transendocytosis is dependent on ligand expression level. (A). Overlaid FACs histograms of ligand-GFP expression on clonally expanded CHO cell lines used in subsequent transendocytosis assay. **(B).** FACs plots of transendocytosis assays with CellTrace Violet (CTV) labelled CD80I2R-GFP CHO cells alone co-incubated with CHO cells with or without CTLA4 at a 3:1 ratio for 3 hours, with ligand remaining quantified as % remaining compared to no CTLA4 conditions in **(C).**
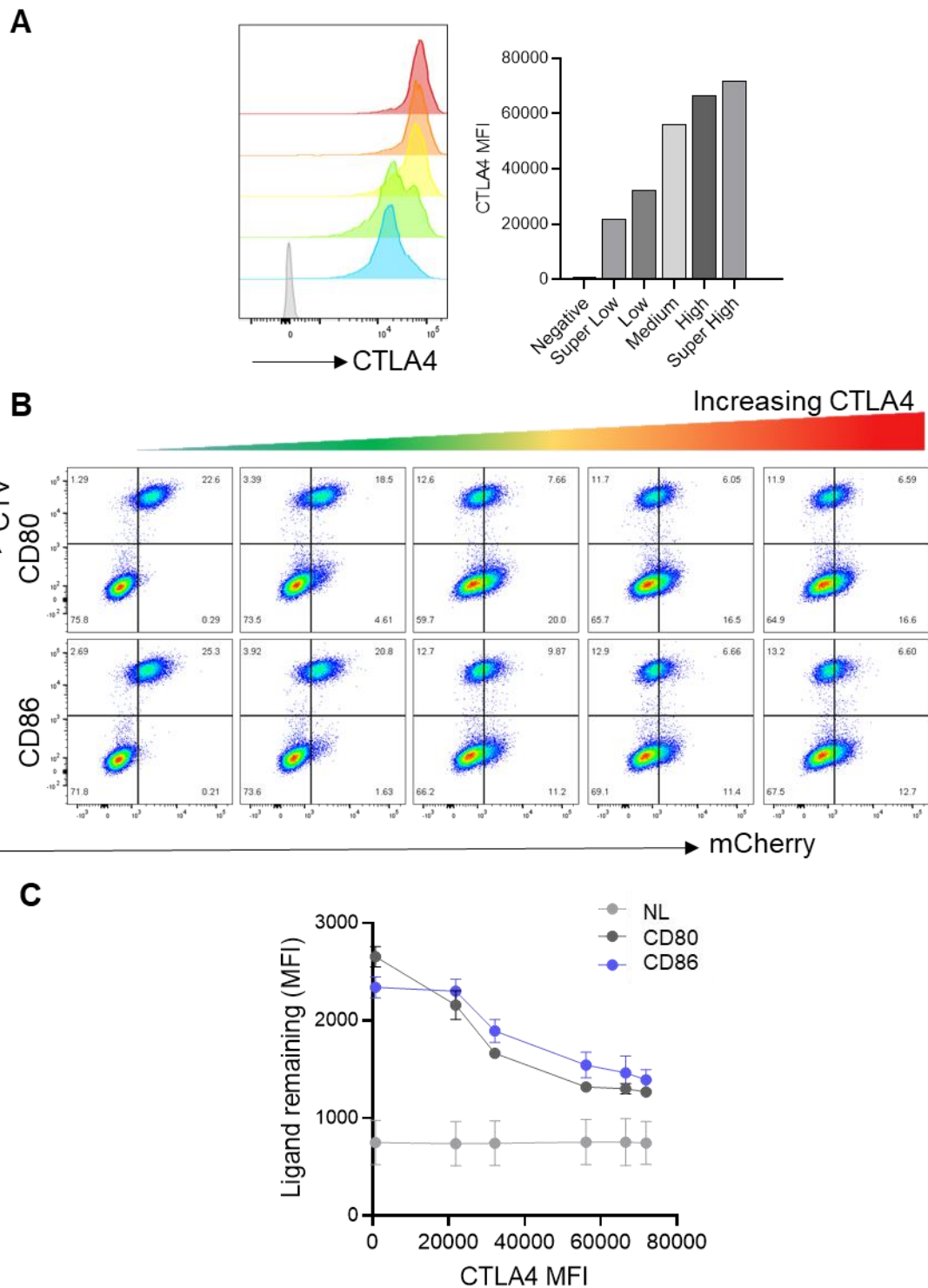
Figure 4. 8. Transendocytosis of CD80 and CD86 is dependent on CTLA4 expression level. (A). CTLA4 levels on FACs Aria sorted Jurkat lines transduced with CTLA4. (B). FACs plots of transendocytosis assays with CellTrace Violet (CTV) labelled CD80-or CD86-mCherry DG75 cells alone co-incubated with Jurkat cells from (A) at a 1:3 ratio for 4 hours. (C). Ligand MFI from CTV+ cells following the transendocytosis assay in B, with a no ligand control (NL). N=4 from 3 independent repeats shown +- SD.

4.2.4. Monomeric CTLA4 can transendocytose CD80 and CD86, but is less efficient for CD86

To investigate how bivalency of CTLA4 influenced the characteristics of CD80 and CD86 transendocytosis, we used our monomeric CTLA4 mutant CTLA4 C157A in a transendocytosis assay at a 1:1 ratio with ligand expressing cells, ensuring equal expression of both C157A and CTLA4 WT (**Figure 4.9A**).

Interestingly, transendocytosis showed that whilst CTLA4 C157A was able to transendocytose CD80 to a comparable extent to WT, it was less effective in removal of CD86, seen by more GFP remaining on CTV+ cells (**Figure 4.9B, upper quadrants**). This was observed as more CD86-GFP remaining relative to the start of the assay (**Figure 4.9C**).

Despite comparable removal, CD80 showed typical accumulation in CTLA4 WT cells, but was clearly reduced with CTLA4 C157A **(Figure 4.9B, box gate).** Remarkably, whilst CD86 showed some accumulation into CTLA4 WT, especially at 1 hour, this was absent in CTLA4 C157A conditions **(Figure 4.9B & D).** These data show the accumulation of ligand in recipient cells relates to the strength of interaction between CTLA-4 and its ligands.

To determine whether this absence of ligand accumulation was due to degradation post-internalization we used NH_4Cl to neutralize lysosomal pH, thereby preventing degradation. Strikingly, addition of NH_4Cl rescued accumulation of CD80 (**Figure 4.10A**) and CD86 (**Figure 4.10B**) in both CTLA4 WT and C157A cells, seen by more GFP in CTV-ve cells. This observation confirmed that all ligands undergo transendocytosis but suggested more rapid degradation for CD86 post-internalization in the absence of NH_4Cl.

Kinetic analysis of ligand accumulation within recipients with time (**blue shaded quadrants, Figure 4.10B**) showed CTLA4 C157A had reduced CD80 accumulation compared to CTLA4 WT. Likewise, CD86 also accumulated less in CTLA4 C157A lines compared to WT (**Figure 4.10D**). These observations support differential rate of ligand degradation post-internalisation.

Another key observation is whilst NH4Cl treatment did not impair CD80 removal by CTLA4 WT, seen by similar levels of CD80-GFP (**red quadrants, upper panel Figure 4.10A),** NH4Cl treatment increased the level of GFP for all other conditions (**red quadrants, lower panel Figure 4.10A. Figure 4.10B).** The fold-change in ligand-GFP remaining +/- NH4Cl is shown in **Figure 4.10E,** demonstrating a larger impact of NH4Cl on ligand removal for the monovalent ligand: receptor combinations.

One interpretation of these data is that pH modulation by NH_4Cl affects weaker interactions such as CD86 more markedly than CD80. This is because removal of CD86 is more reliant on pH-dependent dissociation to permit CTLA4 recycling. Therefore, if you prevent dissociation by increasing pH (as with NH_4Cl treatment) then you inhibit CTLA4 function seen as an increase in remaining ligand. In contrast, CD80 transendocytosis does not rely on pH-dependent dissociation of CTLA4 for removal and therefore is less affected by NH_4Cl treatment (Kennedy et al., 2022). The above results suggest that the weaker, monovalent CTLA4 C157A interaction with CD80 is more sensitive to pH modulation, and therefore may allow pH-dependent dissociation and CTLA4 recycling to permit efficient transendocytosis, in the face of weaker avidity.
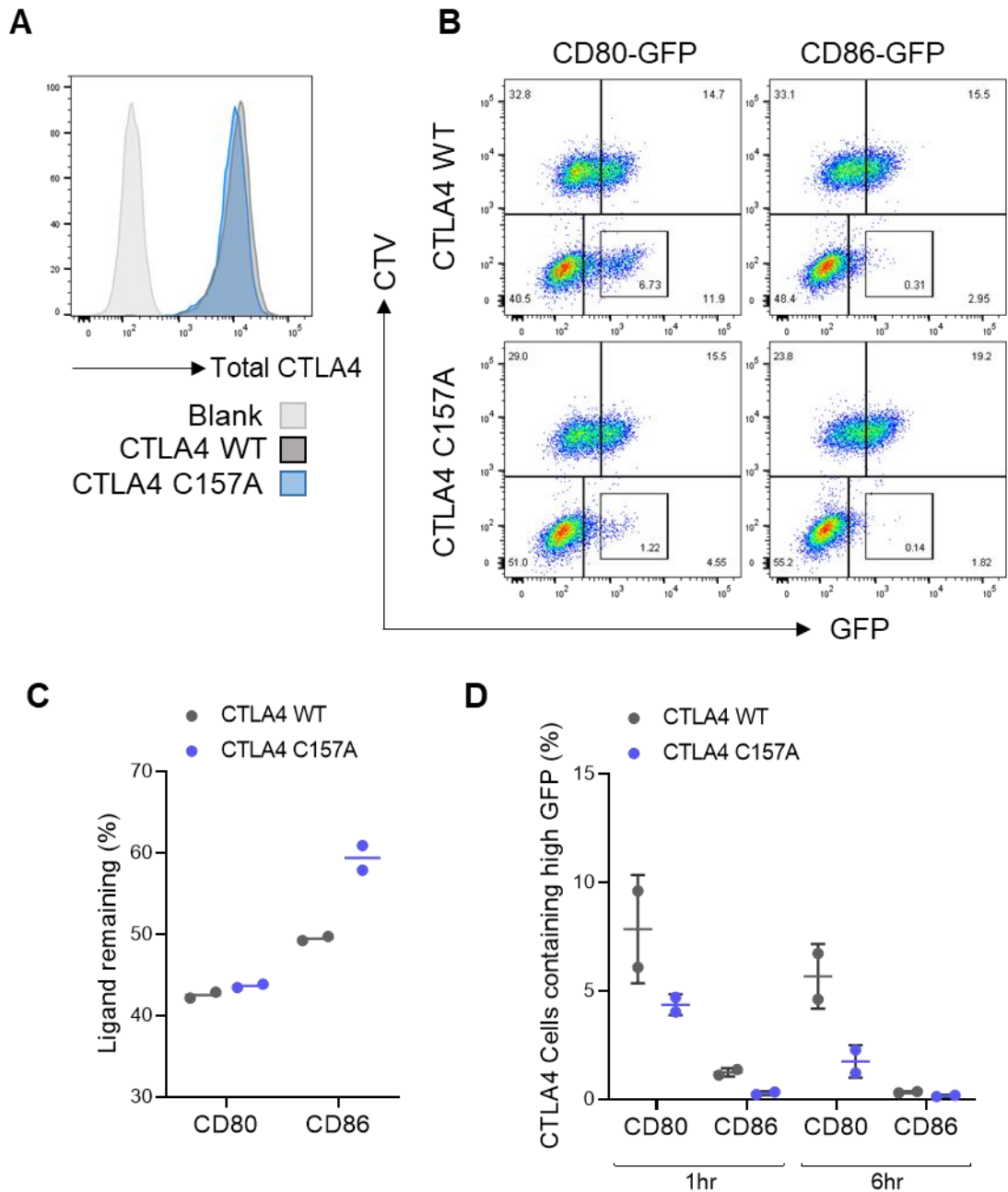
Figure 4. 9. Monomeric CTLA4 can transendocytose both CD80 and CD86, but is impaired in CD86 transendocytosis. (A). CHO cells expressing CTLA4 WT or CTLA4 C157A were stained for total CTLA4 (F8-AF647) for 1hr. **(B).** Transendocytosis assays were carried out with CHO cells in (A). and CellTrace Violet (CTV) labelled CD80-GFP or CD86-GFP CHO cells at a 1:1 ratio for 6 hours. CTV-ve GFPhigh cells are gated by box in Q3. GFP MFI from CTV+ve cells at 6 hours relative to 0 hours is quantified in as a % **(C),** and GFP MFI from CTV-ve cells at 1 hour and 6 hours relative to 0 hours quantified in **(D).** Data presented from 2 independent experiments shown +- SD
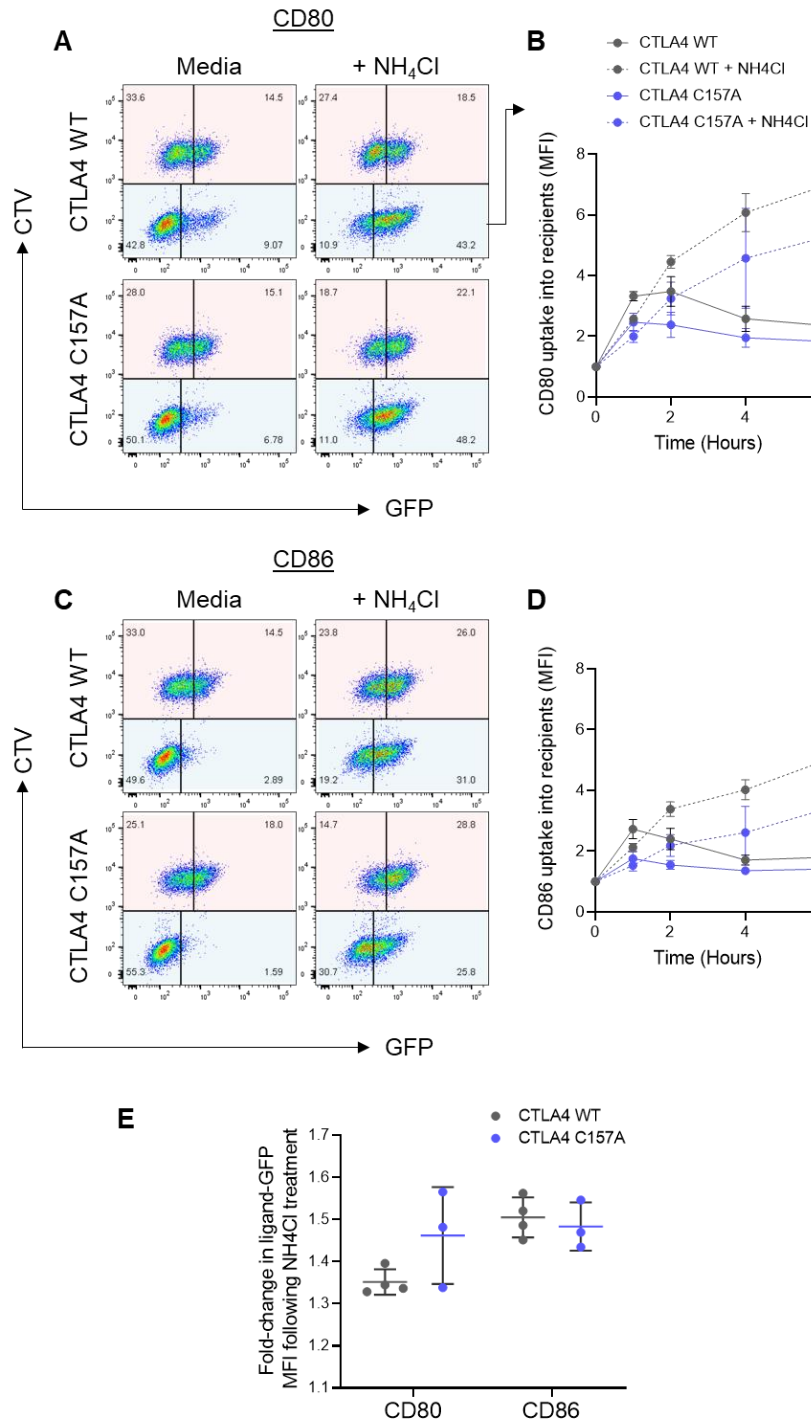
Figure 4. 10. NH₄Cl treatment rescues ligand degradation and reveals monovalent CTLA4 transendocytosis is more sensitive to pH changes. Transendocytosis assays were carried out for 6 hours using CHO cells expressing CTLA4 WT or CTLA4 C157A at a 1:1 ratio with CellTrace Violet labelled CD80-GFP (A). or CD86-GFP (C). with or without 50μM NH₄Cl . (B) and (D) show full kinetic analysis of GFP MFI in CTV-ve CTLA4+ cells of CD80-GFP and CD86-GFP respectively (blue quadrant) (E). Impact of NH₄Cl treatment on ligand downregulation as quantification of GFP levels on CTV+ve donor cells with treatment divided by no treatment following, 6 hours of transendocytosis (red shaded). Data from 3 independent experiments shown +- SD.

Since the above analysis suggested differences in ligand processing post-internalization, we used confocal microscopy to analyze transendocytosis at a cellular level (**Figure 4.11A**). CHO cell lines expressing CTLA4 WT or C157A were plated on glass coverslips with either CD80-GFP or CD86-GFP CHO cells overnight at a 1:3 ratio, to ensure CTLA4 cell access to ligand. The cells were then fixed and permeabilized before staining for intracellular CTLA4 (red) and a nuclear stain (blue) and observing GFP tagged ligand uptake (green).

Confocal microscopy analysis showed that whilst CD80-GFP accumulated in CTLA4 WT cells in large vesicles, accumulation into CTLA4 C157A cells resulted in significantly smaller vesicles, comparable to CD86-GFP vesicles in CTLA4 WT cells. CD86 also clearly accumulated in vesicles following CTLA4 C157A mediated transendocytosis, however there were visually fewer vesicles and cells containing vesicles were rarer (**Figure 4.11A**). Quantification of the number of ligand vesicles per cell reflected these observations, showing maximal puncta with CD80 into CTLA4 WT, with the least following CD86 transendocytosis by CTLA4 C157A (**Figure 4.11B**). Whilst the number of CD80 vesicles in CTLA4 C157A expressing cells was not significantly less than CTLA4 WT, the vesicles themselves were smaller, and showed less co-localization with CTLA4 (**Figure 4.11C and D).** Likewise, lower affinity CD86 ligand accumulated in significantly larger vesicles with more colocalization following transfer by CTLA4 WT than C157A (**Figure 4.11C and D)**. Therefore, weaker avidity appeared to influence co-localization and vesicle size, particularly for CTLA4 C157A:CD86 interactions.

Taken together, this data shows that whilst CTLA4 C157A can still efficiently transendocytose both CD80 and CD86, there were phenotypic changes in processing of the ligand post-internalization with regards to

intracellular accumulation and CTLA4 co-localization. For CD80, CTLA4 C157A was as efficient at removal, with results suggesting loss of bivalency reducing overall binding strength being compensated for by increased pH dissociation and thus CTLA4 recycling. In contrast, CD86 already uses the mechanism of dissociation and recycling for transendocytosis by CTLA4 WT, and therefore loss of bivalency reduces binding strength to the point transendocytosis efficiency is impaired.
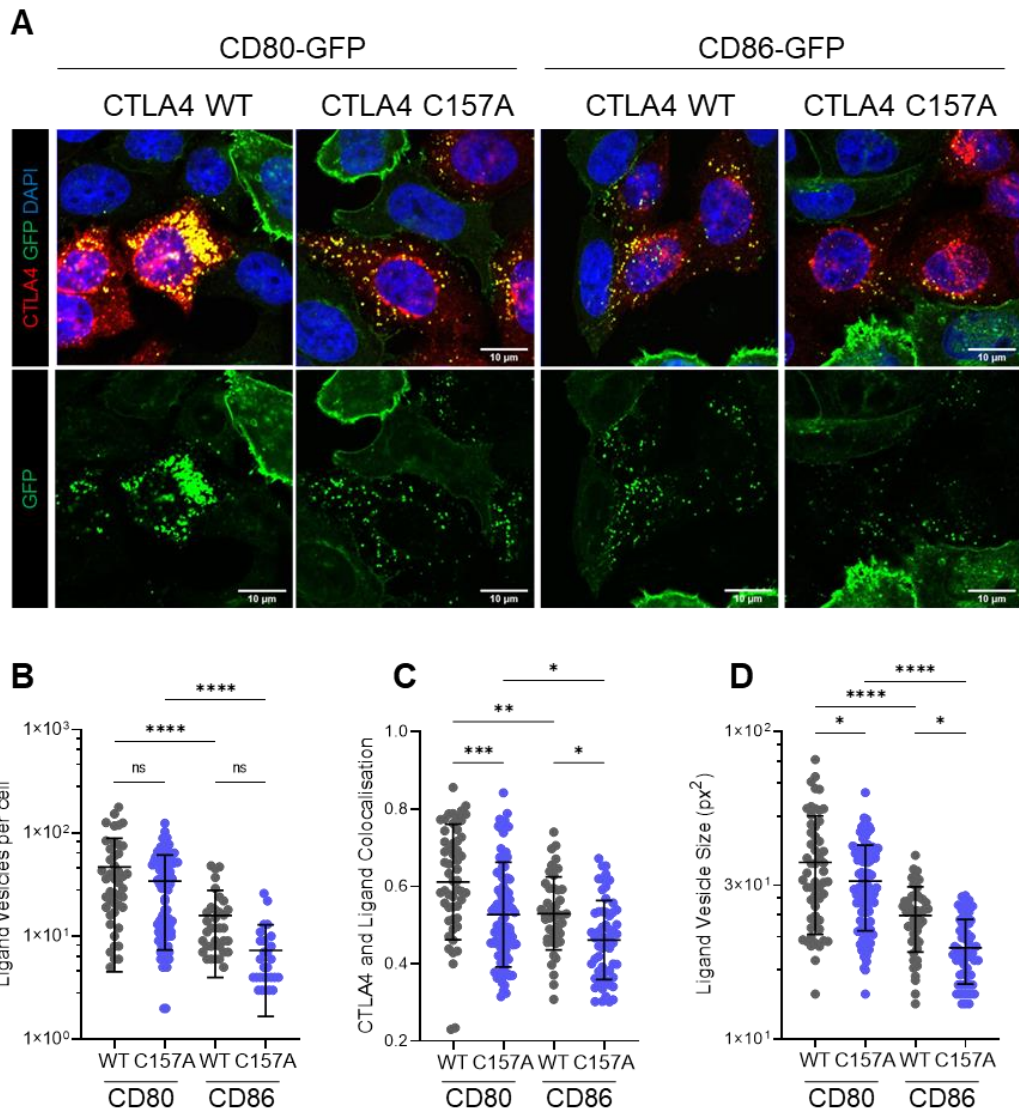
Figure 4. 11. Confocal microscopy shows CTLA4 and CD80 co-localisation in large intracellular vesicles is dependent on CTLA4 dimerisation. (A). Confocal analysis of overnight transendocytosis in CHO cells with CTLA4 WT or CTLA4 C157A (red) and CD80-GFP or CD86-GFP (green) at a 1:3 ratio. Nuclei are stained with DAPI (blue). Scale bar = 10µm. Graph shows analysis of number of ligand vesicles per CTLA4+ cells **(B),** CTLA4:ligand colocalization (C) and the average size of ligand vesicles per CTLA4 cell (D) Data is from >10 images, representative of 2 individual experiments +- SD, analysed by one-way ANOVA ns = p>0.05 *p≤0.05, **p≤0.01,***p≤0.001, ****p≤0.0001. Quantification was performed in CellProfiler.

165

4.2.5. Loss of high avidity CD80:CTLA4 interaction paradoxically enhances CTLA4 mediated transendocytosis

We next performed a set of experiments, using a CD80 mutant with impaired dimerisation (CD80I2R) to investigate the contribution of ligand bivalency to this process to see if this recapitulated the monomeric CTLA4 C157A phenotype.

First, we generated CHO cell lines transduced with CD80-, CD86- and CD80I2R-GFP and selected equally expressing clones based on their GFP tag expression (**Figure 4.12A**). These lines were then CTV labelled and used in a transendocytosis assay with CTLA4 expressing cells at a 1:1 ratio for the indicated time points. As seen in Figure **4.12B**, CD80 and CD86 were removed at comparable rates, as previously observed. Strikingly, despite theoretical loss of avidity, CD80I2R underwent rapid removal from the cell surface, with nearly complete ligand removal after 6 hours transendocytosis. Kinetic quantitation of the MFI of donor (CTV+) populations corroborated these observations, showing CD80I2R underwent transendocytosis at a significantly increased rate compared to CD80 and CD86 (**Figure 4.12C**).

Furthermore, whilst CD80 showed the usual phenotype of detectable acquisition by CTLA4 cells, CD80I2R did not show similar levels of detectable CD80 especially at later time points, making it more similar to CD86 in this respect.. Full kinetic analysis of ligand detection inside CTLA4 cells following transendocytosis showed CD80I2R was internalized, and detection lost following a CD86-like trajectory (**Figure 4.12D**). Again, these data supported the idea that monovalent interaction leads to reduced detection inside CTLA4 cells after

transendocytosis (without compromising ligand removal) compatible with the possibility of more rapid ligand degradation.

To confirm that loss of ligand post-internalisation was due to ligand degradation, we again used NH$_4$Cl treatment. Addition of NH$_4$Cl rescued CD80-, CD86- and CD80I2R-GFP accumulation within the CTLA4 containing cells, as previously demonstrated (**Figure 4.13A**). However, extended analysis of the gated donor populations (CTV+, black box) revealed that, NH$_4$Cl treatment had a larger impact on the ability of CTLA4 to deplete CD86 compared to CD80. Strikingly, NH$_4$Cl treatment had the largest impact on CTLA4 mediated depletion of CD80I2R, impairing ligand removal by ~60% (**Figure 4.13B**). Thus weaker, monovalent interactions were more dependent on intracellular pH for efficient ligand removal. Together, these observations suggest an alternate route of trafficking for monovalent vs. bivalent CD80 ligand post-transendocytosis as well as a different requirement for pH driven dissociation to facilitate transendocytosis.
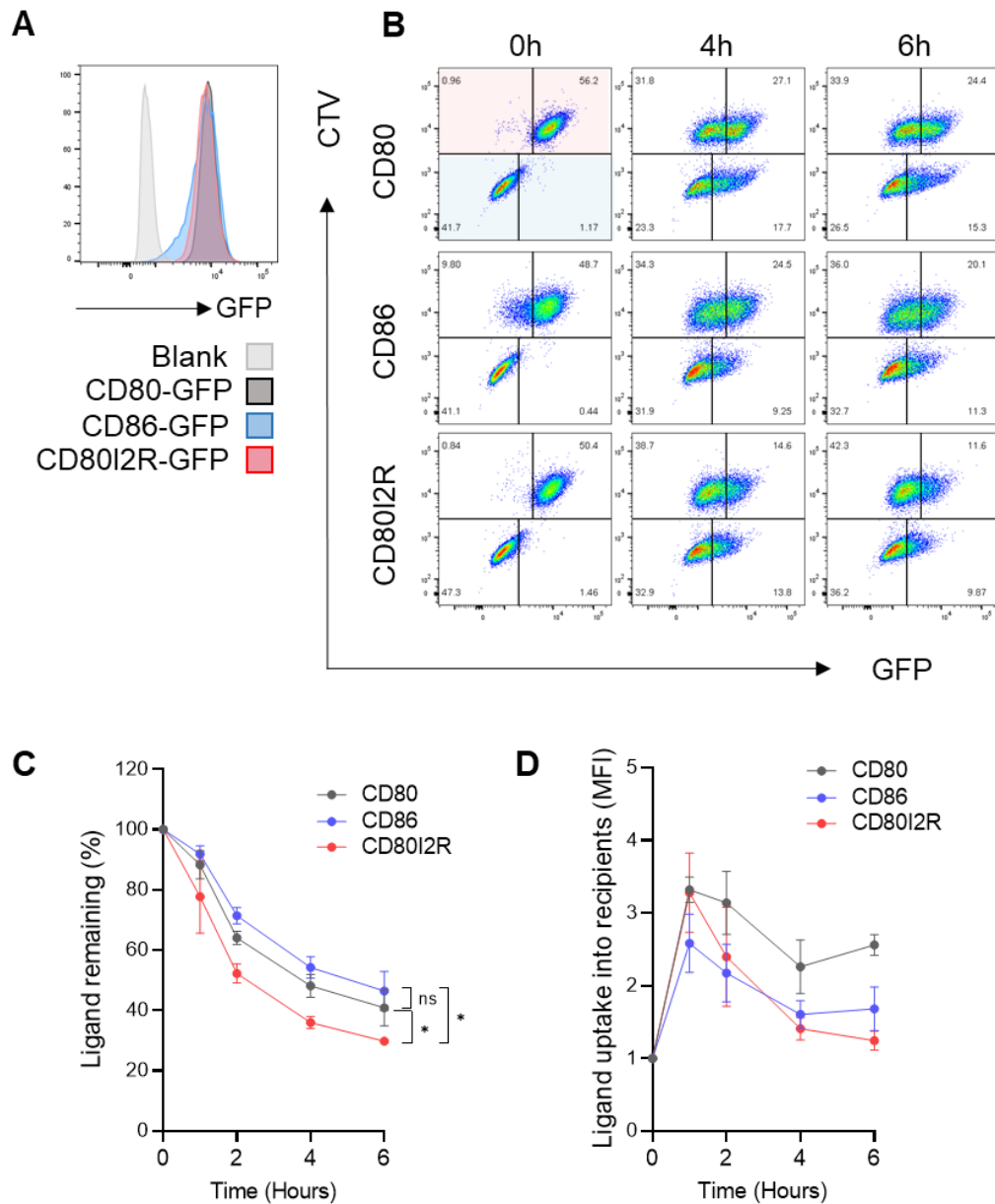
Figure 4. 12. Loss of CD80 avidity paradoxically enhances rate of CTLA4 mediated transendocytosis. (A). Flow cytometry histograms of GFP MFI from CHO cells expressing CD80-GFP, CD86-GFP, CD80I2R-GFP or untransduced CHO cells. **(B).** Time-course transendocytosis assay using cells in **(A)** labelled with CellTrace Violet (CTV) and incubated with CHO cells expressing CTLA4 at a 1:1 ratio at the indicated time points. Gating strategy used for full kinetics are quantified for ligand loss from CTV+ cells, red shaded quadrant **(C)** and ligand gain into CTV- cells, blue shaded quadrant **(D)** relative to 0 hours. Data shown from 3-4 individual experiments +- SEM, analysed by one-way ANOVA at the 6 hour time point only (ns = p>0.05 *p≤0.05, **p≤0.01,***p≤0.001, ****p≤0.0001).
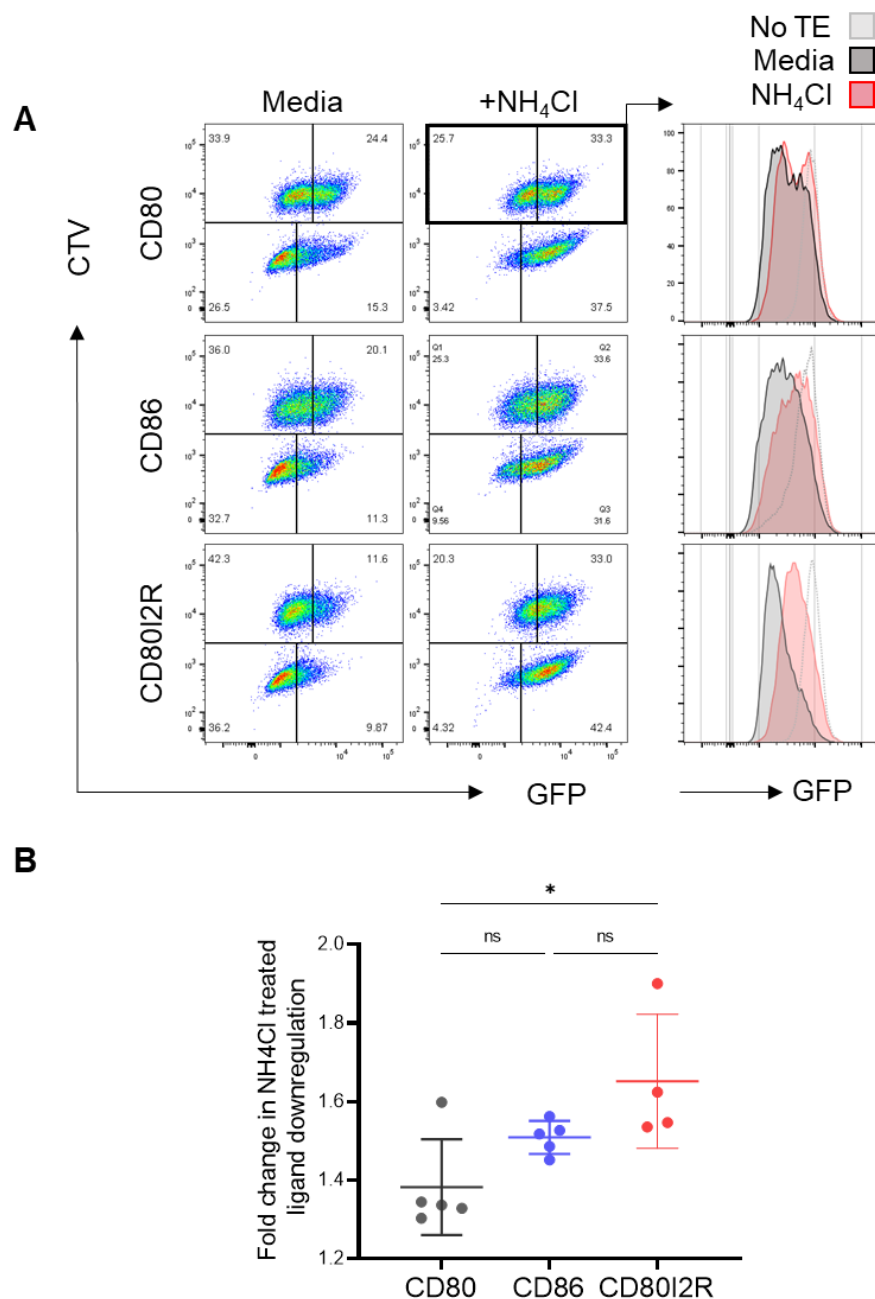
Figure 4. 13. Transendocytosis of wild-type CD80 is less impaired by NH4Cl treatment, compared to monovalent ligands. (A). CellTrace Violet labelled CHO cells expressing CD80-, CD86- or CD80I2R-GFP we incubated at a 1:1 ratio with CTV- CHO cells expressing CTLA4 for 4 hours with or without 50μM NH₄Cl. FACs plots and overlaid histograms gated on CTV+ cells (black box) are shown. **(B).** Impact of NH₄Cl treatment on ligand downregulation as quantification of GFP levels on CTV+ve donor cells with treatment divided by no treatment following 4 hours of transendocytosis (red shaded quadrants). All data from 4-5 independent representative experiments shown, +- SD, analysed by one-way ANOVA ns = p>0.05 *p≤0.05, **p≤0.01,***p≤0.001, ****p≤0.0001.

As we observed decreased CTLA4 colocalisation with CD86 compared to CD80, by microscopy for we speculated CD80I2R might also show increased dissociation. As shown in Figure **4.14A**, whilst CD80 accumulated in large intracellular vesicles, highly colocalized with CTLA4, both CD86 and CD80I2R ligand-containing vesicles were more punctate and showed less colocalisation with CTLA4 vesicles than CD80. CellProfiler analysis using an automated pipeline validated these observations, suggesting smaller ligand vesicles with CD86 and CD80I2R, as well as significantly less CTLA4 colocalisation with ligand (**Figure 4.14B**). Overall, these results supported flow cytometry data suggesting monovalent ligands (CD80I2R and CD86) dissociate from CTLA4 following internalization, whilst dimeric, bivalent CD80 remains bound.

It is known that CTLA4 traffics through intracellular organelles via an endocytic pathway that requires a pH gradient from early endosomes (~pH 6.5) with increasing acidification moving toward lysosomes (~pH 4.5). As we observed an increased dependency on pH for transendocytosis, and increased ligand dissociation from CTLA4 post-internalisation via microscopy for CD80I2R compared to CD80, we sought to determine if this could be driven by pH changes. For this, we used DG75 cell lines expressing equal levels of CD80, CD86, CD80I2R or a high-affinity CD86 mutant, CD86-H113L. We then incubated these cells with CTLA4-Ig directly conjugated to APC for 30 minutes before washing in buffers of decreasing pH and detecting remaining CTLA4-Ig-APC by flow cytometry. CTLA4-Ig showed robust binding to CD80 at every pH with a 10% reduction at pH 4.5 compared to 7.5 (neutral pH). In contrast, CTLA4-Ig dissociated from CD86 under acidic condition (~80% reduction). Whilst binding of CTLA4-Ig to CD80I2R did not dissociate as readily as CD86 at low pH, there was a significant increase in dissociation when compared to CD80, showing

~30% loss in binding at pH 4.5. This level of pH dependent dissociation was also seen with a CD86 variant CD86-H113L (~30%), suggesting the H113L mutation increases CTLA4 binding by modulating pH dependency **(Figure 4.15A and B).**

Taken together, these results suggested monovalent ligands are more likely to dissociate from CTLA4 within lower pH compartments compared with bivalent CD80 dimers.
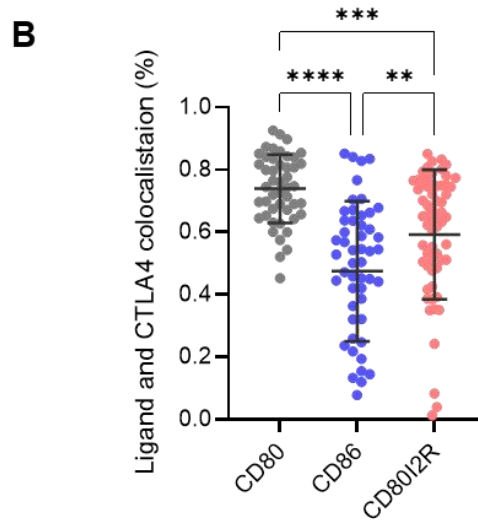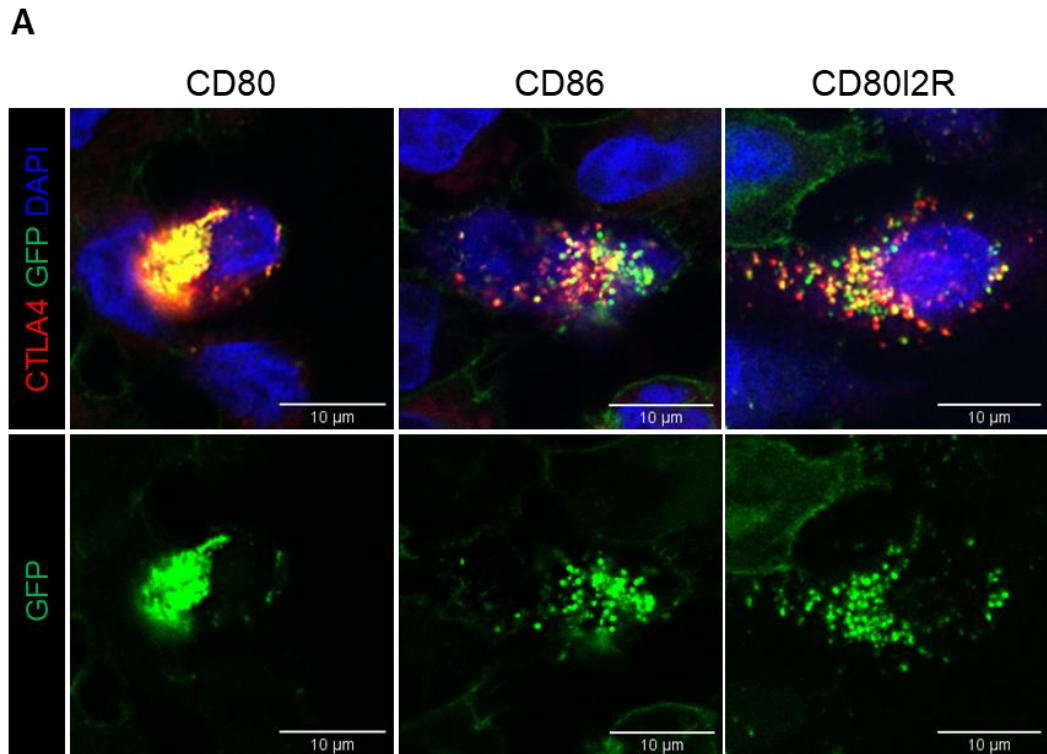
Figure 4. 14. Confocal microscopy analysis following CTLA4 transendocytosis reveals CD80I2R has a CD86-like phenotype. (A). Confocal microscopy analysis following 6 hour transendocytosis of CHO CTLA4 at a 1:1 ratio with CD80-, CD86- or CD80I2R-GFP. Cells stained with anti-CTLA4 (C19; Red), and nuclear stain (DAPI; blue), and analysed for GFP (green). Scale bar = 10μm **(B).** Analysis of colocalization of CTLA4 and GFP (%). Data is from >40 cell per condition, representative of 2 individual experiments as mean +- SD, analysed by one-way ANOVA ns = p>0.05 *p≤0.05, **p≤0.01,***p≤0.001, ****p≤0.0001. Quantification was performed in CellProfiler.

A
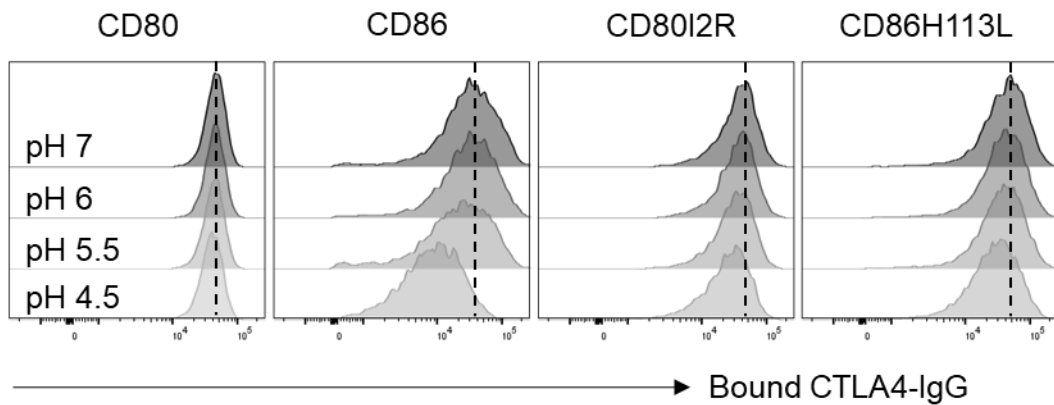
B
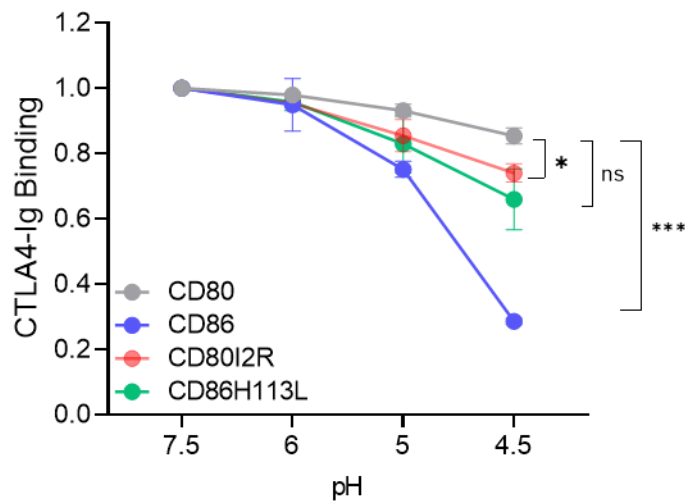
Figure 4. 15. CTLA4 binding to CD80I2R is more pH sensitive,:a high-affinity CD86 phenotype. CHO cells expressing CD80-, CD86-, CD80I2R- or CD86H113L-GFP were stained with 10µg/ml of Abatacept (CTLA4-Ig)-APC at 4ºC for 30 minutes before 3 washes in buffers of indicated pHs. FACs histograms shown in **(A).** and quantified in **(B).** Data shown as mean +- SD from 2 independent experiments, analysed by two-way ANOVA ns = p>0.05 *p≤0.05, **p≤0.01,***p≤0.001, ****p≤0.0001. Quantification was performed in CellProfiler.

4.2.6. Dimerisation is required for CD80 induced CTLA4 ubiquitination

Having observed an increased rate of transendocytosis of CD80I2R, in addition to augmented dissociation from CTLA4 in a manner more like CD86, we wanted to study the fate of CTLA4 following transendocytosis. For this, we used a biochemical approach to assess post-translational modification or degradation of CTLA4 itself. Experiments were initially performed with WT CD80 and CD86, as it was important to understand natural ligand behavior before comparing avidity mutants.

We co-incubated CHO cells expressing CTLA4 with CHO cells expressing no ligand (NL), CD80-GFP or CD86-GFP at various time-points to allow transendocytosis before lysis and analysis by western blotting for CTLA4. This revealed a CD80 induced time-dependent increase in the molecular weight of CTLA4 (**Figure 4.16A,** seen as upward smearing, red box), indicative of post-translational modification, which was absent following ligation of CD86.

As a highly endocytic protein, CTLA4 not only undergoes rapid recycling, but also has a short half-life due to lysosomal degradation (Qureshi et al., 2012a). Moreover, previous work in our lab had suggested CTLA4 ubiquitination via the lysine rich CTLA4 tail as a key signal in directing CTLA4 for lysosomal degradation (Kaur, 2014; Kennedy et al., 2022). Therefore, we repeated this experiment using a CTLA4 mutant lacking all C-terminal lysine residues (CTLA4 Kless). As seen in **Figure 4.16B & 4.16C**, CD80 did not induce a change in molecular weight of CTLA4 Kless, suggesting this modification was CTLA4 ubiquitination. Additional experiments supporting this modification is a result of ubiquitination are also included in our recent publication (Kennedy et al., 2022).

We then tested CD80I2R in this assay to determine the impact of dimerisation on ubiquitination. Intriguingly, transendocytosis with CD80I2R-GFP did not result in post-translational modification of CTLA4 **(Figure 4.16D**). Moreover, a lower molecular weight band was identified (~15kDa) following CD80 ligation, but not following CD86 or CD80I2R, potentially indicating a CTLA4 degradation product. Together, this data suggested ubiquitination was dependent on bivalent ligand binding.

To investigate this in further detail, we performed an immunoprecipitation via the ligand-GFP-tag to isolate only CTLA4 bound to ligand following 4-hour transendocytosis and blotted for ubiquitin. In this experiment, we used both CTLA4 Kless and a CTLA4 mutant lacking the 36 aa CTLA4 tail (Δ36) as a control. As shown in **Figure 4.17A**, precipitation via CD80 effectively pulled down CTLA4, CTLA4 Kless and CTLA4Δ36.. Precipitations with CD86-GFP recovered ~20% CTLA4 WT, consistent with weaker affinity and dissociation as previously observed in **Figure 4.4.** Blotting for ubiquitin revealed a strong ubiquitination signal following CD80 isolation of CTLA4 WT, seen as a smear between 37-100 kDa and consistent with multiple ubiquitination of CTLA4 (**Figure 4.17A**). In contrast, this signal was not seen following CD80 immunoprecipitation with CTLA4 Kless or Δ36 or following CD86 isolation of CTLA4. These observations are therefore consistent with CD80 driving ubiquitination of lysine residues in the CTLA4 tail.

To determine whether higher order lattice formation was required for this fate, we repeated this GFP immunoprecipitation with monomeric CTLA4 C157A, and monovalent ligand CD80I2R. **Figure 4.17B**. shows that precipitation via CD80- and CD80I2R-GFP effectively isolated both CTLA4 WT and C157A

although there was a ~20% reduction in CTLA4 C157A recovery. In addition, again CD86 failed to isolate CTLA4 C157A, as shown previously **Figure 4.4**). Blotting for ubiquitin revealed that whilst a signal was again seen (albeit weaker than previously observed, likely due to alternate lysis buffer used) following CD80 isolation of CTLA4 WT, ubiquitin was not seen in complex within any other condition.
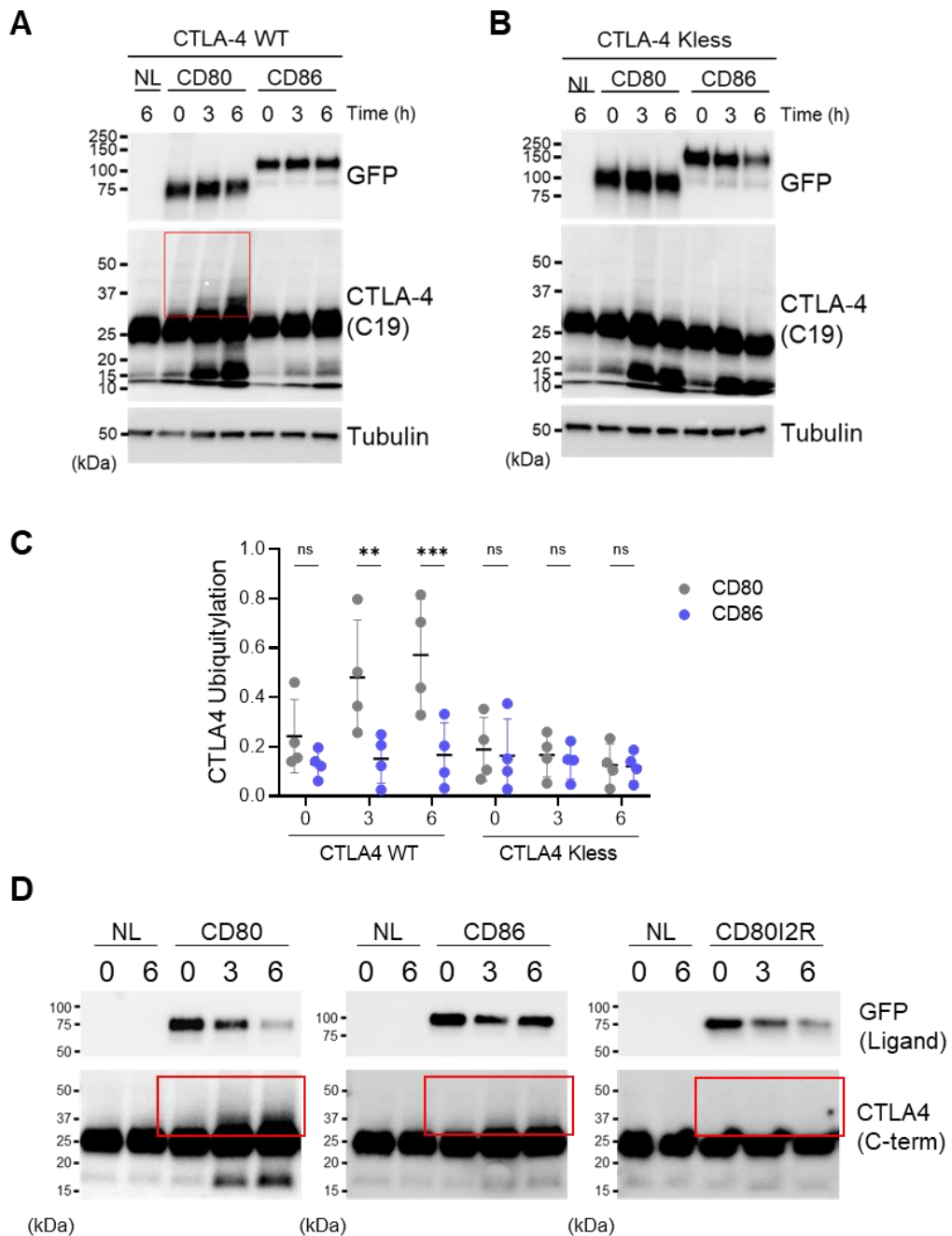
Figure 4. 16. Transendocytosis of CD80 results in lysine dependent CTLA4 post-translational modification. Western blot analysis of total lysates following transendocytosis at indicated time points of CHO CTLA4-WT **(A)** or CTLA4-Kless **(B)** with CHO CD80-GFP, CD86-GFP or cells expressing no ligand (NL) at a 3:1 ratio. Lysates blotted for anti-CTLA4 (C19), anti-GFP and Tubulin. **(C).** Quantification of anti-CTLA4 blots in **(A)** and **(B)** showing >25kDa smear density relative to 25kDa band. Data shown as mean +- SD from 3 independent experiments, analysed by two-way ANOVA ns = $p > 0.05$, **$p \leq 0.01$,***$p \leq 0.001$. Quantification was performed in ImageJ, **(D).** Same as **(A)** with CD80 (left), CD86 (middle) and CD80I2R (right). Increased Mw CTLA4 indicated by red box.

7
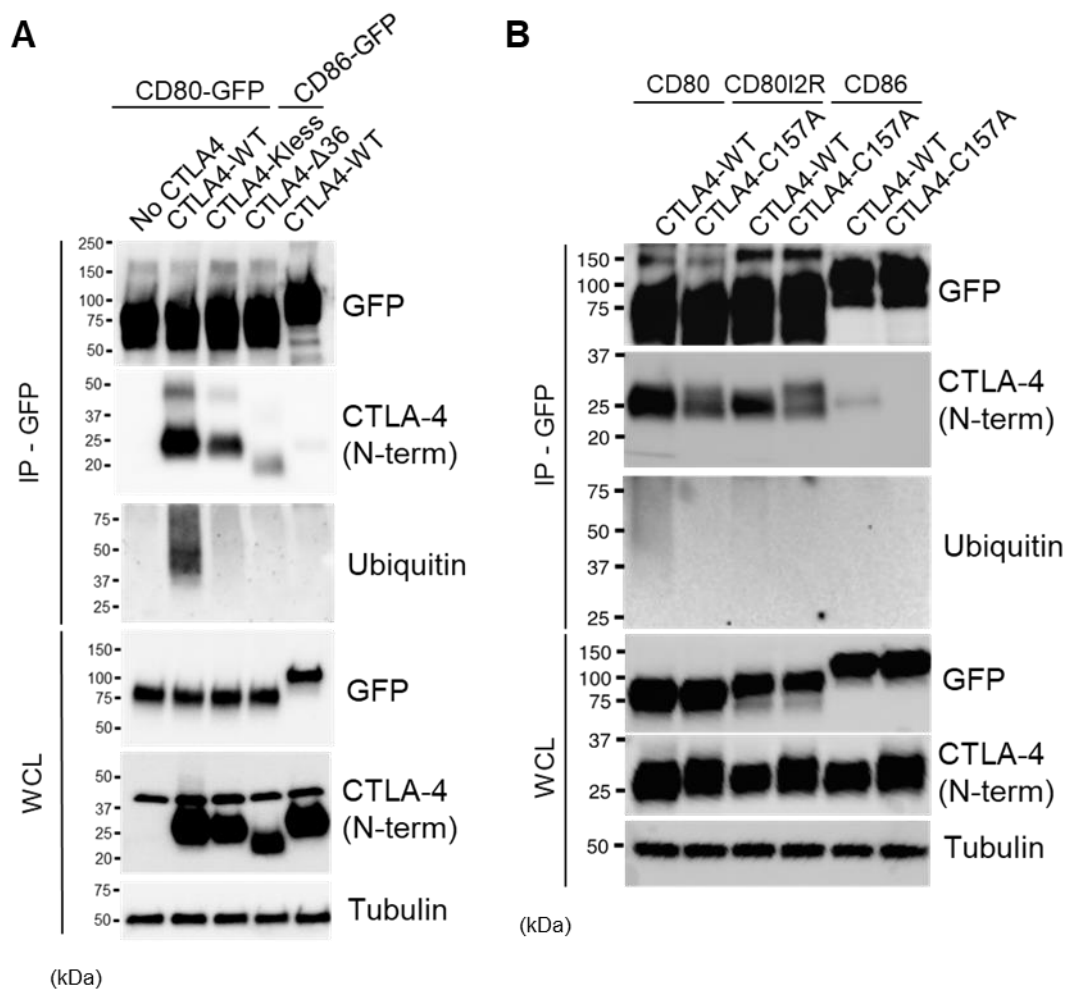
Figure 4. 17. Ligand immunoprecipitation following transendocytosis shows CD80 remains complexed with ubiquitinated CTLA4, in a manner dependent on bivalent binding. (A). Western blot analysis of CHO transendocytosis was performed at a 3:1 ratio for 4 hours followed by immunoprecipitation of CD80-GFP or CD86-GFP using GFP-Trap beads. Precipitates from CTLA4-WT, CTLA4-Kless and CTLA4-4 lacking a cytoplasmic domain (Δ36) were blotted for GFP, CTLA4 (N-term), and ubiquitin, with whole cell lysates (WCL) also blotted for tubulin. **(B)** Experiment in **(A)** was repeated with CHO CTLA4 WT and C157A cells mixed with CD80-, CD80I2R- and CD86- GFP CHO cells.

Whilst this observation supported that CD80 induced ubiquitination was dependent on CTLA4 lattice formation due to a bivalent interaction, this did not exclude the possibility CTLA4 ubiquitination was not observed simply because less CTLA4 was co-precipitated, due to lower avidity/affinity interactions and/or increased dissociation. Therefore, we repeated the transendocytosis experiments, but performed immunoprecipitation of all ubiquitin-associated proteins, before blotting for CTLA4.

As shown in **Figure 4.18A**, following transendocytosis with CD80 we observed a time-dependent increase in the amount of CTLA4 recovered by ubiquitin immunoprecipitation. In contrast, CD86 was clearly unable to drive ubiquitination of CTLA4, with no increase in the amount of CTLA4 recovered by ubiquitin immunoprecipitation above that of the no ligand control. Interestingly, not only did CD80 drive an increase in a 37kDa CTLA4 band (the molecular weight of CTLA4 + ubiquitin), but also in the intensity of the 25kDa band of CTLA4. As 25kDa is the molecular weight of native CTLA4, this observation suggested that CTLA4 was potentially associated with a ubiquitinated partner. Therefore, when isolating all ubiquitinated proteins, this protein in complex with unmodified CTLA4. In support of this hypothesis, a 25kDa species of CTLA4 was also recovered by ubiquitin immunoprecipitation following CD80 transendocytosis with CTLA4 Kless. Moreover, whilst a 37kDa band was clearly detectable for CTLA4 WT in the no ligand control, and following incubation with CD86 ligand, it was never present in CTLA4 Kless conditions. Consequently, we concluded that there is a constant basal level of CTLA4 ubiquitination on lysine residues, likely involved in its characteristic high turnover, that was selectively enhanced by CD80 ligation, but not CD86.

To confirm our hypothesis that this difference is a result of CD80 being able to form higher-order structures, we tested monomeric CD80I2R and CTLA4 C157A. As shown in **Figure 4.18B**, we once more saw an increase in ubiquitinated CTLA4 WT following transendocytosis with CD80, but not with CD86. Moreover, as predicted, CD80I2R did not increase CTLA4 ubiquitination, supporting CD80 dimerisation and bivalent binding as a key step in CTLA4 ubiquitination.

Surprisingly, in contrast to immunoprecipitations via the ligand-GFP tag, isolation of ubiquitinated proteins identified that CD80 also drove ubiquitination of CTLA4 C157A, as shown by an increase in the amount of CTLA4 recovered. One possibility is that despite lacking a disulphide bond, CD80 dimers can still cluster CTLA4, or CTLA4 may still form non-covalent dimers in some settings (akin to CD80 I2R), perhaps allowing ubiquitination to proceed.

Taken together, we concluded that CTLA4 clustering is a likely key step in CTLA4 ubiquitination and that CD80 dimerisation is essential for this mechanism of CTLA4 regulation, but that CTLA4 C157A does not completely disrupt this process.
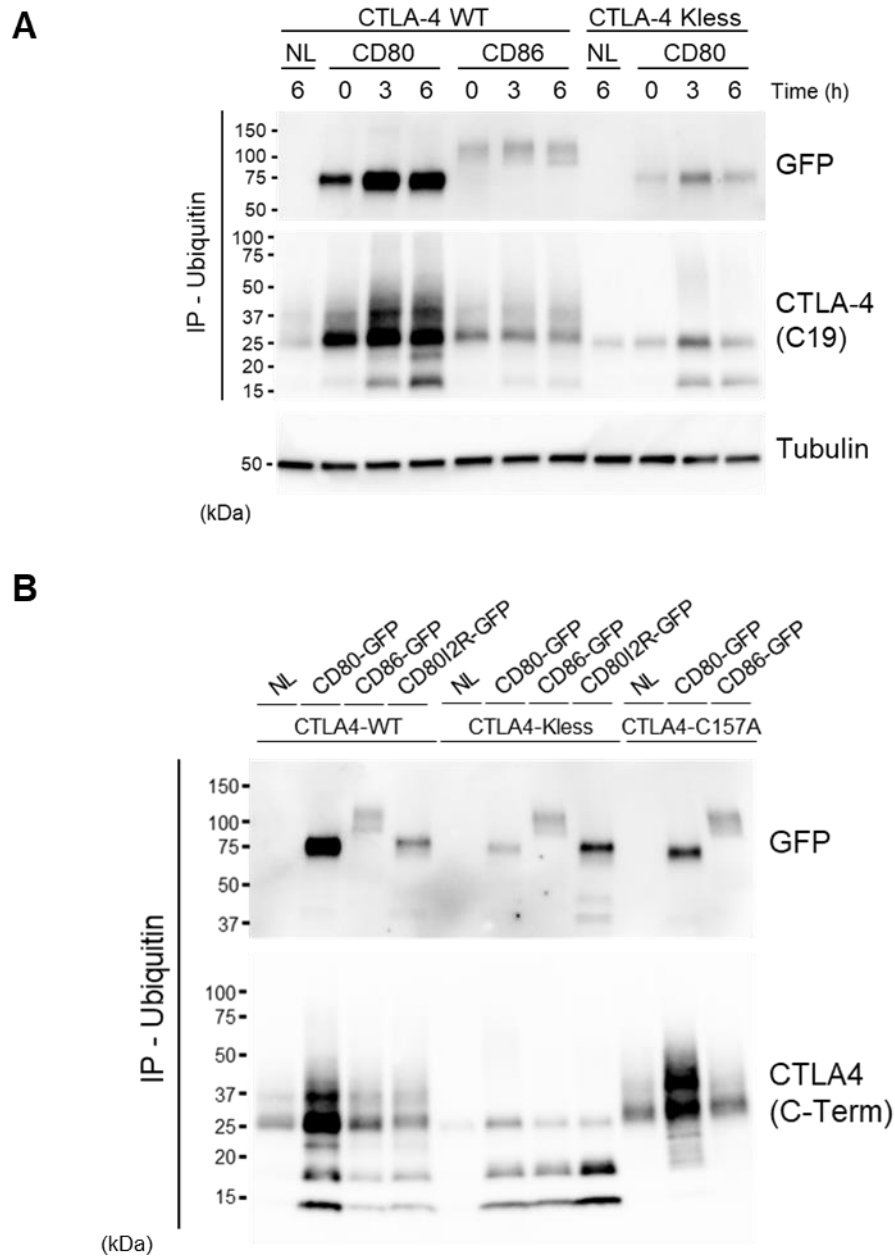
Figure 4. 18. CD80I2R does not drive CTLA4 ubiquitination. (A). Western blot analysis of transendocytosis assay from CHO CTLA4 WT or Kless incubated at a 1:5 ratio with CHO CD80- of CD86-GFP, or CHO cells expressing no ligand (NL) at indicated times, before immunoprecipitation of ubiquitin. Lysates post-IP were blotted using anti-GFP and anti-CTLA4 (C-term), with whole cell lysates (WCL) blotted for tubulin. **(B).** Transendocytosis assay followed by ubiquitin immunoprecipitation as in **(A).** With CHO CTLA4-WT, CTLA4-Kless and CTLA4-C157A with CHO CD80-, CD86- or CD80I2R. All blots representative of at least 3 independent experiments.

4.2.7. *Cis* interaction of CD80:PDL1 increases CD80 transendocytosis efficiency and prevents CTLA4 ubiquitination

Observations so far led us to hypothesize that the dimerisation status of CD80 influences outcomes for CTLA4 mediated transendocytosis. As shown in Chapter 3, we identified co-expression of PDL1 can bind at the CD80 dimer interface and disrupt CD80 homodimerisation. Therefore, we wanted to test whether similar phenotypic changes with regards to increased rate of transendocytosis and inability to promote ubiquitination were also observed when PDL1 was co-expressed with CD80.

For this, we employed our transendocytosis assay using CHO cells expressing CD80-, CD86-, CD80I2R- or CD80-GFP expressed in *cis* with PDL1 tagged with mCherry, incubated overnight with CHO cells with or without CTLA4 at a 1:3 receptor to ligand ratio. As shown in **Figure 4.19A**, the presence of CTLA4 allowed near complete depletion of all ligands from the CTV+ cells due to transendocytosis. Notably, whilst CD80 remained detectable in the CTV-recipient cells (lower right quadrant, red box) when expressed alone, CD80I2R and CD80 in the presence of PDL1 did not show evidence of ligand uptake despite effective removal (**Figure 4.19A**). These data are again consistent with dimeric interactions between CTLA4 and its ligand leading to more obvious detection of captured ligand, whereas monomeric CD80 ligands behave more like CD86.

Subsequently, we performed kinetic analysis to monitor how the presence of PDL1 affects loss of CD80 over time (**Figure 4.19B, data provided by Dr Alan Kennedy**). Strikingly, we saw that not only did loss of CD80 from the donor cell continue over time in both the presence and absence of PDL1, but PDL1 co-

expression appeared to have an enhanced rate of transendocytosis, as seen previously with CD80I2R. Furthermore, PDL1 had no effect on the rate of transendocytosis of CD86, supporting that there is no interaction between PDL1 and CD86.
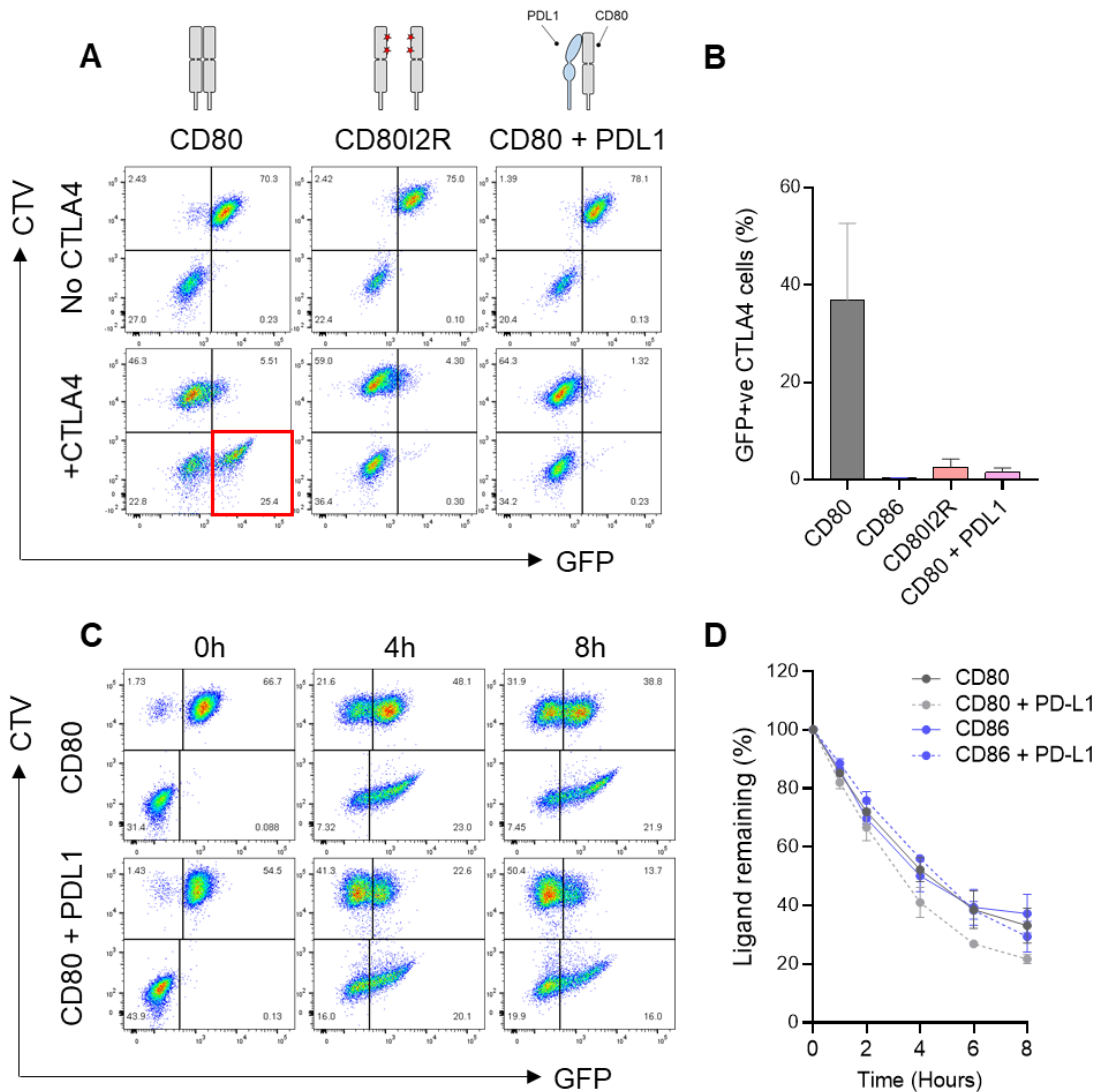
Figure 4. 19. CTLA4 mediated transendocytosis of CD80 in the presence of PDL1 displays a CD80I2R phenotype. (A). Transendocytosis assay using CHO cells expressing CD80-GFP, CD80I2R-GFP or CD80-GFP with PDL1-mCherry co-expressed, labelled with CellTrace Violet (CTV) and incubated with CHO cells expressing no receptor, or CTLA4 at a 1:3 ratio overnight. Red box shows ligand gain into CTV- cells, with % GFP+CTV- from all conditions in **(B).** **(C).** Transendocytosis assay of CHO CTLA4 cells incubated at a 1:3 ratio with CTV labelled CD80-GFP alone or CD80-GFP with PDL1-co-expressed, at times indicated. Performed by Dr. Alan Kennedy **(D).** Full kinetic analysis of **(C).** with additional data for CD86-GFP +- PDL1 co-expression shown. All data from 3 independent repeats shown +- SD.

Despite efficient depletion of CD80, PDL1 itself was not removed by CTLA4 even by 21 hours (**Figure 4.20A**), demonstrating the remarkable specificity of CTLA4 transendocytosis. Following this observation, we hypothesized that CTLA4 binds CD80 in a manner which stabilizes CD80 dimers and potentially disrupts the CD80:PDL1 *cis* interaction, leaving PDL1 behind. To test whether this was due to CTLA4 being a dimer, we also performed transendocytosis with CTLA4 C157A. As a monomer, we predicted that C157A would not stabilise CD80 homodimers However, we observed that CTLA4 C157A did not result in PDL1 depletion from the donor expressing cell (**Figure 4.20A and B**) and transendocytosis was still highly specific for CD80.
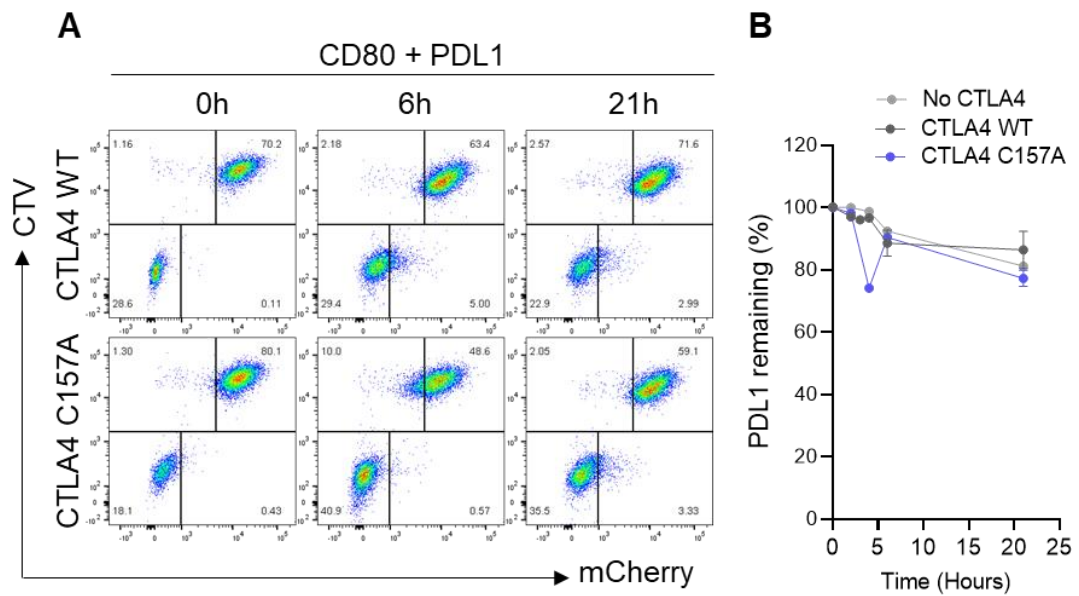
Figure 4. 20. PD-L1 is not removed with CD80 during transendocytosis with either dimeric or monomeric CTLA4. (A) CHO cells expressing CTLA4 WT or CTLA4 C157A were incubated with CellTrace Violet (CTV) labelled CHO cells co-expressing CD80-GFP and PDL1-mCherry at a 3:1 ratio at indicated time points, with full kinetic analysis shown in **(B).** All data from 3 independent repeats shown +- SD.

Since transendocytosis assays suggested CD80 in the presence of PDL1 displayed a CD80I2R-like phenotype, we speculated that PDL1 should also impair CD80 induced ubiquitination of CTLA4. To test this, we performed a ubiquitin immunoprecipitation following transendocytosis with CHO cells expressing CTLA4, mixed with CHO cells expressing CD80, CD86 or CD80I2R-GFP alone, or co-expressed with PDL1-mCherry. As previously observed, an increased molecular weight species of CTLA4 was isolated following CD80 ligation, representing ubiquitinated CTLA4, but not following CD86 or CD80I2R ligation. Co-expression of PDL1 and CD80 clearly reduced the amount of ubiquitinated CTLA4 seen (red box), in line with our hypothesis that CD80 dimerisation was required for this phenotype (**Figure 4.21**). Notably, whilst both CD80 and CD80I2R were recovered in this pull-down (GFP blot, top panel), reflecting high-affinity binding to CTLA4, PDL1 was never recovered, as seen by absence of mCherry signal following immunoprecipitation, suggesting it dissociates from CD80 for transendocytosis.

We wanted to strengthen our ubiquitin observations by studying ligand induced ubiquitination using additional experimental methods. Therefore, we opted to perform a proximity ligation assay (PLA). The principle of *in situ* PLA is depicted in **Figure 4.22A**, where two primary antibodies against proteins of interest are subsequently detected by specialized secondary antibodies conjugated to two corresponding oligos (PLA probes). If oligos are within proximity (<40nm), they ligate and undergo rolling circle amplification. The resultant circular DNA is detected by complimentary oligos coupled to fluorochromes, and are thus detectable by fluorescent microscopy as discrete dots.

PLA staining was performed using antibodies against CTLA4 and ubiquitin following CHO transendocytosis experiments using CD80, CD86, CD80I2R or CD80 + PDL1, to monitor the level of CTLA4 ubiquitination. Resulting composite images are shown in (**Figure 4.22B**) and PLA signal alone shown in (**Figure 4.22C**). Consistent with biochemical data, background ubiquitination was evident in the presence of CD86 and CD80I2R, but CD80 significantly increased the number of PLA puncta, representing an increase in the association between ubiquitin and CTLA4. Moreover, when PDL1 was expressed with CD80, the PLA signal was reduced (29.7 dots/cell for CD80 vs 18.1 dots/cell for CD80+PDL1) (**Figure 4.22D**). Accordingly, this data supports that CD80 dimerisation is required to induce CTLA4 ubiquitination and disrupted by PDL1.
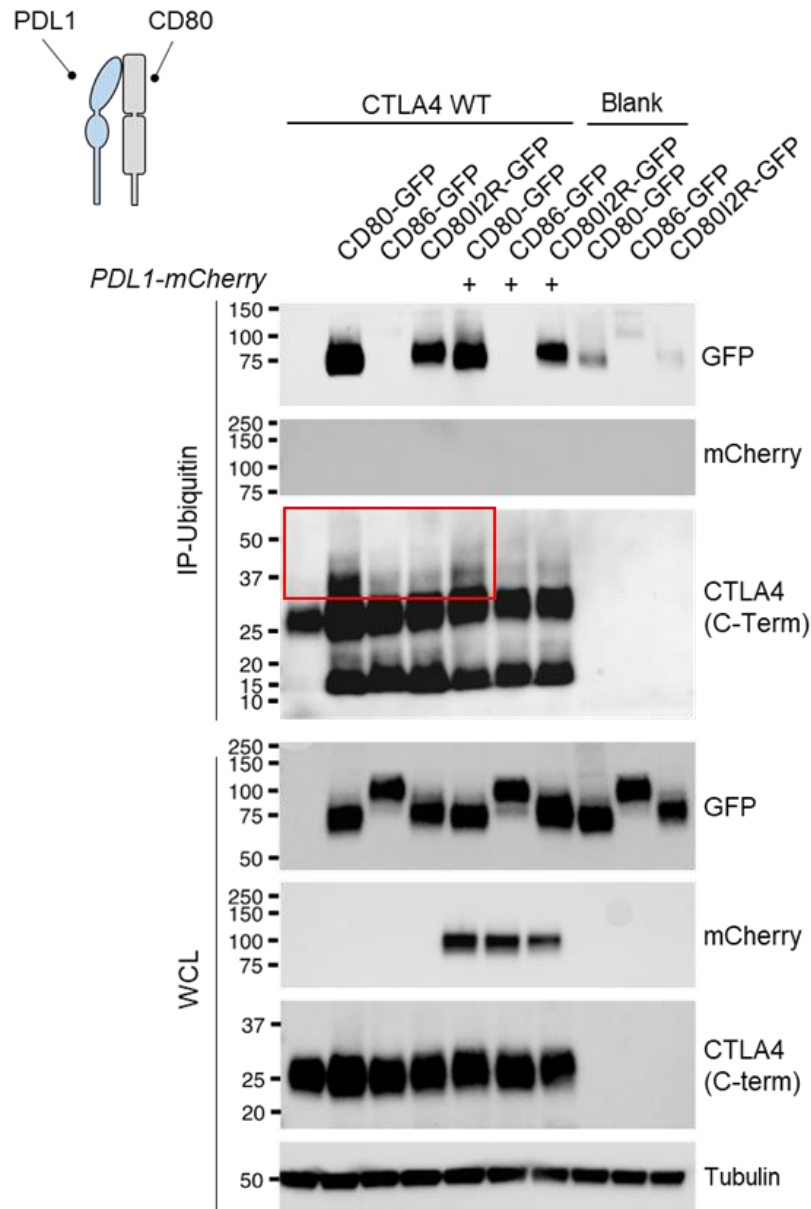
Figure 4. 21. *Cis* **expression of PDL1 impairs CD80 in inducing CTLA4 ubiquitination.** Western blot analysis of transendocytosis assay from CHO CTLA4 WT or untransduced (Blank) lines incubated at a 1:5 ratio with CHO CD80- of CD86-GFP, CD80I2R-GFP either alone or co-expressed with PDL1-mCherry for 4 hours, before immunoprecipitation of ubiquitin. Lysates post-IP were blotted using anti-GFP, anti-mCherry and anti-CTLA4 (C-term), with whole cell lysates (WCL) blotted for the same, as well as tubulin. Data representative of 2 similar experiments.
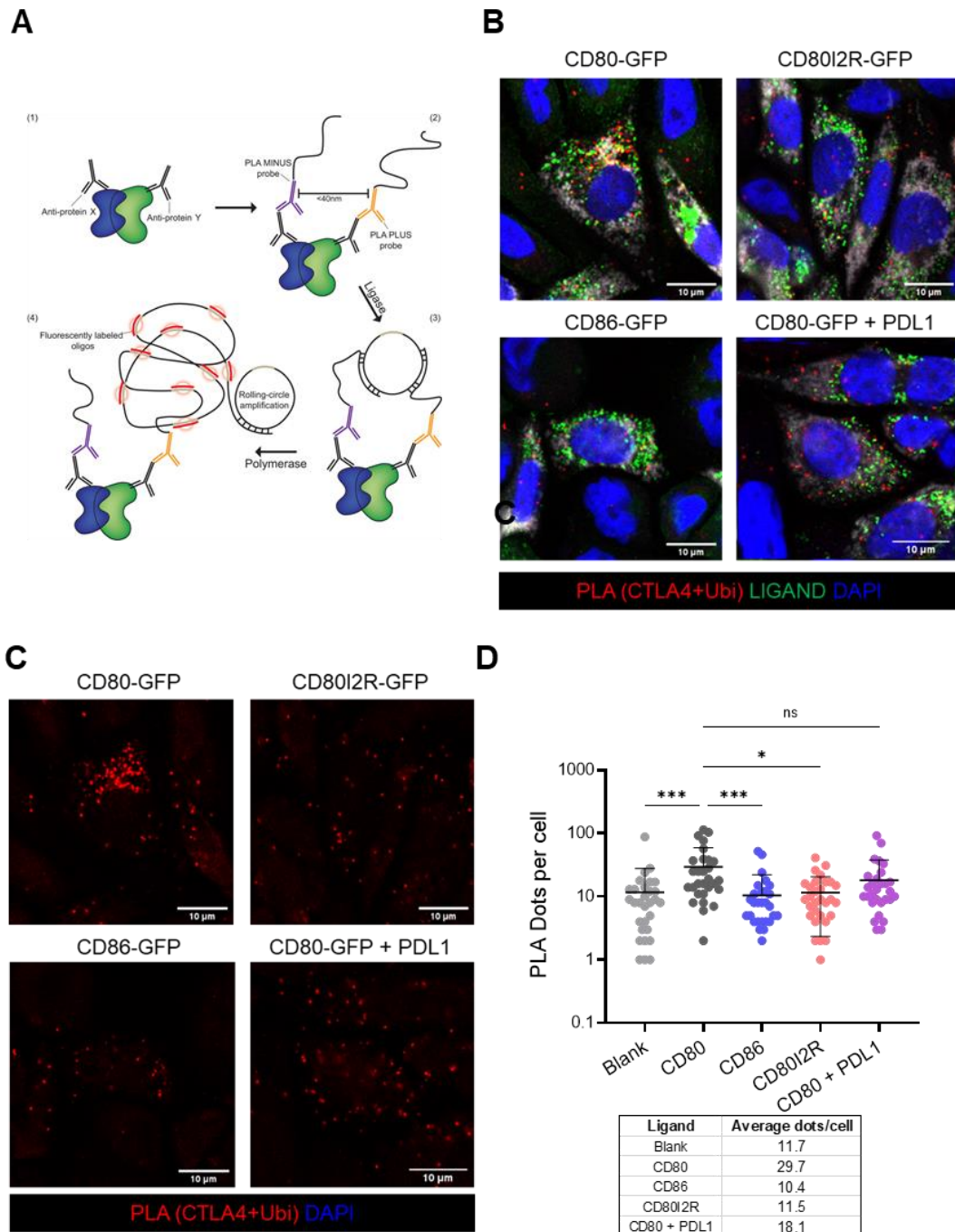
Figure 4. 22. Proximity ligation assay (PLA) for visualization of CTLA4:CD80:Ubiquitin complexes by confocal microscopy. (A) Cartoon representation of PLA **(B)** PLA analysis of overnight transendocytosis in CHO cells with CTLA4 WT and CD80-GFP, CD80I2R-GFP, CD86-GFP of CD80-GFP with PDL1 (green) at a 1:3 ratio. Primary antibodies against goat-anti-CTLA4 (C19) and mouse-anti-ubiquitin (PD41), with resultant PLA signal (red). **(C).** As in **(B),** showing only PLA signal. Nuclei are stained with DAPI (blue). Scale bar = 10μm. **(D)** Analysis of PLA signal. Data from 30 cells per condition, representative of 2 individual experiments as mean +- SD, analysed by Kruskal-Wallis test. ns = p>0.05 *p≤0.05, **p≤0.01,***p≤0.001, ****p≤0.0001. Quantification was performed in CellProfiler.

4.2.8. CTLA4 Kless mutant reveals monovalent ligand transendocytosis efficiency is dependent on the ability of CTLA4 to recycle

Previous studies in the lab confirmed that the CTLA4 Kless mutant showed increased recycling to the cell surface compared to CTLA4 WT, since it was not trafficked via ubiquitin-dependent pathways for degradation (Kennedy et al., 2022). Therefore, to address whether recycling of CTLA4 following dissociation of ligand was responsible for the increase in transendocytosis efficiency for CD80I2R and CD80 bound to PDL1, we used the CTLA4 Kless mutant in a transendocytosis assay.

For this, CHO cells expressing CD80, CD80I2R, CD80 + PDL1 or CD86 were co-incubated at a 3:1 ratio with CTLA4 WT or Kless for 6 hours. As shown in **Figure 4.23A**, CTLA4 WT depleted CD80I2R (47.2% CTV+GFP-) and CD80 + PDL1 (46.8% CTV+GFP-) equivalently and more efficiently than CD80 WT (38.4% CTV+GFP-). In this experiment, CD86 expression was unfortunately lower than other ligand lines, and therefore was almost completely degraded at this time point.

As shown in **Figure 4.23A** CTLA4 Kless was less efficient at removing CD80 compared to CTLA4 WT. In contrast, CTLA4 Kless exhibited a clear advantage in transendocytosis of CD80I2R, CD80+PDL1 and CD86 (**Figure 4.23A, red shaded quadrants**). Quantification of ligand removal by CTLA4 Kless relative to CTLA4 WT supported these observations **(Figure 4.23B)**, suggesting the ability of CTLA4 to recycle underpins transendocytosis efficiency of monovalent ligands. Moreover, whilst CD80I2R, CD80+PDL1 and CD86 were undetectable in CTV- CTLA4 Kless recipients, CD80 was more readily detectable, even over CTLA4 WT (**Figure 4.23A, blue shaded quadrants**).
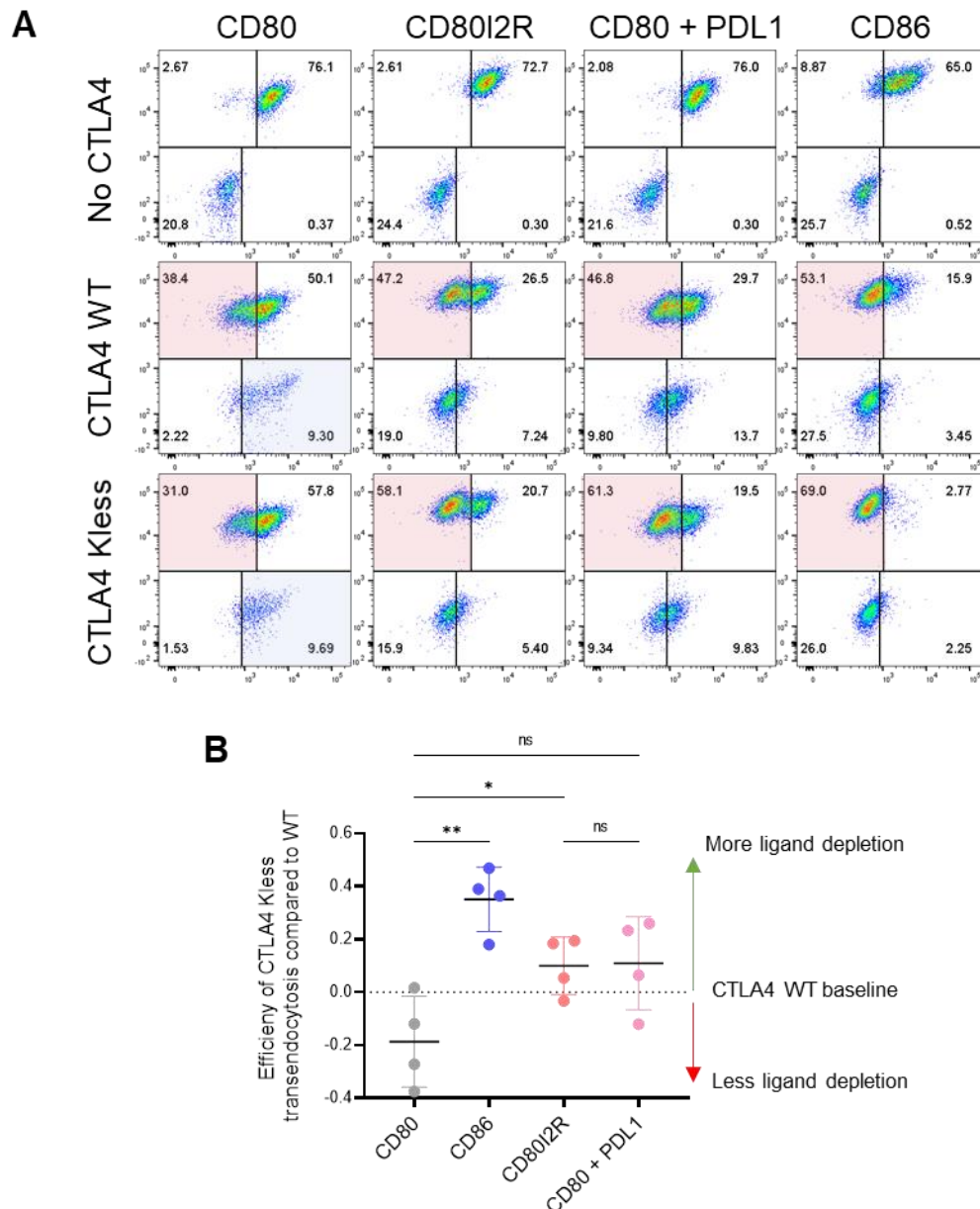
Figure 4. 23. CTLA4 Kless is more efficient at monovalent ligand transendocytosis, but impaired in bivalent ligand transendocytosis. (A) Untransduced CHO cells (no CTLA4) or CHO cells expressing CTLA4 WT or CTLA4 Kless were incubated at a 1:3 ratio with CellTrace Violet (CTV) labelled CHO cells expressing CD80-, CD80I2R-, CD86-GFP or CD80-GFP co-expressed with PDL1-mCherry for 6 hours. FACs analysis shows CTV vs ligand-GFP. **(B)** GFP MFI from quadrants highlighted in red box in **(A)** are quantified as change in ligand depletion by CTLA4 Kless, compared to CTLA4 WT. Data shown from 4 similar experiments as mean +- SD, analysed by One-Way ANOVA. ns = p>0.05 *p≤0.05, **p≤0.01,***p≤0.001, ****p≤0.0001.

To understand these observations, we used confocal microscopy to assess CTLA4 WT and Kless dissociation from ligand following transendocytosis. The presence of PDL1 resulted in smaller intracellular vesicles and increased dissociation as seen by decreased CTLA4 and ligand co-localization (**Figure 4.24)**. This phenotype is remarkably like CD80I2R and CD86 and supports all prior observations regarding similarities with monovalent ligands.

Strikingly, following transendocytosis with CTLA4 Kless, CD80 appeared highly colocalized with CTLA4 in circular 'donut' structures, as opposed to typical punctate vesicles observed with CTLA4 WT (**Figure 4.25, top panel, white arrow**). In contrast, CD86, CD80I2R and CD80+PDL1 did not exhibit this phenotype in the CTLA4 Kless conditions, and instead were comparable to CTLA4 WT conditions showing CTLA4 dissociation and small ligand puncta (**Figure 4.25**). Moreover, examination of the CTLA4 channel alone (**Figure 4.25,** middle panel, top row) suggested that following transendocytosis of CD80, there was minimal CTLA4 Kless remaining that was not complexed with ligand. This is unlike all other ligand conditions, where vesicular cytoplasmic CTLA4 was readily observed. Together, these data support our conclusions that bivalent CTLA4:CD80 interactions traffic via a ubiquitin dependent pathway due to lack of complex dissociation, whereas monovalent ligand dissociate from CTLA4 in a lysine independent manner.
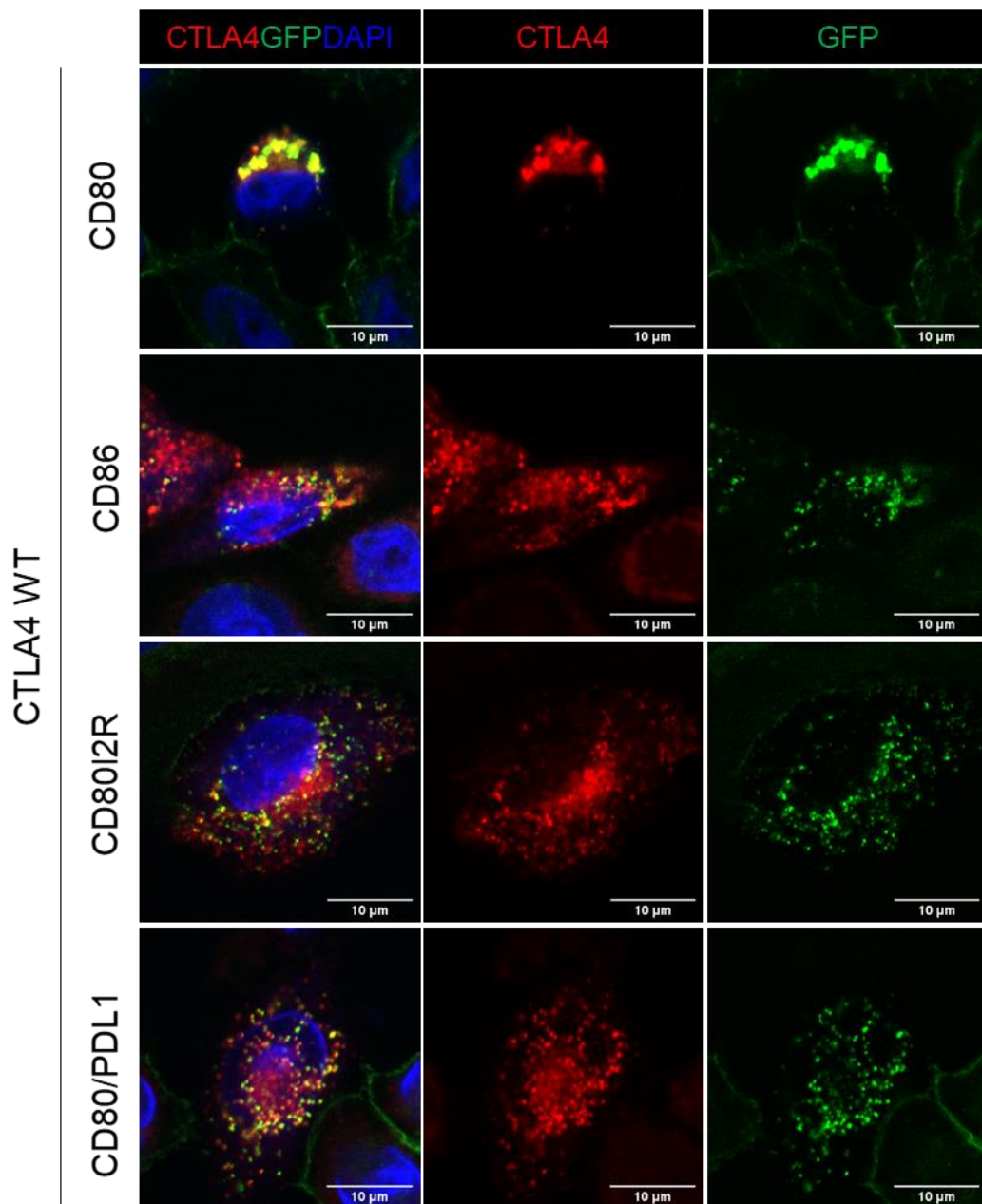
Figure 4. 24. PDL1 co-expression permits CD80 dissociation following transendocytosis, suggestive of a monovalent ligand:CTLA4 interaction. Confocal microscopy analysis following 6 hour transendocytosis of CHO CTLA4 at a 1:1 ratio with CD80-, CD86- or CD80I2R-GFP, or CD80-GFP co-expressed with PDL1-mCherry. Cells stained with anti-CTLA4 (C19; Red), and nuclear stain (DAPI; blue), and analysed for GFP (green). Figure shows composite image (left), CTLA4 only (middle) or ligand only (right). 1 representative cell from >100 cells from >10 images are displayed. Scale bar = 10µm.
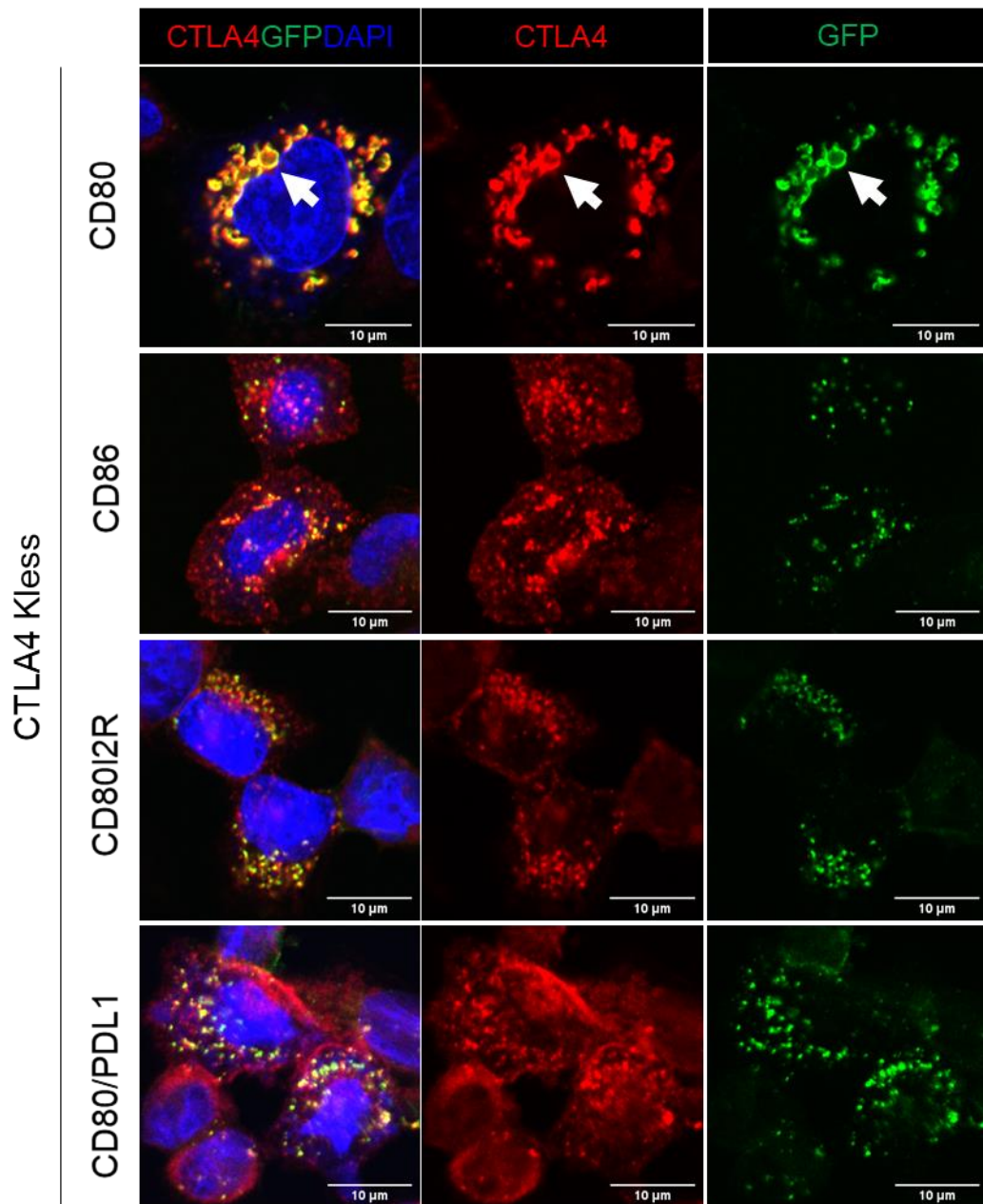
Figure 4. 25. Loss of CTLA4 lysine residues impacts trafficking of bivalent CD80:CTLA4 complexes. Confocal microscopy analysis following 6 hour transendocytosis of CHO CTLA4 Kless at a 1:1 ratio with CD80-, CD86- or CD80I2R-GFP, or CD80-GFP co-expressed with PDL1-mCherry. Co-localized 'donut' structures indicated by white arrows. Cells stained with anti-CTLA4 (C19; Red), and nuclear stain (DAPI; blue), and analysed for GFP (green). Figure shows composite image (left), CTLA4 only (middle) or ligand only (right). 1 representative cell from >100 cells from >10 images are displayed. Scale bar = 10μm.

Due to these observations, we hypothesized that transendocytosis of dimeric CD80 would impair CTLA4 function by remaining bound and being trafficked to lysosomes. In contrast, monovalent ligands dissociate and CTLA4 function is retained by permitting recycling. To test this concept, we performed the transendocytosis assay outlined in **Figure 4.26A**. Here, we used CTV labelled DG75 cells expressing CD80, CD86, CD80I2R or a no ligand control with Jurkat CTLA4 WT or CTLA4 Kless overnight, before adding CTFR labelled DG75 lines expressing mCherry tagged ligand as a re-challenge. Following 6 hours of incubation, we measured transendocytosis efficiency only from the re-challenge, ligand-mCherry line. Here, when Jurkat CTLA4 lines were incubated with DG75 expressing no ligand overnight, CD86-mCherry depletion was readily observed from both CTLA4 WT and CTLA4 Kless (**Figure 4.26B**). However, following initial CD80 transendocytosis, re-challenge CD86-mCherry depletion was impaired as shown as a reduction in CTFR+mCherry- cells (28.4% vs 14.7%, red shaded quadrants). In contrast, overnight incubation with CD86 or CD80I2R did not impair subsequent ligand depletion to the same extent, supporting that these ligands permit continued CTLA4 recycling and retention of function (**Figure 4.26B)**.

Remarkably, following CD80 transendocytosis by CTLA Kless, CD86-mCherry depletion was completely blocked (**Figure 4.26B,** blue shaded quadrants). This was not the case following CD86 or CD80I2R pre-incubation, which again showed CD86-mCherry was able to be removed via transendocytosis. Kless function was therefore consistently blocked by CD80, preventing transendocytosis of CD86 as well as other re-challenge ligands shown as graphs in **Figure 4.26C**. Taken together, this suggests that transendocytosis of CD80 in its dimeric form can regulate CTLA4 function by directing CTLA4 down

a ubiquitin dependent pathway whereas CTLA4 Kless function is blocked and cannot proceed down this route. Conversely, CD86 and CD80I2R do not require CTLA4 lysine residues for resultant trafficking and therefore function is not blocked by removal of CTLA4 lysine residues.
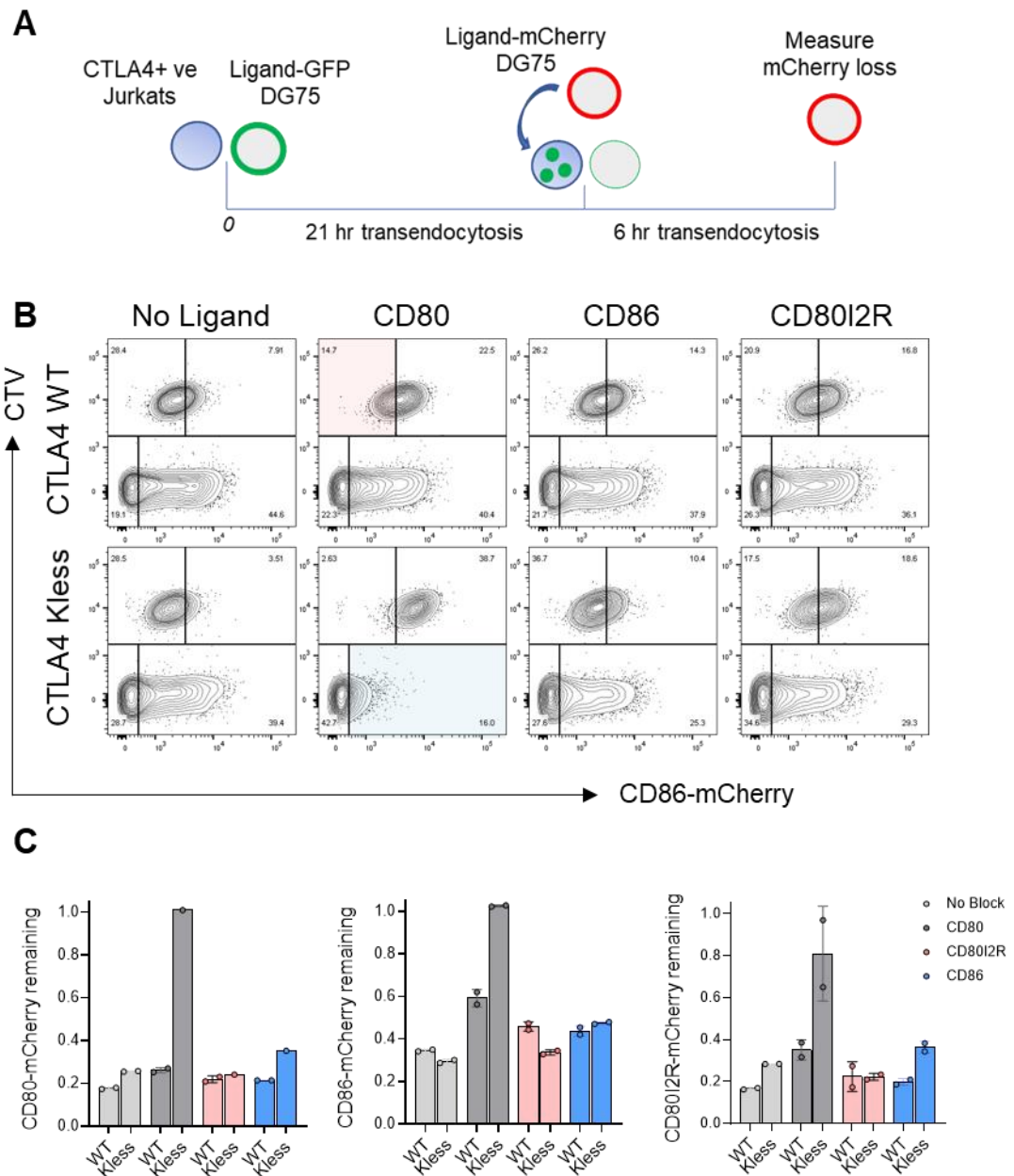
Figure 4. 26. CD80 dimers negatively regulate CTLA4 function by directing CTLA4 down a ubiquitination dependent pathway. (A). Schematic of experiment protocol. Jurkat cells expressing CTLA4 WT or Kless were incubated with CTFR labelled untransduced DG75 cells, or DG75 cells transduced with CD80-GFP, CD86-GFP or CD80I2R-GFP for 21 hours. DG75 cells expressing – mCherry ligands were stained with CTV and added to previous conditions before incubation for 6 hours to measure subsequent TE. Cells were analyzed by flow cytometry for mCherry depletion from CTV+ cells. (**B**). Representative FACs plots for CD86-mCherry depletion from assay described in (A) Ligands cells across the top indicate the primary ligand bearing target. (C). Quantification of CD80-mCherry (left), CD86-mCherry (middle) and CD80I2R-mCherry (right) depletion after 6 hours TE, following 21 hour TE of CD80-, CD86 or CD80I2R-GFP or no TE, with CTLA4 WT and CTLA4 Kless. Data shown from 2 technical repeats as mean +- SD.

4.3. Discussion

CTLA4 is renowned for its inhibitory function on T cells, but its precise mechanism of action is not fully understood (Rowshanravan et al., 2018b). Specifically, whilst CTLA4 controls CD28 co-stimulation by transendocytosis of their shared ligands, it remains elusive why there are two ligands with strikingly differing biophysical characteristics and expression profiles.

We recently proposed a model aimed at explaining these differences following an in-depth comparison of CD80 and CD86 (Kennedy et al., 2022). In this model, the stable high affinity CD80:CTLA4 interaction results in ubiquitination of CTLA4, trafficking the complex towards lysosomes. In contrast, the low affinity CD86:CTLA4 interaction is too weak to survive low pH endosomal compartments, resulting in dissociation and CTLA4 re-entry into the default pathway of CTLA4 recycling (See introduction **Figure 1.4**). In this chapter, we consider the biophysical properties of CTLA4 and its ligands providing a structural explanation underpinning this divergence in CTLA4 fate (**Figure 4.27**).

4.3.1. CTLA4 can compensate for loss of bivalency through increased dissociation and recycling following CD80 transendocytosis

Our first observation is that despite being a monomer, CTLA4 C157A shows no obvious defect in the ability to bind CD80. The CTLA4 crystal structure places the 'MYPPPY' binding motif on the alternate face of that required for CTLA4 dimerisation, such that C157A mutation should not impair CD80 binding (Stamper et al., 2001). In turn, we show that despite loss of avidity, CTLA4 C157A can remove CD80 by transendocytosis as effectively as CTLA4 WT. The CTLA4:CD80 crystal structure shows periodic arrays are dependent on CTLA4

199
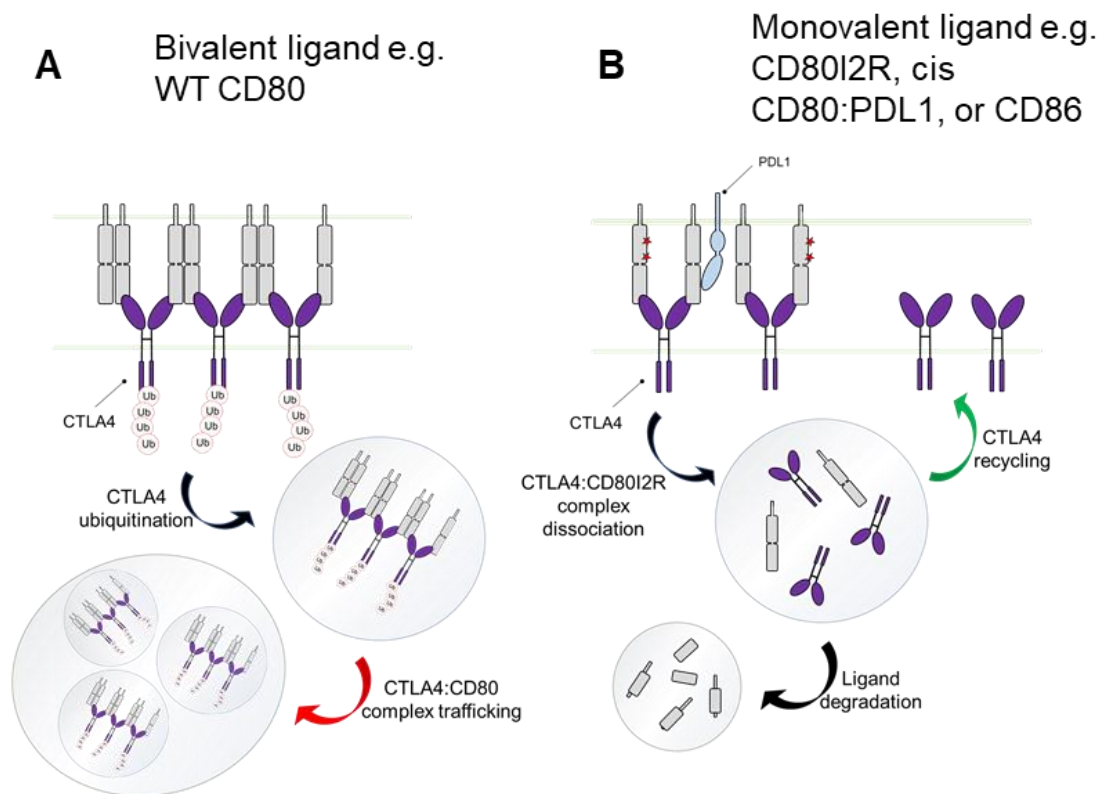
Figure 4. 27. Proposed model: lattice formation by CTLA4:CD80 bivalent interaction is required for CTLA4 ubiquitination following transendocytosis. (A). CTLA4:CD80 lattice formation permits high avidity binding, directing CTLA4 ubiquitination, complex survival in low pH compartments and trafficking to late endosomes/lysosomes **(B).**. CD80I2R, or CD80 expressed in *cis* with PDL1 does not homodimerize and thus binds monovalently to CTLA4. Monovalent CTLA4:CD\80 interactions do not result in CTLA4 ubiquitination, are favoured in complex dissociation in low pH compartments allowing CTLA4 recycling, with CD80 destroyed in lysosomes.

being a homodimer, and therefore it is likely lattices are not formed by a monomeric CTLA4 C157A:CD80 interaction (Stamper et al., 2001). Moreover, a bivalent CTLA4:CD80 interaction is approximately 200-fold stronger than a monovalent equivalent (Greene et al., 1996). Therefore, it may seem paradoxical that CD80 removal would be as efficient. However, an explanation can be based on the differential trafficking of CD80 and CD86 following CTLA4 transendocytosis. That is, if lattice formation is assumed to not occur following a monovalent interaction due to inability to bridge two CD80 dimers, then the loss of an avid CTLA4:CD80 complex increases the probability of CTLA4 dissociating, due to lack of ubiquitination directing the complex towards the recycling pathway, allowing CTLA4 to be re-used for TE.

In support of dissociation, we demonstrate a reduction in CD80 accumulation following transendocytosis by CTLA4 C157A compared to WT, consistent with a loss of phenotypic large, colocalized complexes usually seen for CTLA4 WT:CD80 interactions by microscopy. Together, this suggests CD80 is more rapidly degraded following transendocytosis by CTLA4 C157A, likely due to increased dissociation from weaker binding. Indeed, lysosomal inhibition via NH_4Cl treatment recovers CD80 accumulation. Ligand-receptor complex dissociation following clathrin-mediated endocytosis is well-recognized for many immune functions, such as maintaining extracellular cytokine and chemokine gradients (Lakadamyali et al., 2006; Schwartz, 1995). For example, chemokine receptor CCR7 binds and internalizes its ligand CCL19 before ligand-receptor dissociation in early endosomes permits CCL19 degradation and CCR7 recycling, required for maintenance of chemokine sensing for lymphocyte homing (Otero et al., 2006). Moreover, CTLA4 possesses many similarities to recycling receptor EGFR, where endosomal dissociation based on binding strength

determines whether ligand: EGFR complexes are sorted into the recycling pathway, as with TGFα ligand binding, or degradative pathway, as with EGF ligand binding (Roepstorff et al., 2009). Intriguingly, our lab recently identified a patient-derived CTLA4 R70Q mutation associated with autoimmunity that has ~ 10-fold lower affinity for CD80, but regulation of CD80 is broadly as efficient as CTLA4 WT. Using this mutant, we found evidence of increased, pH dependent dissociation (Kennedy et al., 2022). Together, our data reveals a functional resilience of CD80 removal, as CTLA4 can recover optimal function when faced with a defect that impairs overall binding strength. Moreover, CD86 appears to exploit this approach to be efficiently removed.

4.3.2. Ligand-induced clustering regulates CTLA4 ubiquitination

Despite evidence of increased dissociation, we observed CTLA4 C157A was able to be ubiquitinated following CD80 ligation, suggesting monomeric CTLA4 can still be trafficked towards lysosomes. Whilst counterintuitive, this observation can be explained by considering the influence of CD80 bivalent binding. As a homodimer, CD80 may be able to cluster CTLA4 C157A sufficiently to enable ubiquitination. Ligand induced receptor clustering is a long-standing mechanism to regulate key processes such as receptor internalization, downregulation and more recently, ubiquitination (Haglund and Dikic, 2012; Moody et al., 2015; Waterman and Yarden, 2001). Moreover, high expression of CTLA4 C157A within our cell lines teamed with high receptor membrane motility means an increased chance of clustering regardless of CTLA4 covalent linkage, a common feature in cell signaling studies (Cebecauer et al., 2010; Hartman and Groves, 2011). An alternate possibility is that CTLA4 possesses residues that enable non-covalent dimerisation, and therefore lattice formation is retained.

Indeed, a previous study suggest mutation at C157 is insufficient to enable complete monomerization, and as a result showed no defect in CD80 dependent accumulation of CTLA4 C157S into the cSMAC (Darlington et al., 2005). Consequently, whether monomeric CTLA4 is degraded or recycled may depend on the concentration of CD80 and whether CTLA4 can form effective non-covalent interactions similarly to CD80. These effects may therefore be influenced by cell number and ligand/receptor expression level. It would therefore be of interest to test whether monomeric CTLA4 can retain the correct control of CD80 in settings of low ligand expression. How ubiquitination regulates the process of transendocytosis is discussed further in **section 4.3.5**.

4.3.3. Insights into the molecular mechanism of transendocytosis from monomeric CTLA4

Surprisingly, CTLA4 C157A had a reduced ability to bind CD86-Ig, and immunoprecipitation using CD86 was unable to recover CTLA4 C157A. We also found that capture of CD86 by CTLA4 C157A transendocytosis is less efficient than CTLA4 WT. This is surprising given that CD86 only binds as a monomer to CTLA4, making it unclear why it is affected by making CTLA4 monomeric.

Indeed, a bivalent receptor has an avidity advantage leading to an increase in binding strength essentially by forcing binding site proximity and favoring rebinding following dissociation. A bivalent CTLA4:CD86 interaction, as a result of CTLA4 being a homodimer, may therefore be at the lowest binding threshold biologically required for transendocytosis and thus correct control of CD28, with a monovalent CTLA4 being less competitive with CD28 due to loss of avidity. Theoretically, if CTLA4 is disrupted by mutations that affect affinity or avidity, CD86 is less efficiently bound, CD28 responses are augmented, and

immune balance is dysregulated. In support of this hypothesis, our recent patient identified CTLA4 R70Q mutant, which presents clinically with autoimmune symptoms, showed a specific defect in CD86 binding, thus loss of control of CD86 is likely to be important for driving autoimmune responses (Kennedy et al., 2022). Moreover, recent data from our lab maintains that multiple other clinically identified CTLA4 mutations consistently effect transendocytosis efficiency of CD86, more than CD80. Intriguingly, this includes a heterozygous CTLA4 C157F mutation, which also impairs dimerisation (Alan Kennedy, personal communication).

Altogether, these data support a model whereby monomeric CTLA4 can account for loss of avidity of CD80 by increasing the ability to dissociate, in a manner dependent on CD80 clustering. However, the weaker affinity CTLA4:CD86 interaction already utilizes this mechanism. Thus, a loss in avidity which impairs binding strength limits transendocytosis, potentially augmenting CD28 co-stimulation.

4.3.4. The optimal ligand for transendocytosis is high affinity and low avidity

Despite a loss of avidity resulting from absence of CD80 bivalency, our data suggest that CD80I2R is the most efficient target for CTLA4 transendocytosis. This is explained by considering the characteristics of CTLA4 transendocytosis which contribute to its overall efficiency. First is ligand affinity: CD80 binds with 10-fold higher affinity than CD86, and this is likely unchanged with CD80I2R. Therefore, when CTLA4 engages CD80I2R at the cell surface, it binds with K_{on} rates equivalent to those of WT CD80. Second is avidity: CD80:CTLA4 interaction forms an avid lattice, increasing the overall strength of

204

CD80:CTLA4 binding several orders of magnitude over its monomeric affinity of 0.2µM (Linsley et al., 1994, Stamper et al., 2001). This presumably results in lengthened receptor occupancy times and significantly slower 'off' rates, as determined by quantitative analysis of binding kinetics using surface plasmon resonance (Greene et al., 1996). Together, affinity and avidity contributions influence the propensity to dissociate, and so influence recycling of unbound CTLA4. Furthermore, we show rapid depletion of CD80I2R with an increased rate of ligand degradation by flow cytometry and smaller less co-localised vesicles by confocal microscopy. Similar observations were also seen when CD80 is expressed as a heterodimer with PDL1 (see **section 3.3.4**) suggesting that monomeric ligands have a propensity to dissociate from CTLA4 and to undergo more rapid degradation. Thus, our results support the idea that optimal ligand is high affinity, permitting rapid binding to CTLA4 at the surface, but low avidity, allowing dissociation and recycling. Indeed, mathematical modelling of CTLA4 transendocytosis identified that optimal removal is not based on the highest available affinity of ligand, but rather the availability of CTLA4 to recycle (Khailaie et al., 2018).

Our results also demonstrate a dependency of monovalent ligand (particularly CD86) transendocytosis on pH, and we observed that NH_4Cl treatment inhibits the ability to deplete CD86 and CD80I2R more markedly than CD80. We postulate that due to pH neutralization dissociation is reduced, and recycling of empty CTLA4 diminished. This observation aligns with our data showing CD86 removal was inhibited by BafA in Tregs (Kennedy et al., 2022). Consistent with this, NH_4Cl and BafA have been shown to inhibit recycling of TfR, polymeric IgA and Megalin receptors (Henkel et al., 1998). Moreover, following CD80 ligation, CTLA4:CD80 complexes are reported to localize to low pH Rab7+

compartments, indicative of late endosomes and lysosomes, whereas CD86 trended towards Rab5+ and LRBA compartments, indicative of early endosomes (Kennedy et al., 2022). Whilst not directly assayed, our data show increased dissociation at low pH for CD80I2R, thus we would expect a CD86 pattern of localisation. Taken together, we show the differential intracellular characteristics of CD80 and CD86 is dictated by both valency and affinity, which influence CTLA4 ubiquitination, ligand binding and ligand degradation.

4.3.5. CD80 negatively regulates CTLA4 but only when a homodimer

A key question becomes how is differential CTLA4 processing regulated. In this Chapter, we show CD80 induces ubiquitination of CTLA4 whilst CD86 does not and propose that dimeric CD80:CTLA4 clustering is a pre-requisite for ubiquitination and directing CTLA4 trafficking away from recycling. Interestingly, EGFR, which has striking similarities to CTLA4, undergoes continuous de- and re-ubiquitination via kinase regulation. If ligand remains bound, kinase activity is maintained, and ubiquitination persists (Eden et al., 2013; Sigismund et al., 2013). This parallels our observations that only highly avid, stable CD80:CTLA4 complexes are ubiquitinated. Moreover, multiple studies demonstrate activation of ubiquitin ligases because of substrate clustering, supporting the idea that multivalency and avidity plays a fundamental role in targeting proteins for ubiquitination (Lafont et al., 2001; Zeng et al., 2020; Chen et al., 2021). For example, Mund et al., identified that activation of HECT domain E3 ubiquitin ligases requires clustering of proteins with PY-motifs (Mund and Pelham, 2018). Indeed, extended dimer-dimer interactions resulting from lattice formation generate highly concentrated regions of CD80 and CTLA4 at the cell surface. Whilst the exact E3 ubiquitin-ligases that control CTLA4 are not yet known, links

have been observed between CTLA4 and E3 ubiquitin-ligases GRAIL, (Anandasabapathy et al., 2003), Cbl-b, and Itch. While T cells deficient in Cbl-b and Itch display a hyperproliferative and activated phenotype, typical of those seen in CTLA4 KO mice, their relationship to CTLA-4 function remains unclear (Bachmaier, 2000; Hoff et al., 2010). It will be of great interest to determine the ligase responsible for CTLA4 ubiquitination following CD80 transendocytosis, as it could represent a therapeutic target. Likewise, manipulating CD80 dimerisation could potentially enhance CTLA4 function and be a viable treatment for autoimmune conditions.

While the precise details of CTLA4 ubiquitination remain to be clarified, studying a CTLA4 molecule lacking lysine residues (CTLA4 Kless) gave us further insights. Canonically, ubiquitination of membrane and endocytosed proteins is linked to their degradation in lysosomes. However, ubiquitination is also linked to receptor internalization and trafficking. For example, poly-ubiquitination required for internalisation of the Interferon-α receptor as well as other cellular processes e.g., scaffolding (Hicke et al., 2003; Suresh et al., 2007). Differential ubiquitin-chain length and linkage types, as well as sub-cellular location of ubiquitination, dictates function (Clague et al., 2010). The ability to recover both CTLA4 WT and CTLA4 Kless via ubiquitin-immunoprecipitation Indicates that CTLA4 is continuously associated with a ubiquitinated partner. Indeed, the CTLA4 tail contains a 'PTEP' motif, with 'PxxP' a common motif required for SH3 containing proteins such as E3 ligases (Stamenova et al., 2007). Specifically, a PTAP motif has been identified as a viral trafficking motif via the MVB pathway of degradation (Dorweiler et al., 2006), thus constitutive association and low level ubquitination by an associated ligase would explain our findings and indicate that crosslinking by CD80 can then increase ligase activity.

Interestingly, our Kless CTLA-4 mutant showed no impairment in ligand internalisation, suggesting that ubiquitination is not required for the transendocytosis process and that the cell surface is likely not the most important site of ubiquitination following CD80 transendocytosis. Strikingly, post-internalization we observe that WT CD80 accumulated in large, highly co-localized vesicles with CTLA4 by confocal microscopy This may be consistent with CTLA4:CD80 complexes trafficking via the ubiquitin-dependent pathway to multivesicular bodies (MVB). MVB are formed by ubiquitin-dependent budding of endosomal membranes prior to fusion of these vesicles with lysosomes (Reggiori et al., 2001). The role of ESCRT proteins, which are integral to MVB trafficking would therefore be an area of CTLA-4 biology worthy of investigation.

Interestingly, CTLA4 Kless, which is unable to be poly-ubiquitinated, does not accumulate in large punctate vesicles but instead is sequestered into 'doughnut' structures, with along with WT CD80. Multiple studies support that this phenotype is indicative of membrane staining of intracellular vesicles(Chen et al., 2010; Midekessa et al., 2021; Wimmer et al., 2006). Intriguingly, the MVB pathway is regulated by the endosomal sorting complexes required for transport (ESCRT) machinery (Raiborg et al., 2009), where ESCRT complexes are located on endosomal membranes, bind to poly-ubiquitinated cargo of ubiquitin ligases, and generate MVBs by inward budding of endosomal membranes. Furthermore, the ESCRT machinery has been shown to have a critical role in EGFR recycling (Baldys et al., 2009). Therefore, following a CD80:CTLA4 Kless interaction, CTLA4 Kless could be trafficked towards endosomes by association with ubiquitin ligases, but the final step of poly-ubiquitination does not occur leaving CTLA-4 on the limiting membrane of MVB rather than being processed into intra-lumenal vesicles. Importantly, this further supports the idea that some of this

trafficking is dependent on CD80 bivalent binding, as CTLA4 Kless does not exhibit this phenotype with CD80I2R as a ligand.

In addition, due to loss of trafficking via ubiquitin-dependent pathways, the CTLA4 Kless mutant possesses increased recycling capabilities. Indeed, this regulation resembles other recycling receptors such as PAR2 (Jacob et al., 2005), and Neurokinin-1 receptor (Cottrell et al., 2006), where enhanced recycling is observed in the absence of lysine residues. In line with our model that monovalent ligands more readily exploit CTLA4 recycling due to increased dissociation (**Figure 4.27**), we show that CTLA4 Kless is more efficient at removal of CD86, CD80I2R and CD80 in the presence of PDL1 preventing CD80 homdimerisation. Interestingly, patients with LRBA deficiency, a protein required for CTLA4 recycling, exhibit severe immune dysregulation, highlighting the functional importance of reusing CTLA4 (Hou et al., 2017; Lo et al., 2015b). Indeed, our lab recently reported transendocytosis with CTLA4 lines lacking LRBA specifically impaired transendocytosis of CD86 over CD80 (Kennedy et al., 2022).

4.3.6. *Cis* expression of PDL1 disrupts CD80:CTLA4 lattice formation, permitting CTLA4 recycling

It is now clear that the CD80:PDL1 heterodimer restricts PDL1:PD1 binding. Whilst Zhao et al., suggested that the CD80:PDL1 *cis* interaction impair CTLA4 binding (Zhao et al., 2019), our lab recently demonstrated that robust and time dependent transendocytosis of CD80 occurs in the presence of PDL1 arguing against obvious impairment of CTLA4 binding (Kennedy, Robinson et al., 2022). In this study, we further demonstrate that disruption of CD80:CTLA4 lattices by PDL1 enables CD80:CTLA4 complex dissociation and possible

enhancement of CTLA4 transendocytosis due to more rapidly removal by transendocytosis. We further show increased CTLA4:CD80 dissociation and observe a reduction in CTLA4 ubiquitination. Intriguingly, for this phenotype to occur, CD80 must therefore exhibit monovalent binding to CTLA4 suggesting that CTLA4 is unlikely to re-form CD80 dimers at the membrane before transendocytosis. Since CTLA4-Ig binding to CD80 does not recover PD1 binding to PDL1 (Kennedy, Robinson et al., 2022), then CTLA4 binding per se does not dissociate the heterodimer effectively. Significant questions therefore remain as to how CTLA4 can target CD80-PD-L1 heterodimers without removing PDL1 by transendocytosis.

Nonetheless, our data show that CTLA4 becomes a potential regulator of PD1 signaling, by controlling PDL1 availability via transendocytosis. A study by Tekguc et al., amongst others, suggest this can occur by trogocytosis, as PDL1 was revealed even when CTLA4 lacks its cytoplasmic tail (Aucher et al., 2008, Daubeuf et al., 2010, Tekguc et al., 2021). However, analysis of CTLA4-Δ36, where CTLA4 is deficient in transendocytosis indicates that transendocytosis is significantly more effective. Indeed, building on work presented in this thesis we would suggests that not only can CD80 accelerate T cell responses by inhibiting PDL1:PD1 function, but PDL1 can provide negative feedback, enhancing transendocytosis by disrupting CD80 dimer formation.

4.3.7. Summary

Taken together, data in this Chapter reveal the outcome of CTLA4 mediated transendocytosis is influenced by the biophysical properties of the ligands. We provide a new model whereby CD80:CTLA4 lattice formation, requiring dimeric CD80 ligation, maintains CTLA4 interactions post-

transendocytosis and drives ubiquitination of CTLA4. In addition, this study provides the first cell-based evidence which suggests the optimal ligand for transendocytosis is a high-affinity monomeric ligand **(Figure 4.27)**.

Chapter 5: Optimizing Treg cultures for analysis of CTLA4-mediated transendocytosis

5.1. Introduction

Regulatory T cells (Tregs) regulate the immune system by multiple mechanisms, acting to dampen immune responses and prevent autoimmunity. A fundamental characteristic of Tregs is the constitutive expression of CTLA4, with single cell RNA-seq analysis supporting *Ctla4* as a key component of the Treg gene signature, independent of anatomical location (Bhairavabhotla et al., 2016). Targeted loss of CTLA4 expression on FoxP3+ Treg populations results in lethal immune dysregulation (Takahashi et al., 2000), and multiple models identify loss of CTLA4 limits Treg function (Chambers et al., 1997; Tivol et al., 1997; Wing et al., 2008). We therefore wanted to evaluate methods for ex-vivo isolation and expansion of Tregs in order to study CTLA4 function in these cells.

In this Chapter we aimed to optimise a method of *in vitro* Treg purification and expansion with an aim of maximising potential CTLA4 expression. We show that Tregs isolated and expanded with a fixed TCR stimulus and APCs expressing CD86 show increased FoxP3 and CTLA4 expression, compared to those stimulated with CD80 as a CD28 ligand. This increased CTLA4 expression correlates with an increase in the functional capacity of Tregs, as CD86 stimulated Tregs are more efficient at transendocytosis. We then used expanded Tregs in transendocytosis assays, with results supporting the concept that CD80 transendocytosis results in CTLA4 ubiquitination and trafficking via low pH compartments, whereas CD86 dissociates from CTLA4 post-internalisation in a primary cell model, consistent with data from our model systems. Furthermore, we used our monovalent CD80 mutant, CD80I2R to test whether the ability to

form homodimers, and therefore CTLA4:CD80 lattices at the cell membrane influences CD28 and CTLA4 function.

5.2. Results

5.2.1. Total CD4+ T Cells are unable to efficiently downregulate CD80 or CD86 from artificial APCs *in vitro*

Our group has previously demonstrated that primary CD4+ T cell blasts can capture CD80 and CD86 from CHO cells and primary DCs *in vitro* in a manner dependent on CTLA4 level (Qureshi et al., 2011.; Schubert et al., 2014). However, the extent of ligand downregulation has not been routinely assessed. Given that ligand depletion revealed insights into the differential mechanisms utilized by bivalent and monovalent ligands in cell lines, we wanted to investigate this in primary T cell systems, hypothesizing depletion of CD80/CD86 from DG75s would be observed following co-incubation with primary T cells. For this, we generated T cell blasts by stimulating total CD4+ cells for 5 days using anti-CD3/anti-CD28 activator beads in the presence of IL2. T cell blasts were then cultured with DG75 cells expressing CD80 or CD86 with a C-terminal GFP tag, or untransduced cells, in the presence of anti-human-CD3 and IL2 overnight. **(Figure 5.1A**).

Analysis of the CD4+ population demonstrated GFP acquisition was readily observed following both CD80 and CD86 in a manner that was dependent on CTLA4 level, with more ligand accumulating in cells with a higher CTLA4 MFI **(Figure 5.1B, flow panels, black box)**. This accumulation was blocked by anti-ligand antibodies, confirming specificity of ligand-GFP uptake and consistent with transendocytosis occurring (**Figure 5.1B, right hand graph**). However, despite

acquisition, overnight incubation with CD4 T cells resulted in little depletion of either CD80-GFP or CD86-GFP from CD4-CTLA4- DG75 cells, as levels were the same as in anti-ligand conditions (**Figure 5.1C, histograms**). These observations suggested that whilst both CD80 and CD86 are acquired by CD4+ T cell blasts by transendocytosis, this assay did not allow quantification of ligand removal as a measure of transendocytosis efficiency as minimal ligand depletion was observed. This is likely due to the high expression and synthesis of ligand in transduced donor cells relative to CTLA-4 expression by CD4 cells.
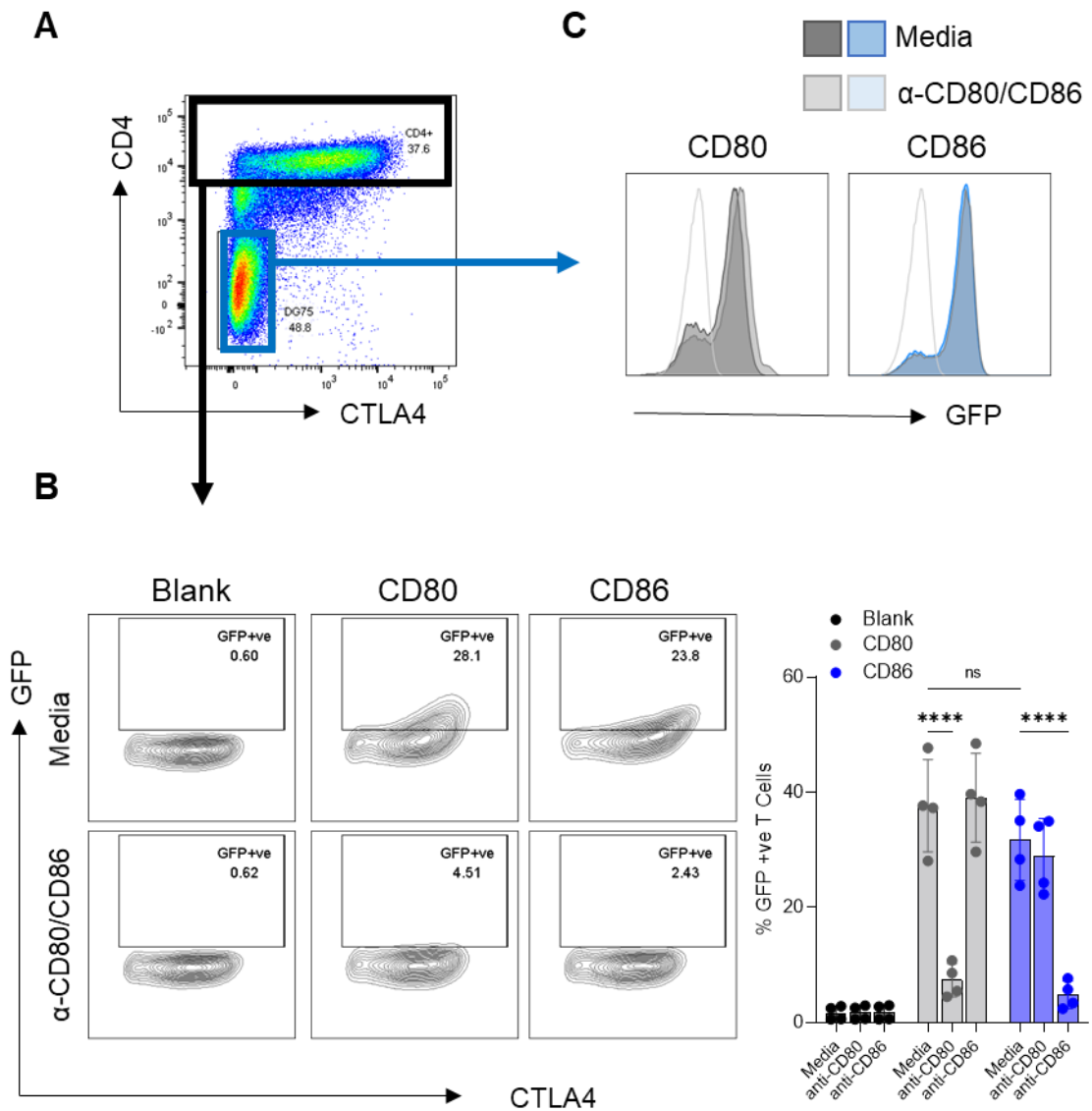
Figure 5. 1. Limited transendocytosis of ligand by CD4+ cells is observed overnight. (A) Total CD4 cells were stimulated with CD3/CD28 Dynabeads at a 2:1 ratio for 5 days, in the presence of 100IU IL2. Beads were then removed, before incubation with untransduced DG75 (blank), or DG75 cells expressing CD80- or CD86-GFP for 21 hours +/- anti-CD80 or anti-CD86 antibody. Cells were stained for CD4 and CTLA4 and assessed by flow cytometry. **(B)** CD4 cells were gated on CD4+ (black box) and analyzed for GFP uptake, with quantification showing the % GFP+ ± SD from 4 donors, analysed by 2-way ANOVA, ns = p>0.05 *p≤0.05, **p≤0.01,***p≤0.001, ****p≤0.0001. **(C)** DG75s were gated as CD4-CTLA4- (blue box) and analysed for GFP expression.

As transendocytosis efficiency is dependent on CTLA4 expression, we considered that the CTLA4 level on CD4 T Cell blasts was insufficient for robust ligand depletion. Recently, we identified that on FoxP3+ cells CTLA4 expression is selectively enhanced by CD86 vs CD80 (Halliday et al., 2020). Therefore, we used CD86 co-stimulation to generate T cell blasts to determine if this increased CTLA4 expression and detectable ligand removal. For this, we stimulated CD4 cells with a 2:1 cell ratio of glutaraldehyde-fixed DG75 cells expressing CD80-GFP or CD86-GFP for 5 days and performed a transendocytosis assay by overnight incubation with CTV-labelled CD80- or CD86-mCherry expressing DG75 cells.

As expected, FoxP3+ Treg frequency (**Figure 5.2A**), and CTLA4 levels in both Teff and Treg populations were increased following CD86 stimulation, compared to CD80 (**Figure 5.2A and B**). However, whilst CD80-mCherry and CD86-mCherry were detectable in T cells following transendocytosis, there was no difference between initial stimulation conditions (**Figure 5.2C, blue shaded quadrants**). Moreover, little ligand depletion was observed by either CD80 or CD86 stimulated T cells of either ligand (**Figure 5.2C, red shaded quadrants**). As differences in CD80, CD86 were not observable, we concluded that expanded CD4+ T cells and DG75 B cells may not be optimal to study the nuances of CTLA4 mediated transendocytosis.
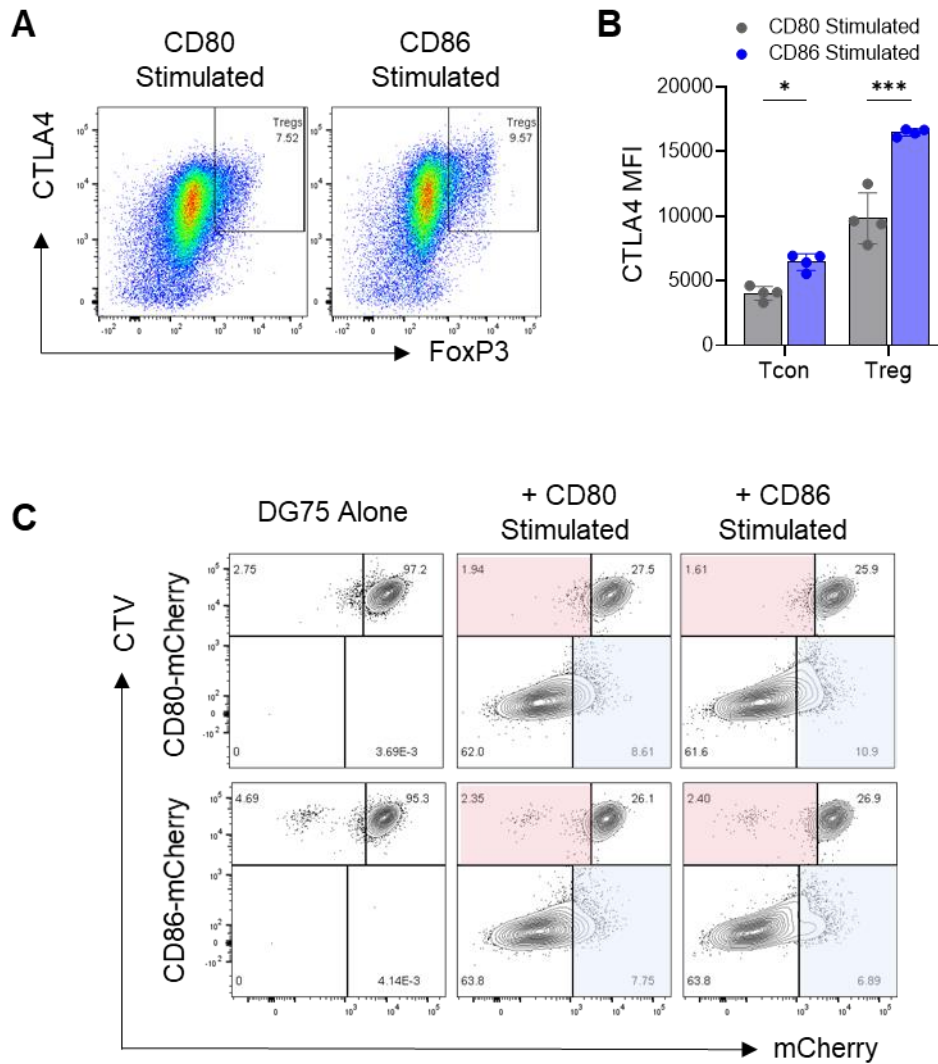
Figure 5. 2. CD86 stimulated CD4+ T cells express higher CTLA4 but are not more efficient at transendocytosis. (A) Total CD4+ cells were stimulated at a 2:1 ratio for 5 days with glutaraldehyde fixed DG75 cells expressing CD80 or CD86, in the presence of 100IU IL2 and assessed by flow cytometry for FoxP3 and CTLA4. **(B)** Quantification of CTLA4 MFI from FoxP3- (Tcon) and FoxP3+ (Treg) populations following stimulation from 4 independent donors ± SD, analysed by 2-way ANOVA, ns = p>0.05 *p≤0.05, **p≤0.01,***p≤0.001, ****p≤0.0001. **(C)** Representative plots from a transendocytosis assay. Stimulated T cells were co-incubated overnight with CellTrace Violet (CTV) labelled DG75 cells expressing CD80-mCherry or CD86-mCherry at a 3:1 ratio. Ligand acquisition shown by blue shading, ligand loss by red shading.

5.2.2. Purified Tregs are more efficient at CD80 transendocytosis

Previous work has demonstrated that whilst activated Teff cell subsets are capable of CTLA4 mediated transendocytosis, Tregs are optimal for this suppressive function as they constitutively express CTLA4 at higher levels (Ovcinnikovos et al., 2019). Indeed, experiments using T cell blasts only included a population of ~10% Tregs. We therefore hypothesized purified Tregs would enable more efficient transendocytosis *in vitro* and thus developed a protocol to allow Treg isolation and expansion.

Leukocyte reduction cones (LRS) cones were enriched for CD4+ cells and CD25+ cells isolated by positive selection using magnetic beads. The CD25+ cells were further stained for CD127, CD25 and CD4, and CD4+CD25+CD127low cells were sorted by flow cytometry. The gating strategy for cell sorting is depicted in **Figure 5.3.A**. CD4 purity following enrichment was 92.2% (±4% s.d.), whilst cell sorting increased purity to 99.7% (±0.4% s.d.). Whilst CD25 positive selection resulted in 55.6% (±2.3% s.d.) CD25+ve population, cell sorting increased this to 98.9% (±1.2% s.d.). Cells from CD25- and CD25+ pre- and post-sort fractions were then phenotyped for FoxP3 and CTLA4 expression. Sorted CD25+ cells were also FoxP3+ and enriched for CTLA4 **Figure 5.3B**. Therefore, this strategy allowed stringent purification of the CD25+CD127loFoxP3+ Treg population.
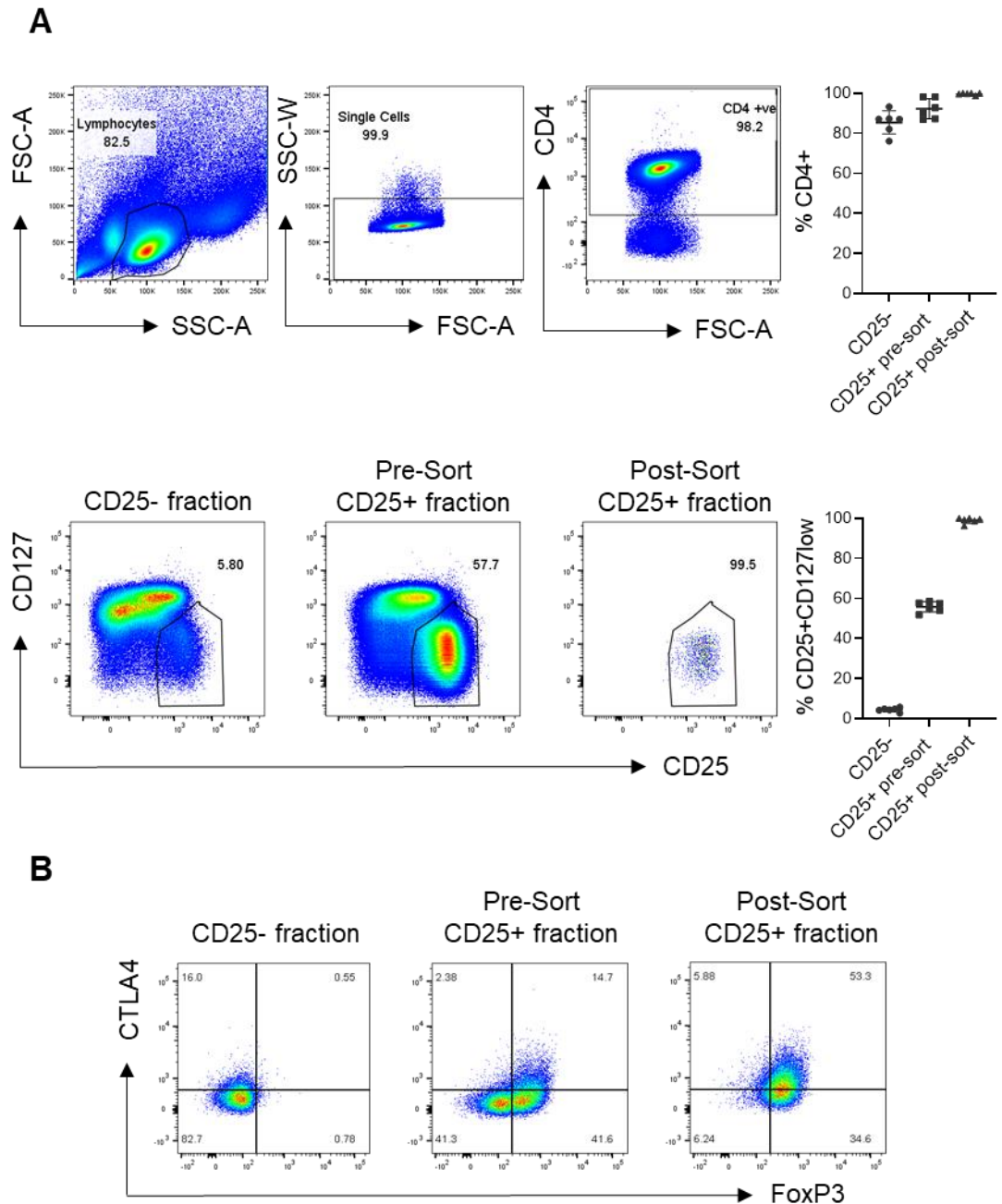
Figure 5. 3. Flow Cytometry cell sorting strategy and purity of CD25+CD127loFoxP3+ Treg subsets. Blood from leukocyte reduction cones was enriched for CD4 cells and selected for CD25+ cells using magnetic bead positive selection. Cells were stained and sorted by FACs to purify CD25+CD127loFoxP3+ Tregs. **(A)** Gating strategy to identify CD25+CD127lo lymphocytes for sorting. Analysis shows purity of CD25- and CD25+ subsets pre- and post-FACs sorting. Frequency of CD4+, and CD25+CD127lo from indicated subsets from 6 donors ± SD. **(B)** Representative plots following intracellular CTLA4 and FoxP3 staining from pre and post sorted fractions.

For expansion, purified Tregs and CD25-ve Teffs were stimulated by incubation with a 1:1 ratio of irradiated mouse L cells expressing CD80, to provide co-stimulation, and anti-CD3 crosslinked by Fc-receptor on L cells as a TCR stimulus. Both Treg and CD25-ve populations were restimulated after 7 days, before analysis for FoxP3 and CTLA4 expression on Day 12 (**Figure 5.4**). We observed that purified Tregs were consistently >95% FoxP3+CTLA4+ and expressed 10.8-fold (±5.4 n=8) higher CTLA4 compared with CD25- cells.

We next assessed whether expanded Tregs were able to deplete ligand from DG75 cells by performing transendocytosis assays using DG75 cells expressing CD80-mCherry or CD86-mCherry (**Figure 5.5**).

We observed that acquisition of both CD80- and CD86-mCherry was readily detectable and time-dependent, consistent with transendocytosis occurring. Strikingly, acquisition of CD80 was much more efficient than previously observed for T cell blasts (**Figure 5.2**), with all Tregs containing mCherry ligand by 8 hours (**Figure 5.5A,** blue box). In contrast, CD86 accumulation was observed but at lower levels than CD80, consistent with our model of differential ligand degradation following CTLA4 mediated internalisation. Unfortunately, despite high CTLA4 expression and FoxP3 purity, Tregs were unable to effectively deplete CD80 or CD86 (**Figure 5.5A, red box; quantified in Figure 5.5B**). This was surprising considering ligand is readily acquired but could be explained by *de novo* synthesis of CD80 and CD86 by the viral promoter occurring at a rate more rapid than that of ligand loss due to CTLA-4 transendocytosis.

We therefore repeated the assay with the same method of Treg purification but increased ratio of Tregs to DG75 cells (**Figure 5.6**). This revealed that

increasing Treg: DG75 ratio enabled detection of CD80 depletion in a Treg cell dependent manner, supporting the idea that CTLA4 was saturated when lower number of Tregs were present, thus preventing detectable downregulation **(Figure 5.6A)**.   Interestingly, CD80 transendocytosis efficiency saturated at a 10:1 Treg to DG75 ratio, (**Figure 5.6B**). Despite successfully observing loss of CD80, we again saw no loss of CD86 even at high Treg: DG75 ratios (**Figure 5.6C**), albeit that CD86 accumulated into the Treg cells.

Taken together, these results suggest that CD80 is a better target for CTLA4 mediated transendocytosis by primary Tregs than CD86, as ligand loss is more readily detected. As CD80 binds CTLA4 with high affinity and avidity, forming lattice structures with CTLA4, cell-cell contact times are likely enhanced, allowing longer for CTLA4 to perform its function. As a lower affinity ligand, CD86 transendocytosis is likely more dependent on a stable cell:cell contact. Indeed, cell synapse formation could be influenced by stimulation-dependent upregulation of adhesion proteins not identified in this system. In addition, our recently published model predicts that CD86 transendocytosis is dependent on the ability of CTLA4 to recycle (Kennedy et al., 2022). As rate of CTLA4 recycling is increased in activated T cells, linked to CD28 and TCR downstream signaling, it may be that the CTLA4 on Tregs is not rapidly recycling and therefore is less efficient at CD86 removal with a stronger TCR stimulus required.
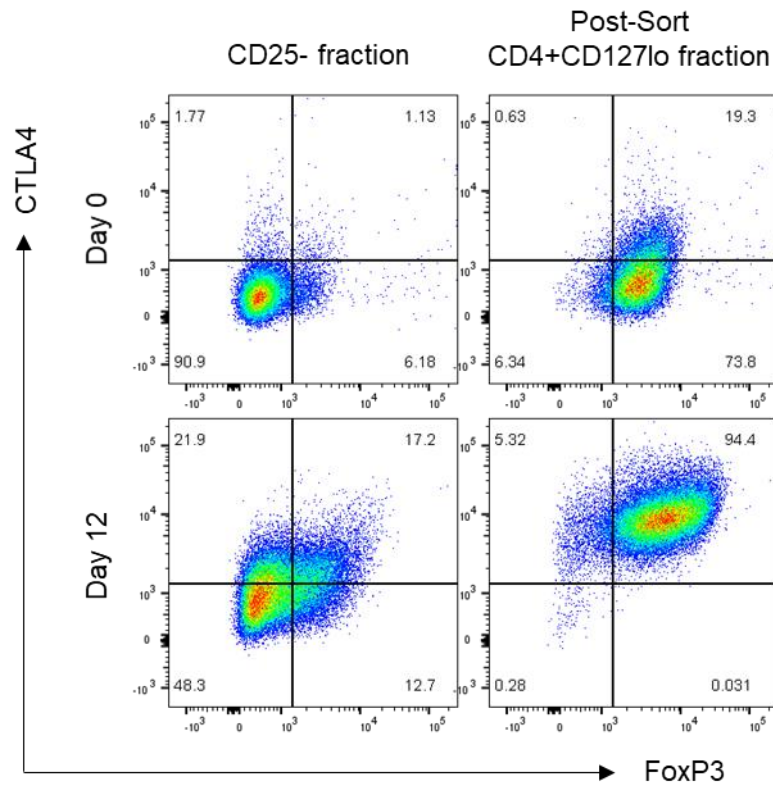
Figure 5. 4. Sorted Tregs maintain FoxP3 purity and express high CTLA4 levels following 12 days of expansion. Blood from leukocyte reduction cones was enriched for CD4 cells and selected for CD25+ cells using magnetic bead positive selection. CD25- and +ve fractions Cells were stained and sorted by FACs to purify CD25+CD127loFoxP3+ Tregs, before expansion by incubating with soluble anti-CD3 and irradiated L cells expressing CD80. Plots show flow cytometry analysis of CTLA4 and FoxP3 expression at Day 0 or following 12 days of expansion, gated on total CD4+ subsets, representative of >8 donors.
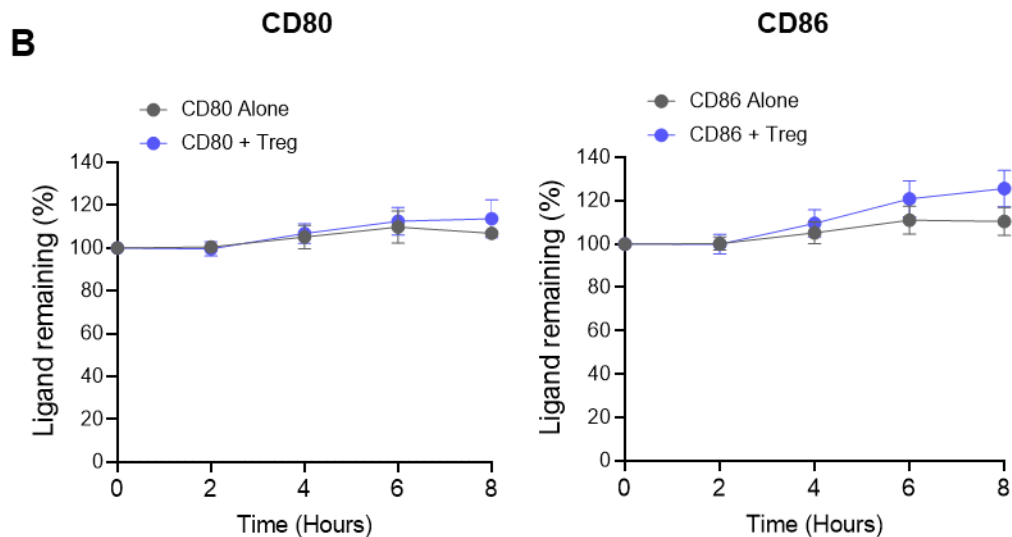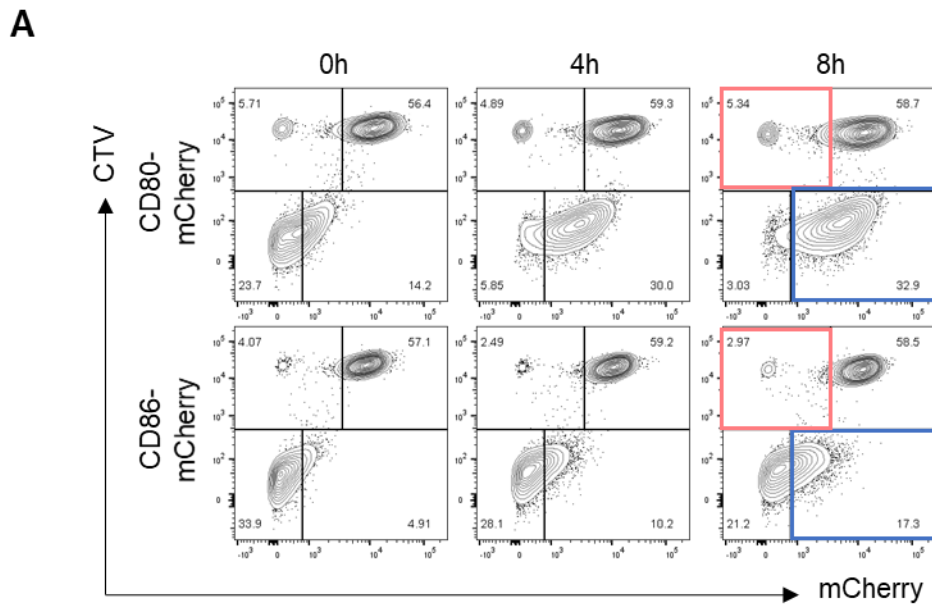
Figure 5. 5. L cell stimulated primary Tregs do not efficiently deplete ligand at a 1:1 ratio, despite internalisation. (A) Representative plots from a transendocytosis assay. Purified Tregs were expanded for 12 days, before co-incubation with CellTrace Violet (CTV) labelled DG75 cells expressing CD80-mCherry or CD86-mCherry, plated at a 1:1 ratio, for 0-8 hours. Blue box indicates ligand acquisition, red box indicates ligand depletion. **(B)** CD80 (left graph) and CD86 (right graph) depletion quantified as percentage mCherry MFI from CTV+ populations relative to 0 hours, from DG75 cells alone, or when co-incubated with Tregs. Data collated from 3 donors ± SD.
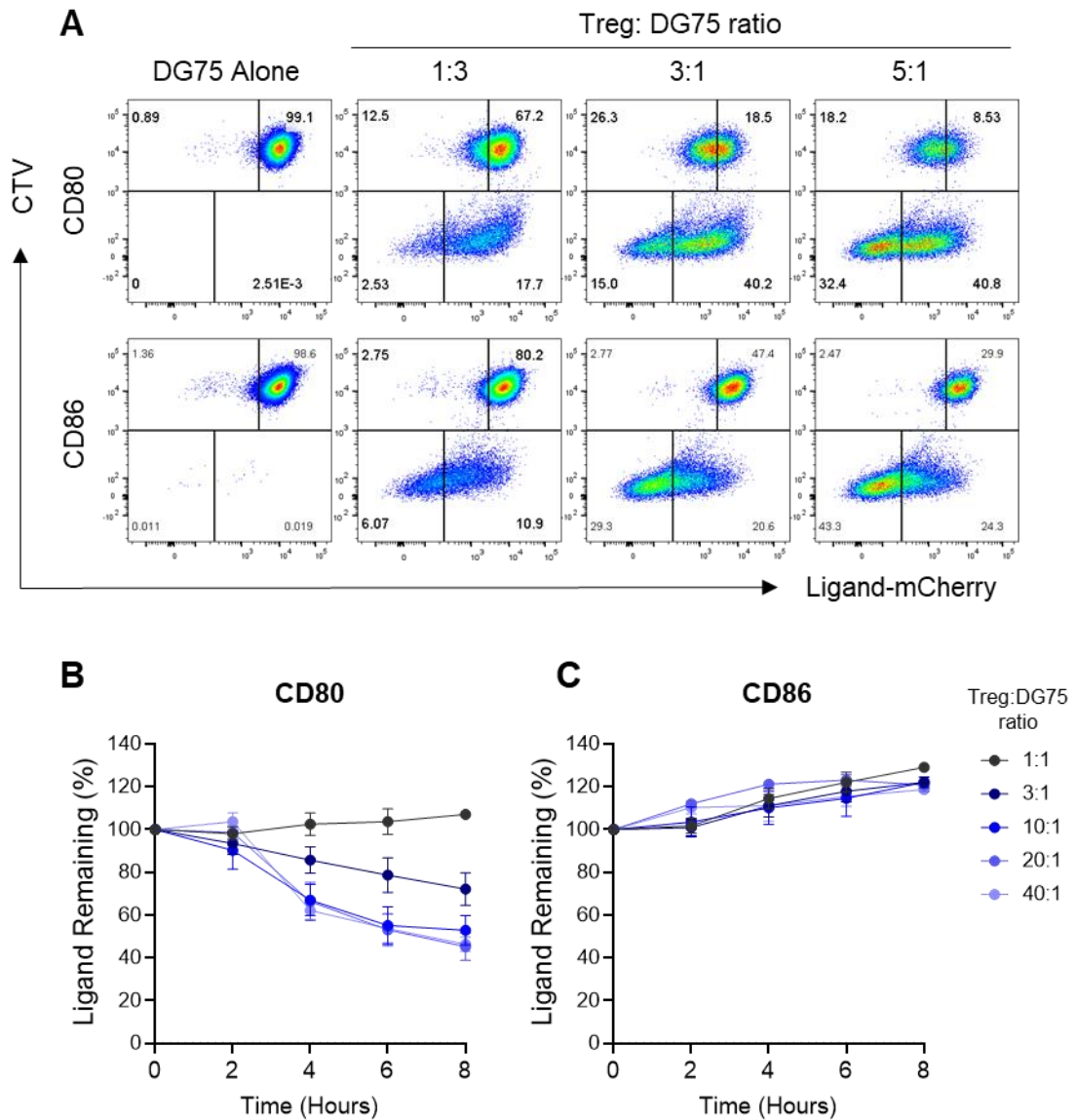
Figure 5. 6. CD80 is efficiently depleted by L cell stimulated primary Tregs.
(A) Representative plots following 8 hours transendocytosis. Purified Tregs were expanded for 12 days, before co-incubation with CellTrace Violet (CTV) labelled DG75 cells expressing CD80-mCherry or CD86-mCherry at indicated ratios for 0-8 hours. **(B)** CD80 and **(C)** CD86 depletion quantified as percentage mCherry MFI from CTV+ populations relative to 0 hours at indicated Treg:DG75 ratios. Data collated from 3 donors ± SD.

5.2.3. CD86 co-stimulation results in increased CTLA4 expression and a more activated Treg phenotype

We next considered how CD80 and CD86 co-stimulation may influence cultured Treg phenotype and transendocytic function. For this, we isolated and sorted Tregs, and then stimulated T cells with soluble anti-CD3 and DG75 cells expressing either CD80 or CD86. The DG75 cells were X-ray irradiated to prevent their expansion.

The frequency of FoxP3+ Tregs, and level of FoxP3 and CTLA4 were analyzed after 7 days. Representative flow cytometry plots following stimulation are shown in **Figure 5.7A**. The frequency of FoxP3+CTLA4 high cells was significantly higher following stimulation with CD86 than with CD80, and compared with no co-stimulation (**Figure 5.7B**). In addition, CD86 stimulation resulted in higher expression of both FoxP3 and CTLA4, compared to CD80 stimulated (**Figure 5.7C, D**). These observations suggested that despite its lower affinity, CD86 can provide a qualitatively better costimulatory signal than CD80, which results in a more activated regulatory T cell phenotype.

We further analysed the phenotype of expanded Tregs for CD28-dependent activation markers CD25, ICOS and PD1. Whilst both CD80 and CD86 expanded cells expressed high levels of CD25, levels were enhanced following co-stimulation with CD86 more than CD80 (**Figure 5.8A**). Similarly, CD86 stimulation resulted in higher levels of both ICOS and PD1 than CD80 stimulation (**Figure 5.8B, C**), indicating more effective CD28 stimulation.
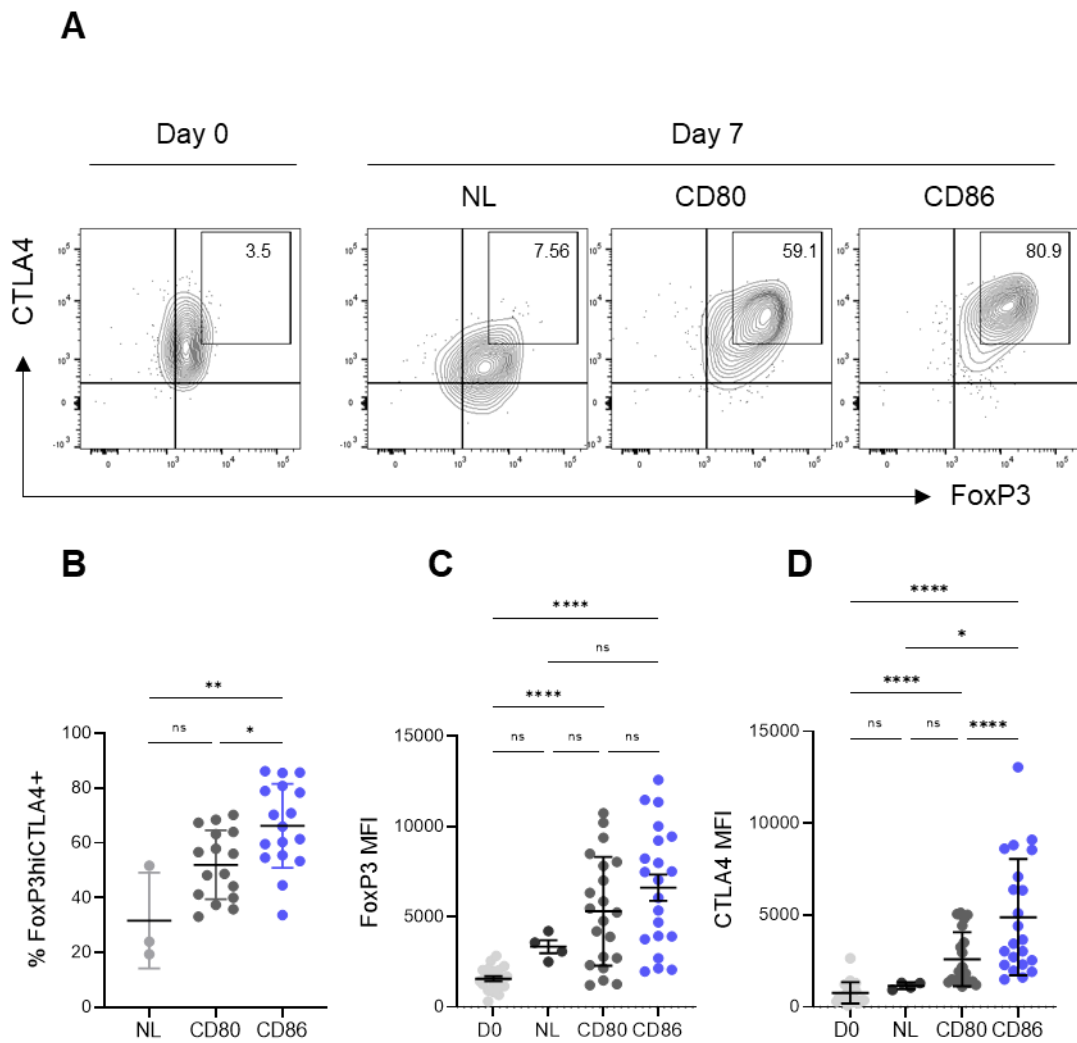
Figure 5. 7. CD86-CD28 co-stimulation enhances FoxP3 and CTLA4 expression. CD25+CD127lo Treg cells were isolated from blood and purified by cell sorting. Purified Tregs were cultured for 7 days with DG75 cells expressing CD80, CD86 or no ligand (NL) with 1µg/ml anti-human-CD3 with 1000IU of IL2. After 7 days, levels of CTLA4 and FoxP3 were assessed by flow cytometry, with representative FACS plots in **(A).** FoxP3 and CTLA4 high cells were gated. (B). Frequency of CTLA4+FoxP3high cells. **(C)** FoxP3 and **(D)** CTLA4 MFIs of total CD4+ cells were also assessed. Data from 3-16 independent donors ± SD, analysed by one-way ANOVA paired analysis, ns = p>0.05 *p≤0.05, **p≤0.01,***p≤0.001, ****p≤0.0001.
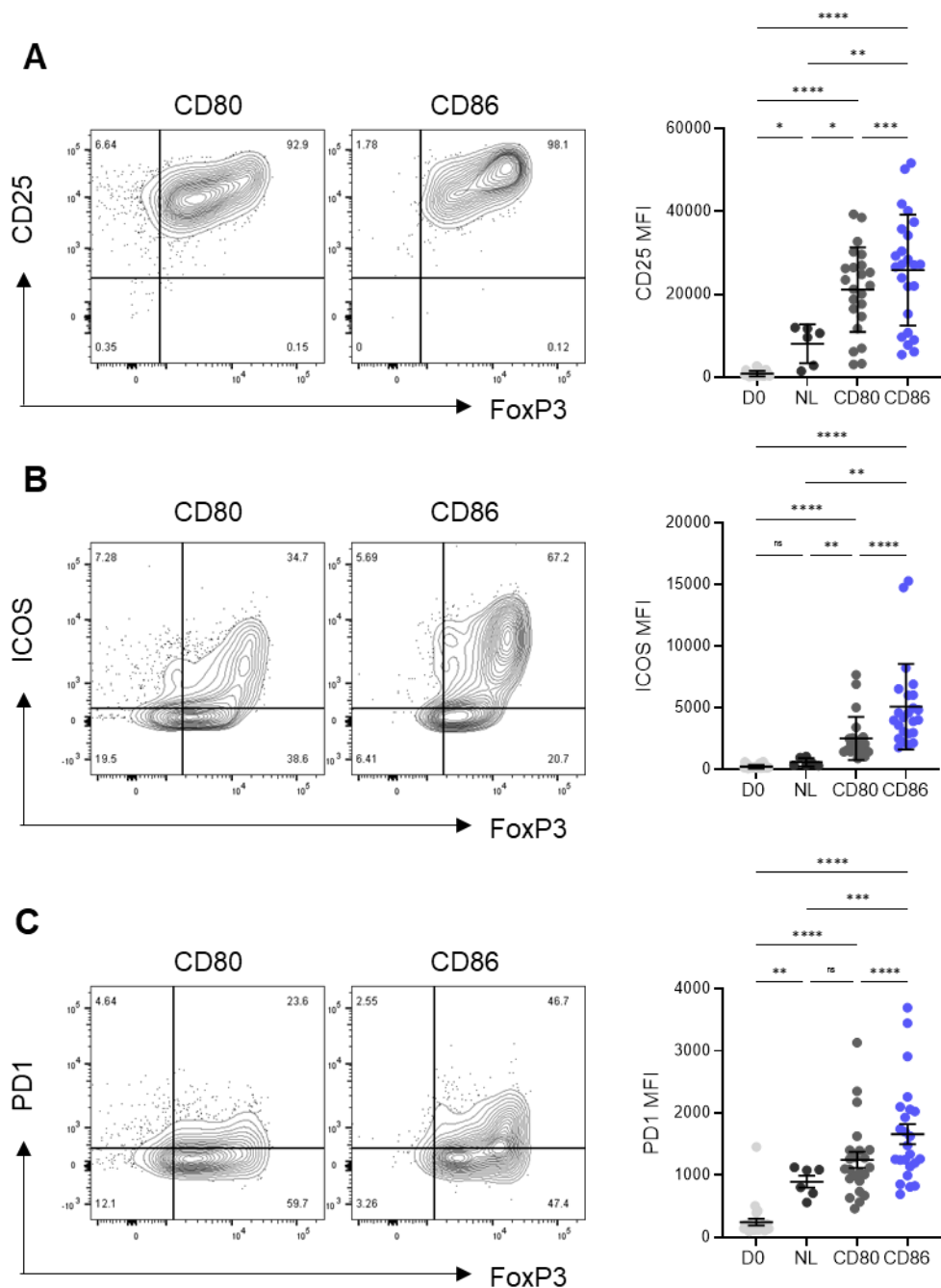
Figure 5. 8. CD86-CD28 costimulation enhances CD25, ICOS and PD1 expression compared to CD80. CD25+CD127lo Treg cells were isolated from blood and purified by cell sorting. Purified Tregs were cultured for 7 days with DG75 cells expressing CD80, CD86 or no ligand (NL) with 1µg/ml anti-human-CD3 with 1000IU of IL2. After 7 days, levels of **(A)** CD25, **(B)** ICOS and **(C)** PD1 were assessed by flow cytometry, with representative FACS plots against FoxP3 expression, and MFIs of total CD4+ cells displayed. Data from 6-24 independent donors ± SEM, analysed by one-way ANOVA paired analysis, ns = p>0.05 *p≤0.05, **p≤0.01,***p≤0.001, ****p≤0.0001.

To observe whether ligand was transferred via transendocytosis during expansion, Tregs were imaged by confocal microscopy. Expanded Tregs were stained for intracellular CTLA4, and GFP was stained using an anti-GFP antibody to increase level of detection. Due to limitations with sourcing suitable anti-CD80/CD86 antibodies for confocal microscopy applications, staining for ligand itself was not possible.

As expected, we clearly observed presence of intracellular vesicles containing CTLA4, and saw acquisition of both CD80-GFP and CD86-GFP into CTLA4+ve Tregs (**Figure 5.9**). Interestingly, we saw that CD80 accumulated in vesicles highly colocalised with CTLA4, whereas CD86 did not, supporting our model that CD80 remains bound to CTLA4 post-internalisation, whereas CD86 dissociates due to a weaker interaction. More work is required to understand how this phenotype influences CD28 responses and Treg growth.
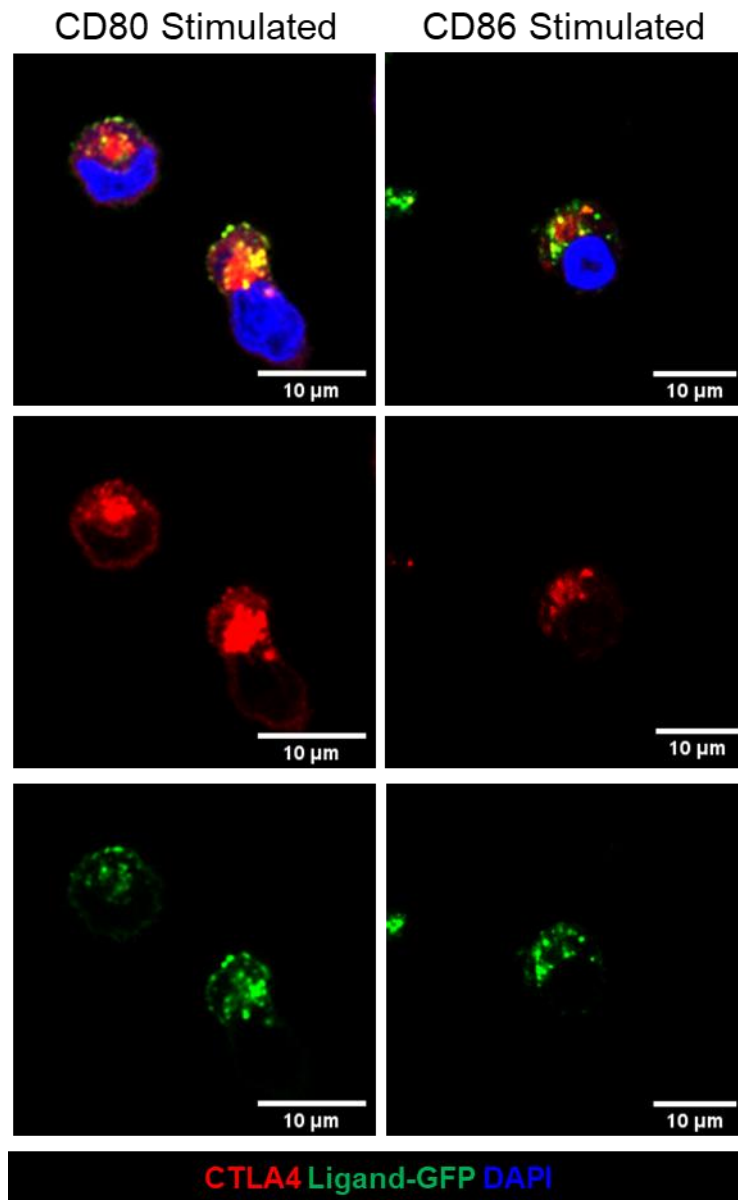
Figure 5. 9. CD80 acquired by Tregs following co-stimulation co-localizes with CTLA4. CD25+CD127lo Treg cells were isolated from blood and purified by cell sorting. Purified Tregs were cultured for 7 days with DG75 cells expressing CD80 or CD86 with 1µg/ml anti-human-CD3 with 1000IU of IL2 replenished every 2-3 days. Cells were stained with anti-CTLA4 (red), anti-GFP (green) and nuclear stain DAPI (blue) and analysed by confocal microscopy. Scale bars = 10µM.

5.2.4. CD86 stimulated Tregs show enhanced CTLA4 transendocytosis

As we identified CD86 stimulated Tregs expressed higher CTLA4, we then considered if this correlated to increased transendocytic function. To study transendocytosis *in vitro*, we restimulated Tregs at Day 7 to allow expansion and analysed resultant phenotypes at Day 10 and Day 14.

We observed that following re-stimulation, Tregs continued to upregulate CTLA4, with maximal expression by day 10 (3 days post-restimulation) (**Figure 5.10A, quantified in B**). In addition, re-stimulation enhanced FoxP3 expression, generating a higher frequency of CTLA4+FoxP3 high cells (**Figure 5.10C**). These results suggested the optimal time to use the Tregs in functional transendocytosis assays was 10 days post-isolation where FoxP3 and CTLA4 expression was highest.

In subsequent TE assays we observed that both CD80 and CD86 were depleted from APC following 16 hours incubation, shown by a reduction in mCherry from the CTV+ population. Moreover, CD86 stimulated Tregs were significantly better at transendocytosis, than CD80 stimulated Tregs. This was seen by both increased ligand-mCherry acquisition (**Figure 5.11A**) and significantly more ligand depletion from CTV+ populations (**Figure 5.11B and C**). Therefore, enhanced CTLA4 expression following CD86 stimulation resulted in more functional Tregs with regards to transendocytosis. It is also possible that CD80 expression on Tregs following CD80 stimulation contributes to this phenotype, by acting as an internal CTLA4 ligand and blocking its function, however further experiments will be needed to test this hypothesis.

From this experiment, it was clear there was significant donor-donor variation in transendocytosis efficiency. We therefore plotted CTLA4 expression against ligand expression and observed that both CD80 and CD86 depletion was highly correlated with CTLA4expression, with CD80 more efficiently removed than CD86, as shown by lower levels of ligand remaining at low CTLA4 levels (**Figure 5.12**). Taken together, this data suggests that CD80 and CD86 transendocytosis is dependent on CTLA4 expression level, with CTLA4 expression highly donor dependent.
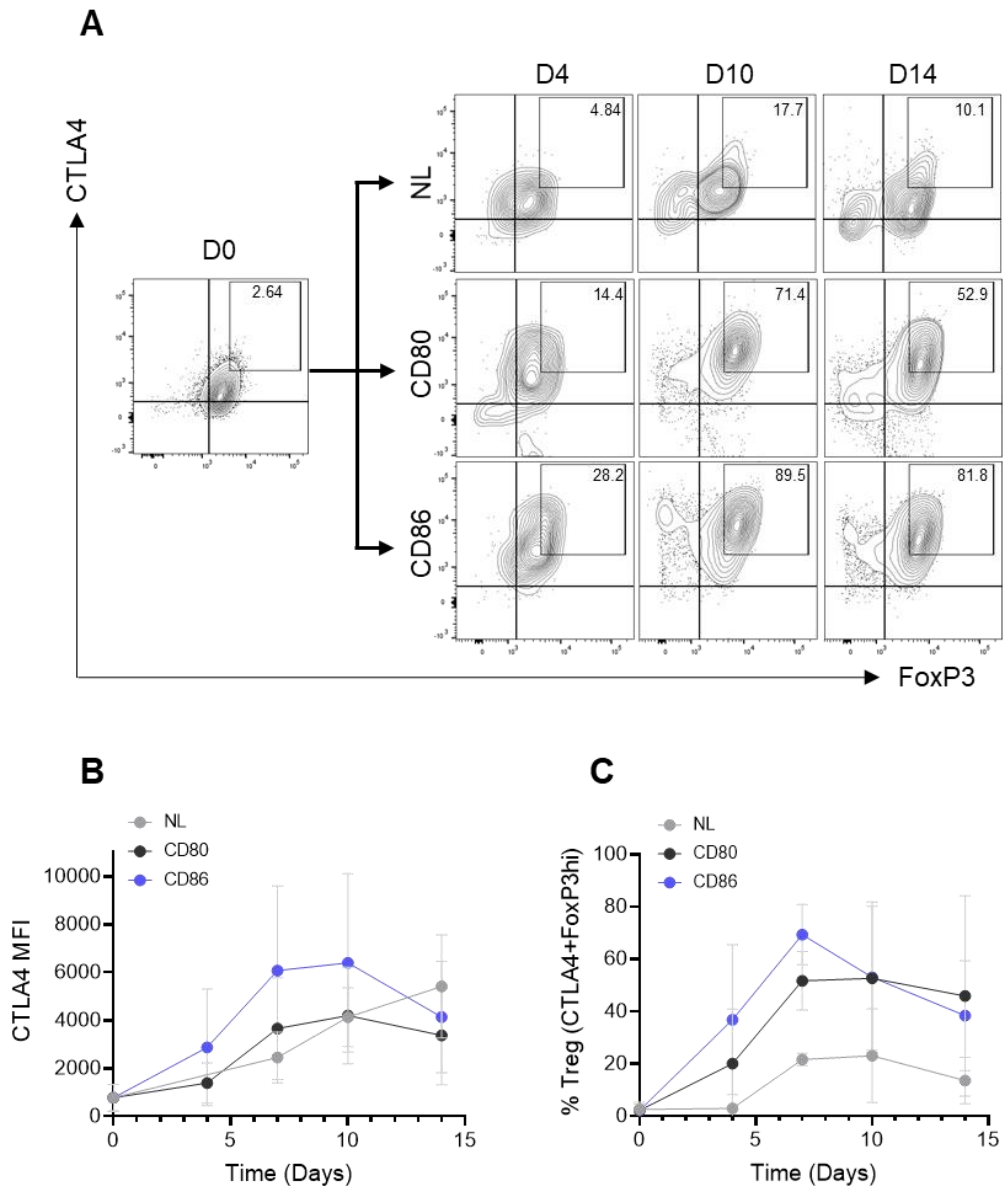
Figure 5. 10. CTLA4 level on CD86 stimulated Tregs peaks at day 10 post-isolation. CD25+CD127lo Treg cells were isolated from blood and purified by cell sorting. Purified Tregs were cultured for 7 days with DG75 cells expressing CD80, CD86 or no ligand (NL) with 1µg/ml anti-human-CD3 with 1000IU of IL2. After 7 days, cells were restimulated by addition of fresh DG75 cells and same dose anti-human CD3. Levels of CTLA4 and FoxP3 were assessed by flow cytometry on Day 4, 7, 10 and 14 during the culture. **(A)** FACS plots showing expression of FoxP3 and CTLA4. High expressing cells are gated with frequencies shown. **(B).** CTLA4 MFIs of total CD4+ cells. **(C)** Frequency of CTLA4+FoxP3high cells. Data from 6 independent donors ± SD.
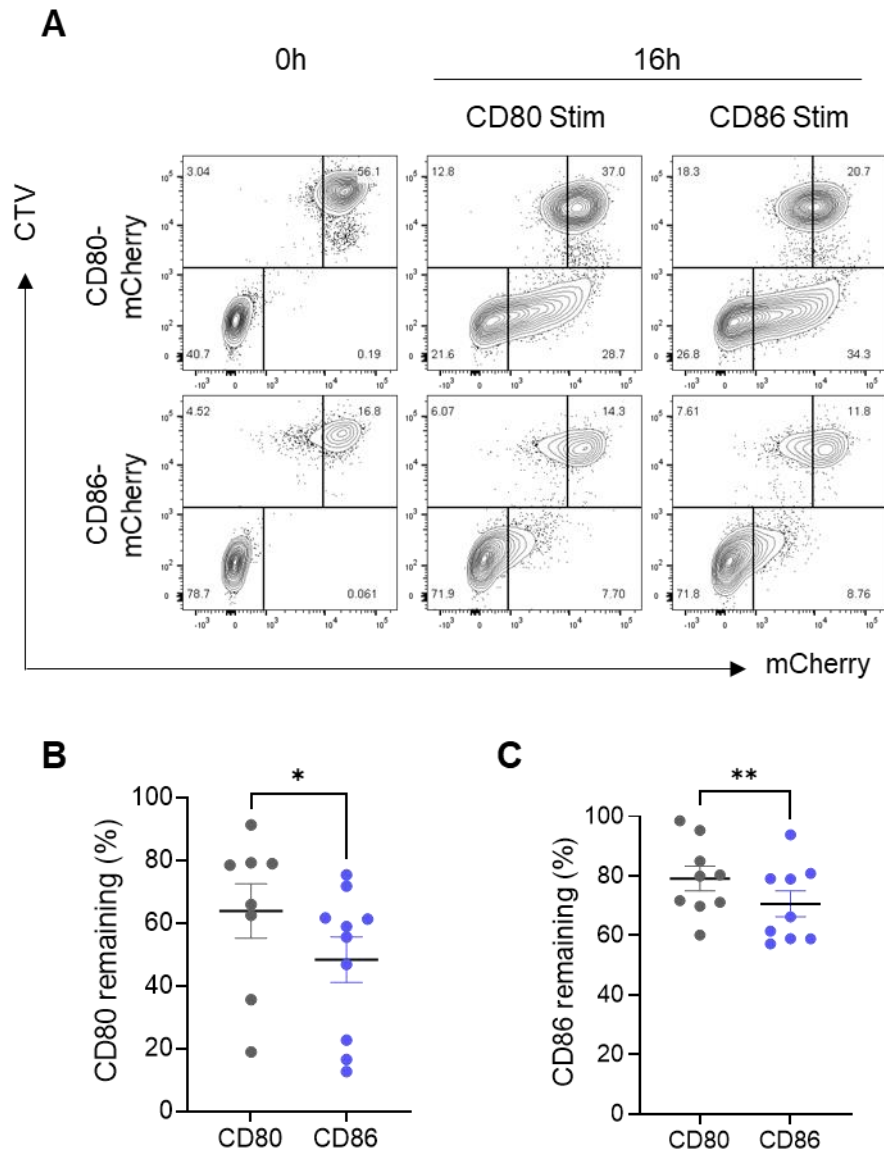
Figure 5. 11. Tregs stimulated by CD86 are more efficient at transendocytosis. CD25+CD127lo Treg cells were isolated from blood and purified by cell sorting. Purified Tregs were cultured for 10 days with DG75 cells expressing CD80 or CD86 with 1µg/ml anti-human-CD3 with 1000IU of IL2. Tregs were then incubated at a 1:1 ratio with Cell Trace Violet (CTV) labelled DG75 cells expressing CD80-mCherry or CD86-mCherry for 0 and 16 hours. **(A)** FACs plots showing CTV against mCherry expression. **(B & C)** Graphs show percentage of CD80-mCherry **(B)** or CD86-mCherry **(C)** remaining at 16 hours, relative to 0 hours. Data from 9 donors, represented as mean ± SEM, analysed by paired T-test, ns = p>0.05 *p≤0.05, **p≤0.01,***p≤0.001, ****p≤0.0001.
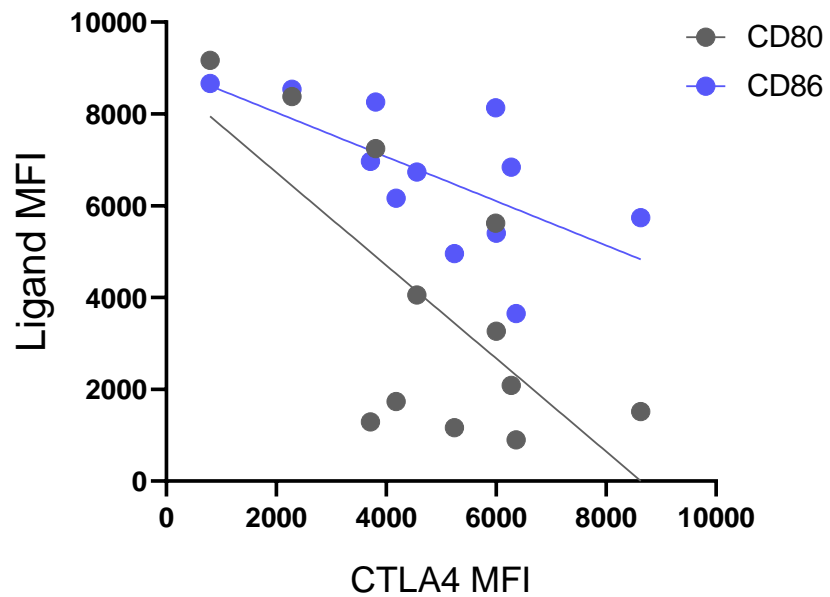
Figure 5. 12. CD80 and CD86 transendocytosis efficiency is dependent on CTLA4 level. Purified Tregs were cultured for 10 days with DG75 cells expressing CD80 (black dots) or CD86 (blue dots) with 1µg/ml anti-human-CD3 with 1000IU of IL2. Tregs were then incubated at a 2:1 ratio with Cell Trace Violet (CTV) labelled DG75 cells expressing CD80-mCherry (full circles) or CD86-mCherry (open circles) for 16 hours, before analysis of mCherry expression on CTV+ cells. Tregs were stained separately for CTLA4 expression. Graph shows ligand downregulation vs CTLA4 expression from 12 donors.

5.2.5. Treg recapitulate the key features of CD80 and CD86 transendocytosis

Having generated highly functional Tregs at sufficient numbers for scalable *in vitro* assays, we used CD86 expanded Tregs to test features of our proposed model of transendocytosis (**Figure 4.27**), in a primary Treg.

To test whether CD80 accumulated inside CTLA4 expressing Treg at a higher level than CD86, we varied DG75 to Treg ratios from 5:1 to 1:20 (DG75:Treg) to ensure ligand uptake. As expected, there was increased transendocytosis, when more Tregs were present of both CD80 and CD86 (**Figure 5.13A, B**). However, CD80 consistently accumulated in more Tregs to a significantly higher level than CD86 (**Figure 5.13A, C**). This increased accumulation of CD80 and rapid loss of CD86 is consistent with our observations in cell line models, and is related to CD86 dissociation from CTLA4.

We next tested how addition of pH modulator Bafilomycin A (BafA) during transendocytosis affected primary Tregs. (**Figure 5.14**)., We observed nearly complete depletion of both CD80- and CD86-mCherry by 21 hours at 10:1 Treg: DG75 ratio and whilst CD80 removal was unaffected by BafA addition, CD86 removal was significantly inhibited (**Figure 5.14, red boxes**). Moreover, Baf A treatment also rescued ligand acquisition into Tregs, showing that CD86 was being degraded post-internalisation (blue boxes). Therefore, we concluded that CTLA4 mediated transendocytosis of CD86 is reliant on pH dependant dissociation in Tregs, in support of our model.
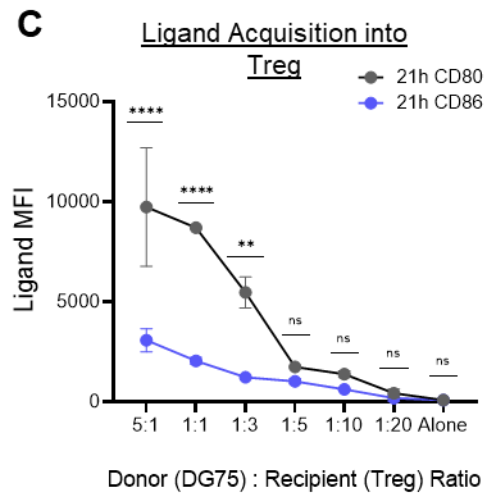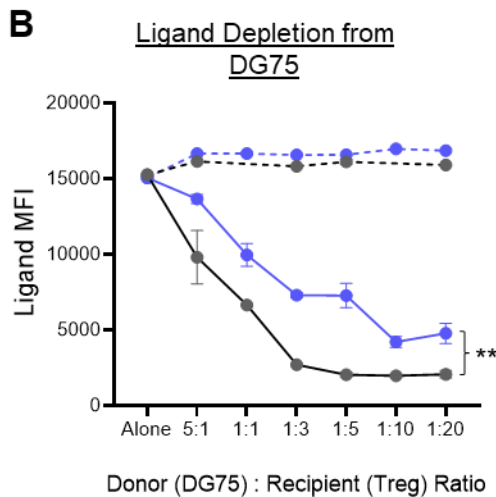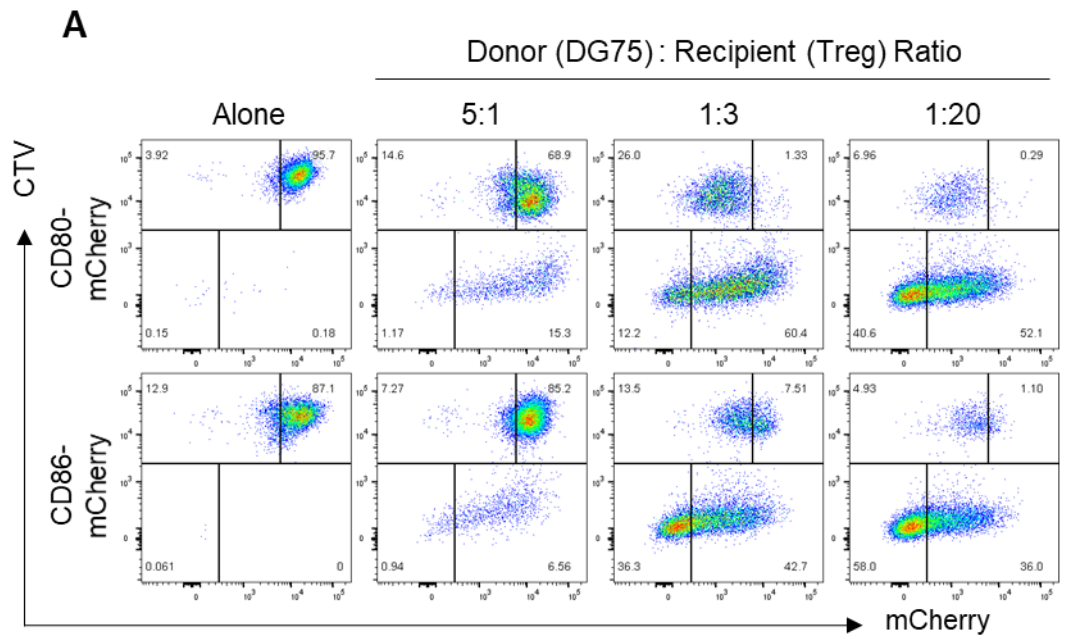
Figure 5. 13. CD80 accumulates more than CD86 in Tregs following transendocytosis. Purified Tregs were cultured for 10 days with DG75 cells expressing CD86 with 1µg/ml anti-human-CD3 with 1000IU of IL2. Tregs were then incubated at indicated ratios with Cell Trace Violet (CTV) labelled DG75 cells expressing CD80-mCherry or CD86-mCherry for 16 hours. **(A)** FACs plots of mCherry vs CTV to observe ligand uptake and removal. **(B-C)** Graphs shows mCherry level in CTV+ DG75 cells showing ligand loss **(B)** or CTV- Treg cells showing ligand uptake **(C).** Data collated from 3 independent donors, represented as mean ± SD, analysed by two-way ANOVA, ns = p>0.05 *p≤0.05, **p≤0.01,***p≤0.001, ****p≤0.0001.
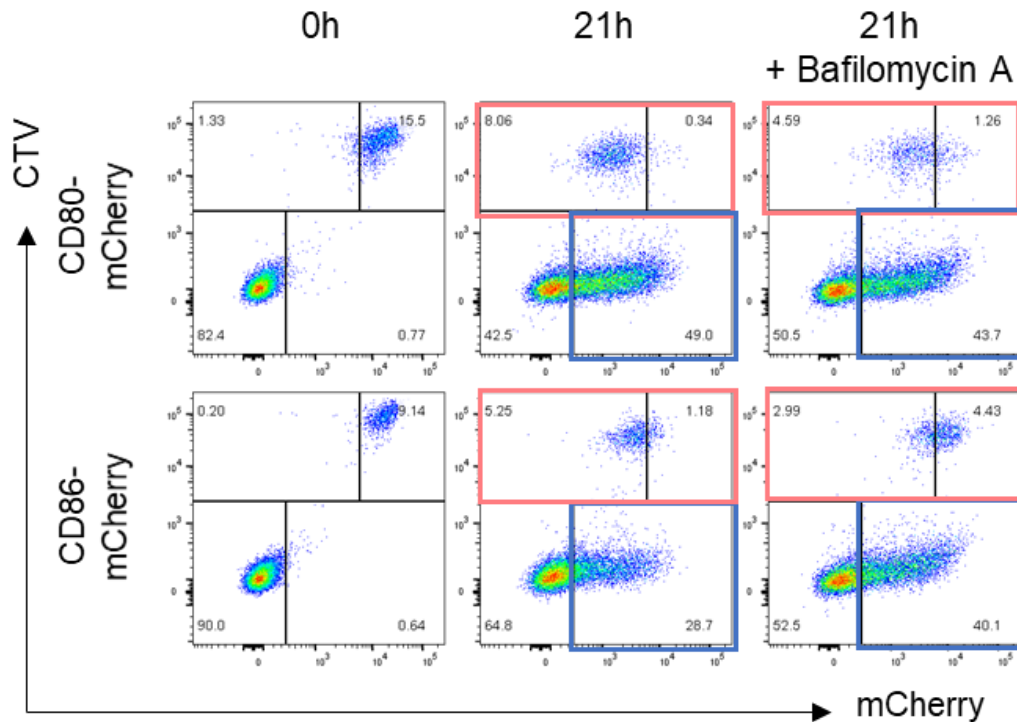
Figure 5. 14. Transendocytosis of CD86 is sensitive to lysosomal inhibition. Purified Tregs were cultured for 10 days with DG75 cells expressing CD86 with 1µg/ml anti-human-CD3 with 1000IU of IL2. Tregs were then incubated at 10:1 Treg:DG75 ratio with Cell Trace Violet (CTV) labelled DG75 cells expressing CD80-mCherry or CD86-mCherry for 21 hours, with or without 50nM Bafilomycin A. FACs plots of mCherry vs CTV to observe ligand uptake (blue gate) and removal (red gate).

Another key difference identified in cell lines is that CD80 induces ubiquitination of CTLA4, dependant on whether CD80 is a monomer or a dimer. To confirm CTLA4 ubiquitination following CD80 engagement in primary Tregs, we incubated Tregs with DG75s expressing CD80- or CD86-GFP, or no ligand (NL) for 6 hours, before lysing cells and performing an immunoprecipitation with ubiquitin-trap beads. As expected, CD80 transendocytosis resulted in ubiquitination of CTLA4, with a strong CTLA4 signal post-IP at both the native CTLA4 molecular weight (25kDa) and a higher molecular weight, indicating both increased association with a ubiquitinated partner and direct ubiquitin post-translational modification (**Figure 5.15**). In contrast, CD86 did not result in CTLA4 ubiquitination. Moreover, the CTLA4 signal at 25kDa was enhanced by addition of BafA for both CD80 and CD86. and treatment prevents dissociation. Together these data provide further support that CTLA4 is ubiquitinated in Tregs depending on whether CD80 or CD86 is ligated

To investigate whether ubiquitination of CTLA4 by CD80 results in a resulted in a reduction of CTLA4 at the cell surface, we asked how much available CTLA4 there was following transendocytosis of CD80 and CD86. For this, we co-incubated expanded Tregs at a 3:1 ratio with CTV labelled DG75 cells expressing CD80-mCherry, CD86-mCherry or a no ligand (NL) control overnight. This ratio was used to ensure all Tregs contained ligand, shown in **Figure 5.16A**. We then added 10µg/ml of anti-CTLA4-APC at 37ºC for 60 minutes. Tregs were then gated as CTV-ve and analysed for anti-CTLA4-APC by flow cytometry, allowing detection of antibody uptake into Tregs due to available cycling CTLA4.

We observed that anti-CTLA4 uptake was markedly reduced following CD80 transendocytosis, whilst transendocytosis of CD86 had no significant

impact on the level of cycling CTLA4 (**Figure 5.16B**). Interestingly, although non-significant, cycling CTLA4 following CD86 transendocytosis had an increased trend over NL controls, potentially due to augmented CD28 co-stimulation by CD86 supporting CD86 as the better CD28 ligand in settings of high CTLA4.
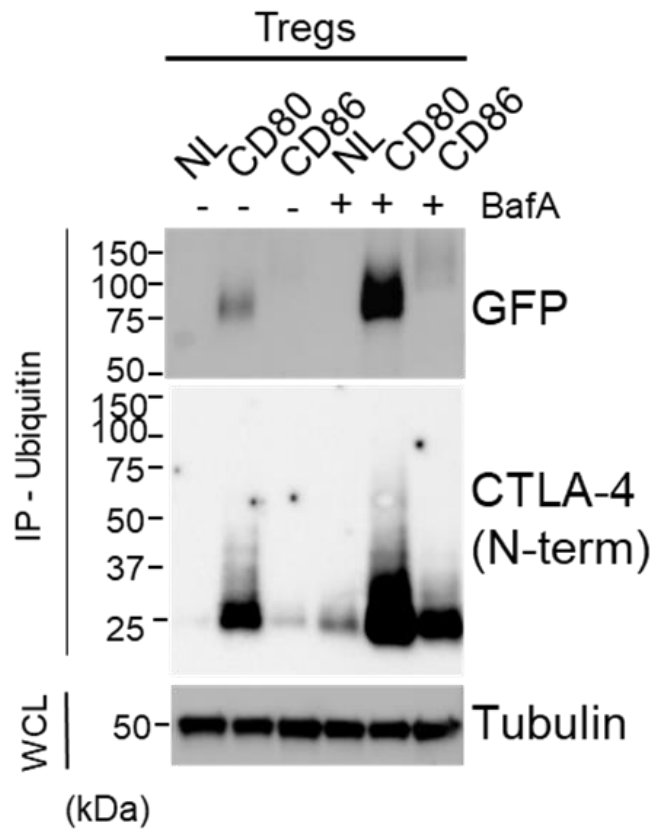
Figure 5. 15. CD80 drives CTLA4 ubiquitination in primary Tregs. Purified Tregs were cultured for 21 days, with DG75s expressing CD86-mCherry with 1µg/ml anti-human-CD3 and 1000IU of IL2 Expanded Tregs were incubated at a 1:5 ratio with DG75s expression no ligand (NL), CD80- or CD86-GFP for 6 hours, in the presence or absence of 50nM Bafilomycin A. Cell cultures were then lysed, before immunoprecipitation (IP) by ubiquitin. Lysates were analysed post-IP by Western Blot using anti-GFP, anti-CTLA4 (N-term clone EPR1572) and whole cell lysates (WCL) analysed for tubulin as a loading control.
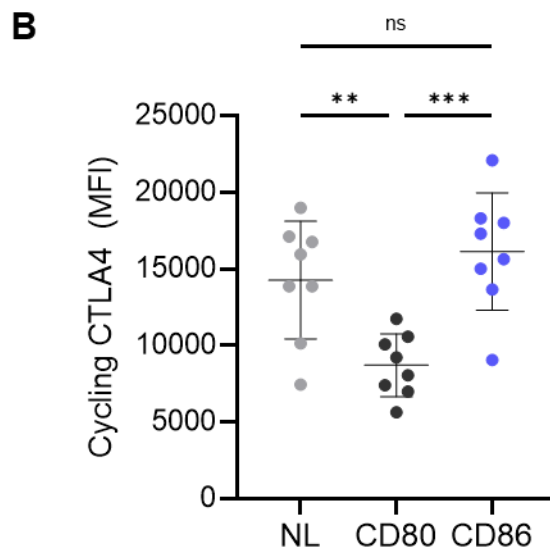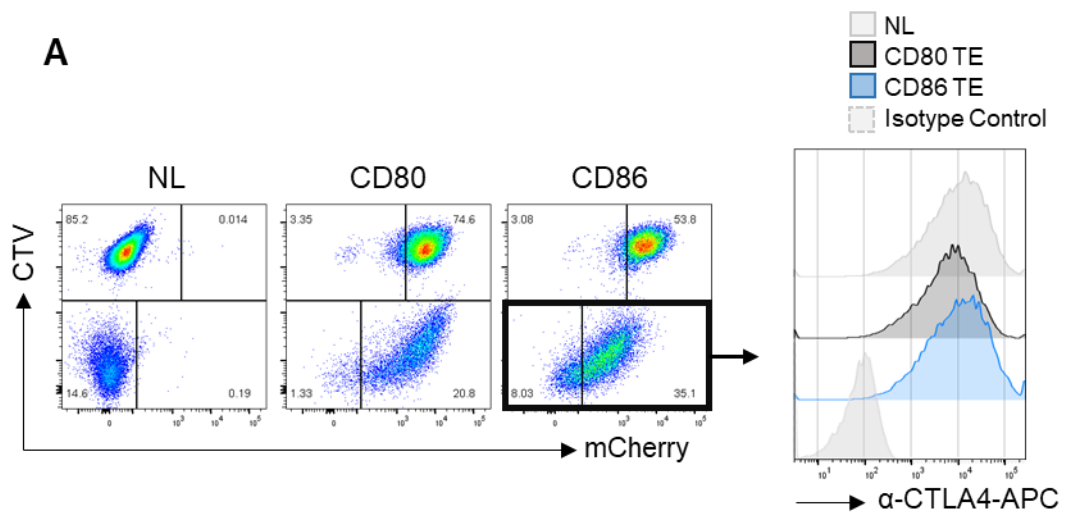
Figure 5. 16. CD80 transendocytosis reduces available CTLA4. Detection of available CTLA4 in expanded Tregs following overnight transendocytosis (TE) of Cell Trace Violet (CTV) labelled DG75 B cells expressing CD80, CD86 or without ligand (NL). **(A)** FACs plots of TE assay. Histograms show available CTLA-4 measured using anti-CTLA-4 antibody at 37°C for 60min, gated on CTV- Treg population (black box) and MFI of CTLA-4 staining quantified **(B).** Data from 8 independent repeats collated from 3 donors ± SD, analysed by one-way ANOVA.

5.2.6. Loss of CD80 avidity enhances CTLA4 mediated transendocytosis due to ability to dissociate from CTLA4 in Tregs

In the previous chapter we showed that ubiquitination of CTLA4 by CD80 is dependent on its ability to dimerise and form high avidity lattices with CTLA4. We also identified that CD80I2R did not enhance CTLA4 ubiquitination, and dissociated from CTLA4 post-internalisation, permitting CTLA4 recycling. We therefore wanted to investigate the influence of bivalency on endogenous CTLA4 using our monovalent CD80I2R mutant in primary Treg models.

First, we tested whether increased transendocytosis efficiency was observed by comparing CD80 and CD80I2R. It is important to note that our resultant cell line expressed 37% more CD80I2R-mCherry than our CD80-mCherry cell line (**Figure 5.17A)**, which is likely influence transendocytosis efficiency. Nevertheless, DG75 CD80 and CD80I2R-mCherry were co-cultured with expanded Tregs at a 1:10 ratio, and transendocytosis measured over time.

We observed (**Figure 5.17B**) a time dependent depletion of both CD80 and CD80I2R. We found that CD80I2R showed better accumulation into Tregs, with the majority containing high levels of CD80I2R by 8 hours (53%), compared to CD80 (36%) (**Figure 5.17B**). Whilst an increased rate of ligand depletion was not readily observed in the raw FACs plots, quantification of MFI relative to 0 hours showed CD80I2R was removed an increased rate compared to CD80 (**Figure 5.17C**). Therefore, these data suggested that CD80I2R showed an increased rate of transendocytosis, however, these experiments need further work.
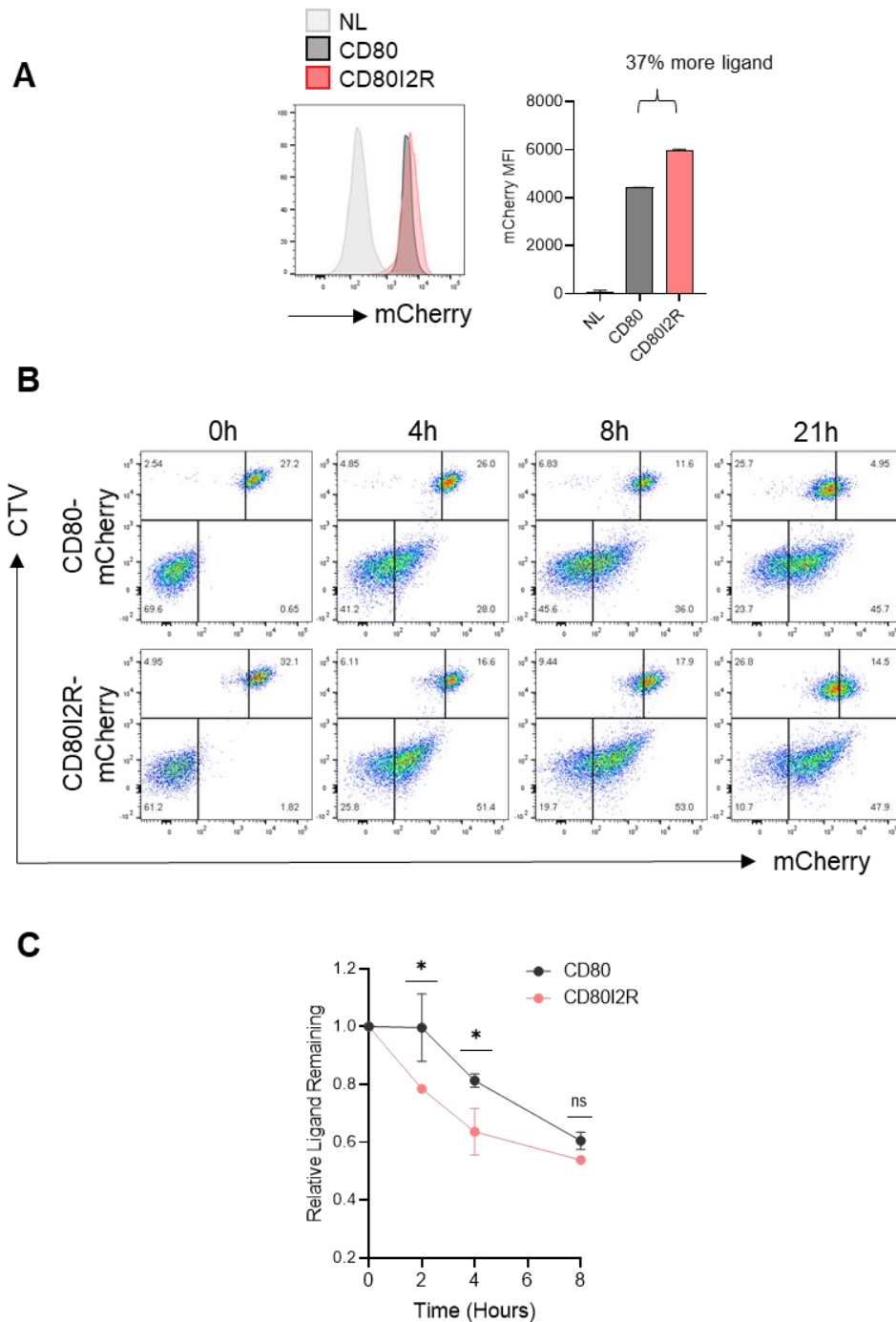
Figure 5. 17. Loss of CD80 avidity enhances CTLA4 mediated transendocytosis in Tregs. (A) Histograms and graph show ligand-mCherry levels in DG75 lines expressing CD80 and CD80I2R-mCherry post sorting. **(B)** FACs plots of transendocytosis assay with expanded Tregs incubated with CellTrace Violet labelled DG75 CD80- or CD80I2R-mCherry at a 10:1 ratio at indicated time points. **(C)** Graph shows quantification of mCherry signal in CTV+ cells, relative to 0 hours. Data from 2 donors ± SD, analysed by 2-way ANOVA ns = p>0.05 *p≤0.05.

Next, we used confocal microscopy to determine if the monovalent CD80 dissociated from CTLA4 post-internalisation. For this, we incubated expanded Tregs with DG75s expressing CD80-, CD80I2R- and CD86-mCherry overnight, before staining for intracellular CTLA4 (green) and mCherry. Following transendocytosis, CD80 accumulated in large intracellular vesicles highly co-localised with CTLA4, in keeping our proposed model. In contrast, CD80I2R was internalised into Tregs, but the ligand clearly showed significantly less co-localisation with CTLA4 (red>yellow), and large CTLA4 vesicles were not commonly seen **(Figure 5.18)**. This phenotype was also seen following CD86 transendocytosis.

Our model based on data from cell lines in **Chapter 4** (**Figure 4.27**) showed transendocytosis of CD80 results in internalisation, ubiquitination and continued association with CTLA4. In contrast, CD86 dissociated in a pH dependant manner, permitting unoccupied CTLA4 to recycle to the cell surface after transendocytosis. Taken together, the data presented here showed similar observations in primary Tregs supporting that the general features proposed in our model also occurs in a physiological cell type.

.
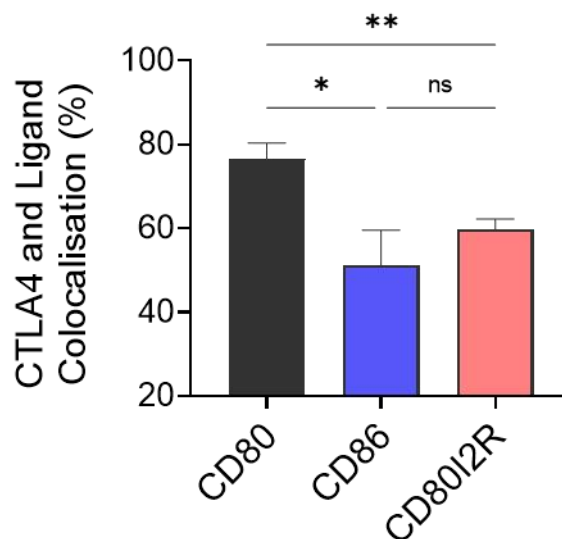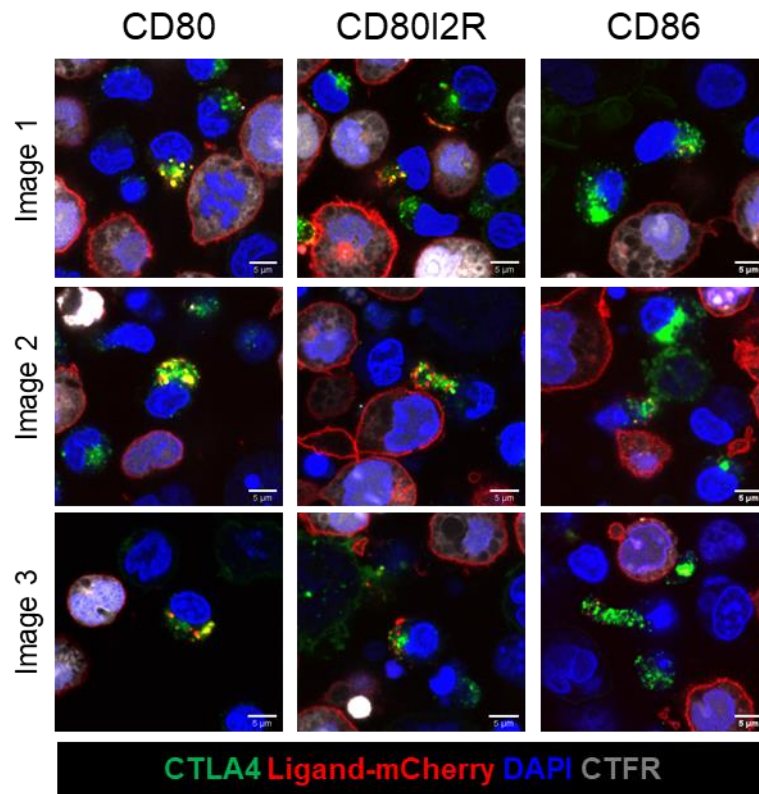
Figure 5. 18. Monovalent ligands dissociate from CTLA4 following internalisation in Treg models. Confocal microscopy analysis following 6-hour transendocytosis of expanded Tregs and CD80-, CD86- or CD80I2R-mCherry at a 5:1 ratio. Cells stained with anti-CTLA4 (C19; Green), and nuclear stain (DAPI; blue), and analysed for mCherry (red). Colocalisation of CTLA4 and ligand quantified using CellProfiler and data from >30 cells from 2 separate experiments shown +- SEM. Scale bar = 5µm. Analysed by 2-way ANOVA ns = $p>0.05$ *$p≤0.05$ **$p≤0.01$.

5.2.7. CD80I2R is a better CD28 ligand than CD80, in the presence of CTLA4

Finally, we considered how changes in valency / avidity of CD80 this would influence CD28 co-stimulation. we hypothesised that loss of bivalency would reduce the bias of CTLA4>CD28 in CD80 binding. Consequently, we tested our monovalent CD80 ligand, CD80I2R, in our Treg expansion protocol, using purified and sorted Treg populations

Strikingly, whilst the phenotypic difference of CD86 stimulation compared to CD80 was seen, CD80I2R also resulted in expansion of CTLA4+FoxP3high Tregs greater than CD86 (~35% compared to ~21%, **Figure 5.19A, B**). In addition, level of CTLA4 expression following stimulation was also quantified. Again, CD86 resulted in increased levels of CTLA4 relative to CD80, but interestingly, CD80I2R induced CTLA4 levels like CD86 and above that of CD80 (**Figure 5.19C**).

To assess whether increased FoxP3high cell frequency was due to cell differentiation or increased proliferation we phenotyped Tregs for the proliferation marker Ki67. We observed that CD80I2R expansion resulted in a significantly greater number of cells expressing Ki67 over both CD80 and CD86. Intriguingly, Ki67 expression correlated with FoxP3 expression, with a higher proportion of FoxP3+Ki67+ cells following CD80I2R stimulation (**Figure 5.20A**) than CD80 or CD86. This suggested that the higher frequency of CTLA4+FoxP3high Tregs was due to rapid proliferation of a pre-existing FoxP3+ cell. Further, we also looked at ICOS as a marker of CD28 engagement, again observing a significant increase in ICOS following CD80I2R and CD86 expansion, compared to CD80 (**Figure 5.20B**).

Overall, observations using monovalent CD80 (CD80I2R) for Treg expansion support that the best ligand for Treg activation is a monovalent high-affinity ligand. Whilst only preliminary data is shown here, this warrants further investigation to see whether this is from a reduction in the ability to be sequestered by CTLA4, due to loss of ability to form CD80:CTLA4 lattices, or by another, currently unclear mechanism.
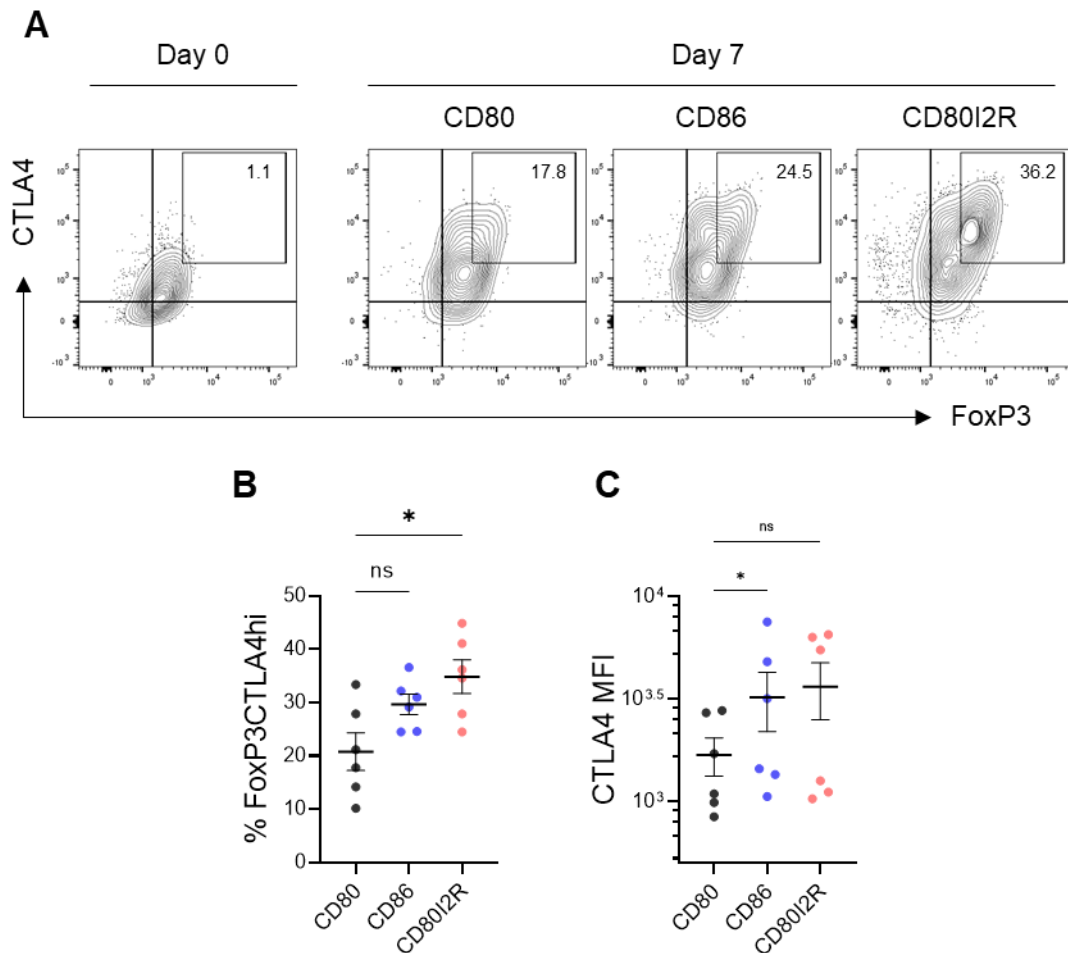
Figure 5. 19. CD80I2R co-stimulation enhances FoxP3 and CTLA4 expression compared to CD80 WT. CD25+CD127lo Treg cells were isolated from blood and purified by cell sorting. Purified Tregs were cultured for 7 days with DG75 cells expressing CD80, CD86 or CD80I2R with 1µg/ml anti-human-CD3 and 1000IU of IL2. After 7 days, levels of CTLA4 and FoxP3 were assessed by flow cytometry, with representative FACS plots in **(A).** FoxP3 and CTLA4 high cells were gated. **(B).** Frequency of CTLA4+FoxP3high cells**. (C)** CTLA4 MFIs of total CD4+ cells were also assessed. Data from 6 donors ± SEM, analysed by one-way ANOVA ns = p>0.05 *p≤0.05 **p≤0.01.
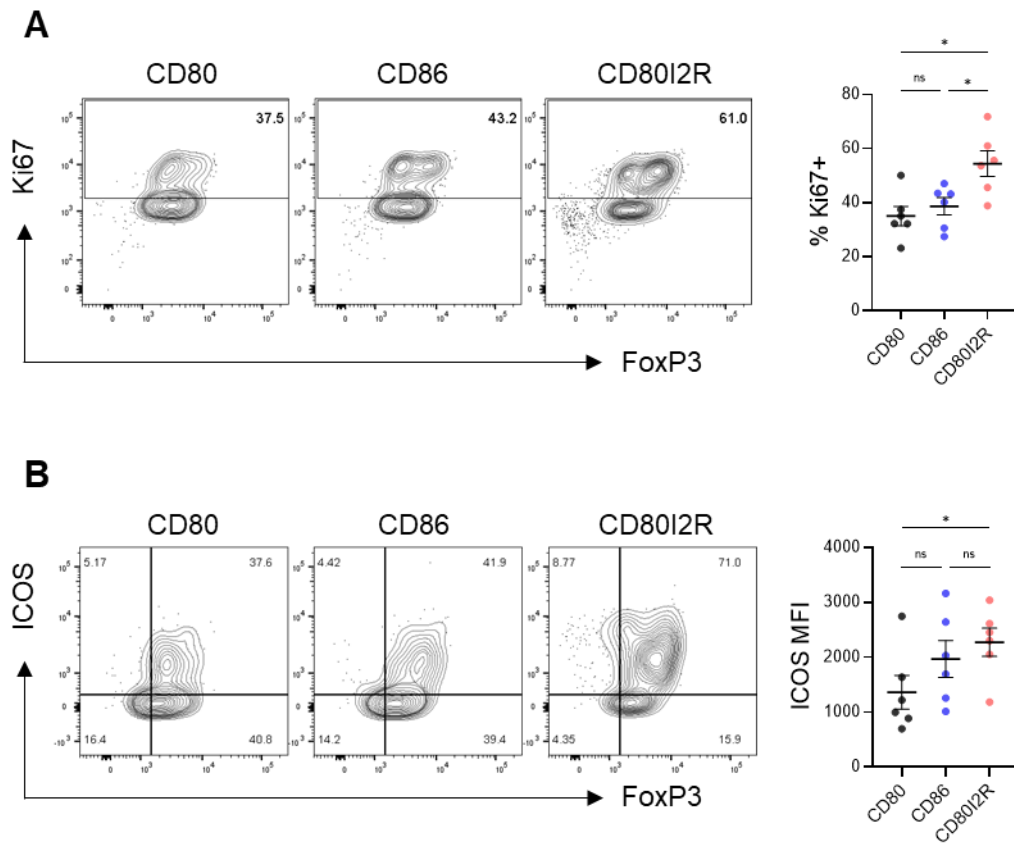
Figure 5. 20. CD80I2R costimulation enhances Ki67 and ICOS expression compared to CD80. CD25+CD127lo Treg cells were isolated from blood and purified by cell sorting. Purified Tregs were cultured for 7 days with DG75 cells expressing CD80, CD86 or CD80I2R with 1µg/ml anti-human-CD3 and 1000IU of IL2. After 7 days, frequency of Ki67+ cells **(A),** and expression levels of ICOS **(B)**. Data from 6 independent donors ± SEM, analysed by one-way ANOVA ns = p>0.05 *p≤0.05 **p≤0.01.

5.3. Discussion

Given the critical role of CTLA4 in Treg it is of interest to study CTLA4 biology on this cell-type *in vitro*. Prior to this Chapter, we gained insights into the molecular mechanism of CTLA4 mediated transendocytosis, where CD80 and CD86 ligands drive alternate fates for CTLA4 in cell line models (Kennedy et al., 2022). Further insight to the biology that dictates these fates at a molecular level, revealed that when CD80 exhibits monovalent binding to CTLA4, this results in lack of ubiquitination, increased dissociation, and chance for CTLA4 to recycle. In this Chapter, we optimised a method for primary Treg purification and expansion, allowing us to study these outcomes in a physiologically relevant cell type, and further study the influence of dimerisation/bivalency within this system.

5.3.1. Dimerisation in the CTLA4:CD28 system influences CD28 co-stimulatory responses

It is established that CD28 co-stimulation is required for Treg activation and proliferation (Guo et al., 2008; Zhang et al., 2013). However, whether CD80 and CD86 differ in CD28 co-stimulatory responses on Treg populations has had limited attention. A major finding from this Chapter is that the phenotype of Tregs is markedly different depending on whether they were stimulated by artificial APCs expressing CD80, or CD86. Specifically, we show co-stimulation provided by CD86 enhanced the expression of FoxP3 and CTLA4, in addition to ICOS, CD25 and PD1 when compared to CD80. These results are in line with our recent publication in non-cultured Treg purified from memory CD4+ populations (Halliday et al., 2020). Together these data suggest that CD86 is the superior CD28 ligand, despite the fact CD80 binds CD28 with higher affinity (Van Der Merwe et al., 1997). Whilst at first paradoxical, these results may be explained

by considering the biophysical properties of the ligands and the influence of CTLA4 expression. Due to the high level of CTLA4 on Tregs, it is probable that the high-avidity interaction with CD80 results in a strong CTLA4>CD28 bias, as predicted by affinity studies and computational modelling (Collins et al., 2002; Khailaie et al., 2018). Therefore, in the presence of CTLA4, CD80 is restricted from CD28 binding whereas the reduced bias of CD86 for CTLA4 enables an increased proportion of ligand to bind to CD28.

Previous studies have reported that CTLA4 blockade increases CD4+CD25- T cell proliferation by CD80, but not CD86, supporting that CTLA4 counterbalances CD80 more effectively than CD86 and supporting CD80 is the major ligand for CTLA4 (Manzotti et al., 2006). Moreover, Halliday et al., identified that CTLA4 KO normalises the CD80 and CD86 differences, enhancing ICOS expression because of CD80 driven expansion (Halliday et al., 2020). Together, these observations may provide biological explanations for prior conflicting interpretations of the role of CD80 versus CD86 blockade in autoimmune disease settings (Lang et al., 2002; MacPhee et al., 2001; Odobasic et al., 2008; Saegusa et al., 2000). For example, anti-CD80 antibodies reduce the incidence of experimental allergic encephalomyelitis (EAE), thought to a T regulatory follicular helper cell mediated disease, where CTLA4 is expressed at high levels (Racke et al., 1995). In this setting, blocking CD80 may cause CTLA4 to better target CD86 thus limiting CD86-CD28 hyper-activation responses. This nuanced control of Treg activation phenotype is likely to have important implications for understanding cellular pathogenesis of disease. Likewise, these observations could provide further understanding to the mechanism of action of therapeutic anti-CTLA4 antibodies. CTLA4 blockade has been shown to increase Treg:Teff ratios by expanding CD4+FoxP3+ populations within tumour microenvironments

in vivo, but studies often fail to consider whether CD80 or CD86 mediated co-stimulation is driving this expansion (Kavanagh et al., 2008; Marangoni et al., 2021; Sharma et al., 2019). Together, the affinity bias within the CTLA4-CD28 system accounts for why CD86 can be a 'better' ligand for CD28, as it is less controlled by CTLA4. Such understanding may therefore have implications in disease settings.

The idea biophysical differences in CD80 and CD86 ligands dictates the level of cell intrinsic CTLA4 vs CD28 competition is also supported by our observations with our monovalent CD80 mutant, CD80I2R. Here, we found that stimulation and expansion with CD80I2R ligands results in increased Treg activation seen by increase in CTLA4 and ICOS expression, compared to both WT CD80 and CD86. As these markers are downstream of CD28 activation, it is likely this phenotype is due to enhanced CD28 engagement and signalling. In addition, CD80I2R stimulation results in an increased percentage of FoxP3+ T cells as well as those expressive Ki67. In line with biophysical predictions, loss of bivalency in the CD80:CTLA4 interaction will prevent lattice formation and high avidity interactions, thereby reducing the CTLA4>CD28 bias seen by CD80 (Merwe et al., 1997; Collins et al., 2002). As a result, the presence of CTLA4 will therefore have less impact on the ability of monovalent CD80 to interact with CD28, compared to bivalent CD80. Similarly, PDL1 can inhibit CD80 dimer formation by interacting in *cis*, forming a PDL1:CD80 heterodimer which can also bind monovalently to CTLA4 (Kennedy, Robinson et al., 2022, Garrett-Thomson et al., 2020; Guan et al., 2016; Khan et al., 2015; Sugiura et al., 2019b; Thibult et al., 2013). The influence of this interaction on CD28 signalling will therefore be of considerable interest.

5.3.2. Potential insights into the mechanism of CD28 signalling

A further area of investigation is whether in the absence of CTLA4, CD86 is still a better CD28 ligand than CD80 despite being lower affinity. An alternative possibility is that the nature of CD86 binding to CD28 is different to that of CD80, which allows a different downstream signalling cascade or more effective triggering to be initiated. Indeed, the CD28 signalling pathway has not been entirely defined, and whilst the crystal structure of CD28 has been generated, the structure of CD28 comparing CD80 vs CD86 has not been reported (Evans et al., 2005; Baker et al., 2009; Nakajima et al., 1997; Toma et al., 2022). Mutational studies identify different amino acids bind to different parts of the ligand, accounting for different reported affinities (Truneh et al., 1996). Importantly, CD86 binds to CD28 with rapid on- and off- rates (Linsley et al., 1994). In our study, we have a fixed amount of TCR stimulus and thus the only variable is the co-stimulation provided. Assuming both ligands bind monovalently to CD28, the differences in affinity would suggest that CD80 should remain bound for longer, with K_{off} values corresponding to half-times of receptor occupancy of ~21s and ~4s for CD80 and CD86, respectively (Greene et al., 1996). One possibility is CD86 may be able to provide a 'pulse-like' or "serial engagement" of CD28, amplifying downstream signalling by increasing the number of receptors which are triggered. This mechanism of receptor triggering has been reported for other receptors with low-affinity ligands, such as the TCR with low affinity peptide:MHC (Chen et al., 2017; Dushek et al., 2009). An additional consequence of this low-affinity binding may be a reduced cell-adhesion time. Importantly, ligand-binding kinetics are known to be rate-limiting for cell-cell interactions, such as seen for integrins (Li et al., 2021), and it is therefore plausible CD86 binds with low-affinity to enhance cell diffusion and rapidly activate many cells.

Important to this discussion is the emerging literature which challenges the valency properties of the CD28 receptor. Whilst commonly thought to bind ligand monovalently due to steric interference at the membrane proximal end of CD80, Sanchez-Lockhart et al., challenged this view (Sanchez-Lockhart et al., 2014). They suggested TCR inside-out signalling induces conformational changes in the CD28 dimer interface which permit bivalent ligand binding, with disruption of a single-ligand binding site in a CD28 dimer limiting receptor recruitment to the immunological synapse ((Sanchez-Lockhart et al., 2014, 2011)). Linked to this idea, other reports suggest monovalent binding of CD28 despite existing as a homodimer is a mechanism to prevent activation in the absence of TCR ligation, as artificial bivalent CD28 ligation induced responses in the absence of TCR engagement (Dennehy et al., 2006). The question of CD28 bivalency is also supported by the CD28: superagonistic 5.11A Fab′ co-crystal structure, demonstrating bivalent antibody binding, however conventional anti-CD28 antibodies e.g. 7.3B6 are topologically constrained (Lühder et al., 2003). Given the phenotypic differences resulting from CD80 vs CD86 ligation of CD28, further investigation into the valency properties of the CD28 receptor will likely warrant further investigation.

5.3.3. Expanded Tregs permit study of CTLA4 transendocytosis *in vitro*

The main aim of this Chapter was to establish an *in vitro* method of Treg purification and expansion that allowed quantitative study of CTLA4 transendocytosis. Here, we demonstrated the ability to robustly detect ligand inside Tregs expanded following CD86 co-stimulation. Crucially, the level of acquisition of both ligands was more obviously observed here than in previously published reports using expanded total CD4+ cells gated on induced Treg

populations i.e. a higher percentage of T cells were found to contain ligand (Ovcinnikovs et al., 2019; Qureshi et al., 2011). As well as ligand acquisition, CD80 and CD86 removal from the DG75 was also used as a measure of transendocytosis efficiency. This is a measure that is not frequently used to study transendocytosis but has some key implications for determining the differential mechanisms of transendocytosis used by CD86 and CD80, discussed in more detail in **Chapter 4**.

Further, Tregs stimulated by DG75s resulted in depletion of CD86, with CD86 stimulated Tregs being more efficient than those grown on CD80. This increased efficiency was likely due to increased CTLA4 expression increasing the probability of ligand binding and cell-contact times to the point they permit transendocytosis. Treg-APC contact *in vivo* has been shown to last for 3-4 minutes (Breart et al., 2006; Tang et al., 2006; Matheu et al., 2015). Together, the idea of an increase in factors which aid cell-cell adhesion is becoming increasingly key for removal of CD86.

As a result of optimisation of a protocol that enables measurement of Treg transendocytosis efficiency, we therefore used CD86 stimulation to generate Tregs going forward. Using Treg we observed that CD80 was readily detectable inside the Treg, in contrast to CD86, even when similar amounts of ligand had been removed. Alongside this observation was that depletion of CD86 was more sensitive to lysosomal inhibition, as treatment with BafA prevents CD86 depletion and revealed CD86 accumulation inside the Treg. Therefore, this data provided primary T cell evidence that CD80 and CD86 follow different trafficking pathways post-internalisation in alignment with our proposed model (Kennedy et al., 2022). Furthermore, the observation that CD80, but not CD86 induces ubiquitination of

CTLA4 in Tregs, is consistent with our previous finings and provides evidence that CD80 directs CTLA4 to lysosomes.

Finally, we also used our optimised method of Treg isolation and expansion to study the importance of CTLA4:CD80 lattice formation dimer -dimer interaction in controlling CTLA4 fate. We observed an increase in the efficiency of transendocytosis with CD80I2R, alongside increased dissociation from CTLA4 observed by microscopy. Whilst this model is discussed in **Chapter 4**, here we show further evidence that this concept is valid in a physiologically relevant cell type, therefore supporting this biology occurs *in vivo* to regulate immune function.

5.3.4. Summary

As a result of work presented in this Chapter, we demonstrate a method of human Treg isolation and expansion that results in high CTLA4 expression. Consequently, we use our Treg expansion protocol to confirm fundamental differences in the mechanism of CD80 vs CD86 mediated CTLA4 transendocytosis, as well as study the impact of ligand dimerisation within this system.

We show that this expansion protocol uses CD86 as a co-stimulatory ligand to activate Tregs and promote CTLA4 expression, as CD86 potentially exhibits less CTLA4>CD28 bias based on biophysical predications compared to CD80, and thus engages CD28 more effectively. In support of these predictions, we show loss of CD80 bivalency increases CD28 engagement shown by an increase in CTLA4 expression on Tregs stimulated with our CD80I2R mutant.

Chapter 6: Overall discussion and future perspectives

The CD28-CTLA4 system is critical in immune regulation, possessing a delicate interplay whereby CD28 determines T cell activation and cytokine production, and CTLA4 prevents overactivation by promoting T cell anergy. From the work presented here, it is apparent the biophysical properties of receptor interactions with their shared ligands, CD80 and CD86, dictate key functional outcomes. With 10-fold higher affinity, and an additional avidity advantage due to the ability to bind bivalently and form lattice-like structures with CTLA4, the CD80 homodimer is highly divergent from its counterpart, CD86. With CD80 dimerisation potentially regulated by *cis* expression with PDL1, how dimerisation contributes to the process of CTLA4 transendocytosis is of crucial understanding.

In this thesis, we saw that the stable dimer-dimer interaction between CTLA4 and CD80 resulted in ubiquitination of CTLA4, and survival of the complex in low-pH compartments post-internalisation. This data, alongside further evidence recently published in our Nature Immunology article, suggests CD80 targets CTLA4 toward lysosomes, effectively disabling CTLA4 and preventing further ligand removal (Kennedy et al., 2022). Critically, we were able to show that this regulation is a result of CD80:CTLA4 bivalent binding and lattice-induced clustering as our monovalent CD80 mutant, CD80I2R, did not trigger CTLA4 ubiquitination. This finding also potentially answers why CD86 as a ligand is also not coupled to CTLA4 ubiquitination, because as a monomer, it is unable to form the lattice-structures which appear critical for this induction. With this phenotype uncovered, further investigation into factors which regulate ubiquitination, as well as the direct ubiquitin ligase responsible in Tregs, is warranted. Degradation of CTLA4 itself was not directly assayed in these experiments. Thus, whilst CTLA4

function was attenuated, we are unable to conclude that ubiquitination is directly linked to CTLA4 degradation per se. Exploring the type and nature of ubiquitin linkage will be a significant next step in the further study of the molecular mechanism of CTLA4 transendocytosis.

We were able to observe both CD80I2R and when CD80 was expressed in *cis* with PDL1 (CD80:PDL1), showed evidence of increased dissociation from CTLA4 post-internalisation, with the ability of CTLA4 to continue transendocytosis retained. Consistent with this, we were able to demonstrate with both CD80I2R and CD80:PDL1, that the reduction in CTLA4 binding strength because of loss of avidity enhancement (but unchanged affinity) increased the efficiency of CTLA4 transendocytosis, as CTLA4 had a higher propensity to recycle and remove further ligand. With this in mind, further experiments utilising affinity mutants, e.g. the high affinity variant CD86-H113L would be useful to study these differences. Further, whilst we were able to robustly show these features in cell-line models, only aspects of this model were demonstrated in primary Tregs. This work would benefit from further investigation into the impact of dimerisation within primary models, whereby key features such as an increased rate of transendocytosis, increased ligand degradation post-internalisation and loss of ubiquitination would be predicted to be observed following CTLA4 transendocytosis with CD80I2R and CD80:PDL1 on Tregs. Indeed, our cell-line models neglect the impact of adhesion proteins, and other factors e.g. level of TCR stimulation, which influence CTLA4 biology. Therefore, whilst our methodology reveals insight into the molecular mechanism of transendocytosis, how this process impacts functional responses regarding Treg proliferation and phenotype will be a key area of further exploration.

In line with the above, we observed differences in the phenotype of Tregs stimulated by CD80 versus CD86, with evidence that dimerisation plays a role by influencing the level of CTLA4:CD28 competition, and therefore CD28 engagement. Data shown here, with additional results from our labs recent publication (Halliday et al., 2020), showed that stimulation with CD86 resulted in greater CTLA4 expression, alongside increased ICOS and PD1, than CD80, akin to strong CD28 signalling. Interestingly, we observed a similarly enhanced phenotype when T cells were stimulated with CD80I2R allowing us to form a hypothesis that the avidity influence from CTLA4:CD80 homodimer interactions are required to efficiently prevent CD28 engaging with CD80. This additional influence of avidity within the system has inevitable implications for the emerging literature aiming to understand the *cis*-CD80:PDL1 interaction, whereby it should be known that the CD28 stimulus received may not be equivalent when comparing CD80 and CD80:PDL1 mediated activation.

Collectively, we have provided new insights into the mechanism of CTLA4 transendocytosis at a molecular level, accounting for why CD80 and CTLA4 exist as homodimers. In addition, we have developed a method of Treg expansion that will allow this model to be explored in a primary setting, permitting further exploration into additional influence of Treg components and influencing factors. Given the fundamental role of the CTLA4:CD28 pathway in immune regulation, our results provide crucial molecular detail which broaden our understanding of the system and present new opportunities to exploit CTLA4 for immunotherapy.

References

Akbari O, Freeman GJ, Meyer EH, Greenfield EA, Chang TT, Sharpe AH, Berry G, DeKruyff RH, Umetsu DT., 2002. Antigen-specific regulatory T cells develop via the ICOS-ICOS-ligand pathway and inhibit allergen-induced airway hyperreactivity. Nat Med. 8(9), 1024-32.

Alam, S.M., Travers, P.J., Wung, J.L., Nasholds, W., Redpath, S., Jameson, S.C., Gascoigne, N.R.J., 1996. T cell-receptor affinity and thymocyte positive selection. Nature 381, 616–620.

Alam MS., 2018. Proximity Ligation Assay (PLA). Curr Protoc Immunol. 123(1), 58.

Albiges, L., Medina Rodriguez, L., Kim, S.-W., Im, S.-A., Carcereny, E., Rha, S.Y., Tran, B., Oliveira, J., Maroto-Rey, P., Su, W.-C., Voskoboynik, M., Rodriguez-Vida, A., Costa, L., Ascierto, P.A., Insa Molla, M.A., Wang, Y., Gainer, S.D., Subramaniam, D.S., Voss, M.H., 2022. Safety and clinical activity of MEDI5752, a PD-1/CTLA-4 bispecific checkpoint inhibitor, as monotherapy in patients (pts) with advanced renal cell carcinoma (RCC): Preliminary results from an FTIH trial. Journal of Clinical Oncology 40, 107–107.

Alegre, ML., Frauwirth, K. & Thompson, C., 2001. T-cell regulation by CD28 and CTLA-4. Nat Rev Immunol **1**, 220–228.

Alkan C, Coe BP, Eichler EE., 2011. Genome structural variation discovery and genotyping. Nat Rev Genet 12(5), 363-76.

Altman, A., Kong, K.F., 2019. pH-sensitive anti-CTLA4 antibodies: yes to efficacy, no to toxicity. Cell Res 29, 601–602.

Anandasabapathy, N., Ford, G.S., Bloom, D., Holness, C., Paragas, V., Seroogy, C., Skrenta, H., Hollenhorst, M., Fathman, C.G., Soares, L., 2003. GRAIL: An E3 ubiquitin ligase that inhibits cytokine gene transcription is expressed in anergic CD4+ T cells. Immunity 18, 535–547.

Anderson, M.S., Venanzi, E.S., Klein, L., Chen, Z., Berzins, S.P., Turley, S.J., von Boehmer, H., Bronson, R., Dierich, A., Benoist, C., Mathis, D., 2002. Projection of an immunological self shadow within the thymus by the aire protein. Science 298, 1395–1401.

Anton, O.M., Peterson, M.E., Hollander, M.J., Dorward, D.W., Arora, G., Traba, J., Rajagopalan, S., Snapp, E.L., Christopher Garcia, K., Waldmann, T.A.,

Long, E.O., 2020. Trans-endocytosis of intact IL-15Rα–IL-15 complex from presenting cells into NK cells favors signaling for proliferation. Proc Natl Acad Sci U S A 117, 522–531.

Anton van Der Merwe, P., Bodian, D.L., Daenke, S., Linsley, P., Davis, S.J., 1997. CD80 (B7-1) Binds Both CD28 and CTLA-4 with a Low Affinity and Very Fast Kinetics. J. Exp. Med 185, 393–403.

Anton van der Merwe P, Davis SJ, Shaw AS, Dustin ML., 2000. Cytoskeletal polarization and redistribution of cell-surface molecules during T cell antigen recognition. Semin Immunol 12, 5-21.

Appleman, L.J., Berezovskaya, A., Grass, I., Boussiotis, V.A., 2000. CD28 Costimulation Mediates T Cell Expansion Via IL-2-Independent and IL-2-Dependent Regulation of Cell Cycle Progression. The Journal of Immunology 164, 144–151.

Aruffo, A., Seed, B., 1987. Molecular cloning of a CD28 cDNA by a high-efficiency COS cell expression system. Proc Natl Acad Sci U S A 84, 8573–8577.

Aucher A, Magdeleine E, Joly E, Hudrisier D., 2008. Capture of plasma membrane fragments from target cells by trogocytosis requires signaling in T cells but not in B cells. Blood 15, 5621-8.

Bachmaier K, Krawczyk C, Kozieradzki I, Kong YY, Sasaki T, Oliveira-dos-Santos A, Mariathasan S, Bouchard D, Wakeham A, Itie A, Le J, Ohashi PS, Sarosi I, Nishina H, Lipkowitz S, Penninger JM., 2000. Negative regulation of lymphocyte activation and autoimmunity by the molecular adaptor Cbl-b. Nature 13, 211-6.

Bachmann, M.F., Gallimore, A., Jones, E., Ecabert, B., Acha-Orbea, H., Kopf, M., 2001. Normal pathogen-specific immune responses mounted by CTLA-4-deficient T cells: A paradigm reconsidered. Eur J Immunol 31, 450–458.

Bachmann, M.F., Köhler, G., Ecabert, B., Mak, T.W., Kopf, M., 1999. Cutting edge: lymphoproliferative disease in the absence of CTLA-4 is not T cell autonomous. J Immunol 163, 1128–31.

Baldys, A., Raymond, J.R., 2009. Critical role of ESCRT machinery in EGFR recycling. Biochemistry 48, 9321–9323.

Belardi, B., Son, S., Felce, J.H., Dustin, M.L., Fletcher, D.A., 2020. Cell–cell interfaces as specialized compartments directing cell function. Nat Rev Mol Cell Biol 21, 750–764.

Bhairavabhotla, R., Kim, Y.C., Glass, D.D., Escobar, T.M., Patel, M.C., Zahr, R., Nguyen, C.K., Kilaru, G.K., Muljo, S.A., Shevach, E.M., 2016. Transcriptome Profiling of Human FoxP3+ Regulatory T Cells. Hum Immunol 77, 201.

Bhatia, S., Edidin, M., Almo, S.C., Nathenson, S.G., 2005a. Different cell surface oligomeric states of B7-1 and B7-2: Implications for signaling. Proc Natl Acad Sci U S A 102, 15569–15574.

Bianchi, M.E., 2007. DAMPs, PAMPs and alarmins: all we need to know about danger. J Leukoc Biol 81, 1–5.

Boomer JS, Green JM. An enigmatic tail of CD28 signaling., 2010. Cold Spring Harb Perspect Biol 2(8):a002436.

Borriello, F., Sethna, M.P., Boyd, S.D., Schweitzer, A.N., Tivol, E.A., Jacoby, D., Strom, T.B., Simpson, E.M., Freeman, G.J., Sharpe, A.H., 1997. B7-1 and B7-2 have overlapping, critical roles in immunoglobulin class switching and germinal center formation. Immunity 6, 303–313.

Breart B, Bousso P., 2006. Cellular orchestration of T cell priming in lymph nodes. Curr Opin Immunol. 18, 483-90.

Brown, Z.J., Heinrich, B., Ma, C., Yu, S.J., Zhang, Q., Fu, Q., Sandhu, M., Agdashian, D., Korangy, F., Greten, T.F., 2018. CTLA-4 blockade induces indoleamine 2,3-dioxygenase where treatment with 1- methyl-d-tryptophan displays greater treatment effect in tumors with high ido expression. HPB 20, S54–S55.

Brunkow, M.E., Jeffery, E.W., Hjerrild, K.A., Paeper, B., Clark, L.B., Yasayko, S., Wilkinson, J.E., Galas, D., Ziegler, S.F., Ramsdell, F., 2001. Disruption of a new forkhead / winged-helix protein , scurfin , results in the fatal lymphoproliferative disorder. 2001. Nature, 68–73.

Buchbinder EI, Desai A., 2016. CTLA-4 and PD-1 Pathways: Similarities, Differences, and Implications of Their Inhibition. Am J Clin Oncol. 39, 98-106.

Burnett, D.L., Parish, I.A., Masle-Farquhar, E., Brink, R., Goodnow, C.C., 2017. Murine LRBA deficiency causes CTLA-4 deficiency in Tregs without progression to immune dysregulation. Immunol Cell Biol 95, 775–788.

Butte, M.J., Keir, M.E., Phamduy, T.B., Sharpe, A.H., Freeman, G.J., 2007. PD-L1 interacts specifically with B7-1 to inhibit T cell proliferation. Immunity 27, 111.

Butte, M.J., Peña-Cruz, V., Kim, M.J., Freeman, G.J., Sharpe, A.H., 2008. Interaction of human PD-L1 and B7-1. Mol Immunol 45, 3567–3572.

Calistri, A., Munegato, D., Toffoletto, M., Celestino, M., Franchin, E., Comin, A., Sartori, E., Salata, C., Parolin, C., Palù, G., 2015. Functional Interaction Between the ESCRT-I Component TSG101 and the HSV-1 Tegument Ubiquitin Specific Protease. J Cell Physiol 230, 1794–1806.

Cano RLE, Lopera HDE. Introduction to T and B lymphocytes. In: Anaya JM, Shoenfeld Y, Rojas-Villarraga A, et al., editors. Autoimmunity: From Bench to Bedside [Internet]. Bogota (Colombia): El Rosario University Press; 2013 Jul 18. Chapter 5.

Cao, X., Cai, S.F., Fehniger, T.A., Song, J., Collins, L.I., Piwnica-Worms, D.R., Ley, T.J., 2007. Granzyme B and Perforin Are Important for Regulatory T Cell-Mediated Suppression of Tumor Clearance. Immunity 27, 635–646.

Cebecauer, M., Spitaler, M., Sergé, A., Magee, A.I., 2010. Signalling complexes and clusters: Functional advantages and methodological hurdles. J Cell Sci 123, 309–320.

Cederbom L, Hall H, Ivars F., 2000. CD4+CD25+ regulatory T cells down-regulate co-stimulatory molecules on antigen-presenting cells. Eur J Immunol. 30, 1538-43.

Chakrabarti, P., Pal, D., 2001. The interrelationships of side-chain and main-chain conformations in proteins. Prog Biophys Mol Biol 76, 1–102.

Chambers, C.A., Sullivan, T.J., Allison, J.P., 1997. Lymphoproliferation in CTLA-4-deficient mice is mediated by costimulation-dependent activation of CD4+ T cells. Immunity 7, 885–895.

Chan, A.C., Dalton, M., Johnson, R., Kong, G.H., Wang, T., Thoma, R., Kurosaki, T., 1995. Activation of ZAP-70 kinase activity by phosphorylation of tyrosine 493 is required for lymphocyte antigen receptor function. EMBO Journal 14, 2499–2508.

Janeway CA Jr, Travers P, Walport M, et al. Immunobiology: The Immune System in Health and Disease. 5th edition. New York: Garland Science; 2001. Principles of innate and adaptive immunity.

Chaudhri, A., Xiao, Y., Klee, A.N., Wang, X., Zhu, B., Freeman, G.J., 2018. PD-L1 Binds to B7-1 Only In Cis on the Same Cell Surface. Cancer Immunol Res 6, 921–929.

Chen, B., Jiang, Y., Zeng, S., Yan, J., Li, X., Zhang, Y., Zou, W., Wang, X., 2010. Endocytic sorting and recycling require membrane phosphatidylserine asymmetry maintained by TAT-1/CHAT-1. PLoS Genet 6, 1–19.

Chen, J., Almo, S.C., Wu, Y., 2017. General principles of binding between cell surface receptors and multi-specific ligands: A computational study. PLoS Comput Biol 13.

Chen, Z., Oh, D., Biswas, K.H., Zaidel-Bar, R., Groves, J.T., 2021. Probing the effect of clustering on epha2 receptor signaling efficiency by subcellular control of ligand-receptor mobility. Elife 10, 1–19.

Cheng, G., Yu, A., Malek, T.R., 2011. T-cell tolerance and the multi-functional role of IL-2R signaling in T-regulatory cells. Immunol Rev 241, 63–76.

Cheng, X., Veverka, V., Radhakrishnan, A., Waters, L.C., Muskett, F.W., Morgan, S.H., Huo, J., Yu, C., Evans, E.J., Leslie, A.J., Griffiths, M., Stubberfield, C., Griffin, R., Henry, A.J., Jansson, A., Ladbury, J.E., Ikemizu, S., Carr, M.D., Davis, S.J., 2013. Structure and interactions of the human programmed cell death 1 receptor. J Biol Chem 288, 11771–11785.

Chinen, T., Kannan, A.K., Levine, A.G., Fan, X., Klein, U., Zheng, Y., Gasteiger, G., Feng, Y., Fontenot, J.D., Rudensky, A.Y., 2016. An essential role for the IL-2 receptor in T reg cell function. Nat Immunol 9, 1322-1333.

Choi JM, Kim SH, Shin JH, Gibson T, Yoon BS, Lee DH, Lee SK, Bothewell A.L., Lim J.S, Lee S.K., 2008. Transduction of the cytoplasmic domain of CTLA-4 inhibits TcR-specific activation signals and prevents collagen-induced arthritis. Proceedings of the National Academy of Sciences of the United States of America. 2008 105, 19875-19880.

Ciechanover, A., Schwartz, A.L., Dautry Varsat, A., Lodish, H.F., 1983. Kinetics of internalization and recycling of transferrin and the transferrin receptor in a human hepatoma cell line. Effect of lysosomotropic agents. Journal of Biological Chemistry 258, 9681–9689.

Clague, M.J., Urbé, S., 2010. Ubiquitin: Same molecule, different degradation pathways. Cell 143, 682–685.

Cohen, L.D., Zuchman, R., Sorokina, O., Müller, A., Dieterich, D.C., Armstrong, J.D., Ziv, T., Ziv, N.E., 2013. Metabolic Turnover of Synaptic Proteins: Kinetics, Interdependencies and Implications for Synaptic Maintenance. PLoS One 8, 63191.

Colin R. F. Monks, Benjamin A. Freiberg, Hannah Kupfer, N.S.& A.K., 1998. Three-dimensional segregation of supramolecular Monks 1998. Nature 340, 764–766.

Collins, M., Ling, V., Carreno, B.M., 2005. The B7 family of immune-regulatory ligands. Genome Biol 6, 1–7.

Collins, A. v., Brodie, D.W., Gilbert, R.J.C., Iaboni, A., Manso-Sancho, R., Walse, B., Stuart, D.I., van der Merwe, P.A., Davis, S.J., 2002a. The interaction properties of costimulatory molecules revisited. Immunity 17, 201–210.

Concepcion Revilla Calvo, B., Amsen, D., Kruisbeek, A.M., 1997. Cytotoxic T Lymphocyte Antigen 4 (CTLA-4) Interferes with Extracellular Signal-regulated Kinase (ERK) and Jun NH 2-terminal Kinase (JNK) Activation, but Does Not Affect Phosphorylation of T Cell Receptor and ZAP70. J. Exp. Med 186, 1645–1653.

Corcoran, K., Jabbour, M., Bhagwandin, C., Deymier, M.J., Theisen, D.L., Lybarger, L., 2011. Ubiquitin-mediated regulation of CD86 protein expression by the ubiquitin ligase membrane-associated RING-CH-1 (MARCH1). Journal of Biological Chemistry 286, 37168–37180.

Corse, E., Allison, J.P., 2012. Cutting Edge: CTLA-4 on Effector T Cells Inhibits In Trans. The Journal of Immunology 189, 1123–1127.

Cottrell, G.S., Padilla, B., Pikios, S., Roosterman, D., Steinhoff, M., Gehringer, D., Grady, E.F., Bunnett, N.W., 2006. Ubiquitin-dependent down-regulation of the neurokinin-1 receptor. Journal of Biological Chemistry 281, 27773–27783.

Craig L. Bennett, Jacinda Christie, Fred Ramsdell, Mary E. Brunkow, Polly J. Ferguson, Luke Whitesell, Thaddeus E. Kelly, Frank T. Saulsbury, Phillip F. Chance, Hans D. Ochs, 2001. The immune dysregulation, polyendocrinopathy, enteropathy, X-linked syndrome (IPEX) is caused by mutations of FOXP3. Nat Genet 27, 20–21.

Curran, M.A., Montalvo, W., Yagita, H., Allison, J.P., 2010. PD-1 and CTLA-4 combination blockade expands infiltrating T cells and reduces regulatory T and myeloid cells within B16 melanoma tumors. Proc Natl Acad Sci U S A 107, 4275–4280.

Darlington, P.J., Kirchhof, M.G., Criado, G., Sondhi, J., Madrenas, J., 2005. Hierarchical Regulation of CTLA-4 Dimer-Based Lattice Formation and Its

Biological Relevance for T Cell Inactivation. The Journal of Immunology 175, 996–1004.

Daubeuf S, Aucher A, Bordier C, Salles A, Serre L, Gaibelet G, Faye JC, Favre G, Joly E, Hudrisier D., 2010. Preferential transfer of certain plasma membrane proteins onto T and B cells by trogocytosis. PLoS One 14:e8716.

David D. Chaplin, 2010. Overview of the immune response. Journal of Allergy and Clinical Immunology 125, S345.

Davis, M.M., Bjorkman, P.J., 1988. The T cell receptor genes and T-cell recognition. Nature 334, 395–402.

Davis, S., van der Merwe, P. 2006. The kinetic-segregation model: TCR triggering and beyond. Nat Immunol 7, 803–809.

Dennehy, K.M., Elias, F., Zeder-Lutz, G., Ding, X., Altschuh, D., Lühder, F., Hünig, T., 2006. Cutting Edge: Monovalency of CD28 Maintains the Antigen Dependence of T Cell Costimulatory Responses. The Journal of Immunology 176, 5725–5729.

Deppong CM, Bricker TL, Rannals BD, Van Rooijen N, Hsieh CS, Green JM., 2013. CTLA4Ig inhibits effector T cells through regulatory T cells and TGF-β. J Immunol 15, 3082-9.

Deppong, C.-S., Hsieh, J.M., Green, C.-W.J., Lio, L.F., Dodson, C.M., 2022. Precursors Cytokine Responsive Regulatory T Cell − CD28 Facilitates the Generation of Foxp3. J Immunol 184, 6007–6013.

Derbinski, J., Gäbler, J., Brors, B., Tierling, S., Jonnakuty, S., Hergenhahn, M., Peltonen, L., Walter, J., Kyewski, B., 2005. Promiscuous gene expression in thymic epithelial cells is regulated at multiple levels. Journal of Experimental Medicine 202, 33–45.

Derbinski, J., Schulte, A., Kyewski, B., Klein, L., 2016. Promiscuous gene expression in medullary thymic epithelial cells mirrors the peripheral self. Journal of Immunology 196, 2915–2922.

Mayle KM, Le AM, Kamei DT., 2012 The intracellular trafficking pathway of transferrin. Biochim Biophys Acta. 1820, 264-81.

Dorweiler, I.J., Ruone, S.J., Wang, H., Burry, R.W., Mansky, L.M., 2006. Role of the Human T-Cell Leukemia Virus Type 1 PTAP Motif in Gag Targeting and Particle Release. J Virol 80, 3634–3643.

Dushek, O., Das, R., Coombs, D., 2009. A Role for Rebinding in Rapid and Reliable T Cell Responses to Antigen. PLoS Comput Biol 5, e1000578.

Eden, Emily R. Fangtian Huang, Alexander Sorkin, Clare E Futter, 2013. The role of EGF receptor ubiquitination in regulating its intracellular traffic. Traffic 13, 329–337.

Esensten, J.H., Helou, Y.A., Chopra, G., Weiss, A., Bluestone, J.A., 2016. CD28 Costimulation: From Mechanism to Therapy. Immunity 44, 973–988.

Evans, E.J., Esnouf, R.M., Manso-Sancho, R., Gilbert, R.J.C., James, J.R., Yu, C., Fennelly, J.A., Vowles, C., Hanke, T., Walse, B., Hünig, T., Sørensen, P., Stuart, D.I., Davis, S.J., 2005. Crystal structure of a soluble CD28-Fab complex. Nat Immunol 6, 271–279.

Fallarino, F., Grohmann, U., Vacca, C., Bianchi, R., Orabona, C., Spreca, A., Fioretti, M.C., Puccetti, P., 2002. T cell apoptosis by tryptophan catabolism. Cell Death Differ 9, 1069–1077.

Felce, J.H., Davis, S.J., 2012. Unraveling receptor stoichiometry using BRET. Front Endocrinol (Lausanne) 3, 1–4.

Finn PW, He H, Wang Y, Wang Z, Guan G, Listman J, Perkins DL., 1997. Synergistic induction of CTLA-4 expression by costimulation with TCR plus CD28 signals mediated by increased transcription and messenger ribonucleic acid stability. J Immunol. 158, 4074-81.

Fisher, P., Ungar, D., 2016. Bridging the gap between glycosylation and vesicle traffic. Front Cell Dev Biol 4, 1–12.

Fontenot, J.D., Gavin, M.A., Rudensky, A.Y., 2003. Foxp3 programs the development and function of CD4+CD25+ regulatory T cells. Journal of Immunology 198, 986–992.

Ganesan A, Moon TC, Barakat KH., 2018. Revealing the atomistic details behind the binding of B7-1 to CD28 and CTLA-4: A comprehensive protein-protein modelling study. Biochim Biophys Acta Gen Subj. 1862, 2764-2778.

Garrett-Thomson, S.C., Massimi, A., Fedorov, E. v., Bonanno, J.B., Scandiuzzi, L., Hillerich, B., Seidel, R.D., Love, J.D., Garforth, S.J., Guha, C., Almo, S.C., 2020. Mechanistic dissection of the PD-L1:B7-1 co-inhibitory immune complex. PLoS One 15, 1–28.

Gaudino, S.J., Kumar, P., 2019. Cross-talk between antigen presenting cells and T cells impacts intestinal homeostasis, bacterial infections, and tumorigenesis. Front Immunol 10, 1–14.

Generous, AR, Harrison, OJ, Troyanovsky, RB, Mateo, M, Navaratnarajah, CK, Donohue, RC, Pfaller, CK, Alekhina, O, Sergeeva, AP,

Indra, I, Thornburg, T, Kochetkova, I, Billadeau, DD, Taylor, MP, Troyanovsky, SM, Honig, B, Shapiro, L & Cattaneo, R 2019, 'Trans-endocytosis elicited by nectins transfers cytoplasmic cargo, including infectious material, between cells', Journal of cell science, 132(16).

Girard T, Gaucher D, El-Far M, Breton G, Sékaly RP., 2014. CD80 and CD86 IgC domains are important for quaternary structure, receptor binding and co-signaling function. Immunol Lett. 161, 65-75.

Glinos, D.A., Soskic, B., Williams, C., Kennedy, A., Jostins, L., Sansom, D.M., Trynka, G., 2020. Genomic profiling of T-cell activation suggests increased sensitivity of memory T cells to CD28 costimulation. Genes Immun 21, 390–408.

Gogishvili, T., Lühder, F., Goebbels, S., Beer-Hammer, S., Pfeffer, K., Hünig, T., 2013. Cell-intrinsic and-extrinsic control of Treg-cell homeostasis and function revealed by induced CD28 deletion. Eur. J. Immunol 43, 188–193.

Golubovskaya V, Wu L., 2016. Different Subsets of T Cells, Memory, Effector Functions, and CAR-T Immunotherapy. Cancers 8, 36

Good-Jacobson, K.L., Song, E., Anderson, S., Sharpe, A.H., Shlomchik, M.J., 2012. CD80 expression on B cells regulates murine T follicular helper development, germinal center B cell survival and plasma cell generation. J Immunol 188, 4217.

Grakoui, A., Bromley, S.K., Sumen, C., Davis, M.M., Shaw, A.S., Allen, P.M., Dustin, M.L., 1999. The immunological synapse: A molecular machine controlling T cell activation. Science 285, 221–227.

Green, D.R., Droin, N., Pinkoski, M., 2003. Activation-induced cell death in T cells. Immunol Rev 193, 70–81

Green, J.M., Noel, P.J., Sperling, A.I., Walunas, T.L., Gray, G.S., Bluestone, J.A., Thompson, C.B., 1994. Absence of B7-dependent responses in CD28-deficient mice. Immunity 1, 501–508.

Greene, J.A.L., Leytze, G.M., Emswiler, J., Peach, R., Bajorath, J., Cosand, W., Linsley, P.S., 1996. Covalent dimerization of CD28/CTLA-4 and oligomerization of CD80/CD86 regulate T cell costimulatory interactions. Journal of Biological Chemistry 271, 26762–26771.

Greenwald, R., 2001. CTLA-4 Regulates Induction of Anergy In Vivo. Immunity 14, 145–155.

Guan H, Wan Y, Lan J, Wang Q, Wang Z, Li Y, Zheng J, Zhang X, Wang Z, Shen Y, Xie F., 2016. PD-L1 is a critical mediator of regulatory B cells and T cells in invasive breast cancer. Sci Rep, 6: 35651.

Guntermann, C., Alexander, D.R., 2002. CTLA-4 Suppresses Proximal TCR Signaling in Resting Human CD4+ T Cells by Inhibiting ZAP-70 Tyr319 Phosphorylation: A Potential Role for Tyrosine Phosphatases. The Journal of Immunology 168, 4420–4429.

Guo, F., Iclozan, C., Suh, W.-K., Anasetti, C., Yu, X.-Z., Yu, Z., Lee, H., 2008. CD28 Controls Differentiation of Regulatory T Cells from Naive CD4 T Cells 1. J Immunol 181, 2285–2291.

Haglund, K., Dikic, I., 2012. The role of ubiquitylation in receptor endocytosis and endosomal sorting. J Cell Sci 125, 265–275.

Halliday, N., Williams, C., Kennedy, A., Waters, E., Pesenacker, A.M., Soskic, B., Hinze, C., Hou, T.Z., Rowshanravan, B., Janman, D., Walker, L.S.K., Sansom, D.M., 2020. CD86 Is a Selective CD28 Ligand Supporting FoxP3+ Regulatory T Cell Homeostasis in the Presence of High Levels of CTLA-4. Front Immunol 11, 1–13.

Hansen, J.D., Pasquier, L. du, Lefranc, M.P., Lopez, V., Benmansour, A., Boudinot, P., 2009. The B7 family of immunoregulatory receptors: A comparative and evolutionary perspective. Mol Immunol 46, 457–472.

Harikumar KG, Yan Y, Xu TH, Melcher K, Xu HE, Miller LJ., 2017. Bioluminescence Resonance Energy Transfer (BRET) Assay for Determination of Molecular Interactions in Living Cells. Bio Protoc. 7(22):e2904.

Harper K, Balzano C, Rouvier E, Mattéi MG, Luciani MF, Golstein P., 1991. CTLA-4 and CD28 activated lymphocyte molecules are closely related in both mouse and human as to sequence, message expression, gene structure, and chromosomal location. J Immunol. 147(3), 1037-44.

Hartman, N.C., Groves, J.T., 2011. Signaling clusters in the cell membrane. Curr Opin Cell Biol 23, 370–376.

Hathcock, K.S., Laszlo, G., Pucillo, C., Linsley, I.P., Hodes, R.J., 1994. Comparative Analysis of B7-1 and B7-2 Costimulatory Ligands: Expression and Function. J Exp Med, 180(2), 631-40.

Hefazi, M., Bolivar-Wagers, S., Blazar, B.R., 2021. Regulatory T Cell Therapy of Graft-versus-Host Disease: Advances and Challenges. Int J Mol Sci 22.

Henkel, J.R., Apodaca, G., Altschuler, Y., Hardy, S., Weisz, O.A., 1998. Selective perturbation of apical membrane traffic by expression of influenza M2, an acid-activated ion channel, in polarized Madin-Darby canine kidney cells. Mol Biol Cell 9, 2477–2490.

Hicke L, Dunn R., 2003. Regulation of membrane protein transport by ubiquitin and ubiquitin-binding proteins. Annu Rev Cell Dev Biol. 19, 141-72.

Hoff, H., Kolar, P., Ambach, A., Radbruch, A., Brunner-Weinzierl, M.C., 2010. CTLA-4 (CD152) inhibits T cell function by activating the ubiquitin ligase Itch. Mol Immunol 47, 1875–1881.

Holdorf AD, Green JM, Levin SD, Denny MF, Straus DB, Link V, Changelian PS, Allen PM, Shaw AS., 1999. Proline residues in CD28 and the Src homology (SH)3 domain of Lck are required for T cell costimulation. J Exp Med. 1999, 190(3), 375-84.

Homann, D., Dummer, W., Wolfe, T., Rodrigo, E., Theofilopoulos, A.N., Oldstone, M.B.A., von Herrath, M.G., 2006. Lack of Intrinsic CTLA-4 Expression Has Minimal Effect on Regulation of Antiviral T-Cell Immunity. J Virol 80, 270–280.

Hong, SW., Krueger, P.D., Osum, K.C. Dileepan, T., Herman, A., Mueller, D., Jenkins, M., 2022. Immune tolerance of food is mediated by layers of CD4^{+} T cell dysfunction. Nature 607, 762–768.

Hori, S., Nomura, T., Sakaguchi, S., 2003. Control of regulatory T cell development by the transcription factor Foxp3. Journal of Immunology 198, 981–985.

Hou, T.Z., Verma, N., Wanders, J., Kennedy, A., Soskic, B., Janman, D., Halliday, N., Rowshanravan, B., Worth, A., Qasim, W., Baxendale, H., Stauss, H., Seneviratne, S., Neth, O., Olbrich, P., Hambleton, S., Arkwright, P.D., Burns, S.O., Walker, L.S.K., Sansom, D.M., 2017. Identifying functional defects in patients with immune dysregulation due to LRBA and CTLA-4 mutations. Blood 129, 1458–1468.

Hu, H., Rudd, C.E., Schneider, H., 2001. Src Kinases Fyn and Lck Facilitate the Accumulation of Phosphorylated CTLA-4 and Its Association with PI-3 Kinase in Intracellular Compartments of T-Cells. Biochem Biophys Res Commun 288, 573–578.

Hünig, T., Schimpl, A., 1998. The IL-2 Deficiency Syndrome. In: Durum, S.K., Muegge, K. (eds) Cytokine Knockouts. Contemporary Immunology. Humana Press, Totowa, NJ.

Ikemizu, S., Gilbert, R.J.C., Fennelly, J.A., Collins, A. v., Harlos, K., Jones, E.Y., Stuart, D.I., Davis, S.J., 2000. Structure and Dimerization of a Soluble Form of B7-1. Immunity 12, 51–60.

Itoh, M., Takahashi, T., Sakaguchi, N., Kuniyasu, Y., Shimizu, J., Otsuka, F., Sakaguchi, S., 1999. Thymus and autoimmunity: production of CD25+CD4+ naturally anergic and suppressive T cells as a key function of the thymus in maintaining immunologic self-tolerance. J Immunol 162, 5317–26.

Jacob, C., Cottrell, G.S., Gehringer, D., Schmidlin, F., Grady, E.F., Bunnett, N.W., 2005. c-Cbl mediates ubiquitination, degradation, and down-regulation of human protease-activated receptor 2. Journal of Biological Chemistry 280, 16076–16087.

Janman, D., Hinze, C., Kennedy, A., Halliday, N., Waters, E., Williams, C., Rowshanravan, B., Hou, T.Z., Minogue, S., Qureshi, O.S., Sansom, D.M., 2021. Regulation of CTLA-4 recycling by LRBA and Rab11. Immunology 164, 106–119.

Jansson, A., Barnes, E., Klenerman, P., Harlén, M., Sørensen, P., Davis, S.J., Nilsson, P., 2005. A Theoretical Framework for Quantitative Analysis of the Molecular Basis of Costimulation. The Journal of Immunology 175, 1575–1585.

Kaur, S., Qureshi, O.S., Sansom, D.M., 2013. Comparison of the Intracellular Trafficking Itinerary of CTLA-4 Orthologues. PLoS One 8, 60903.

Kavanagh, B., O'Brien, S., Lee, D., Hou, Y., Weinberg, V., Rini, B., Allison, J.P., Small, E.J., Fong, L., 2008. CTLA4 blockade expands FoxP3+ regulatory and activated effector CD4 + T cells in a dose-dependent fashion. Blood 112, 1175–1183.

Kennedy, A., Robinson, M., Hinze, C., Waters, E., Williams, C., Halliday, N., Dovedi, S., Sansom, D.M., 2023. CTLA-4 regulates PD-L1-PD-1 interactions via transendocytosis of CD80. EMBO Journal 42, e111556.

Kennedy A, Waters E, Rowshanravan B, Hinze C, Williams C, Janman D, Fox TA, Booth C, Pesenacker AM, Halliday N, Soskic B, Kaur S, Qureshi OS, Morris EC, Ikemizu S, Paluch C, Huo J, Davis SJ, Boucrot E, Walker LSK, Sansom DM., 2022. Differences in CD80 and CD86 transendocytosis reveal CD86 as a key target for CTLA-4 immune regulation. Nat Immunol 23, 1365-1378.

Khailaie, S., Rowshanravan, B., Robert, P.A., Waters, E., Halliday, N., Badillo Herrera, J.D., Walker, L.S.K., Sansom, D.M., Meyer-Hermann, M., 2018. Characterization of CTLA4 Trafficking and Implications for Its Function. Biophys J 115, 1330–1343.

Khan, A.R., Hams, E., Floudas, A., Sparwasser, T., Weaver, C.T., Fallon, P.G., 2015. PD-L1hi B cells are critical regulators of humoral immunity. Nature Communications 6, 1–16.

Khattri, R., Auger, J.A., Griffin, M.D., Sharpe, A.H., Bluestone, J.A., 1999. Lymphoproliferative disorder in CTLA-4 knockout mice is characterized by CD28-regulated activation of Th2 responses. J Immunol 162, 5784–91.

Khoury, S.J., Rochon, J., Ding, L., Byron, M., Ryker, K., Tosta, P., Gao, W., Freedman, M.S., Arnold, D.L., Sayre, P.H., Smilek, D.E., 2017. ACCLAIM: A randomized trial of abatacept (CTLA4-Ig) for relapsing-remitting multiple sclerosis. Multiple Sclerosis 23, 686–695.

Klein L, Kyewski B, Allen PM, Hogquist KA., 2014. Positive and negative selection of the T cell repertoire: what thymocytes see (and don't see). Nat Rev Immunol. 14(6), 377-91.

Koorella, C., Nair, J.R., Murray, M.E., Carlson, L.M., Watkins, S.K., Lee, K.P., 2014. Novel regulation of CD80/CD86-induced phosphatidylinositol 3-kinase signaling by NOTCH1 protein in interleukin-6 and indoleamine 2,3-dioxygenase production by dendritic cells. J Biol Chem 289, 7747–7762.

Kovacs, B., Parry, R. V., Ma, Z., Fan, E., Shivers, D.K., Freiberg, B.A., Thomas, A.K., Rutherford, R., Rumbley, C.A., Riley, J.L., Finkel, T.H., 2005. Ligation of CD28 by Its Natural Ligand CD86 in the Absence of TCR Stimulation Induces Lipid Raft Polarization in Human CD4 T Cells. The Journal of Immunology 175, 7848–7854.

Kronenberg M, Rudensky A., 2005. Regulation of immunity by self-reactive T cells. Nature. 2005 435, 598-604.

Krummel, M.F., Allison, J.P., 1996. CTLA-4 engagement inhibits IL-2 accumulation and cell cycle progression upon activation of resting T cells. J Exp Med 183, 2533–2540.

Krummel, M.F., Allison, J.P., 1995. CD28 and CTLA-4 have opposing effects on the response of T cells to stimulation. J Exp Med 182, 459.

Krummel, M.F., Sjaastad, M.D., Wulfing, C.W., Davis, M.M., 2000. Differential clustering of CD4 and CD3ζ during T cell recognition. Science (1979) 289, 1349–1352.

Kryczanowsky, F., Raker, V., Graulich, E., Domogalla, M.P., Steinbrink, K., 2016. IL-10–Modulated Human Dendritic Cells for Clinical Use: Identification of a Stable and Migratory Subset with Improved Tolerogenic Activity. The Journal of Immunology 197, 3607–3617.

Kufareva, I., Stephens, B., Gilliland, C.T., Wu, B., Fenalti, G., Hamel, D., Stevens, R.C., Abagyan, R., Handel, T.M., 2013. A Novel Approach for Quantifying GPCR Dimerization Equilibrium Using Bioluminescence Resonance Energy Transfer. Methods Mol Biol 1013, 93.

Kunkl, M., Amormino, C., Frascolla, S., Sambucci, M., de Bardi, M., Caristi, S., Arcieri, S., Battistini, L., Tuosto, L., 2020. CD28 Autonomous Signaling Orchestrates IL-22 Expression and IL-22-Regulated Epithelial Barrier Functions in Human T Lymphocytes. Front Immunol 11, 1–13.

Kunkl M, Sambucci M, Ruggieri S, Amormino C, Tortorella C, Gasperini C, Battistini L, Tuosto L., 2019. CD28 Autonomous Signaling Up-Regulates C-Myc Expression and Promotes Glycolysis Enabling Inflammatory T Cell Responses in Multiple Sclerosis. Cells 11, 575.

Lafont, F., Simons, K., 2001. Raft-partitioning of the ubiquitin ligases Cbl and Nedd4 upon IgE-triggered cell signaling. Proc Natl Acad Sci U S A 98, 3180–3184.

Lakadamyali, M., Rust, M.J., Zhuang, X., 2006. Ligands for clathrin-mediated endocytosis are differentially sorted into distinct populations of early endosomes. Cell 124, 997–1009.

Lang, T.J., Nguyen, P., Peach, R., Gause, W.C., Via, C.S., 2002. In Vivo CD86 Blockade Inhibits CD4+ T Cell Activation, Whereas CD80 Blockade Potentiates CD8+ T Cell Activation and CTL Effector Function. The Journal of Immunology 168, 3786–3792.

Lau, K.S., Partridge, E.A., Grigorian, A., Silvescu, C.I., Reinhold, V.N., Demetriou, M., Dennis, J.W., 2007. Complex N-Glycan Number and Degree of Branching Cooperate to Regulate Cell Proliferation and Differentiation. Cell 129, 123–134.

Leung, H.T., Bradshaw, J., Cleaveland, J.S., Linsley, P.S., 1995. Cytotoxic T lymphocyte-associated molecule-4, a high-avidity receptor for CD80 and CD86,

contains an intracellular localization motif in its cytoplasmic tail. J Biol Chem 270, 25107–25114.

Li J, Yan J, Springer TA., 2021. Low-affinity integrin states have faster ligand-binding kinetics than the high-affinity state. Elife 2;10:e73359.

Lin, D.Y.W., Tanaka, Y., Iwasaki, M., Gittis, A.G., Su, H.P., Mikami, B., Okazaki, T., Honjo, T., Minato, N., Garboczi, D.N., 2008. The PD-1/PD-L1 complex resembles the antigen-binding Fv domains of antibodies and T cell receptors. Proc Natl Acad Sci U S A 105, 3011–3016.

Lindsten T, Lee KP, Harris ES, Petryniak B, Craighead N, Reynolds PJ, Lombard DB, Freeman GJ, Nadler LM, Gray GS., 1993. Characterization of CTLA-4 structure and expression on human T cells. J Immunol. 151(7), 3489-99.

Ling, V., Wu, P.W., Finnerty, H.F., Agostino, M.J., Graham, J.R., Chen, S., Jussiff, J.M., Fisk, G.J., Miller, C.P., Collins, M., 2001. Assembly and annotation of human chromosome 2q33 sequence containing the CD28, CTLA4, and ICOS gene cluster: Analysis by computational, comparative, and microarray approaches. Genomics 78, 155–168.

Linsley, P.S., Bradshaw, J., Greene, J.A., Peach, R., Bennett, K.L., Mittler, R.S., 1996. Intracellular trafficking of CTLA-4 and focal localization towards sites of TCR engagement. Immunity 4, 535–543.

Linsley PS, Greene JL, Brady W, Bajorath J, Ledbetter JA, Peach R., 1994. Human B7-1 (CD80) and B7-2 (CD86) bind with similar avidities but distinct kinetics to CD28 and CTLA-4 receptors. Immunity 1(9), 793-801.

Linsley, P.S., Ledbetter, J.A., 1993. The role of the CD28 receptor during T cell responses to antigen. Annu Rev Immunol 11, 191–212.

Linsley, P.S., Nadler, S.G., Bajorath, J., Peach, R., Leung, H.T., Rogers, J., Bradshaw, J., Stebbins, M., Leytze, G., Brady, W., Malacko, A.R., Marquardt, H., Shaw, S.Y., 1995. Binding stoichiometry of the cytotoxic T lymphocyte-associated molecule-4 (CTLA-4): A disulfide-linked homodimer binds two CD86 molecules. Journal of Biological Chemistry 270, 15417–15424.

Liu, H., Hu, B., Xu, D., Liew, F.Y., 2022. and CTLA4 , β Murine Colitis: The Role of IL-10, TGF-Regulatory T Cells Cure + CD25 + CD4. J Immunol References 171, 5012–5017.

Liu, W., Putnam, A.L., Xu-yu, Z., Szot, G.L., Lee, M.R., Zhu, S., Gottlieb, P.A., Kapranov, P., Gingeras, T.R., Barbara, B.F., Clayberger, C., Soper, D.M., Ziegler, S.F., Bluestone, J.A., 2006. CD127 expression inversely correlates with

FoxP3 and suppressive function of human CD4+ T reg cells. Journal of Experimental Medicine 203, 1701–1711.

Lo, B., Zhang, K., Lu, W., Zheng, L., Zhang, Q., Kanellopoulou, C., Zhang, Y., Liu, Z., Fritz, J.M., Marsh, R., Husami, A., Kissell, D., Nortman, S., Chaturvedi, V., Haines, H., Young, L.R., Mo, J., Filipovich, A.H., Bleesing, J.J., Mustillo, P., Stephens, M., Rueda, C.M., Chougnet, C.A., Hoebe, K., McElwee, J., Hughes, J.D., Karakoc-Aydiner, E., Matthews, H.F., Price, S., Su, H.C., Rao, V.K., Lenardo, M.J., Jordan, M.B., 2015. Patients with LRBA deficiency show CTLA4 loss and immune dysregulation responsive to abatacept therapy. Science 349, 436–440.

Lopez-Herrera, G., Tampella, G., Pan-Hammarström, Q., Herholz, P., Trujillo-Vargas, C.M., Phadwal, K., Simon, A.K., Moutschen, M., Etzioni, A., Mory, A., Srugo, I., Melamed, D., Hultenby, K., Liu, C., Baronio, M., Vitali, M., Philippet, P., Dideberg, V., Aghamohammadi, A., Rezaei, N., Enright, V., Du, L., Salzer, U., Eibel, H., Pfeifer, D., Veelken, H., Stauss, H., Lougaris, V., Plebani, A., Gertz, E.M., Schäffer, A.A., Hammarström, L., Grimbacher, B., 2012. Deleterious mutations in LRBA are associated with a syndrome of immune deficiency and autoimmunity. Am J Hum Genet 90, 986–1001.

Lühder, F., Huang, Y., Dennehy, K.M., Guntermann, C., Müller, I., Winkler, E., Kerkau, T., Ikemizu, S., Davis, S.J., Hanke, T., Hünig, T., 2003. Topological requirements and signaling properties of T cell-activating, anti-CD28 antibody superagonists. Journal of Experimental Medicine 197, 955–966.

MacPhee, I.A.M., Turner, D.R., Yagita, H., Oliveira, D.B.G., 2001. CD80(B7.1) and CD86(B7.2) Do not have distinct roles in setting the Th1/Th2 balance in autoimmunity in rats. Scand J Immunol 54, 486–494.

Mandelbrot, D.A., McAdam, A.J., Sharpe, A.H., 1998. B7-1 or B7-2 is required to produce the lymphoproliferative phenotype in mice lacking CTLA-4. J. Exp. Med. 189, 435.

Manzotti, C.N., Liu, M.K.P., Burke, F., Dussably, L., Zheng, Y., Sansom, D.M., 2006. Integration of CD28 and CTLA-4 function results in differential responses of T cells to CD80 and CD86. Eur J Immunol 36, 1413–1422.

Marangoni, F., Zhakyp, A., Corsini, M., Geels, S.N., Carrizosa, E., Thelen, M., Mani, V., Prüßmann, J.N., Warner, R.D., Ozga, A.J., di Pilato, M., Othy, S., Mempel, T.R., 2021. Expansion of tumor-associated Treg cells upon disruption of a CTLA-4-dependent feedback loop. Cell 184, 3998-4015.e19.

Marasco, M., Berteotti, A., Weyershaeuser, J., Thorausch, N., Sikorska, J., Krausze, J., Brandt, H.J., Kirkpatrick, J., Rios, P., Schamel, W.W., Köhn, M., Carlomagno, T., 2020. Molecular mechanism of SHP2 activation by PD-1 stimulation. Sci Adv 6: eaay4458.

Marie, J.C., Letterio, J.J., Gavin, M., Rudensky, A.Y., 2005. TGF-β1 maintains suppressor function and Foxp3 expression in CD4 +CD25+ regulatory T cells. Journal of Experimental Medicine 201, 1061–1067.

Martin Werner, J., Mellins, E., Sethi, D., Wieczorek, M., Abualrous, E.T., Sticht, J., Álvaro-Benito, M., Stolzenberg, S., Noé, F., Freund, C., 2017. Major Histocompatibility Complex (MHC) Class i and MHC Class ii Proteins: Conformational Plasticity in Antigen Presentation. Article 8, 1.

Martínez-Martín, N., Fernández-Arenas, E., Cemerski, S., Delgado, P., Turner, M., Heuser, J., Irvine, D.J., Huang, B., Bustelo, X.R., Shaw, A., Alarcón, B., 2011. T Cell Receptor Internalization from the Immunological Synapse Is Mediated by TC21 and RhoG GTPase-Dependent Phagocytosis. Immunity 35, 208–222.

Matheu, M.P., Othy, S., Greenberg, M.L., Dong, T.X., Schuijs, M., Deswarte, K., Hammad, H., Lambrecht, B.N., Parker, I., Cahalan, M.D., 2015. Imaging regulatory T cell dynamics and CTLA4-mediated suppression of T cell priming. Nat Commun 6:6219.

Midekessa, G., Godakumara, K., Dissanayake, K., Hasan, M.M., Reshi, Q.U.A., Rinken, T., Fazeli, A., 2021. Characterization of extracellular vesicles labelled with a lipophilic dye using fluorescence nanoparticle tracking analysis. Membranes (Basel) 11, 779.

Migliano, S.M., Teis, D., 2018. ESCRT and Membrane Protein Ubiquitination. Prog Mol Subcell Biol 57, 107–135.

Miller Christina Baker AE Kevin Cook AE Beth Graf AE Mariano Sanchez-Lockhart AE Katherine Sharp AE Xia Wang AE Barbara Yang AE Takeshi Yoshida, J.A., Miller, J., Baker Á K Cook Á B Graf Á M Sanchez-Lockhart Á K Sharp Á X Wang Á B Yang Á T Yoshida, Á.C., 2009. Two pathways of costimulation through CD28. Immunol Res 45, 159–172.

Milligan, G., Ward, R.J., Marsango, S., 2019. GPCR homo-oligomerization. Curr Opin Cell Biol 57, 40–47.

Misra, N., Bayry, J., Lacroix-Desmazes, S., Kazatchkine, M.D., Kaveri, S. v., 2004. Cutting Edge: Human CD4+CD25+ T Cells Restrain the Maturation and

Antigen-Presenting Function of Dendritic Cells. The Journal of Immunology 172, 4676–4680.

Mogensen, T.H., 2009. Pathogen recognition and inflammatory signaling in innate immune defenses. Clin Microbiol Rev 22, 240–273.

Moody, P.R., Sayers, E.J., Magnusson, J.P., Alexander, C., Borri, P., Watson, P., Jones, A.T., 2015. Receptor Crosslinking: A General Method to Trigger Internalization and Lysosomal Targeting of Therapeutic Receptor:Ligand Complexes. Molecular Therapy 23, 1888–1898.

Mund, T., Pelham, H.R., 2018. Substrate clustering potently regulates the activity of WW-HECT domain– containing ubiquitin ligases. Journal of Biological Chemistry 293, 5200–5209.

Nakajima, A., Watanabe, N., Yoshino, S., Yagita, H., Okumura, K., Azuma, M., 1997. Requirement of CD28-CD86 co-stimulation in the interaction between antigen-primed T helper type 2 and B cells. Int Immunol 9, 637–644.

Nakayama, M., 2014. Antigen presentation by MHC-dressed cells. Front Immunol 5, 1–8.

Nikolich-Žugich, J., Slifka, M.K., Messaoudi, I., 2004. The many important facets of T-cell repertoire diversity. Nat Rev Immunol 4, 123–132.

Norisada, J., Fujimura, K., Amaya, F., Kohno, H., Hirata, Y., Oh-hashi, K., 2018. Application of NanoBiT for Monitoring Dimerization of the Null Hong Kong Variant of α-1-Antitrypsin, NHK, in Living Cells. Mol Biotechnol 60, 539–549.

Oderup C, Cederbom L, Makowska A, Cilio CM, Ivars F., 2006. Cytotoxic T lymphocyte antigen-4-dependent down-modulation of costimulatory molecules on dendritic cells in CD4+ CD25+ regulatory T-cell-mediated suppression. Immunology. 118(2), 240-9.

Odobasic, D., Leech, M.T., Xue, J.R., Holdsworth, S.R., 2008. Distinct in vivo roles of CD80 and CD86 in the effector T-cell responses inducing antigen-induced arthritis. Immunology 124, 503.

Oh-Hashi K, Hirata Y, Kiuchi K., 2016. SOD1 dimerization monitoring using a novel split NanoLuc, NanoBit. Cell Biochem Funct. 34(7), 497-504.

Ohue, Y., Nishikawa, H., 2019. Regulatory T (Treg) cells in cancer: Can Treg cells be a new therapeutic target? Cancer Sci 110, 2080–2089.

Otero, C., Groettrup, M., Legler, D.F., 2019. Ligands: Recycling versus Degradation Opposite Fate of Endocytosed CCR7 and Its. J Immunol References 177, 2314–2323.

Ovcinnikovs, V., Ross, E.M., Petersone, L., Edner, N.M., Heuts, F., Ntavli, E., Kogimtzis, A., Kennedy, A., Wang, C.J., Bennett, C.L., Sansom, D.M., Walker, L.S.K., 2019. CTLA-4-mediated transendocytosis of costimulatory molecules primarily targets migratory dendritic cells. Sci Immunol 4.

Pagès, F., Ragueneau, M., Rottapel, R., Truneh, A., Nunes, J., Imbert, J., Olive, D., 1994. Binding of phosphatidyl-inositol-3-OH kinase to CD28 is required for T-cell signalling. Nature 369, 327–329.

Palacios, E.H., Weiss, A., 2004. Function of the Src-family kinases, Lck and Fyn, in T-cell development and activation. Oncogene 23, 7990–8000.

Parekh, V. v, Lalani, S., Kim, S., Halder, R., Azuma, M., Yagita, H., Kumar, V., Wu, L., van Kaer, L., 2009. PD-1/PD-L Blockade Prevents Anergy Induction and Enhances the Anti-Tumor Activities of Glycolipid-Activated Invariant NKT Cells 1. The Journal of Immunology 182, 2816–2826.

Parry, R. v, Chemnitz, J.M., Frauwirth, K.A., Lanfranco, A.R., Braunstein, I., Kobayashi, S. v, Linsley, P.S., Thompson, C.B., Riley, J.L., 2005. CTLA-4 and PD-1 Receptors Inhibit T-Cell Activation by Distinct Mechanisms. Mol Cell Biol 25, 9543–9553.

Paust S, Lu L, McCarty N, Cantor H., 2004. Engagement of B7 on effector T cells by regulatory T cells prevents autoimmune disease. Proc Natl Acad Sci U S A., 101(28), 10398-403.

Peach, R.J., Bajorath, J., Naemura, J., Leytze, G., Greene, J., Aruffo, A., Linsley, P.S., 1995. Both extracellular immunoglobin-like domains of CD80 contain residues critical for binding T cell surface receptors CTLA-4 and CD28. J Biol Chem 270, 21181–21187.

Pennock, N.D., White, J.T., Cross, E.W., Cheney, E.E., Tamburini, B.A., Kedl, R.M., 2013. T cell responses: naive to memory and everything in between. Adv Physiol Educ 37, 273–283.

Pentcheva-Hoang T, Egen JG, Wojnoonski K, Allison JP., 2004. B7-1 and B7-2 selectively recruit CTLA-4 and CD28 to the immunological synapse. Immunity 21(3), 401-13.

Pinto, B.F., Medeiros, N.I., Teixeira-Carvalho, A., Fiuza, J.A., Eloi-Santos, S.M., Nunes, M.C.P., Silva, S.A., Fontes-Cal, T.C.M., Belchior-Bezerra, M., Dutra, W.O., Correa-Oliveira, R., Gomes, J.A.S., 2022. Modulation of Regulatory T Cells Activity by Distinct CD80 and CD86 Interactions With CD28/CTLA-4 in Chagas Cardiomyopathy. Front Cardiovasc Med 9, 1–14.

Pontoux, C., Banz, A., & Papiernik, M., 2002. Natural CD4 CD25(+) regulatory T cells control the burst of superantigen-induced cytokine production: the role of IL-10. International immunology, 14 2, *233-9.*

Prasad KV, Cai YC, Raab M, Duckworth B, Cantley L, Shoelson SE, Rudd CE., 1994. T-cell antigen CD28 interacts with the lipid kinase phosphatidylinositol 3-kinase by a cytoplasmic Tyr(P)-Met-Xaa-Met motif. Proc Natl Acad Sci U S A 29, 2834-8.

Qureshi, O.S., Kaur, S., Hou, T.Z., Jeffery, L.E., Poulter, N.S., Briggs, Z., Kenefeck, R., Willox, A.K., Royle, S.J., Rappoport, J.Z., Sansom, D.M., 2012. Constitutive Clathrin-mediated Endocytosis of CTLA-4 Persists during T Cell Activation. Journal of Biological Chemistry 287, 9429–9440.

Qureshi, O.S., Zheng, Y., Nakamura, K., Attridge, K., Manzotti, C., Schmidt, E.M., Baker, J., Jeffery, L.E., Kaur, S., Briggs, Z., Hou, T.Z., Futter, C.E., Anderson, G., Walker, L.S.K., Sansom, D.M., 2011. Trans-Endocytosis of CD80 and CD86: A Molecular Basis for the Cell-Extrinsic Function of CTLA-4. Science 332, 600–603.

Racke, M.K., Scott, D.E., Quigley, L., Gray, G.S., Abe, R., June, C.H., Perrin, P.J., 1995. Distinct roles for B7-1 (CD-80) and B7-2 (CD-86) in the initiation of experimental allergic encephalomyelitis. Journal of Clinical Investigation 96, 2195–2203.

Raffin, C., Vo, L.T., Bluestone, J.A., 2020. Treg cell-based therapies: challenges and perspectives. Nat Rev Immunol 20, 158–172.

Raiborg, C., Stenmark, H., 2009. The ESCRT machinery in endosomal sorting of ubiquitylated membrane proteins. Nature 458, 445–452.

Raker, V.K., Domogalla, M.P., Steinbrink, K., 2015. Tolerogenic dendritic cells for regulatory T cell induction in man. Front Immunol 6, 1–11.

Reggiori, F., Pelham, H.R.B., 2001. Sorting of proteins into multivesicular bodies: Ubiquitin-dependent and -independent targeting. EMBO Journal 20, 5176–5186.

Riha, P., Rudd, C.E., 2010. CD28 co-signaling in the adaptive immune response. Self/Nonself - Immune Recognition and Signaling 1, 231–240.

Roepstorff, K., Grandal, M.V., Henriksen, L., Louise, S., Knudsen, J., Lerdrup, M., Grøvdal, L., Willumsen, B.M., van Deurs, B., 2009. Differential Effects of EGFR Ligands on Endocytic Sorting of the Receptor. Traffic 10, 1115–1127.

Roifman CM., 2000. Human IL-2 receptor alpha chain deficiency. Pediatr Res. 48, 6-11.

Rowshanravan, B., Halliday, N., Sansom, D.M., 2018. CTLA-4: A moving target in immunotherapy. Blood 131, 58–67.

Rudd CE, Taylor A, Schneider H., 2009. CD28 and CTLA-4 coreceptor expression and signal transduction. Immunol Rev. 229(1), 12-26.

Ruocco, M.G., Pilones, K.A., Kawashima, N., Cammer, M., Huang, J., Babb, J.S., Liu, M., Formenti, S.C., Dustin, M.L., Demaria, S., 2012. Suppressing T cell motility induced by anti-CTLA-4 monotherapy improves antitumor effects. J Clin Invest 122.

Saegusa, K., Ishimaru, N., Yanagi, K., Haneji, N., Nishino, M., Azuma, M., Saito, I., Hayashi, Y., 2000. Treatment with anti-CD86 costimulatory molecule prevents the autoimmune lesions in murine Sjogren's syndrome (SS) through up-regulated Th2 response. Clin Exp Immunol 119, 354–360.

Sahoo, N.C., Rao, K.V.S., Natarajan, K., 2002. CD80 expression is induced on activated B cells following stimulation by CD86. Scand J Immunol 55, 577–584.

Sakaguchi S, Sakaguchi N, Asano M, Itoh M, Toda M., 1995. Immunologic self-tolerance maintained by activated T cells expressing IL-2 receptor alpha-chains (CD25). Breakdown of a single mechanism of self-tolerance causes various autoimmune diseases. J Immunol 155, 1151-64.

Salahpour, A., Espinoza, S., Masri, B., Lam, V., Barak, L.S., Gainetdinov, R.R., 2012. BRET biosensors to study GPCR biology, pharmacology, and signal transduction. Front Endocrinol (Lausanne) 3, 1–9.

Salavessa, L., Lagache, T., Malardé, V., Grassart, A., Olivo-Marin, J.C., Canette, A., Trichet, M., Sansonetti, P.J., Sauvonnet, N., 2021. Cytokine receptor cluster size impacts its endocytosis and signaling. Proc Natl Acad Sci USA 118.

Salazar-Fontana, L.I., Barr, V., Samelson, L.E., Bierer, B.E., 2003. CD28 Engagement Promotes Actin Polymerization Through the Activation of the Small Rho GTPase Cdc42 in Human T Cells. The Journal of Immunology 171, 2225–2232.

Salomon, B., Lenschow, D.J., Rhee, L., Ashourian, N., Singh, B., Sharpe, A., Bluestone, J.A., 2000. B7/CD28 costimulation is essential for the homeostasis of the CD4+CD25+ immunoregulatory T cells that control autoimmune diabetes. Immunity 12, 431–440.

Sanchez-Lockhart, M., Kim, M., Miller, J., 2011. Cutting edge: A role for inside-out signaling in TCR regulation of CD28 ligand binding. J Immunol 187, 5515–5519.

Sanchez-Lockhart, M., Rojas, A. v, Fettis, M.M., Bauserman, R., Higa, T.R., 2014. T Cell Receptor Signaling Can Directly Enhance the Avidity of CD28 Ligand Binding. PLoS One 9, 89263.

Sansom, D.M., 2015. Moving CTLA-4 from the trash to recycling. Science (1979) 349, 377–378.

Sansom, D.M., 2000. CD28, CTLA-4 and their ligands: who does what and to whom? Immunology 101, 169.

Sansom, David M., Manzotti, C.N., Zheng, Y., 2003. What's the difference between CD80 and CD86? Trends Immunol 24, 314–9.

Sansom, D.M., Walker, L.S.K., 2019. Dimers Aren't Forever: CD80 Breaks up with PD-L1. Immunity 51, 972–974.

Santra S, Barouch DH, Sharpe AH, Letvin NL., 2000. B7 co-stimulatory requirements differ for induction of immune responses by DNA, protein and recombinant pox virus vaccination. Eur J Immunol 30, 2650-9.

Schneider H, da Rocha Dias S, Hu H, Rudd CE., 2001. A regulatory role for cytoplasmic YVKM motif in CTLA-4 inhibition of TCR signaling. Eur J Immunol. 2001 31, 2042-50.

Schneider, H., Martin, M., Agarraberes, F.A., Yin, L., Rapoport, I., Kirchhausen, T., Rudd, C.E., 1999. Cytolytic T lymphocyte-associated antigen-4 and the TCR zeta/CD3 complex, but not CD28, interact with clathrin adaptor complexes AP-1 and AP-2. J Immunol 163, 1868–79.

Schneider, H., Rudd, C.E., 2014. Diverse Mechanisms Regulate the Surface Expression of Immunotherapeutic Target CTLA-4. Front Immunol 5.

Schneider, H., Schwartzberg, P.L., Rudd, C.E., 1998. Resting Lymphocyte Kinase (Rlk/Txk) Phosphorylates the YVKM Motif and Regulates PI 3-Kinase Binding to T-Cell Antigen CTLA-4. Biochem Biophys Res Commun 252, 14–19.

Schneider, H., Valk, E., Leung, R., Rudd, C.E., 2008. CTLA-4 Activation of Phosphatidylinositol 3-Kinase (PI 3-K) and Protein Kinase B (PKB/AKT) Sustains T-Cell Anergy without Cell Death. PLoS One 3, 3842.

Schubert, D., Bode, C., Kenefeck, R., Hou, T.Z., Wing, J.B., Kennedy, A., Bulashevska, A., Petersen, B.-S., Schäffer, A.A., Grüning, B.A., Unger, S., Frede, N., Baumann, U., Witte, T., Schmidt, R.E., Dueckers, G., Niehues, T.,

Seneviratne, S., Kanariou, M., Speckmann, C., Ehl, S., Rensing-Ehl, A., Warnatz, K., Rakhmanov, M., Thimme, R., Hasselblatt, P., Emmerich, F., Cathomen, T., Backofen, R., Fisch, P., Seidl, M., May, A., Schmitt-Graeff, A., Ikemizu, S., Salzer, U., Franke, A., Sakaguchi, S., Walker, L.S.K., Sansom, D.M., Grimbacher, B., 2014. Autosomal dominant immune dysregulation syndrome in humans with CTLA4 mutations. Nature Medicine. 2014 Dec;20(12):1410-1416. DOI: 10.1038/nm.3746.

Schwartz, A.L., 1995. Receptor cell biology: Receptor-mediated endocytosis. Pediatr Res 38, 835–843.

Schwartz, J.-C.D., Zhang, X., Fedorov, A.A., Nathenson, S.G., Almo, S.C., 2001. Structural basis for co-stimulation by the human CTLA-4/B7-2 complex. Nature 410, 604–608.

Serwas, N.K., Hoeger, B., Ardy, R.C., Stulz, S. v., Sui, Z., Memaran, N., Meeths, M., Krolo, A., Yüce Petronczki, Ö., Pfajfer, L., Hou, T.Z., Halliday, N., Santos-Valente, E., Kalinichenko, A., Kennedy, A., Mace, E.M., Mukherjee, M., Tesi, B., Schrempf, A., Loizou, J.I., Kain, R., Bidmon-Fliegenschnee, B., Schickel, J.N., Glauzy, S., Huemer, J., Garncarz, W., Salzer, E., Pierides, I., Bilic, I., Thiel, J., Priftakis, P., Banerjee, P.P., Förster-Waldl, E., Medgyesi, D., Huber, W.D., Orange, J.S., Meffre, E., Sansom, D.M., Bryceson, Y.T., Altman, A., Boztug, K., 2019. Human DEF6 deficiency underlies an immunodeficiency syndrome with systemic autoimmunity and aberrant CTLA-4 homeostasis. Nature Communications 10, 1–15.

Shahinian, A., Pfefer, K., Lee, K.P., Kündig, T.M., Kishihara, K., Wakeham, A., Kawai, K., Ohashi, P.S., Thompson, C.B., Mak, T.W., 1993. Differential T cell costimulatory requirements in CD28-deficient mice. Science (1979) 261, 609–612.

Sharma, A., Subudhi, S.K., Blando, J., Scutti, J., Vence, L., Wargo, J., Allison, J.P., Ribas, A., Sharma, P., 2019. Anti-CTLA-4 immunotherapy does not deplete Foxp3 þ regulatory T cells (Tregs) in human cancers. Clinical Cancer Research 25, 1233–1238.

Sharpe, A.H., 2009. Mechanisms of costimulation. Immunol Rev 229, 5–11.

Shental-Bechor, D., Levy, Y., 2008. Effect of glycosylation on protein folding: A close look at thermodynamic stabilization. Proc Natl Acad Sci U S A 105, 8256–8261.

Sheppard, K.A., Fitz, L.J., Lee, J.M., Benander, C., George, J.A., Wooters, J., Qiu, Y., Jussif, J.M., Carter, L.L., Wood, C.R., Chaudhary, D., 2004. PD-1 inhibits T-cell receptor induced phosphorylation of the ZAP70/CD3ζ signalosome and downstream signaling to PKCθ. FEBS Lett 574, 37–41.

Shevach, E.M., Thornton, A.M., 2014. tTregs, pTregs, and iTregs: similarities and differences. 2014. Regulatory cells in health and disease 250, 88-102.

Shiratori, T., Miyatake, S., Ohno, H., Nakaseko, C., Isono, K., Bonifacino, J.S., Saito, T., 1997. Tyrosine phosphorylation controls internalization of CTLA-4 by regulating its interaction with clathrin-associated adaptor complex AP-2. Immunity 6, 583–589.

Sigismund, S., Algisi, V., Nappo, G., Conte, A., Pascolutti, R., Cuomo, A., Bonaldi, T., Argenzio, E., Verhoef, L.G.G.C., Maspero, E., Bianchi, F., Capuani, F., Ciliberto, A., Polo, S., di Fiore, P.P., 2013. Threshold-controlled ubiquitination of the EGFR directs receptor fate. EMBO Journal 32, 2140–2157.

Sobhani, N., Tardiel-Cyril, D.R., Davtyan, A., Generali, D., Roudi, R., Li, Y., 2021. CTLA-4 in regulatory T cells for cancer immunotherapy. Cancers (Basel) 13, 1–18.

Soskic, B., Jeffery, L.E., Kennedy, A., Gardner, D.H., Hou, T.Z., Halliday, N., Williams, C., Janman, D., Rowshanravan, B., Hirschfield, G.M., Sansom, D.M., 2021. CD80 on Human T Cells Is Associated With FoxP3 Expression and Supports Treg Homeostasis. Front Immunol 11, 1–12.

Speeckaert, R., van Geel, N., 2017. Targeting CTLA-4, PD-L1 and IDO to modulate immune responses in vitiligo. Exp Dermatol 26, 630–634.

Stamenova, S.D., French, M.E., He, Y., Francis, S.A., Kramer, Z.B., Hicke, L., 2007. Ubiquitin Binds to and Regulates a Subset of SH3 Domains. Mol Cell 25, 273–284.

Stamper, Carin C, Tobin, J.F., Erbe, D. v, Stahl, M.L., Seehra, J., Somers, W.S., Mosyak, L., 2001. Crystal structure of the B7-1/CTLA-4 complex that inhibits human immune responses. Nature 410, 608–611.

Stamper, Carin C., Zhang, Y., Tobin, J.F., Erbe, D. v., Ikemizu, S., Davis, S.J., Stahl, M.L., Seehra, J., Somers, W.S., Mosyak, L., 2001. Crystal structure of the B7-1/CTLA-4 complex that inhibits human immune responses. Nature 410, 608–611.

Staub, O., Rotin, D., 2006. Role of ubiquitylation in cellular membrane transport. Physiol Rev 86, 669–707.

Sugár, I.P., Das, J., Jayaprakash, C., Sealfon, S.C., 2017. Multiscale Modeling of Complex Formation and CD80 Depletion during Immune Synapse Development. Biophys J 112, 997–1009.

Sugiura, D., Maruhashi, T., Okazaki, I.M., Shimizu, K., Maeda, T.K., Takemoto, T., Okazaki, T., 2019a. Restriction of PD-1 function by cis-PD-L1/CD80 interactions is required for optimal T cell responses. Science (1979) 364, 558–566.

Suresh Kumar, K.G., Barriere, H., Carbone, C.J., Liu, J., Swaminathan, G., Xu, P., Li, Y., Baker, D.P., Peng, J., Lukacs, G.L., Fuchs, S.Y., 2007. Site-specific ubiquitination exposes a linear motif to promote interferon-α receptor endocytosis. Journal of Cell Biology 179, 935–950.

Surh, C.D., Sprent, J., 1994. T-cell apoptosis detected in situ selection in the thymus. Nature 372, 100–103.

Tai, X., van Laethem, F., Sharpe, A.H., Singer, A., 2007. Induction of autoimmune disease in CTLA-4-/- mice depends on a specific CD28 motif that is required for in vivo costimulation. Proc Natl Acad Sci U S A 104, 13756–13761.

Takahashi, T., Tagami, T., Yamazaki, S., Uede, T., Shimizu, J., Sakaguchi, N., Mak, T.W., Sakaguchi, S., 2000. Immunologic Self-Tolerance Maintained by Cd25+Cd4+Regulatory T Cells Constitutively Expressing Cytotoxic T Lymphocyte–Associated Antigen 4. Journal of Experimental Medicine 192, 303–310.

Takatsu K, Horikawa K., 2006. Interleukin-5 regulates genes involved in B-cell terminal maturation. Immunology. 118, 497-508.

Takeuchi, O., Hoshino, K., Kawai, T., Sanjo, H., Takada, H., Ogawa, T., Takeda, K., Akira, S., 1999. Differential Roles of TLR2 and TLR4 in Recognition of Gram-Negative and Gram-Positive Bacterial Cell Wall Components. Technology of Japan Science 11, 443–451.

Tang, Q., Henriksen, K.J., Boden, E.K., Tooley, A.J., Ye, J., Subudhi, S.K., Zheng, X.X., Strom, T.B., Bluestone, J.A., 2003. Cutting Edge: CD28 Controls Peripheral Homeostasis of CD4+CD25+ Regulatory T Cells. The Journal of Immunology 171, 3348–3352.

Tang Q, Adams JY, Tooley AJ, Bi M, Fife BT, Serra P, Santamaria P, Locksley RM, Krummel MF, Bluestone JA., 2006. Visualizing regulatory T cell

control of autoimmune responses in nonobese diabetic mice. Nat Immunol. 7(1), 83-92.

Tang, Q., Vincenti, F., 2017. Transplant trials with Tregs: perils and promises. J Clin Invest 127, 2505–2512.

Thibult, M.L., Mamessier, E., Gertner-dardenne, J., Pastor, S., Just-landi, S., Xerri, L., Chetaille, B., Olive, D., 2013. PD-1 is a novel regulator of human B-cell activation. Int Immunol 25, 129–137.

Tivol, E.A., Boyd, S.D., McKeon, S., Borriello, F., Nickerson, P., Strom, T.B., Sharpe, A.H., 1997. CTLA4Ig prevents lymphoproliferation and fatal multiorgan tissue destruction in CTLA-4-deficient mice. The Journal of Immunology 158, 5091–5094.

Tivol, E.A., Gorski, J., 2002. Re-establishing Peripheral Tolerance in the Absence of CTLA-4: Complementation by Wild-Type T Cells Points to an Indirect Role for CTLA-4. The Journal of Immunology 169, 1852–1858.

Toma, H., Sugamura, K., Abe Ohgai, R., Kaibara, N., Koiwai, O., Tanabe, K., Ohnuki, K., Ogawa, S., Ryosuke Watanabe, D., Harada, Y., Takeda, K., 2022. CD28-Mediated Costimulation with CD28 and Play Distinct Roles in Grb2 and Gads Exhibit Different Interactions. J Immunol 177, 1085–1091.

Tomas, A., Futter, C.E., Eden, E.R., 2014. EGF receptor trafficking: Consequences for signaling and cancer. Trends Cell Biol 24, 26–34.

Truneh, A., Reddy, M., Ryan, P., Lyn, S.D., Eichman, C., Couez, D., Hurle, M.R., Sekaly, R.P., Olive, D., Sweet, R., 1996. Differential recognation by CD28 of its cognate counter receptors CD80 (B7.1) and B70 (B7.2): Analysis by site directed mutagenesis. Mol Immunol 33, 321–334.

Trzupek, D., Dunstan, M., Cutler, A.J., Lee, M., Godfrey, L., Jarvis, L., Rainbow, D.B., Aschenbrenner, D., Jones, J.L., Uhlig, H.H., Wicker, L.S., Todd, J.A., Ferreira, R.C., 2020. Discovery of CD80 and CD86 as recent activation markers on regulatory T cells by protein-RNA single-cell analysis. Genome Med 12, 1–22.

Tsushima, F., Yao, S., Shin, T., Flies, A., Flies, S., Xu, H., Tamada, K., Pardoll, D.M., Chen, L., 2007. Interaction between B7-H1 and PD-1 determines initiation and reversal of T-cell anergy. Blood 110, 180-185.

Turvey, S.E., Broide, D.H., 2010. Innate immunity. Journal of Allergy and Clinical Immunology 125, S24–S32.

Verma, N., Burns, S.O., Walker, L.S.K., Sansom, D.M., 2017. Immune deficiency and autoimmunity in patients with CTLA-4 (CD152) mutations. Clin Exp Immunol 190, 1.

Walker LS, Sansom DM., 2015. Confusing signals: recent progress in CTLA-4 biology. Trends Immunol. 36, 63-70.

Walker, L.S.K., 2013. Treg and CTLA-4: Two intertwining pathways to immune tolerance. J Autoimmun 45, 49–57.

Walker LS, Sansom DM., 2011. The emerging role of CTLA4 as a cell-extrinsic regulator of T cell responses. Nat Rev Immunol. 11, 852-63.

Walunas TL, Bakker CY, Bluestone JA., 1996. CTLA-4 ligation blocks CD28-dependent T cell activation. J Exp Med. 183, 2541-50.

Waterhouse, P., Penninger, J.M., Timms, E., Wakeham, A., Shahinian, A., Lee, K.P., Thompson, C.B., Griesser, H., Mak, T.W., 1995. Lymphoproliferative Disorders with Early Lethality in Mice Deficient in Ctla-4. Science (1979) 270, 985–988.

Waterman H, Yarden Y., 2001. Molecular mechanisms underlying endocytosis and sorting of ErbB receptor tyrosine kinases. FEBS Lett 490(3), 142-52.

Watts, C., 1985. Rapid endocytosis of the transferrin receptor in the absence of bound transferrin. J Cell Biol 100, 633–637.

Weihs, F., Wang, J., Pfleger, K.D.G., Dacres, H., 2020. Experimental determination of the bioluminescence resonance energy transfer (BRET) Förster distances of NanoBRET and red-shifted BRET pairs. Anal Chim Acta X 6, 100059.

Westermann-Clark, E., Ballow, M., Walter, J.E., 2022. The new quest in CTLA-4 insufficiency: How to immune modulate effectively? J Allergy Clin Immunol 149, 543–546.

Wherry EJ, Kurachi M. 2015. Molecular and cellular insights into T cell exhaustion. Nat Rev Immunol. 15, 486-99.

Whitehead, G.S., Wilson, R.H., Nakano, K., Burch, L.H., Nakano, H., Cook, D.N., 2012. IL-35 production by inducible costimulator (ICOS)-positive regulatory T cells reverses established IL-17-dependent allergic airways disease. Journal of Allergy and Clinical Immunology 129, 207-215.e5.

Wildin, R.S., Ramsdell, F., Peake, J., Faravelli, F., Casanova, J.L., Buist, N., Levy-Lahad, E., Mazzella, M., Goulet, O., Perroni, L., Dagna Bricarelli, F.,

Byrne, G., McEuen, M., Proll, S., Appleby, M., Brunkow, M.E., 2001. X-linked neonatal diabetes mellitus, enteropathy and endocrinopathy syndrome is the human equivalent of mouse scurfy. Nat Genet 27, 18–20.

Williams, I.R., Unanue, E.R., Immunol, J., Jenkins, M., Schwartz, R., Exp Med, J., Harding, F.A., McArthur, J.G., Gross, J.A., Raulet, D.H., Allison, J.P., Borriello, F., Freeman, G J, Sharpe, A.H., results, unpub-lished, Thomas, K.R., Capecchi, M.R., Freeman, Gordon J, Gribben, John G, Boussiotis, Vassiliki A, Ng, Judy W, Restivo Jr, Vincent A, Lombard, Lisa A, Gray, G.S., Nadler, Lee M, Gribben, J G, Boussiotis, V A, Ng, J W, Restivo Jr, V A, Lombard, L A, Nadler, L M, 1993. Cloning of B7-2: a CTLA-4 Counter-Receptor That Costimulates Human T Cell Proliferation. Science (1979) 262, 909–911.

Wimmer, V.C., Horstmann, H., Groh, A., Kuner, T., 2006. Donut-like topology of synaptic vesicles with a central cluster of mitochondria wrapped into membrane protrusions: A novel structure-function module of the adult calyx of held. Journal of Neuroscience 26, 109–116.

Wing, K., Onishi, Y., Prieto-Martin, P., Yamaguchi, T., Miyara, M., Fehervari, Z., Nomura, T., Sakaguchi, S., 2008. CTLA-4 control over Foxp3+ regulatory T cell function. Science (1979) 322, 271–275.

Xing Y, Hogquist KA., 2012. T-cell tolerance: central and peripheral. Cold Spring Harb Perspect Biol.4(6):a006957.

Yang, Q., Jeremiah Bell, J., Bhandoola, A., 2010. T-cell lineage determination. Immunol Rev 238, 12–22.

Yokosuka, T., Kobayashi, W., Takamatsu, M., Sakata-Sogawa, K., Zeng, H., Hashimoto-Tane, A., Yagita, H., Tokunaga, M., Saito, T., 2010. Spatiotemporal Basis of CTLA-4 Costimulatory Molecule-Mediated Negative Regulation of T Cell Activation. Immunity 33, 326–339.

Zeng J, Santos AF, Mukadam AS, Osswald M, Jacques DA, Dickson CF, McLaughlin SH, Johnson CM, Kiss L, Luptak J, Renner N, Vaysburd M, McEwan WA, Morais-de-Sá E, Clift D, James LC., 2021. Target-induced clustering activates Trim-Away of pathogens and proteins. Nat Struct Mol Biol 28(3), 278-289.

Zenke, S., Sica, M.P., Steinberg, F., Braun, J., Zink, A., Gavrilov, A., Hilger, A., Arra, A., Brunner-Weinzierl, M., Elling, R., Beyersdorf, N., Lämmermann, T., Smulski, C.R., Rohr, J.C., 2022. Differential trafficking of

ligands trogocytosed via CD28 versus CTLA4 promotes collective cellular control of co-stimulation. Nat Commun 13, 1–18.

Zhang, H., Dutta, P., Liu, J., Sabri, N., Song, Y., Li, W.X., Li, J., 2019. Tumour cell-intrinsic CTLA4 regulates PD-L1 expression in non-small cell lung cancer. J Cell Mol Med 23, 535.

Zhang, R., Huynh, A., Whitcher, G., Chang, J., Maltzman, J.S., Turka, L.A., 2013. An obligate cell-intrinsic function for CD28 in Tregs. J Clin Invest 123.

Zhang, Y., Allison, J.P., 1997. Interaction of CTLA-4 with AP50, a clathrin-coated pit adaptor protein. Proc Natl Acad Sci U S A 94, 9273–9278.

Zhang, Y., Du, X., Liu, M., Tang, F., Zhang, P., Ai, C., Fields, J.K., Sundberg, E.J., Latinovic, O.S., Devenport, M., Zheng, P., Liu, Y., 2019. Hijacking antibody-induced CTLA-4 lysosomal degradation for safer and more effective cancer immunotherapy. Cell Res 29, 609–627.

Zhanhua, C., Gan, J.G.-K., lei, L., Sakharkar, M.K., Kangueane, P., 2005. Protein subunit interfaces: heterodimers versus homodimers. Bioinformation 1, 28–39.

Zhao, Y., Lee, C.K., Lin, C.H., Gassen, R.B., Xu, X., Huang, Z., Xiao, C., Bonorino, C., Lu, L.F., Bui, J.D., Hui, E., 2019. PD-L1:CD80 Cis-Heterodimer Triggers the Co-stimulatory Receptor CD28 While Repressing the Inhibitory PD-1 and CTLA-4 Pathways. Immunity 51, 1059-1073.e9.

Zhao H, Liao X, Kang Y., 2017. Tregs: Where We Are and What Comes Next? Front Immunol. 24, 1578.

Zinkernagel, R.F., Doherty, P.C., 1974. Immunological surveillance against altered self components by sensitised T lymphocytes in lymphocytes choriomeningitis. Nature 251, 547–548.

Zuccarino-Catania, G.V., Sadanand, S., Weisel, F.J., Tomayko, M.M., Meng, H., Kleinstein, S.H., Good-Jacobson, K.L., Shlomchik, M.J., 2014. CD80 and PD-L2 define functionally distinct memory B cell subsets that are independent of antibody isotype. Nat Immunol 15, 631.